The Genetic and Functional Basis of Three Inherited Palmoplantar Keratodermas in Human Disease

Dr Thiviyani Maruthappu

Supervisors: Professor David P. Kelsell
Professor Edel A. O'Toole

A Thesis submitted for the degree of PhD

Centre for Cell Biology and Cutaneous Research
Blizard Institute
Bart's & The London School of Medicine & Dentistry
Queen Mary University of London

November 2018

Declaration

I, Thiviyani Maruthappu, confirm that the research included within this thesis is my own work or that where it has been carried out in collaboration with, or supported by others, that this is duly acknowledged below and my contribution indicated. Previously published material is also acknowledged below.

I attest that I have exercised reasonable care to ensure that the work is original, and does not to the best of my knowledge break any UK law, infringe any third party's copyright or other Intellectual Property Right, or contain any confidential material.

I accept that the College has the right to use plagiarism detection software to check the electronic version of the thesis.

I confirm that this thesis has not been previously submitted for the award of a degree by this or any other university.

Dr Thiviyani Maruthappu

Details of Publications, Collaborations, Oral Presentations and Prizes

Publications

Original Peer Reviewed Publications:

Maruthappu T, Posafalvi A, Castelletti S, Delaney PJ, Syrris P, O'Toole EA, Green KJ, Elliott PM, Lambiase PD, Tinker A, McKenna WJ, Kelsell DP.
Loss of function desmoplakin I and II mutations underlie dominant arrhythmogenic cardiomyopathy with a hair and skin phenotype. Br J Dermatol. 2018 Nov 1.

Maruthappu T, McGinty LA, Blaydon DC, Fell B, Määttä A, Duit R, Hawkins T, Braun KM, Simpson MA, O'Toole EA, Kelsell DP
Recessive Mutation in FAM83G Associated with Palmoplantar Keratoderma and Exuberant Scalp Hair. J Invest Dermatol. 2018 Apr;138(4):984-987

Maruthappu T, Chikh A, Fell B, Delaney PJ, Brooke MA, Levet C, Moncada-Pazos A, Ishida-Yamamoto A, Blaydon D, Waseem A, Leigh IM, Freeman M, Kelsell DP
Rhomboid family member 2 regulates cytoskeletal stress-associated Keratin 16. Nat Commun. 2017 Jan 27;8:14174

Invited Reviews:

Ellis A, Risk JM, **Maruthappu T**, Kelsell DP.
Tylosis with oesophageal cancer: Diagnosis, management and molecular
Orphanet J Rare Dis. 2015 Sep 29;10:126

Maruthappu T, Scott CA, Kelsell DP Discovery in genetic skin disease: the impact of high throughput genetic technologies. Genes (Basel). 2014 Aug 4;5(3):615-34

Book Chapter:

Chapter 23.3 Inherited Skin Disease
T Maruthappu & D.P. Kelsell
Oxford Textbook of Medicine 6e
ISBN 9780199652136
Oxford University Press 2018

Oral Presentations

2016
Cutaneous features of Desmoplakin mutations in ARVC
T Maruthappu, S Castelletti, A Posafalvi, P Delaney, P Lambiase, WM McKenna, DP Kelsell
Leducq Foundation Cardiac Research Semi-Annual Meeting, American Heart Association Scientific Symposium, New Orleans 2016

Mutations in FAM83G underlie autosomal recessive Palmoplantar Keratoderma, Leukonychia and Abundant Curly Hair.
T Maruthappu, LA McGinty, A Maatta, K Braun, EA O'Toole and DP Kelsell.
European Society for Dermatology Research: Oral Plenary 2016

Deep Clinical and Molecular Phenotyping in ARVC
A Posafalvi, **T Maruthappu**, S Castelleti, W McKenna, DP Kelsell
European Society of Dermatology Research: Judges Poster Walk 2016

2015
iRHOM2: a novel regulator of wound healing and cancer
T Maruthappu, A Chikh, DP Kelsell.
Invited Speaker British Association of Dermatology Annual Meeting, Professors and Registrars forum July 2015

iRHOM2: a novel regulator of wound healing and cancer.
T Maruthappu, A Chikh, DP Kelsell.
British Society of Investigative Dermatology Annual Meeting April 2015

2014
iRHOM2: a novel regulator of wound healing and cancer
T Maruthappu, A Chikh, DP Kelsell
European Society of Dermatology Research Annual Meeting, September 2014

iRHOM2: a novel regulator of wound healing and cancer
T Maruthappu, A Chikh, DP Kelsell
William Harvey Day Oral Presentation, Barts and The London School of Medicine &Dentistry 2014

Academic Prizes, Awards and Scholarships

2017 Whimster Prize, British Association of Dermatologists (2014-2017)

2017 Hugh Wallace Essay Prize, Royal Society of Medicine (2016-2017)

2017 Psoriasis Gene to Clinic Conference Educational Grant

2016 European Society of Dermatology Research Travel Fellowship

2016 Psoriasis International Network Meeting Scholarship

2015 European Society of Dermatology Poster Prize

2015 British Society of Investigative Dermatology SpR Oral Presentation Prize – Best Paper

2015 Additional MRC funding obtained (£1700)

2014 QMUL William Harvey Day best Oral Presentation Prize

2014 Additional MRC funding (£800)

2014 European Society of Dermatology Research Travel Fellowship

Abstract

The ability of cells to respond to stress is fundamental for survival. The palmoplantar epidermis, by its very nature, is subjected to substantial external forces. At birth, the skin at these sites is similar to the skin elsewhere, however, as we expose it to physical stresses such as walking and gripping, it thickens to adapt. The palmoplantar keratodermas (PPKs) are a heterogeneous group of disorders characterised by abnormal thickening of the palmoplantar epidermis. Causative mutations have been identified in a diverse array of genes, such as those encoding the TNFα sheddase, ADAM17, and the water channel protein, Aquaporin 5.

Three distinct PPK's were studied in order to unravel the molecular basis of their associated diseases. The work presented here identifies the palmoplantar and stress-associated Keratin 16 as a novel interacting protein for iRHOM2, and demonstrates that this regulatory relationship contributes to palmoplantar thickness in Tylosis with Oesophageal Cancer. The deep clinical phenotyping of patients with ARVC caused by dominantly inherited mutations in desmoplakin revealed an unreported cutaneous phenotype of PPK and curly hair which may prove useful in the diagnosis of this complex disease. Finally, this Thesis includes the discovery of the first human disease-causing mutation in *FAM83G*, which presented with a unique phenotype of PPK and abundant curly hair and linked FAM83G to Wnt signaling. By correlating the clinical phenotype with the genotype in each case, and extrapolating from rare monogenic diseases to more common disorders, the PPK's provide a unique resource in which to study the genetic basis of disease.

Table of Contents

List of Figures and Tables

Chapter 1 - Introduction

Chapter 3 – iRHOM2 regulates cytoskeletal stress associated Keratin 16

Chapter 4 - Loss of function Desmoplakin I and II mutations underlie dominant Arrhythmogenic Cardiomyopathy with a hair and skin phenotype

Chapter 5 - Mutations in FAM83G Cause Autosomal Recessive Palmoplantar Keratoderma with Leukonychia and Abundant Curly Hair

Appendices

Abbreviations

3’	3-prime Phosphate
5’	5-prime Phosphate
µ	Micro
A	Ampere
ADAM	A Disintegrin and Metalloprotease
AI	Amelogenesis Imperfecta
AC	Arrythmogenic Cardiomyopathy
ARVC	Arrhythmogenic Right Ventricular Cardiomyopathy
AT	Annealing Temperature
ATP	Adenosine Triphosphate
bp	Base Pair
BSA	Bovine Serum Albumin
°C	Degrees Celsius
Ca2+	Calcium
cAMP	Cyclic Adenosine Monophosphate
cDNA	Coding DNA
cGMP	Cyclic Guanosine Monophosphate
CK1	Casein Kinase 1
Cx	Connexin
DAPI	4’,6-Diamidino-2-Phenylindole
dbSNP	Database of Single Nucleotide Polymorphisms
DEJ	Dermal-Epidermal Junction
dH2O	Distilled Water
ddH2O	Double Distilled Water
DES	Desmin
DMEM	Dulbecco’s Modified Eagle Medium
DMSO	Dimethyl Sulfoxide
DNA	Deoxyribonucleic Acid
dNTP	Deoxyribonucleotide Triphosphate
DP	Dermal Papilla
DSC	Desmocollin
DSG	Desmoglein
DSP	Desmoplakin
dsDNA	Double Stranded DNA
DUF	Domain of unknown function
ECM	Extra Cellular Matrix
EDTA	Ethylenediaminetetraacetic Acid
EGFR	Epidermal Growth Factor Receptor
ELISA	Enzyme-Linked Immunosorbent Assay
EM	Electron Microscopy
FAM83	Family with sequence similarity 83
FBS	Foetal Bovine Serum
g	Grams
GAPDH	Glyceraldehyde 3-Phosphate Dehydrogenase
h	Hour

HCl	Chlorhidric Acid
H&E	Haematoxilin and Eosin
HFH	Hereditary Footpad Hyperkeratosis
Hz	Hertz
ICC	Immunocytochemistry
IF	Intermediate Filament
ICD	Implantable Cardioverter Defibrillator
Ig	Immunoglobulin
IHC	Immunohistochemistry
InDel	Insertion/Deletion
IRS	Inner Root Sheath
iRHOM2/RHBDF2	Rhomboid Family Member 2
JAM	Junction Adhesion Molecule
JUP	Junction Plakoglobin Gene
Kb	Kilo Bases
KD	Knockdown
KDa	Kilo Daltons
KO	Knockout
KRT/K	Keratin
L	Litres
LB Broth	Luria Bertani Broth
LOF	Loss of Function
m	Mili
M	Molar
MAb	Monoclonal Antibody
Mg2+	Magnesium
min	Minute
MMP	Matrix Metallo-Proteases
mRNA	Messenger RNA
n	Nano
NaOH	Sodium Hidroxide
NGS	Next Generation Sequencing
NHK	Normal Human Keratinocytes
NMD	Nonsense mediated decay
NS	Normal Skin
NTP	Non-Targeting Pool
OA	Okadaic Acid
PAb	Polyclonal Antibody
PAGE	Polyacrylamide Gel Electrophoresis
PBS	Phosphate Buffer Saline
PC	Pachyonychia Congenita
PCR	Polymerase Chain Reaction
PFA	Paraformaldehyde
PG	Plakoglobin
pH	Power of Hydrogen
PKP	Plakophilin
PLA	Proximity ligation assay

PLEC	Plectin
PM	Plasma Membrane
PMP	Peripheral Myelin Protein
PPK	Palmoplantar Keratoderma
PSS	Peeling Skin Syndrome
PV	Pemphigus Vulgaris
RNA	Ribonucleic Acid
rpm	Rotations per minute
RT	Room Temperature
RT-PCR	Reverse Transcription PCR
s	Second
SCD	Sudden Cardiac Death
SDM	Site-Directed Mutagenesis
SDS	Sodium Dodecyl Sulphate
siRNA	Small Interfering RNA
shRNA	Small hairpin RNA
SNP	Single Nucleotide Polymorphism
SP	Serine Proteases
SPPK	Striate PPK
TBE	Tris Borate EDTA
TBS	TRIS Buffered Saline
TBS-T	TBS-Tween 20
TCF	Transcription Factor
TFC	Task Force Criteria
TGF	Tumour Growth Factor
TGM	Transglutaminase
TKI	Tyrosine Kinase Inhibitor
TM	Trans Membranous
TMEM	Transmembrane Protein
TOC	Tylosis with Oesophageal Cancer
TRIS	Tris (hydroxymethyl) aminomethane
U	Units
v	Volume
V	Volt
WB	Western Blotting

Acknowledgements

I was extremely fortunate to undertake this PhD in Professor David Kelsell's Lab. I would like to thank David for his patience and perseverance and tirelessly supportive mentorship. My co-supervisor Professor Edel O'Toole has always been an immense source of inspiration throughout both my clinical and academic career. I would like to thank the MRC for funding this PhD through a Clinical Research Training Fellowship (MR/K002740/1)

Many members of the Kelsell group offered their expertise, knowledge and guidance throughout this PhD particularly Dr Anissa Chikh, who supervised the iRHOM2 project and Dr Diana Blaydon. It was also a great pleasure to collaborate with Lisa McGinty, Benjamin Fell, Paul Delaney and Dr Anna Posafalvi.

I would like to thank our collaborators including, Prof Matthew Freeman (Oxford, UK), Dr Gopal Sapkota (Dundee, UK), Prof A Määttä (Durham, UK), Prof Bill McKenna, Prof Andy Tinker, Prof Pier Lambiase (Bart's Heart Centre, UK) and Dr Silvia Castelleti (Pavia, Italy)

I am deeply grateful to my family, Mum, my husband James, Oscar, Rafferty, Atticus and Ben, who have supported and encouraged me throughout the course of this PhD.

Finally, I would like to thank my father, for always believing that I could do more than I ever thought I could, I know you would be proud.

Chapter 1

Introduction

1.1 The Skin

The skin forms our first defense against the hostilities of the external environment, including pressure, water, light, heat, cold, trauma or infection. The skin is composed of several layers, each delineating a particular function. The epidermis comprises the most superficial of the skin and in humans, contains keratinocytes, melanocytes and Langerhans cells. The stratum corneum lies above the epidermis, with a typical basket-weave like pattern, and acts as a semi-permeable barrier to chemicals, infectious agents and prevents water and solute loss from within. Beneath the epidermis lies the dermis, which is highly vascularized and responsible for nutritional support of the epidermal layers. It is composed of a collagen and elastin-containing fibrous matrix. It also contains nerves and therefore mediates cutaneous sensation. Immune surveillance cells reside in the dermis, including Langerhans cells, dermal dendritic cells and leukocytes.

The skin is a highly dynamic structure, and its exact cell population adapts physiologically in response to particular cues such as wound healing. However, skin diseases can occur when the skin is unable to respond appropriately to exogenous challenges. For example, the skin is a highly immunologic organ and circulating immune cells recognize and defend against foreign pathogens. Failure to do so can result in infections such as cutaneous warts and fungal infections. In contrast, mis-direction of the immune system and recognition of "self" as foreign, results in auto-immunity, which, in the skin can manifest as a multitude of diseases including Pemphigus Vulgaris. Auto-antibodies in this disease are directed against the intercellular desmosome, which plays a role in cell-cell adhesion and therefore this disease is characterised by widespread blistering and erosions.

1.2 The Skin as a Marker of Internal Disease

The skin is a remarkable indicator of internal disease. In fact, skin "signs" can pre-date the onset of other more sinister diseases and allow for earlier diagnosis and screening. Several internal malignancies are associated with cutaneous features, which can precede a diagnosis of cancer. For example, the presence of acanthosis nigricans (hyperpigmented velvety thickening of the flexures) can be associated with breast, ovary, uterine or renal carcinomas. Another example is Tylosis with Oesophageal Cancer (TOC), which will be discussed in detail later in this thesis. Cutaneous features of this rare disease include thickened skin overlying

the palms and soles typically present in childhood, and oesophageal cancer in mid to later life.

The skin can therefore reflect underlying internal disease and in some instances, it may be the only visible clue. Inherited cardiocutaneous disease e.g. Naxos syndrome and Arrhythomogenic Right Ventricular Cardiomyopathy (ARVC), are characterised by the early presence of specific skin and hair changes which are linked to potentially fatal cardiac anomalies that present later in life. By identifying cutaneous clues to underlying disease, affected individuals can be diagnosed earlier and enter into appropriate surveillance progammes.

The Kelsell group recently identified the first example of a functional knockout of ADAM17 in humans, as the cause of a recessively inherited neonatal inflammatory skin and bowel syndrome. ADAM17, is a pivotal membrane bound sheddase, whose targets include TNFa and EGFR family ligands. These findings contribute to the increasingly expanding body of evidence that links the skin to internal diseases affecting the gut, joints, heart and central nervous system. In recent years there has been a shift in the way skin research is perceived. It is now widely acknowledged that the skin is a valuable “proof-of principle” organ, which is both convenient to monitor and sample with minimal intervention, and from which we can gain greater insights into complex multi-system diseases.

1.3 The Epidermis

The epidermis consists of four layers whose thickness varies according to site and situation. These layers stratify from the basal layer, the spinous layer, the granular layer to the stratum corneum which is shed during desquamation Keratinocytes make up 80% of the cells forming the epidermal layers, the remaining 20% is composed of other cells such as melanocytes, Langerhans cells, Merkel cells and lymphocytes (Houben et al., 2008).

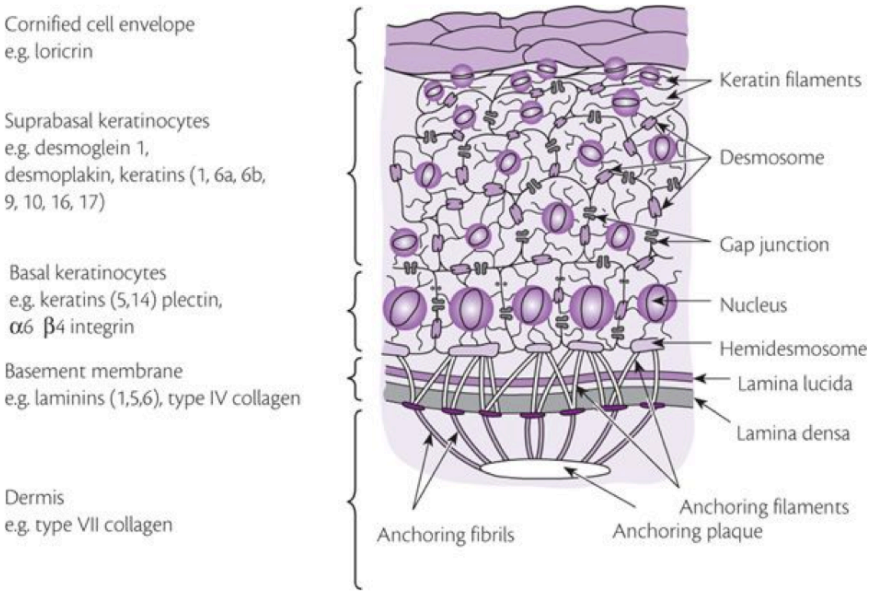

Figure 1.1 A schematic representation of the epidermis illustrating important structures and the site of expression of a number of skin-disease associated proteins (Adapted from Maruthappu & Kelsell, 2018)

Keratinocyte differentiation occurs in the basal layer and is a genetically-programmed carefully regulated process. The basal layer contains mitotically active keratinocytes whose columnar shape is determined by the expression of keratins (K5) and 14 (K14) (Figure 1.1). These keratins also bind hemidesmosomes, through linker proteins Plectin and BPAG1e which determine adhesion of the epidermis to the basement membrane. Melanocytes, another epidermal cell type, produce melanin, which is the pigment in these cells, and are responsible for skin pigmentation. Several studies have shown that the basal layer can exhibit three proliferative potentials, as stem cells, transit amplifying cells and post mitotic cells. Stem cells are capable of forming the entire pilo-sebaceous unit but also the interfollicular epidermis (Wolff et al., 2007). Stem cells will be discussed in greater detail in Chapter 5.

The spinous layer is so named owing to the shape the adopted by the composing keratinocytes, which alters as the cells differentiate into the granular layer. These keratinocytes retain K5 and K10 filaments produced in the basal layer, predominantly localised around the nucleus and tethered to desmosomes, but do not synthesize any new mRNA, instead they produce K1 and K10 specific to this epidermal layer. These keratins are specifically expressed in differentiated/keratinised cells and their downregulation together with the up-regulation of K6 and K16 are a hallmark of hyperproliferative disorders (Wolff et al., 2007). The granular layer is composed of basophilic keratohyalin granule-containing cells which give this layer its characteristic "granular" appearance. These granules contain profilaggrin, keratin filaments and loricrin. This layer is responsible for several characteristics of the epidermal barrier. Release of profilaggrin from the granules results in its calcium-dependent cleavage into filaggrin monomers which aggregate with keratin to form macrofilaments. Filaggrin is eventually degraded into UV protective molecules (Wolff et al., 2007). The final stage of epidermal differentiation in the skin ends with flattened cornified cells that form the stratum corneum. During this differentiation process, regulated apoptosis results in the destruction of the nucleus together with all intracellular components except the keratin filaments and filaggrin matrix.

The corneocytes play an essential role in the regulation of permeability, desquamation, antimicrobial peptide activity, toxin exclusion and selective chemical absorption, which are some of the most critical functions of the extracellular lipid matrix. They also provide mechanical reinforcement, hydration, cytokine-mediated inflammation and protection from UV damage. As such, corneocytes represent the first defence barriers of the human organism against external factors (Egberts et al., 2004, Houben et al., 2007, Fuchs, 1990, Fuchs, 2007).

1.4 The Palmoplantar Epidermis

The ridged skin of the palms and soles (palmoplantar sites) in mammals is uniquely adapted to withstand remarkable physical stress. The skin at this site differs from the skin elsewhere in several ways. Firstly, the stratum corneum is 8-10 times thicker than interfollicular skin (Figure 1.2), the stratum granulosum is absent, it lacks hair and has an increased number of nerve endings and sweat glands. Unlike interfollicular skin, irrespective of an individuals ethnicity, the palmoplantar skin lacks pigmentation (Swensson et al., 1998).

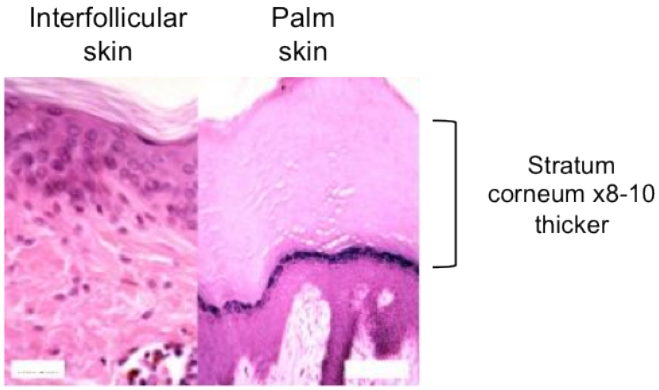

Figure 1.2 Haematoxylin and Eosin stained sections comparing interfollicular skin and palm skin showing markedly increased thickness of the stratum corneum in the palm.

The actual physical resilience of the palmoplantar epidermis is predominantly due to an abundance of cytoskeletal scaffolding proteins known as keratin intermediate filaments. Keratins constitute up to 85% of the protein content of differentiated epithelial cells and provide both flexibility and strength by forming a framework within the cytoplasm. The palmoplantar epidermis contains significantly greater keratin than the interfollicular skin (Swensson and Eady, 1996).

Several genetic skin disorders, known as the Palmoplantar Keratodermas “PPK’s” show a striking predilection for the palms and soles, and can present exclusively at these sites but may not show differences at birth (Swensson et al. 1998).

1.5 The Palmoplantar Keratodermas

The palmoplantar keratodermas (PPK) are a heterogeneous collection of skin disorders characterised by abnormal thickening of the skin of the volar surfaces of the hands and feet. They can be divided clinically into diffuse, focal and punctate types, histologically into epidermolytic and non-epidermolytic types and into hereditary and acquired types. Further subdivisions into simple (involvement of the palms and soles only), complex (involvement of non-volar skin including its appendages and, in certain cases, the buccal mucosa) and syndromic (associated with abnormalities in other bodily systems) are also made(Itin and Fistarol, 2005). Diffuse epidermolytic PPK (EPPK) (Figure 1.3) has been shown to be due to mutations in the gene encoding the palmoplantar specific keratin, KRT9 (Reis et al., 1994); whilst diffuse, non-epidermolytic PPK (NEPPK) has been associated with mutations in KRT1, KRT16 and, recently, the gene encoding the water channel protein, Aquaporin 5(Yang et al., 1994, Blaydon et al., 2013, Terrinoni et al., 2001). In focal PPK, the hyperkeratosis is less extensive and restricted to areas of weight bearing and/or friction (Table 1.1). Quite often the focal PPKs are complex and associated with abnormalities of the hair, nails, teeth and/or sweat glands. There are several types of focal PPK with abnormalities in other organs including hearing loss and cardiomyopathy due to defective gap junctions or desmosomes(Brooke et al., 2012), respectively. Using high throughput sequencing platforms, more genes underlying other forms of keratodermas are also being identified (Maruthappu et al., 2014).

Type of Diffuse PPK	Associated Disorder	Genetic Defect
EPPK (Epidermolytic palmoplantar keratoderma)		Keratin 9
NEPPK (non-epidermolytic PPK)	Umbilical hyperkeratosis	Keratin 1
NEPPK Diffuse Nagashima-type NEPPK		Aquaporin 5 Serpin B7
Syndromic NEPPK (Naxos Disease)	Woolly hair and cardiomyopathy	Plakoglobin Desmoplakin
Vohwinkel's Syndrome	Sensorineural Deafness Ichthyosis	Connexin 26 Loricrin
Erythrokeratoderma variabilis	Generalised erythroderma	Connexin 31
Clouston's syndrome	Alopecia, nail dystrophy sensorineural deafness	Connexin 30 Connexin 30.3
Ectodermal dysplasia skin fragility syndrome	Skin fragility, blistering, abnormal hair growth nail dystrophy and occasionally defective sweating	Plakophilin 1
Mal de Meleda	Hyperhidrosis an perioral erythema	*SLURP-1*
Olmsted syndrome	Perioroficial keratosis	*TRPV3*

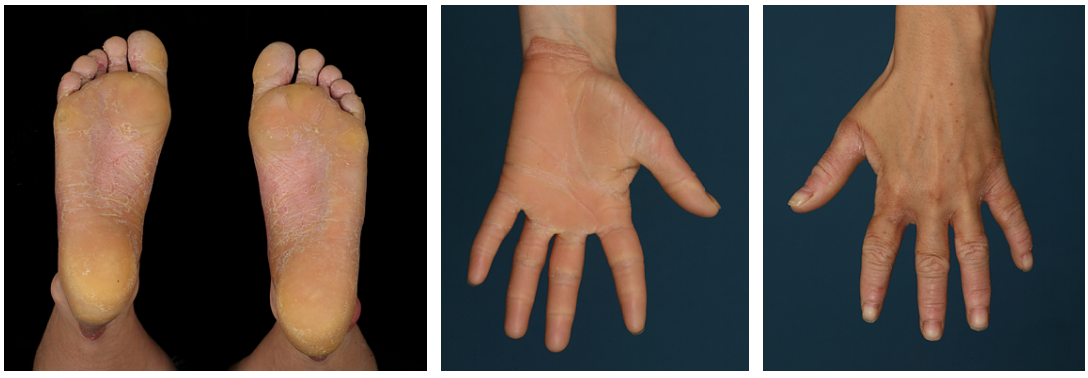

Figure 1.3 Genetics of diffuse palmoplantar keratoderma (adapted from Maruthappu & Kelsell, 2016). Clinical photographs of diffuse non epidermolytic PPK caused by mutations in *AQP5*, images courtesy of Prof E A O'Toole.

Table 1.1 Genetics of focal palmoplantar keratoderma (Adapted from Maruthappu & Kelsell, 2016).

Type of Focal PPK	Associated Disorder	Genetic Defect
Focal NEPPK	Follicular and orogenital hyperkeratosis	Keratin 16
Focal NEPPK (Tylosis)	Oesophageal Cancer, oral and follicular hyperkeratosis	i*RHOM2*
Pachyonychia Congenita	Nail dystrophy, oral lesions, epidermal cysts	Keratin 6A Keratin 6B Keratin 6C Keratin 16 Keratin 17
Striate PPK		Desmoglein 1 Desmoplakin Keratin 1
Papillon-Lefevre		Cathepsin C
Oculocutaneous tyrosinaemia	Photophobia, corneal ulceration, learning disabilities	Tyrosine aminotransferase
Epidermolysis Bullosa Simplex and Junctional EB	Generalised blistering	Keratin 5 Keratin 14 I*TGB4*
Punctate PPK Type 1A (Buschke-Fischer-Brauer Type)		*AAGAB*
Punctate PPK Type 1B		*COL14A1*

1.6 Tylosis with Oesophageal Cancer

Tylosis with oesophageal cancer (TOC; OMIM 148500) is a rare but highly penetrant disease in which affected individuals initially develop a focal non-epidermolytic palmoplantar keratoderma (thickening of the palms and soles, particularly prevalent in areas which undergo repeated trauma) (Figure 1.4A). In addition to oral leukokeratosis, follicular hyperkeratosis. The term "Tylosis" is derived from the Greek tulosis, making a callous, which describes the marked thickening that develops on the palmoplantar epidermis. Importantly, affected individuals carry a very high risk of developing squamous cell carcinoma of the oesophagus (95% by the age of 65 years)(Howel-Evans et al., 1958, Ellis et al., 2015). Although a comparatively rare condition, TOC has been reported to date in five extensive family pedigrees worldwide. It was first described in two large Liverpool families by Howel–Evans et al. (1958). The larger of the two families were reviewed in 1994 (Ellis et al., 1994). At that stage, 345 family members had been identified, 89 of whom had been diagnosed with Tylosis with 57 still alive. A total of 21 Tylotic members had died of oesophageal neoplasia and 11 had died of other causes. It has since been determined that the two Liverpool families are in fact distant kindreds, There is no known increase in the incidence of other common carcinomas in these patients. Similar but smaller pedigrees have been reported from Germany (Hennies et al., 1995), the United States (Stevens et al., 1996), Finland (Saarinen et al, 2012), Spain (Varela et al., 2011) and Brazil (De Souza et al., 2009). The frequency of the disorder in the general population is unknown, but is likely to be less than 1 in 1,000,000.

TOC is inherited as an autosomal dominant trait with complete penetrance. Our group identified three missense mutations in the *RHBDF2* gene, encoding the catalytically inactive rhomboid protein iRhom2 as the underlying cause of this disease in the UK, US and German families (Blaydon et al., 2012) (Figure 1.4B). The UK and US families share the same missense mutation – p.ille186Thr – however the mutation in the German family lies three amino acids away, p.Pro189Leu. In addition, a further missense mutation p.Asp188Asn, has been confirmed in the Finnish family (Saarinen et al., 2012). It is pertinent to note that all three reported mutations lie within three amino acids of one another in the highly conserved N Terminus domain (Figure 1.4C).

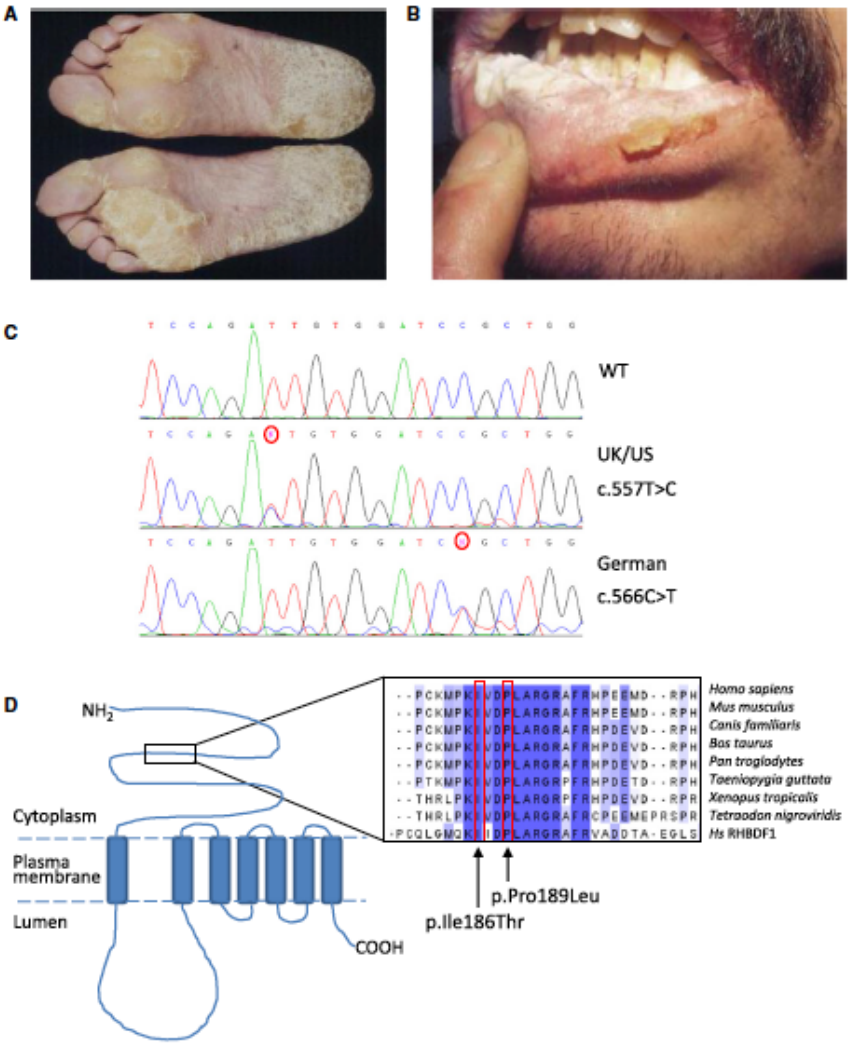

Figure 1.4(A) Focal keratoderma and oral leukokeratoses in patient with TOC. (B) Site of missense mutation in iRHOM2 in UK/US and German TOC kindreds. (C) Structure of iRHOM2 showing clustering of TOC-causing mutations and the high degree of conservation in the affected residues between multiple species.

This obvious clustering of mutations, along with the fact that each residue affected is highly conserved both between species and between iRhom2 and its close family member iRhom1 strongly suggests the mutations alter a site-specific function of iRhom2 to give rise to TOC. In addition to offering strong clues as to the pathogenesis of TOC, this discovery also represents the first linkage of any gene to inherited oesophageal cancer.

1.7 Rhomboid Proteins

Rhomboids are a protease family conserved across all kingdoms of life, whose catalytically active members function as intramembrane proteases, a class of enzyme whose active sites reside within a transmembrane domain, and which function to cleave their substrates within or immediately adjacent to the substrate's own transmembrane domain(s) (Freeman, 2016). The Rhomboid family of proteins were first described in *Drosophilia Melanogaster*, and were identified to play a role in EGFR signaling, by cleaving Spitz which is homologus to human TGFα (Urban et al., 2001). Rhomboids are a family of intramembrane serine proteases, whose active site is located within the lipid bilayer, enabling them to cut substrate transmembrane domains. They play a key role in the release of membrane tethered proteins as a mechanism of intercellular signaling(Freeman, 2004). Mammalian Rhomboids have been subdivided into 4 groups: Secretase A and B, PARL and iRhoms (Bergbold and Lemberg, 2013). The diverse members of this group are universally conserved and fulfill a range of activities such as Regulated Intramembrane Proteolyisis(RIP) and degradation. They are characterised by their structure, comprised of 6 or 7 transmembrane spanning domains in addition to a cytoplasmic N terminus and luminal C terminus (Etheridge et al., 2013).

1.8 Inactive Rhomboids iRHOM1 and iRHOM2

Although the inactive rhomboids iRhom1 and iRhom2 show topological similarity to active Rhomboids, they are proteolytically inactive and lack the necessary catalytic residues present in active rhomboid proteases. iRhoms were initially identified through gene alignment data with known rhomboid proteins. They are highly conserved and exist in all metazoans (Freeman, 2009). All iRhoms have a proline in the x-position of the GxSG catalytic motif, which is predicted to alter rhomboid folding such that proteolytic activity is lost. In accordance with this, all iRhoms tested have not been shown to cleave known rhomboid substrates. iRhom1 and 2 are 57% identical and 69% similar (Lemberg & Freeman 2007). iRhoms have two unique features which differentiate them from other rhomboid proteases (Zettl et al., 2011). The highly conserved N Terminus domain has a numerous potential phosphorylation sites, which could regulate its activity. In addition, both iRhom1 and iRhom2 have an extended cysteine rich loop spanning between the transmembrane domains 1 and 2. This highly conserved region is known as the iRhom homology domain (Zettl et al.,

2011). The high degree of conservation of these two regions suggests they confer an important functional significance. Gain of function mutations in iRhom2 arise as a consequence of missense mutations in its N Terminus and underlie TOC (Blaydon et al., 2012). In addition, iRhom2 has been reported to play a role in the genetics of epithelial ovarian cancers (Wojnarowicz et al., 2012).

In mice, iRhom1 and iRhom2 are expressed in most cell types. Both are highly expressed in the skin and iRhom2 is also significantly expressed in macrophages, although overall iRhom1 is expressed more highly than iRhom2 (Christova et al., 2013). To date, little is known about the function and substrate selectivity of iRhoms in mammals, despite intense investigation. The study of the molecular effects of Tylosis, caused by gain of function mutations in the N terminus region, may shed light on their activity and regulation.

1.9 iRHOMs and ADAM17 (TACE) Maturation/Processing

ADAM17, also known as TNFα converting enzyme (TACE), is a membrane bound metalloproteinase which sheds a diverse range of substrates including TNFα and EGFR family ligands (Gooz et al., 2011).

iRHOM2 has been shown to be a critical regulator of the maturation and processing of ADAM17 (McIlwain et al., 2012, Adrain et al., 2012). In mice, ER-located iRHOM2 binds ADAM17 and promotes its transfer to the golgi, where it undergoes furination, and is cleaved to become the active/mature form. This is subsequently trafficked to the cell surface membrane, where it is able to shed TNFα and its other substrates. In macrophages derived from iRhom2 KO mice, ADAM17 is unable to exit the ER and therefore does not undergo maturation and trafficking and TNFα shedding in response to LPS stimulation is abolished (Adrain et al., 2012). iRHOM2 KO mice appear phenotypically normal, however they do not release TNFα in response to lipopolysaccharide stimulation or bacterial infection as a consequence of reduced ADAM17 activity (McIlwain et al., 2012). There appears to be a degree of functional redundancy in cells other than macrophages between iRHOM1 and iRHOM2 in the trafficking and maturation of ADAM17 (Christova et al., 2013).

1.10 iRHOM2, ADAM17 and TOC

TOC is associated with gain-of-function mutations in the highly conserved cytoplasmic N-terminus of iRHOM2 (Blaydon et al, 2012; Saarinen et al, 2012). This has been shown to result in increased processing and maturation of ADAM17. In mammalian myeloid and epithelial cells, iRHOM2 promotes the maturation and trafficking of ADAM17 in the endoplasmic reticulum and Golgi (Adrain et al., 2012). Activated ADAM17 then transits to the plasma membrane where it is able to cleave its substrates including TNFα, IL6R and EGFR-family ligands (Brooke et al., 2014, Rose-John, 2013) (Figure 1.5A). In TOC-derived keratinocytes, *iRHOM2* mutation leads to high levels of constitutive ADAM17 activity with elevated ectodomain shedding of many of its substrates, which can be effectively inhibited by an ADAM17 sheddase inhibitor (Unpublished data, Matthew Brooke, Figure 1.5 B and C). Furthermore, PMA-stimulated peripheral blood mononuclear cells (PBMCs) from TOC patients also have increased TNFα release compared to control PBMC's (Brooke et al., 2014). In contrast, PBMCs/macrophages from *irhom2*$^{-/-}$ mice have impaired ADAM17 maturation and consequently, TNFα shedding from these cells is almost entirely abolished in response to bacterial stressors (Adrain et al., 2012, McIlwain et al., 2012).

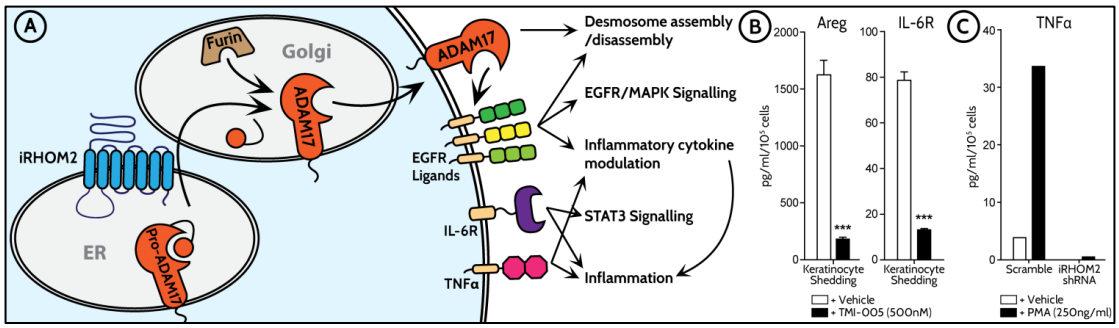

Figure 1.5 (A) Illustration depicts trafficking of ADAM17 by iRHOM2 from the ER to the Golgi where it undergoes maturation by furination and is then transported to the cell membranes where it cleaves a range of substrates such as EGFR ligands, IL6R and TNFα. (B) and (C) Graphs showing production of Amphiregulin (Areg), IL6R and TNFα measured by ELISA in TOC keratinocytes, significantly reduced by the ADAM17 sheddase inhibitor, TMI 005. (Figure courtesy of Matthew Brooke)

1.11 TOC: A Constitutive Wound Healing State

In vitro, TOC keratinocytes also show increased migration in monolayer scratch-wound assays when compared with control keratinocytes (Blaydon et al., 2012). In fact, TOC keratinocytes can close a scratch wound within 4 hours whereas control keratinocytes required 24 hours to close a wound of similar size. Like other squamous cancer cell lines, TOC keratinocytes are also hyperproliferative.

An additional rather unusual feature of the TOC epidermis is the presence of "immature desmosomes". Examination of the desmosomes in skin biopsies from patients with TOC was undertaken by electron microscopy (Brooke et al., 2014). Desmosomes in all layers of TOC epidermis lacked the electron-dense midline seen in mature desmosomes in normal epidermis which suggests that they are in the immature form typically seen in wound healing (Garrod et al 2005).

The presence of increased shedding of ADAM17 substrates implicated in wound healing TNFα, IL6 and IL8, the presence of immature desmosomes, hyperproliferation and increased migratory behaviour all suggest that TOC exhibits features of a constitutive "wound-healing" state (Brooke et al., 2014).

1.12 iRHOM2 Expression in Human Skin and Keratinocytes

In the skin, iRHOM2 typically shows a cell surface membrane and cytoplasmic distribution. This is in contrast to the distribution of iRhom1, whose expression is predominantly basal and cytoplasmic. This is reproducible in cells, when overexpressed with GFP-tagged WT-iRHOM2. In keratinocytes, iRHOM2 is localized to the cytoplasm and cell membrane, however this is not observed in cells derived from non-epithelial sites where it is predominantly located in the ER and cytoplasm (PhD Thesis, Sarah Etheridge 2015). This may suggest a unique role for iRHOM2 in keratinocytes and in the skin. iRHOM2 has previously been shown to be highly expressed in murine macrophages (McIlwain et al 2012, Adrain et al 2012). In the human epidermis, iRHOM2 is also observed brightly in spindle-shaped cells infiltrating the dermis. These cells have been shown to be macrophages by colocalisation studies with the macrophage marker CD68 (PhD Thesis, Sarah Etheridge). This suggests a

dual role for iRHOM2 in the skin – both in the keratinocytes themselves but also in the infiltrating immune cells.

1.13 Keratins and the skin

Keratin intermediate filaments are a large, diverse group of epithelial proteins, which play a key role in the epidermal architecture. Keratin expression is tightly regulated and dependent on epithelial type and stage in differentiation. Much is now known about the expression characteristics of keratins in different cell types as a result of naturally occurring mutations in human diseases or experimental knockout experiments in transgenic mice. These have provided a wealth of information about their likely functions (Moll et al., 1982).

Keratins are composed of a common a-helical rod domain of approximately 310 amino acids flanked by non-helical head (N Terminus) and tail regions (C Terminus) (Figure 1.6). The 4 helical regions are denoted Coil 1A, Coil 1B, Coil 2A and Coil 2B and are combined by "linker" segments (Steinert et al., 1994).

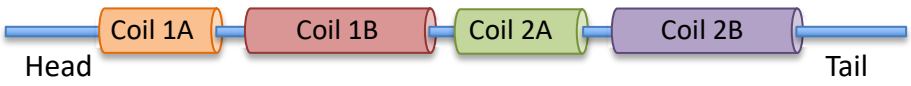

Figure 1.6 Structure of the Keratin filament. Keratins are composed of the non-helical N-terminal head, C-terminal tail and 4 helical rod domains.

Keratins are typically expressed in a pairwise fashion forming heteropolymers composed of one Type I keratin (acidic, K9-20) paired with its specific Type II partner (basic, K1-8) for example K6/K16 and K1/K10. Specific pairs initiate heterodimerisation through their coil-coil domains, forming 10nm filaments which self-assemble to form the keratin filament network (Yamada et al., 2002). Type 1 and 2 pairs are specific, for example, K1 & K10, K5 and 14, K6 and K16 are well described pairings and the expression of Type I and Type II keratins usually occurs as a ratio of 1:1 in all cells (Moll et al., 1982).

Simple epithelia of the liver intestine and pancreas characteristically express K7, K8, K18, K18 and K20. In the the interfollicular epidermis, K5 and K14 are expressed basally, and K1/K10 are confined to the suprabasal layers (Moll et al., 1982, Fuchs and Green, 1980) (Table 1.2).

Keratin	Epithelial Tissue	Partner
Type 1-Simple		
K18	Simple epithelia(liver pancreas, colon, lung	K8, K7
K20	Simple epithelia, gastrointestinal	K8 (K7)
Type 1- Barrier		
K9	Stratified cornifying epithelia; palm and sole	K1
K10	Stratified cornifying; suprabasal	K1
K12	Stratified epithelia; cornea	K3
K13	Stratified epithelia; non cornifying suprabasal	K4
K14	Stratified epithelia; basal	K5
K15	Stratified epithelial hair follicle stem cell	K5
K16	Stratified epithelia; palmoplantar and stress induced	K6a/b
K17	Stratified epithelia; palmoplantar and stress induced	K6b
K19	Simple and stratified epithelia	K8
K23,34	Epithelia	
Type 1 - Structural		
K25-K40	Stratified epithelia, hair follicle sheath and hair fibre	
Type II - Simple		
K7, K8	Simple epithelia	
Type II - Barrier		K18
K1	Stratified cornifying epithelia; suprabasal	K10
K2	Stratified cornifying epithelia; late suprabasal	(K10)
K3	Stratified epithelia, cornea	K12
K4	Stratified epithelia;non-cornifying; suprabasal	K13
K5	Stratified and complex epithelia; basal cells	K14 (K15)
K6a	Stratified epithelia; palmoplantar and stress induced	K16
K6b	Stratified epithelia; palmoplantar and stress induced	K17
K6c	Stratified epithelia	
K76	Stratified cornifying epithelia, oral, suprabasal	(K10)
K78, K79, K80	Epithelia	
Type II -Structural		
K71-86	Stratified epithelia, hair follicle, hair sheath and hair fibre	

Table 1.2 Expression patterns of Type I and II Keratins in human epithelia.

Live cell imaging studies have shown that, rather than being static structures, keratins are highly dynamic and transit between phases of assembly and disassembly (Windoffer et al., 2011, Kolsch et al., 2010, Leube et al., 2011). The "keratin cycle" describes the process by which keratins "turn over" within the cell. It is initiated by "nucleation" of the keratin filaments at the cell periphery proximal to focal adhesions. Elongation of new keratin units then occurs, guided by the actin cytoskeleton, towards the peripheral keratin network. Keratins then move towards the nucleus where they bundle. The cycle is continued when keratin pairs disassemble into oligomers that diffuse into the cytosol (Figure 1.7)(Windoffer et al., 2011), available for the next round of nucleation. This process of filament turnover and rearrangement is important in permitting changes in cell size and shape required for migration and proliferation (Haines and Lane, 2012).

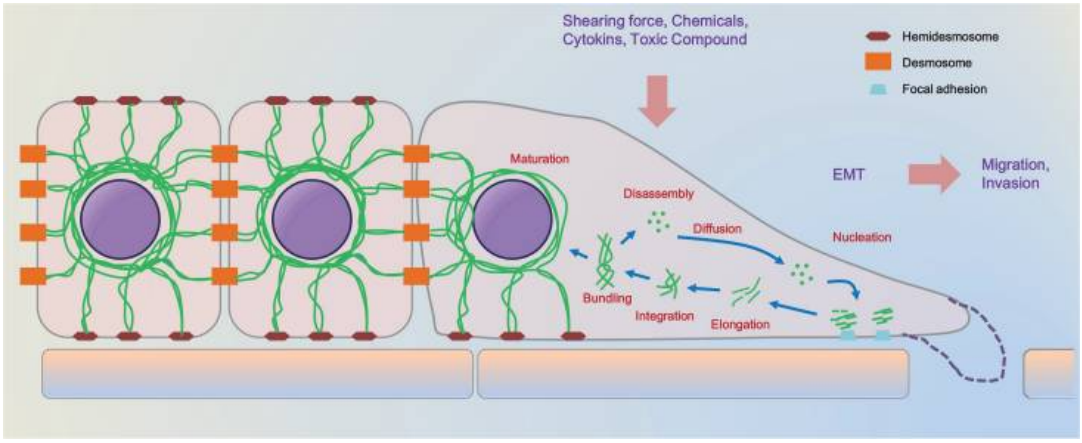

Figure 1.7 Keratin filament cycling: soluble keratins assemble at the cell periphery and polymerise, resulting in elongation. Elongated keratins move towards the nucleus guided by actin, resulting in bundling of keratins around the nucleus. Subsequent disassembly redistributes keratin oligomers to the cytoplasmic pool where they are available for a further cycle of filament formation (Schematic diagram adapted from Kim et al., 2015).

The keratin cytoskeleton is anchored at various sites on the cell membrane, creating a branch-like network that offers mechanical support. Desmoplakin, a major component of the desmosomal adhesion complex, binds Type II keratins by direct interaction between its carboxy terminal and the amino terminal of the type II keratin (Green et al., 2010, Kouklis et al., 1994). Keratins also bind hemidesmosomes, the major junction complexes adhering epithelial cells to the basal layer. Keratins link plectin and BPAG1e at hemidesmosome cell-matrix adhesions. This step required for correct assembly of hemisdesmosomes (Green et al.,2010).

1.14 Keratins in the palmoplantar epidermis

Over 50 Keratin isotypes are expressed in stratified and pseudostratified epithelia however, their precise expression pattern is both site and situation specific. Unlike inter-follicular skin, the ridged skin of the palms and soles is characterized by the constitutive expression of Keratins 6, 16, 17 and uniquely, Keratin 9 (K9) (Swensson et al, 1998). The expression of specific keratins at this site is indicative of regional adaptions of this epidermis to a high cell turnover rate. Of all the epidermal tissues in the body, the palmoplantar epidermis is exposed to the most extreme physical stress, bearing an individuals entire bodyweight millions of times during their lifetime. To withstand this stress, the particular combination of keratins expressed here provides a combination of resilience and flexibility. Early studies considered K16 to be primarily associated with hyperproliferation however, owing to its expression in wound healing and constitutive expression in non-keratinized barrier epithelia such as the oral mucosa and oesophagus it has become clear that its actual function may be to provide flexibility (Swensson et al 1998), (Leigh et al., 1995)(McGowan et al. 1998).

Keratin 9 expression is confined to the suprabasal layers of the palmoplantar epidermis. Mutations in the gene encoding K9 are known to cause epidermolytic palmoplantar keratoderma, a rare dominant-negative skin disorder(Reis et al., 1994). Transgenic mice lacking K9 develop hyperkeratotic calluses and compensatory upregulation of K6 and K16(Fu et al., 2014). K16 knock-out mice also develop a severe inflammatory palmoplantar keratoderma associated with pain and reduced mobility (Lessard and Coulombe, 2012). The two mice studies point to critical roles for K9 and K16 in the proper formation and function of the footpad epidermis.

1.15 Keratins and Disease

Keratinopathies comprise a diverse group of over 60 different diseases which have been linked to inherited keratin changes (www.interfil.org). Although rare, these diseases have provided insight into the functions of specific keratins (Haines and Lane, 2012).

1.15.1 Keratin 1/10

Keratins 1 and 10 are expressed in suprabasal differentiated cells of the epidermis. Loss-of-function mutations in KRT1 or KRT10 underlie Epidermolytic Ichthyosis/bullous congenital ichthyosiform erythroderma (BCIE) (McLean et al., 1999). BCIE is characterized by erythroderma, hyperkeratosis and blistering of the upper layers of the skin. However, it is important to recognize that there is a significant degree of heterogeneity between individuals carrying mutations in KRT1. Palmoplantar keratoderma and generalized malodor are also common features. (Stevens and Rustin, 1994).

1.15.2 Keratin 5/14

The best studied of the keratinopathies is Epidermolyis Bullosa Simplex (EBS), which is a rare, usually autosomal dominant disorder which results from mutations in Keratin 5 or 14(Chen et al., 1995, Stephens et al., 1995). The mutations can occur in the rod domain and can rarely be caused by homozygous recessive K14 knockout. The loss-of-function mutations causing EBS result in dramatically reduced mechanical resilience. Clinically this manifests as widespread severe blistering from birth, which can be fatal, although most patients do present with localised forms. From the study of EBS, it has been ascertained that the primary function of K5 and K14 is to provide mechanical resilience in response to trauma of the epidermis (D'Alessandro et al., 2002, Haines and Lane, 2012, Ishida-Yamamoto et al., 1991).

1.15.3 Keratin 6, 16 and 17

These three keratins are expressed in the skin of the palms and soles as well as the oral mucosa. They are also expressed in sebaceous gland tissue and pathologically in response to

wounding or injury. Hence, together they are known as the "wound healing keratins" (McGowan and Coulombe, 1998) .

Pachyonychia Congenita (PC) is a group of autosomal dominantly inherited genodermatoses caused by mutations in either K6A, K6B, K6C, K16 and K17 (Smith et al., 2005, Terrinoni et al., 2001). The mutations cluster in the Coil 1A or Coil 2B domains of the keratin filament. This disorder is characterised by painful palmoplanter keratoderma, abnormalities of the nails (hyperkeratosis), thickened white plaques affecting the oral mucosa (leukokeratosis) and peri-follicular hyperkeratosis. The exact molecular mechanisms underlying PC remain to be elucidated, it is thought there is a dominant negative effect of the mutant keratin, resulting in disruption of the remaining wild-type intermediate filament network. In support of this, Krt16-null mice develop oral lesions soon after birth and later, a painful palmoplanter keratoderma (Lessard & Coulombe 2012). Attempts have been made to subdivide PC on its genetic basis (PC1 - K6 and K16, PC2 – K17) and develop gentotype-phentotype correlation, however characterization of over 80 PC patients show variability over the clinical features(Wilson et al., 2011).

In addition to inherited keratinopathies, altered keratin expression profiles can be characteristic of specific disease states. An example of this is psoriasis, an inflammatory skin disease in which affected individuals develop widespread red, scaly plaques. Histologically, the psoriatic plaque is characterised by increased expression of Keratin 16 and 17 (Leigh et al., 1995).

1.15.4 Keratins and Cancer

Keratin expression patterns are so specific that when abnormally present, the can be indicative of neoplasia, as such they are widely considered to be tumour biomarkers. Furthermore, they have both a diagnostic and prognostic significance(Karantza, 2011). For example, breast adenocarcinomas constitutively express K7, K8, K18 and K19, and in poorly differentiated breast adenocarcinomas, they can also express K5/6, K14 and K17 (Sorlie et al 2001). Squamous cell carcinomas, independent of their site of origin express K5,14, K6, K16 and K17. In poorly differentiated SCC, K8, K18 and K19 are also observed – usually, their expression is restricted to the liver (Moll et al., 1982, Moll, 1998). Given this role for keratins in cancer, the possibility that the keratins are playing a more direct role in the pathogenesis

of tumour development has arisen. In support of this, there is a growing body of literature highlighting the role of keratins in a variety of cell regulatory processes such as size, shape, proliferation and inflammation. Moreover, studies have shown that keratins could contribute to cancer cell invasion and metastasis. Keratin filament re-organisation into a peri-nuclear ring-like structure, which can occur upon phosphorylation of specific residues, alters the keratin network architecture and "softens" the cytoplasm, which in turn facilitates migration and invasion (Beil et al.,2003, Suresh et al., 2005).

1.15.5 Keratins and Wound Healing

The keratin filament cytoskeleton is highly dynamic and flexible to allow cells to proliferate during growth and migrate during wound healing. This dynamicity is the key to re-organisation and bundling of the keratin filament network in response to shear stress. The expression of Keratins 6, 16 and 17 are all rapidly upregulated in wounded keratinocytes within 2-3 hours of injury (Paladini et al., 1996) at the expense of K1 and K10. This response is exhibited by many complex epithelia and is conserved from amphibians to mammals (McGowan and Coulombe 1998). Wound edge keratinocytes have characteristic features, these "activated" keratinocytes show altered cell adhesion, juxtanuclear reorganization of keratin intermediate filament network and generation of cytoplasmic processes in the direction of cell migration (lamellopodia) (Kolsch et al., 2010, Leube et al., 2011).

1.16 Cell-Cell Connectivity

Cell-cell adhesion is a critical mechanism for maintaining epithelial integrity. It also plays an essential role in regulating communication between cells. Robust cell-cell adhesion in epithelia is maintained by four intercellular junctions, each with unique but complementary functions. The importance of these structures is highlighted by the plethora of human disorders arising from their defect.

1.16.1 Gap Junctions

Gap junctions are aggregates of intercellular channels that permit direct cell-cell transfer of ions (Ca^{2+}, Mg^{2+}) and other small molecules (<1kDa such as cAMP, cGMP and ATP) by diffusion as well as electrical communication of varying conductance. They are evolutionarily conserved and were first identified as ion pathways in conductive cells such as nerves and muscles (Goodenough et al., 1996). They are expressed in virtually all human tissues. Gap junctions are comprised of connexins, which assemble into hexamers to form connexons. The interlocked proteins form channels which cluster into polymorphic plaques containing thousands of individual units. The connexin family of proteins contain over 21 members, named according to their molecular mass (Wei et al., 2004). Their expression pattern is tightly regulated throughout tissue types, each conferring a specific function due to varied permeability to particular molecules and ions (Goldberg et al., 2004). Greater understanding of the role of Gap junctions has come from disorders arising from mutations in specific Gap junction proteins. Mutations in *GJB2* (encoding Cx26) were identified as the primary cause of autosomal recessive non-syndromic hearing loss (Kelsell et al., 1997, Kelsell et al., 2001). As CX26 is the most abundant connexin in the cochlea, its diminished function has a profound effect on hearing. In the skin, *GJB3* mutations have been found to cause autosomal dominantly inherited erythrokeratodermia variabilis (EKV, OMIM 133200) (Wilgoss et al., 1999). Furthermore, mutations in *GJB2* (Cx26) have been linked to congenital hearing loss and PPK (Heathcote et al., 2000).

1.16.2 Adherens Junctions

Adherens junctions mediate adhesion and cell recognition. They are present in epithelia as well as cardiac myocytes and fibroblasts. The major component of adherens junctions are cadherins, which are structurally formed of repeating extracellular cadherin domains and a cytoplasmic region that binds p120 catenin and B-catenin at opposing ends (Oda and Teichi, 2011). Multiple cadherins are expressed in a context specific manner. For example, in the skin E-cadherin is primarily expressed, whereas in the heart and neuronal tissue, this is substituted for N-cadherin.

1.16.3 Tight Junctions

Tight junctions occur at the apical and basolateral domains of epithelia and their main function is to prevent the paracellular passage of fluids, electrolytes and macromolecules (Bonazzi and Cossart, 2011). They are composed of 4 main proteins, occludins, claudins, junction adhesion molecules (JAM) and the coxsackievirus and adenovirus receptor proteins (CAR). Occludins and Claudins have four transmembrane domains and form homodimers via their extracellular loops. JAMs and CARS have only one transmembrane domain and extracellular IgG-like domain that mediates adhesion. These transmembrane components bind to intracellular components which then links them to the actin cytoskeleton. Due to their apical location, tight junctions are frequently targeted by pathogenic organisms to facilitate their invasion into the epidermis.

1.16.4 Desmosomes

Desmosomes are beautifully complex structures located in close proximity to Adherens junctions and are more widely distributed along the lateral membranes. They are named from the Greek words “desmos” meaning bond and “soma” meaning body. They function to tether the intermediate filament cytoskeleton to the plasma membrane, permitting the formation of a flexible structural network within the cell (Green et al., 2000). They are highly adhesive and play a key role in determining the mechanical resistance of the cell and thus are highly expressed at sites which require resistance to high mechanical stress such as the epidermis and cardiac muscle. In cardiac tissue, they additionally provide electromechanical

coupling (Yin and Green 2004). Ultrastructurally, desmosomes appear as multi-layered symmetrical structures, containing a pair of opposing electron-dense plaques between which lies an extracellular region of approximately 35nm width. Between the plaques is central dense midline which is comprised of desmosomal cadherin ectodomains (Desai et al., 2009) Figure 1.8.

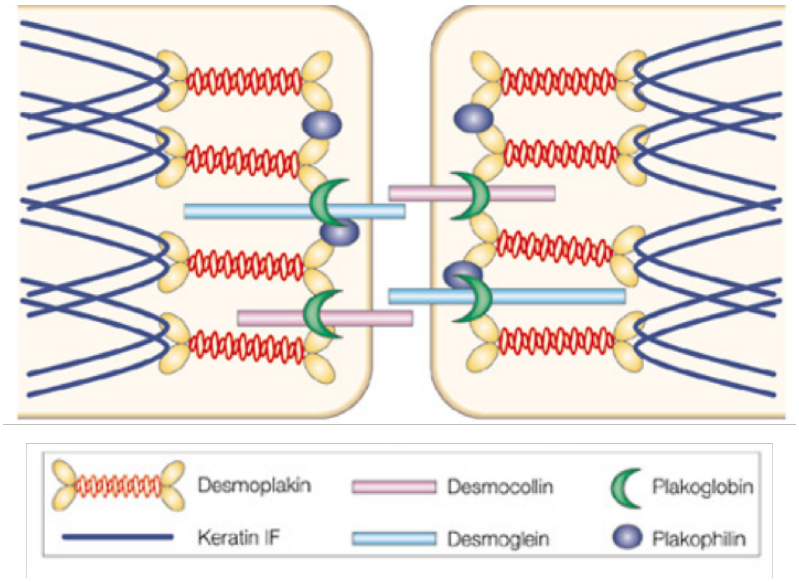

Figure 1.8 Structure of the Desmosomes. Desmosomes are multicomponent structures composed of five key desmosomal proteins and interact with Keratin intermediate filaments to form a flexible structural network within the cell (Schematic diagram adapted from Green & Gaudry 2000).

In addition to the intermediate filaments, desmosomes also interact with microtubules via association of DSP with the microtubule binding protein end-bindin 1 (EB1) (Patel et al., 2014). Through this interaction, it can regulate microtubule organization and dynamics at sites of cell-cell contact. Moreover, desmoplakin-EB1 interactions also influence the localisation and function of gap junction proteins including Connexin 43 (Cx43). Therefore, Desmosomal defects can have a "knock-on" effect on other junctions.

Desmosomal cadherins are similar to the classic cadherins found in adherens junctions. They are subdivided into desmogleins 1-4 and desmocollins 1-3. The genes encoding these proteins are located on Chromosome 18 in both humans and mice (Frank et al., 2001). They are variably expressed in epithelia, for example Dsg1 and Dsc1 are restricted to stratified epithelia. Dsg 4 is predominantly expressed in differentiated layers of the epidermis and hair follicles. The structure of Dsg and Dsc is fairly similar to classical cadherins. They contain a

series of highly conserved extracellular repeat(EC) domains followed by a short transmembrane domain(TM). Desmosomal cadherins are known to bind to other components of the desmosomes such as Plakoglobin and Plakophilins (Green et al., 2000).

The desmosomal armadillo family members include Plakoglobin (Pg) and Plakophilin 1-3 (PKPs 1-3). Like B Catenin, they can also translocate to the nucleus and in fact, the Pkp1b isoform is exclusively nuclear. The primary role of Pg is to link intermediate filaments to the desmosomal plaque. It does so by binding the intracellular domain of desmosomal cadherins and interacting with the N-terminus of the IF-binding protein Desmoplakin. As well as its structural role, Pg can have further signalling properties through its indirect influence on B-catenin signalling (Simcha et al., 1998).

Desmoplakin

The third major component of the desmosome are the plakin family of proteins. Desmoplakin is one of the most well described desmosomal proteins and the most abundant component of the desmosome. It is abundantly expressed in the heart, skin and hair follicle. It has a "dumbbell" shaped structure that is divided into three domains, N Terminus, Rod domain and C Terminus. The N-terminal domain primarily binds to armadillo proteins and to Dsc1a and targets DP to the desmosomal plaque. The central rod domain mediates oligomerisation and the C-terminal domain couples intermediate filaments to the desmosomal plaque by direct interaction with Type I keratin intermediate filaments. Its amino terminus binds directly to plakoglobin and the plakophilins, thereby linking intermediate filaments to the desmosomal plaque. The intermediate filament in question can differ from tissue to tissue. In the skin, it is the keratins that are anchored to desmosomes, whereas in the heart it is desmin, and in other tissues it is vimentin (Desai et al., 2009).

DSP I and II

In humans, the *DSP* mRNA transcript is alternatively spliced to yield two isoforms; Desmoplakin I and Desmoplakin II. DSP II is the shorter form, lacking two thirds of the rod domain. In stratified epithelia, the two isoforms are expressed at nearly equivalent levels however DSPI is the predominant isoform in the heart (Angst et al., 1990, Uzumcu et al., 2006). In 2012, Cabral et al. (Cabral et al.,2012) demonstrated in an elegant series of

experiements using two mutations in DSP that lead to different dosages of the two major DSP splice variants, that DSPII appears to be a key component in intermediate filament stability and desmosome mediated adhesion. Therefore, the two isoforms do not appear to be functionally redundant. They also proposed that changes in the ratio between DSPI and DSPII could influence normal desmosomal function.

1.16.5 Electromechanical coupling in the Heart: The intercalate Disc

The heart is composed of billions of individual cardiomyocytes, which are able to function as a highly co-ordinated structure. Electromechanical coupling between cardiomyocytes occurs at the "intercalate disc", a structure highly concentrated in adhesive and conductive components such as desmosomes, gap junctions and voltage gated channels. The epidermal equivalent to the intercalate disc is the intercellular membrane. Desmosomes of the intercalate disc provide structural integrity by interconnecting actin filaments and desmin filaments (the equivalent of Keratin) of adjacent cells (Patel et al., 2014).

Cardiac connexins include Cx43, Cx40 and Cx 45 (Kanter et al. 1993). Their expression pattern within the heart is complex, but as a general rule, Cx43 is predominantly expressed in the left ventricle. Mouse models with selective ablation of Cx43 have shown that 80% reduction is required to produce a 50% loss of electrical conductance (Gutstein et al.,2001).

In the epidermis, desmoplakin can alter the localisation of Cx43 through its interaction with the microtubule binding protein EB1, providing a mechanism for how desmosomes can regulate Gap junctions (Patel et al., 2014). In the heart, there is also evidence that desmosomal proteins can regulate both Gap junctions and Voltage gated sodium channels. For example, knock-down of PKP-1 results in reduced conduction through Na^+ channels (Cerrone et al., 2012). In ARVC, dominantly inherited mutations in desmosomal proteins such as PKP2, DSP, JUP and DSG2 result in decreased plakoglobin and Cx43 at the intercalate disc (Paul et al., 2013). This is occurs despite the presence of normal cellular levels of these proteins, suggesting impaired trafficking as the underlying pathological mechanism.

1.16.6 Desmosomes in the Heart versus Skin

The proteins which make up the desmosomes in the heart differ to those present in the epidermis, reflecting their function. In cardiomyocytes, DSP, PG, DSC2, DSG2 and PKP2 are the key desmosomal components (Patel et al., 2014) (Figure 1.9).

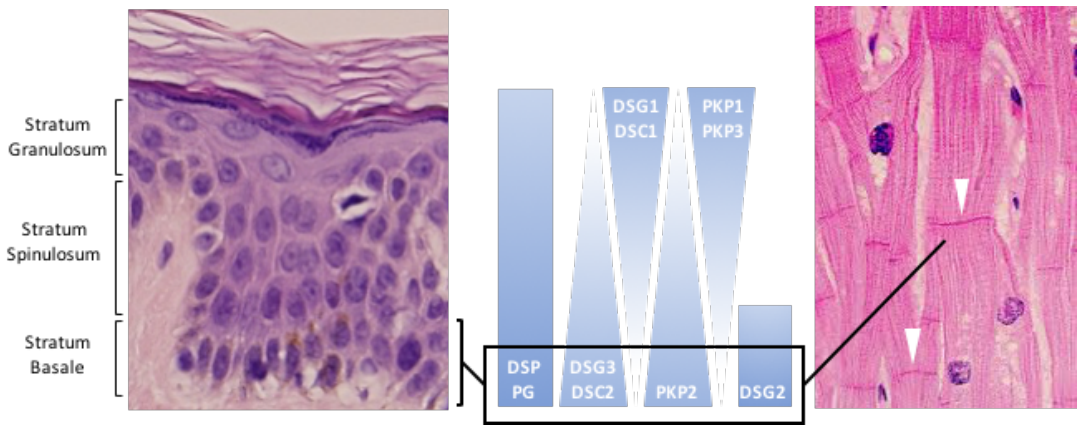

Figure 1.9 Desmosomes in the skin (left) and at the intercalate disc in cardiomyocytes (white arrowhead) express different desmosomal proteins. The desmosomal proteins found in the basal layers of the skin are also found at the intercalate disc. However DSG1, DSC1 PKP1 and PKP3 are only present in the skin.

In the skin, several more desmosomal proteins are expressed depending on the site within the epidermis. The composition of the desmosome varies from basal layers to stratum corneum, presumably reflecting the different functional properties of the desmosome at each site. DSG2 expression is usually restricted to the proliferative basal layer, becoming upregulated in epidermal carcinomas (Brennan & Mahoney 2009). PG, PKP1 and DP expression increases in the suprabasal layers and subsequently DSG1, DSC4 and DSC1 in the granular layers. (Mahoney et al., 2006). The tight regulation of these desmosomal components is thought to reflect their role in driving epidermal morphogenesis, particularly in controlling differentiation.

With regards to the function of individual components, DSG2 and DSC2 function as the key extracellular linkers in the heart. Whereas in the skin, this is performed by DSG1, DSG3, DSG4, DSC1 or DSC3. PKP2 is the sole Plakophilin in the heart, in contrast to the additional presence of PKP1 and PKP3 in the skin. Reflecting their tissue specific expression pattern, human genetic diseases showing skin/ectodermal abnormalities in the absence of cardiac

involvement have been linked to mutations in DSG1, DSG3 and PKP1 (Rickman et al., 1999, Klijuic et al., 2003, McGrath et al., 1997). In contrast, mutations in DSG2, DSC2, DSP, PG, PKP2 (Pilichou et al., 2006, Syrris et al., 2006, Rampazzo et al., 2002, Asimaki et al., 2007) have been linked to cardiac disease without cutaneous manifestations. Further examples of desmosomes in human disease are described below.

1.16.7 Desmosomal Diseases

Much of our understanding into the function of desmosomal proteins have come from diseases arising from their dysfunction. Desmsomal diseases include autoimmune blistering disorders, infectious diseases in addition to an array of cardiocutaneous disorders.

Autoimmune Disorders

As desmosomes primarily function to maintain intercellular adhesion, it is unsurprising that defects in desmosomal proteins are associated with epidermal blistering disorders. Pemphigus vulgaris is an autoimmune blistering disorder caused by autoantibodies targeting DSG1 and DSG3 (Shimizu et al., 1995). It typically presents with superficial blisters and/or erosions frequently affecting the mucous membranes. Histologically, lesional skin demonstrates suprabasal epidermal acantholysis (loss of cohesion between keratinocytes), clefting and blister formation. Patients presenting with limited oral involvement tend to have autoantibodies (IgG) targeting DSG3, whereas involvement of both the skin and mucosa is linked to autoantibodies to both DSG1 and DSG3 (Amagai et al 1991, Ding et al., 1997). The phenotypic differences reflect the expression pattern of these desmosomal cadherins between the skin and mucosal tissues (Shirkata et al., 1998) (Figure 1.10).

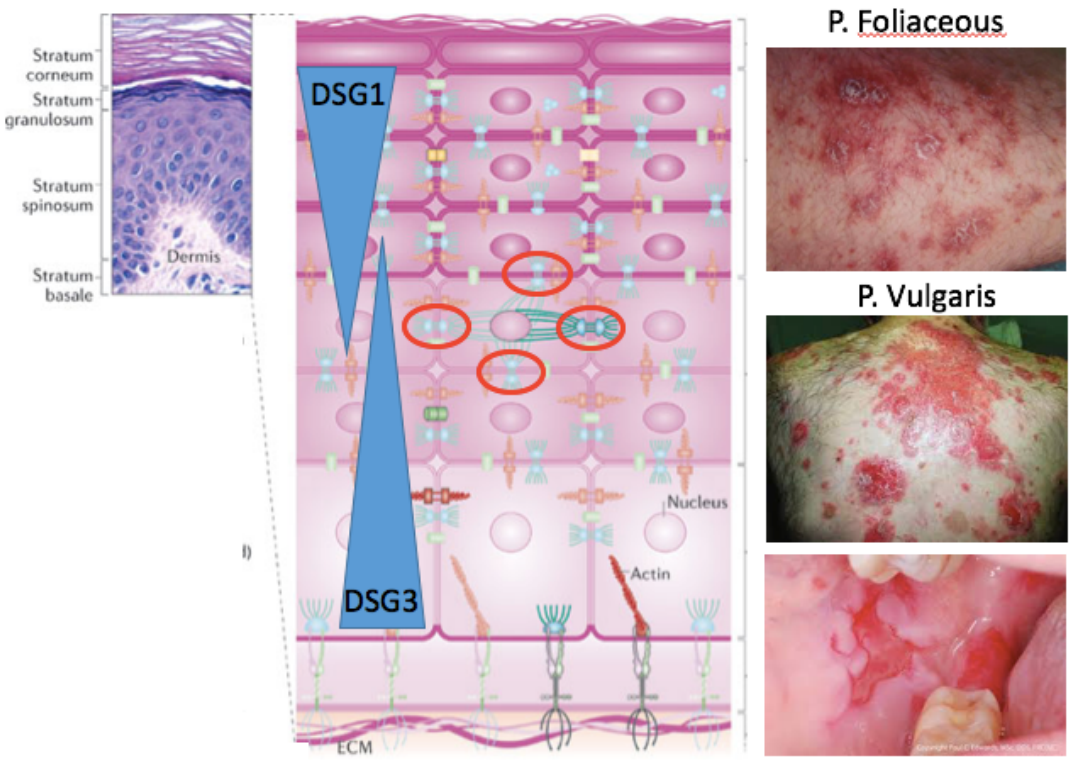

Figure 1.10 Differential expression of DSG1 and DSG3 underlie the phenotypic features of Pemphigus Foliaceous and Pemphigus Vulgaris. Autoantibodies to DSG3 underlie PV, contributing to the development of oral ulceration where this protein is also expressed (Schematic diagram adapted from Simpson et al., 2011).

Pemphigus Foliaceous is a relatively benign form of pemphigus characterised by scaly crusted erosions on an erythematous base. Mucosal involvement is frequently absent. It is caused by autoantibodies to desmoglein 1 which results in very superficial loss of intercellular adhesion as DSG1 is primarily expressed in the granular of the epidermis. However, DSG1 expression in mucosal tissues is very low, explaining the lack of oral involvement in these patients. As PV can be associated with autoantibodies to both DSG1 and DSG3 it is associated with much more severe epidermal and mucosal blistering which can be fatal.

A useful sign when attempting to diagnose PV or PF is the presence of “Nikolsky’s sign”. Gentle rubbing of unaffected skin results in blistering or erosion formation. This clinical sign neatly demonstrates the importance of functional desmosomes in maintaining epithelial integrity in response to mechanical stress.

Infectious Diseases

Some strains of pathogenic Staphylococcus aureus are able to produce exfoliative toxins (ET) targeting the desmosomal cadherin DSG1 (Amagai et al 2000, Amagai et al 2002). Clinically, this can result in either Bullous impetigo or its generalised form, Staphylococcal Scalded Skin Syndrome. Typically, both diseases are characterised by superficial blistering and histologically, there is evidence of keratinocyte acantholysis. The exfoliative toxin is a unique serine protease that shows "lock and key" specificity for DS1 and not DSG3 hence resulting in superficial blistering.

1.16.8 Inherited Cardio-Cutaneous Disease.

Several cardiocutaneous syndromes have been reported to date, often their first presentation may be to dermatologists, in whom early recognition could expedite the diagnosis of more sinister underlying cardiac pathology. The link between the skin and heart is somewhat unsurprising considering their shared embryological derivation from the neural crest, the bilaterally paired strips of cells arising from the ectoderm at the margins of the neural tube. Furthermore, the skin and heart require similar mechanoresilient properties, both being subjected to phenomenal repeated stress and shearing forces. One key property of both tissues is their ability to respond to stress with both flexibility and strength. Desmosomes play an important role in providing these characteristics, as highlighted by the cardiac and cutaneous manifestations of diseases resulting from mutations in desmosomal genes.

Arrhythmogenic Right Ventricular Cardiomyopathy

Arrythmogenic Right Ventricular Cardiomyopathy (ARVC) or Arrythmogenic Cardiomyopathy (AC) is an inherited disorder of the heart muscle with a prevalence of at least 1 in 1000. As there is a high propensity for cardiac arrhythmias in affected individuals, it is the leading cause of cardiac death in individuals <35 years old and contributes to 10% of deaths from undiagnosed cardiac disease in the <65 age group (Sen-Chowdhry et al., 2005). As such, the foremost clinical challenge in ARVC is making an accurate and timely diagnosis. This is complicated by the lack of overt symptoms, vast phenotypic heterogeneity and variability of cardiac findings. At present, diagnosis can be attempted on the basis of comprehensive non-invasive evaluation and fulfilment of clinical criteria outlined by the International ARVC Task

Force (Marcus et al., 2010). ARVC demonstrates a clear familial preponderance, and evaluation of first and second-degree relatives of probands estimates that over 50% of cases are inherited, most frequently as an autosomal dominant trait (Corrado et al., 2017, Sen-Chowdhry et al., 2007) . The genetic basis of ARVC is however complex, in the majority of cases the cause is a mutation in one of the components of the desmosome, as these form the major electromechanical adhesion complex between cardiomyocytes. Mutations have been reported to occur in five desmosomal genes; Plakoglobin (PG), Desmoplakin (DSP) Plakophilin 2 (PKP2), Desmoglein 2 (DSG2) and Desmocollin 2 (DSC2). In 30% of cases, the genetic cause remains unknown (Sen-Chowdhry et al., 2007, Brooke et al., 2012). The 100K genomes project has recruited patients with ARVC but as yet novel genes have not been identified.

Histologically, ARVC may show interstitial fibrosis with fatty replacement. The presence of interstitial fibrosis is a reactive process and occurs in the absence of myocyte necrosis, but in response to triggers such as inflammation and ischaemia. The presence of fatty replacement in the myocardium is an unusual feature, reasonably restricted to ACM. One controversy in the field is nomenclature of the disease, although originally known as ARVC, the involvement of the right heart can be variable and non-classical, predominantly left sided variants have not infrequently been described. Moreover, dual chamber involvement is also relatively common.

Naxos Disease

Naxos disease is a triad of ARVC, woolly hair and diffuse keratoderma which develops at sites of pressure on the palms and soles (Figure 1.11). The disease was first identified on the Greek Island of Naxos, where, despite the autosomal recessive mode of inheritance, the prevalence of the disease exceeds 1 in 1000 (Protonotarios et al., 1986). The initial presenting signs are the cutaneous features which facilitates the recognition of affected individuals in early childhood. Cardiac pathology develops later in life, typically during adolescence but can be as late as the fourth decade. Typically, affected individuals develop palpitations and syncope. The classical ECG findings include QRS prolongation, epsilon waves and inverted T waves in the right precordial leads (V1-3). Ventricular tachycardial/fibrilliation is the commonest cause of morbidity and mortality in these patients, arising from the right ventricle. Later, as the disease progresses the left ventricle can become involved. The annual incidence of sudden cardiac disease is approximately 3% (Delmar and McKenna, 2010).

The causal mutation for Naxos disease is a homozygous two base pair deletion in the gene encoding plakoglobin (JUP 2157del2), which result in premature termination of translation and was first discovered by McKoy et al. (McKoy et al., 2000). Gene sequences were determined by reverse transcriptase PCR from mRNA isolated from skin sample from an affected patient. This was further corroborated in two further independent studies (Protonotarios and Tsatsopoulou 2004, Delmar and McKenna, 2010). In a minority of heterozygotic carriers of *JUP-2157del2* show mild clinical disease expression, such as woolly hair (5/40) and minor cardiac abnormalities (8/40) however none fulfilled the diagnostic criteria of ARVC. (Protonotarios et al., 2004)

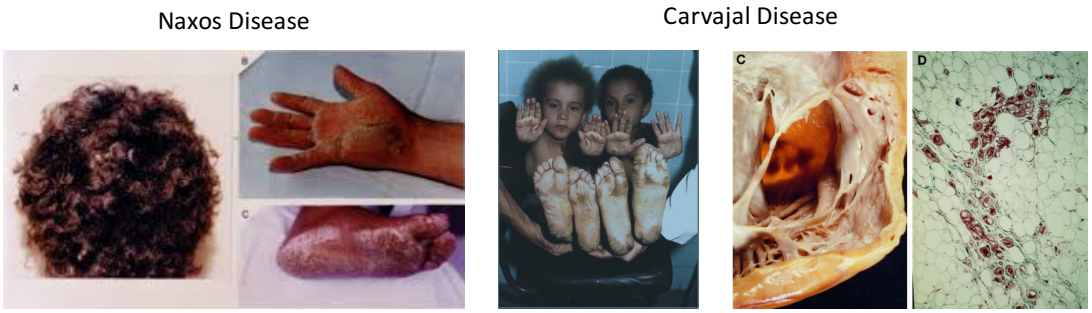

Figure 1.11. Clinical phenotypic features of Naxos Disease and Carvajal Disease. Both diseases can present with a triad of curly hair, palmoplantar keratoderma and cardiomyopathy. Typically, marked fibrofatty replacement is seen within the cardiac ventricles post-mortem, although this is less prominent in Naxos disease.

Carvajal Disease

Recessively inherited homozygous deletion mutations in the last exon in *DSP* were first described in cardiocutaenous syndromes in patients from India and Ecuador (by Dr Luis Carvajal-Huerta). Norgett et al. (Norgett et al.,2000) Using a combination of Autozygosity mapping, denaturing high performance liquid chromatography and sequence analysis, they identified the causative mutation as a homozygous deletion in DSP (7901delG). This results in a premature stop codon and a truncated protein product lacking the C terminus domain of the tail region. Like Naxos disease, Carvajal syndrome is consists of a palmoplantar keratoderma, woolly hair and left dominant arrythomogenic cardiomyopathy (Figure 1.11). However, the PPK differs in Carvajal disease in that it is striate rather than diffuse. Clinically,

the cardiac phenotype is complicated by frequent and complex ventricular arrhythmia and precordial T-wave inversion (V1-3). Post-mortem findings include biventricular cavity enlargement, more severe on the left than the right, focal aneurysms in both ventricles, myocyte loss and replacement fibrosis in the subepicardial layer. Adipose replacement is a less prominent component of the disease.

Alcalai et al., described a large consanguineous family with recessive ARVC caused by a homozygous missense mutation in *DSP* G2375R. Eight family members died suddenly before the age of 35 years, all of whom had woolly hair, xerotic skin from infancy and the presence of skin fragility – vesicular lesions over the peripheries, knees, palms and soles from childhood (Alcalai et al., 2003).

Dominantly Inherited ARVC

DSP

The first gene implicated in the more common, dominantly inherited form of ARVC was Desmoplakin. Using linkage analysis and direct sequencing, the mutation was found to be a missense mutation (S299R) in exon 7 of DSP in an Italian ARVC family, the site of the mutation suppresses a potential phosphorylation site in the N-terminal domain of the protein, necessary for its interaction with plakoglobin. Clinically, the patients developed classical features of ARVC with predominantly right sided precordial T-wave inversion and arrhythmia originating from the right ventricle, presenting clinically as ventricular fibrillation in several family members and in some instances sudden cardiac death (Rampazzo et al., 2002).

PKP2

This armadillo protein is likely to account for the highest proportion of ARVC cases. In large scale ARVC studies from the US and Germany, heterozygous variants in *PKP2* were found to account for 43% and 27% of cases respectively, and up to 70% of familial cases in The Netherlands. The latter was found to result from a founder effect in the Dutch population. The phenotype in this cohort of patients tends to be classical right sided involvement. Skin and hair abnormalities linked to PKP mutations have never been reported. It is likely to be because in the skin, PKP2 is localised to the nucleus rather than the desmosomal plaque, where it is substituted by PKP1 (Syrris et al., 2006).

JUP

Dominantly inherited heterozygous mutations in the gene encoding PG, *JUP* have also been found to cause ARVC. First in a German family, where the mutation (118_119insGCA), results in the insertion of a serine residue at amino acid position 39, which lies within the N-terminal domain of the protein product. The patient was reported to have classical right ventricular disease without skin or hair involvement (Asimaki et al., 2007).

DSG2

The fourth desmosomal protein to be implicated in ARVC is DSG2. Using a candidate gene approach, Pillchou et al. (Pilichou et al., 2006) identified 9 heterozygous mutations in DSG2 (5 missense, 2 insertion-deletions, 1 nonsense and 1 splice site) in 8 of 54 probands. In a further cohort, Syrris et al., (Syrris et al., 2007), described prominent left ventricular involvement in 25% of *DSG2* cases. It has been estimated that mutations in desmosomal cadherins DSG2 and DSC2 account for approximately 10% of cases of ARVC (Sen-Chowdhury et al., 2007)

1.17 Background to the Aims and Hypotheses

It is fascinating to consider that inherited mutations in a multitude of genes can lead to abnormalities of the palmoplantar skin. These mutations affect a remarkable array of genes including structural proteins (e.g. Keratins), adhesion proteins (e.g. desmosomal components) and channel proteins (e.g. connexins) (Maruthappu & Kelsell, 2018). Although involvement of these particular proteins could be predicted to result in PPK's, the discovery of many other responsible genes has been surprising.

Examples include mutations in *TRPV3*, which underlie Olmsted Syndrome (Lin et al., 2012) which presents with PPK and periorifical keratotic plaques. TRPV3 protein belongs to a family of non-selective cation channels, responsible primarily for thermoregulation, and is expressed not only in the skin but also in the brain (Xu et al., 2002). The discovery of this mutation provided novel insight into the role of TRPV3, particularly in the skin.

Many genetic mutations attributed to PPK's present not only with skin disease but also systemic involvement, with the PPK frequently being the only cutaneous manifestation of the disease despite the protein being expressed at other skin sites. For example, mutations in *GJB2* encoding Connexin 26 (Cx26) were found to underlie PPK and congenital deafness

(Kelsell et al., 1997). This discovery led to the finding that Cx26 is expressed at high levels in human cochlear cells as well as the skin. Interestingly, despite high levels of Cx46 in multiple other organ sites including the colon, prostate and breast in humans. (www.proteinatlas.org), deafness and PPK appear to be the only overt manifestations of the mutation.

What these and other discoveries demonstrate, is that the palmoplantar epidermis is an exquisitely sensitive barometer of pathological inherited mutations. As the palmoplantar epidermis is both visible and highly accessible, the PPK's provide a rich resource for genotype-phenotype correlation and their study forms the basis of this Thesis.

1.18 Aims and Hypotheses of this Study

The overarching theme of this Thesis is to investigate the diverse genetic and functional basis of PPK's and their links to human disease. The aims can broadly be subdivided into three components.

1. Identification of Novel Binding partners for iRHOM2 to help elucidate its primary functions in TOC and normal skin, very little is known about the function of iRHOM2 in human skin but it is clearly expressed at the cell surface membrane and individuals with TOC have a clear skin phenotype
2. Exploration of cutaneous phenotypes in ARVC – discovery of novel mechanisms and links to cardiac disease
3. Novel gene discovery in PPKs.

To Investigate these hypotheses, the following approaches were used:

1.

   i) A yeast 2 hybrid screen was employed to identify novel interacting binding partners for iRHOM2.

   ii) In vitro modelling using shRNA *iRHOM2*

   ii) In vivo modelling using *iRHOM2-KO* mice

2.

i) Deep cutaneous and cardiac phenotyping of dominantly inherited *DSP* mutation carriers with ARVC

ii) Molecular characterisation by immunohistochemical staining of patients' skin biopsies

iii) Extraction of cDNA and mRNA from patient skin biopsies to explore the mechanistic basis for the phenotype.

3.

i) Identification of the first human disease-causing mutation in *FAM83G* as a cause of PPK and exuberant hair using a combination of exome and Sanger sequencing.

ii) Using confocal hair analysis and immunohistochemistry of skin biopsies from affected patients, a possible mechanism for the cutaneous phenotype was identified.

Chapter 2

Materials & Methods

2.1 Antibodies

Antibody	Reference code	WB Dilution	ICC/IHC Dilution
RHBDF2 (Rabbit)	HPA018080 (Sigma)	1:500	1:50
RHBDF1 (Rabbit)	Ab81342 (Abcam)	X	1:100
Cytokeratin 16 (Mouse)	LL0025 (Cancer Research UK)	1:500	1:50
Cytokeratin 16 (Rabbit)	Ab76416 (Abcam)	1:500	1:50
Cytokeratin 16 (Rabbit)	Ab182791 (Abcam)	1:500	1:100
Cytokeratin 6 (Mouse)	Ab18586 (Abcam)	X	1:100
Cytokeratin 9 (Rabbit)	gift of D Leslie-Pedrioni (University of Dundee, UK)	X	1:250
Ki-67 (Rabbit)	Ab15580 (Abcam)	X	1:100
Anti-HA (Rat)	3F10 (Roche)	1:500	X
ADAM17 (Rabbit)	Ab2051 (Abcam)	1:500	X
Vinculin (Mouse)	Ab18058 (Abcam)	1:80000	X
GAPDH (Rabbit)	Ab8245 (Abcam)	1:2000	X
DSP (Mouse)	11-5F (kind gift from Kathy Green)	1:1000	1:50
JUP (Mouse)	0BT0651(Abd Serotec)	1:100	1:10
Connexin 43 (Mouse)	Mab3067 (Millipore)	1:2000	1:200
FAM83G (Mouse)	Ab121750 (abcam)	1:1000	1:100
Filaggrin (Rabbit)	Ab81468 (Abcam)	X	1:100
Loricrin (Rabbit)	Ab85679 (Abcam)	X	1:100
Cytokeratin 10 (Rabbit)	Ab9026, (Abcam)	X	1:100
Active B Catenin (Mouse)	Merck Millipore 05-655 Clone 8E7	1:1000	1:100
B Catenin	BD Transduction labs	1:1000	1:100
Anti-GFP (Mouse)	Ab290 (Abcam)	1:500	1:200

2.2 Statistical Analysis

Statistical analyses were carried out using the two-tailed paired Student's t-test $*P \leq 0.05$, $**P \leq 0.01$, $***P \leq 0.001$

2.3 Yeast two-hybrid Analysis

Yeast two-hybrid screening was performed by Hybrigenics Services, S.A.S., Paris, France (http://www.hybrigenics-services.com).

The coding sequence for human iRHOM2 N-terminus (aa. 1-403; GenBank accession number gi:306035188) was PCR-amplified and cloned into pB29 as an N-terminal
fusion to LexA (N-iRHOM2-LexA-C). The construct was checked by sequencing the entire insert and used as a bait to screen a random-primed Human Reconstituted Skin cDNA library constructed into pP6. pB29 and pP6 derive from the original pBTM116 (Vojtek and Hollenberg, 1995; Béranger et al., 1997) and pGADGH (Bartel et al., 1993) plasmids, respectively.

112 million clones (13-fold the complexity of the library) were screened using a mating approach with YHGX13 (mata) yeast strains as previously described (Fromont-Racine et al., 1997). 28 His+ colonies were selected on a medium lacking tryptophan, leucine and histidine. The prey fragments of the positive clones were amplified by PCR and sequenced at their 5' and 3' junctions. The resulting sequences were used to identify the corresponding interacting proteins in the GenBank database (NCBI) using a fully automated procedure. A confidence score was attributed, firstly taking into consideration the redundancy and independency of the prey fragments and reading frames and stop codons in overlapping fragments. Secondly, taking into account the interactions found in all the screens performed at Hybrigenics, using the same library. The scores have been shown to positively correlate with the biological significance of the interaction (Rain et al., 2001; Wojcik et al., 2002).

2.4 Cell Culture

Control (CTRL) and TOC keratinocyte cell lines (previously described in Blaydon et al., 2012) were cultured in Dulbecco's Modified Eagle's Medium (DMEM, Sigma) supplemented with 1% Penicillin/Streptomycin, 10% Foetal Calf Serum, 1% L-glutamine, 1% RM+ supplement (containing EGF) and cultured in a humidified incubator at 10% CO2, 37C. HaCaT cells were cultured in DMEM supplemented with 10% Foetal Calf Serum, 1% L-glutamine and 1% Penicillin/Streptomycin and cultured in a humidified incubator at 10% CO2, 37°C.

After gaining appropriate consent, a skin biopsy from an affected male with PPK was used to produce the PPK K16-R127C cell line. Primary keratinocytes were isolated and grown in the presence of a γ-irradiated 3T3 feeder layer. Cells were immortalized with HPV16 (E6/E7) as described previously (Rheinwald et al., 1975) All experiments were carried out on cells that had been passaged between 10 and 40 times post-immortalization. Cells were cultured in the same conditions described above.

2.5 Western Blotting

Protein preparation from cell lysates:

Cells were grown to confluence on 10cm plates and lysed on ice. The cells were washed twice with ice-cold PBS and 1ml of lysis buffer (Appendix A) added containing a protease inhibitor cocktail (Roche, UK). Cells were left on ice to lyse for 10 minutes. A cell scraper was used to remove cells vigorously from the plate and they were transferred to an eppendorf tube. The lysate were pre-cleared to remove debris by spinning at 13,000G for 10 minutes at 4°C, the supernatant was then removed for protein assay, using the Bradford method (Bio-Rad). Following protein assay, lysate inputs could be calculated for western blotting, for example 20ug of protein per lane, and denaturing 5x Laemelli buffer (0.1 M Tris-HCL (pH6.8), 4% SDS, 20% Glycerol, 0.001% Bromophenol Blue, 1.44 M Beta-mercaptoethanol) added to enable protein epitope availability for probing antibodies. Lysates were either used immediately or stored at -80°C.

SDS-PAGE Electrophoresis

SDS-PAGE Electrophoresis was carried out using equipment from Biorad (Hemel Hempsted, UK). All equipment was cleaned with hot water and 70% ethanol before use. SDS-polyacrylamide gels were prepared with an appropriate polyacrylamide percentage for the protein being detected with higher percentage gels used for lower molecular weights. iRhom2 is around 100KDa and the Keratins are approximately 50KDa in size, so a 10 % gel was used. The resolving gel was first made up, which separates the proteins in the lysates by size. Every 10ml of 10% gel comprised: 2.7 ml double distilled H2O (ddH2O), 2.5 ml 30% polyacrylamide mix (Protogel), 2.5 ml Tris (1.5 M, pH8.8), 0.1 ml SDS (10%), 0.1 ml Ammonium Persulphate (APS, 10%) and 6 µl *N,N,N-Tetramethylethylenediamine* (TEMED). APS and TEMED act as setting agents in the gel. Isopropanol was then added to level the top of the gel and remove air bubbles. The gel was then left to set for around 20 minutes.
Once the resolving gel was set, the isopropanol was removed and the top of the gel washed with ddH2O. The stacking gel was prepared next, which allows loading of the samples. The stacking gel has a lower resistance than the resolving gel, allowing the proteins to 'line up' at the same point before entering the resolving gel. Each 5ml stacking gel contained: 3.4 ml ddH2O; 0.8 ml 30% polyacrylamide mix; 0.63 ml Tris (1 M, pH6.8), 0.05 ml SDS (10%), 0.05ml APS (10%) and 5 µl TEMED. The gel was poured around the combs that form the loading wells at the top of the gel avoiding the formation of air bubbles and left to set for approximately half an hour.

Once the gels had set, they were fitted into the tank and the combs removed. Running buffer (0.3% Tris, 1.44% Glycine, 0.1% SDS in ddH2O) was poured in between the gels and outside the gel but without it touching to prevent a short circuit. The wells of the gel were rinsed to remove any gel debris or unpolymerised gel using a 1ml pipette and running buffer. Protein lysates were heated to 95°C or 5 minutes and then cooled on ice and spun at 13,000rpm for 5 minutes in a bench top centrifuge before loading into the gels. Rainbow ladder (GE Healthcare) was also included in at least one well per gel to allow identification of protein size. The gel was then run for approximately 1 1⁄2 hours at 100V per gel until the dye front from the bromophenol blue in the loading buffer reached the bottom of the gel. The protein has a negative charge (from the SDS in the loading buffer), causing the protein to migrate from negative charge towards positive charge when the electrical current is run through the tank.

Transfer

Transfer of the proteins from the gel onto a nitrocellulose membrane was then carried out. Blotting paper, sponge pads and a piece of nitrocellulose membrane were soaked in transfer buffer (0.3% Tris, 1.44% Glycine, 20% methanol in ddH2O). A cassette was then used to sandwich a sponge pad, two pieces of blotting paper, the gel, the nitrocellulose membrane, two pieces of blotting paper and another sponge pad taking care to avoid air bubbles. Again, the negatively charged protein migrates from negative charge towards positive charge when the electrical current is run through the tank. The gel was therefore placed towards the negative side of the tank and the membrane at the positive side. Once the sandwich was made, the cassette was placed in the tank with transfer buffer and an ice pack to prevent overheating. A current of 350 mA for 2 1⁄2 hours transfer.

Blocking

Once the transfer was complete, the nitrocellulose membranes were blocked in 5% skimmed milk in TBS-Tween (0.1%), which per litre comprises: 2.423 g Trizma HCl, 8.006 g NaCl and 1ml Tween20 in ddH2O. The pH is adjusted to pH7.6 in the 10X stock solution

Antibody Incubation and development.

Primary antibodies were optimized with either 5% skimmed milk, 5% BSA or TBS-Tween depending on the efficacy of the antibody and manufacturers instructions. The membrane was incubated overnight at 4C and then washed 3 times for 5-10 minutes each in TBS-T before addition of a secondary antibody. The secondary antibodies used were either Goat anti-Rabbit or Goat anti-mouse (horse-radish peroxidase conjugated) (Dako Ely Cambridgeshire UK) at a dilution of 1:5000. Membranes were incubated in secondary antibody for 1 hour at room temperature. This was followed by 3 x 5-10 minute washes in TBS-T and visualized using ECL and developed in a dark room using x-ray film and an automated developing system.

Cells were washed in PBS and then lysed using lysis buffer (1M Tris, 2.5M NaCl, 10% Glycerol, 0.5M Glycerophosphate, 1% Tween-20, 0.5% Nonidet P40, 1×EDTA-free Complete Protease

Inhibitor tablet (Roche) for 15 minutes on ice. Extracts were separated on SDS 12% polyacrylamide gels and transferred to a nitrocellulose transfer membrane. The blots were incubated with specific antibodies and developed according to the manufacturer's instructions (ECL Immobilon, Millipore)

2.6 Immunostaining and Image Processing

Cells plated on cover slips or 5µm tissue sections were fixed with either 4% paraformaldehyde (PFA) in PBS for 10 minutes at room temperature, or in ice cold Methanol-Acetone (50:50 mixture) at -20°C for 10 minutes depending on the optimal method for detection of the primary antibodies. The following steps were all carried out at room temperature. Cells were permeabilised with 0.1% Triton X-100 for 10 minutes if PFA fixation was used, then blocked with 5% Goat Serum for 1 hour. Cells or tissue sections were incubated with primary antibody diluted in 5% goat serum overnight at 4°C.

The following day, fixed cells or tissue sections were washed in 3 x 5 minutes in PBS, then incubated with the appropriate Alexa Fluor (Life Technologies) fluorescent secondary antibody for one hour at room temperature. The secondary antibody was diluted 1:800 in 5% goat serum. Cells or tissue sections were washed twice 3 x 5 minutes in PBS, then incubated in DAPI nuclear stain (1:10,000), then washed twice for 10 minutes each and finally mounted onto slides and imaged using the Zeiss 710 confocal microscope (Carl Zeiss).

The quantification of perinuclear localization of K16 filaments was based on the method previously described by Feng & Coloumbe (Feng & Coulombe., 2015). CTRL and TOC cells were quantified in ImageJ by drawing a line from the nuclear envelope across the plasma membrane using the freehand tool and plotting the K16-associated fluorescence signal along this line. K16 filament arrangements were classified as 'perinuclear' when all of the positive filament signals (>50% relative signal intensity, normalized to the maximum fluorescence of the specific cell) were found within 3um from the nuclear membrane. Images were selected randomly and blindly subjected to this quantification. For the final bar graph depicting the percentage of perinuclear cells, 90 images for each of CTRL and TOC from three independent experiments each were quantified. Statistical analysis was performed using the unpaired students t-test.

2.7 Generation of 3D Human Skin Equivalents

Human dermal fibroblasts were embedded in 4 mg/ml collagen 1 matrices at a concentration of 250,000 cells/ml to produce dermal equivalents. After culturing these dermal equivalents for 24H, keratinocytes were seeded on top (30,000 cells/cm^2) and kept in submerged culture for a further 24H. Afterwards, the human skin equivalents were lifted to the air-liquid interface and cultured until day 14 with alternate daily media change, before being PFA-fixed and paraffin-embedded for processing.

2.8 Transfection of Cell Lines with Overexpression DNA constructs

RHBDF2 constructs were prepared by subcloning wildtype RHBDF2 cDNA from Origene clone #SC122961 (Origene) into vector pEGFP-N3. Mutant RHBDF2 constructs were prepared using the QuikChange II site-directed mutagenesis kit (Agilent).

N-terminus RHBDF2 construct was prepared by cloning wildtype RHBDF2- N-terminal domain into vector pEGFP-N3. The plasmid was prepared using In-Fusion HD Cloning kit (Clontech Laboratories, Takara). N-terminus RHBDF2 constructs were a generous gift from Prof M. Freeman (Oxford, UK)

HaCaT cells were grown on coverslips and plated at a density of $2x10^5$ cells per well of a 6 well plate. Transfection was carried out after 24 hours using. Fugene 6 (Roche). The cell-culture medium was changed the next day. Cells were fixed and immunostained 48 hours following transfection.

2.9 Co-Immunoprecipitation

Cells were grown to confluence in 10 cm plates. Plates were washed twice on ice in ice-cold PBS and then lysis buffer was added with a protease inhibitor cocktail (Roche). Lysates collected after 10 minutes and pre-cleared by centrifugation at 13,000 G for 10 minutes at 4°C. The supernatant was removed from the debris pellet and transferred to a clean tube. Protein concentration was calculated using the Bradford Protein Assay system (Bio-Rad). 50µl Dynabeads (Thermo) were prepared according to manufacturers instructions. Antibodies (2-4g) were bound to the beads by incubation at room temperature with rotation for 30 minutes. Species matched IgG (Rabbit IgG sc-2027, Mouse IgG sc-2025, Santa Cruz) were bound to beads as a control. 2mg of protein lysate was added to beads and incubated overnight at 4°C with rotation. The following day beads were washed three times for 5 minutes on ice in 700µl NP-40 wash buffer (50mM Tris pH 8.0, 150mM NaCl, 1mM EDTA, 1% NP40) containing protease and phosphatase inhibitors (Roche) followed by separation on a magnet. Beads were separated from antibody-protein complexes by boiling for 5 minutes in 2x Laemelli buffer and the eluate separated by a magnet loaded onto a gel for SDS-PAGE electrophoresis. The lysate was run alongside as an input for the IP.

2.10 Flexcell Mechanical Stress Assay

The Flexcell FX-4000 Tension System (Flexcell International Corporation), a computer-regulated bioreactor that uses vacuum pressure to apply cyclic or static strain to cells cultured on flexible-bottomed culture plates. It was used to subject a cell monolayer to mechanical stress. HaCaT cells were grown to a near confluence on BioFlex 6-well plates coated with pronectin (Flexcell International Corporation) which contain a flexible membrane in each 35-mm well. Each plate was placed over the loading station containing 6 planar faced posts. Cells were subject to cyclic mechanical stretch with a frequency of 5 Hz and an elongation of amplitude ranging from 10 to 13%. Cells were stretched for 0 hours (unstretched control) and 4 hours, and then prepared for immunocytochemistry as described above.

2.11 Proximity Ligation Assay

PLA was performed using the Duolink in-situ kit (Sigma) according to manufacturers instructions. Cells were plated on coverslips or Bioflex 6 well plates for cell stretching assay (above) and fixed with Methanol Acetone or PFA as described previously. Following fixation, cells were incubated in Duolink blocking solution for 30 minutes at 37°C. Previously optimized primary antibodies were diluted in Duolink Antibody diluent and added to cells, which were incubated overnight at 4°C. The following day the cells were washed in Duolink Wash buffer A 2 x 5mins. The PLA plus and minus probes were diluted 1:5 in antibody diluent and added to the cells which was incubated for 1hr at 37°C. The cells were washed in Duolink Wash buffer A 2 x 5mins. The Ligation-Ligase was prepared according to instructions and applied to cells for 30mins at 37°C. The cells were washed 2 x 2mins in Duolink wash buffer A and the Duolink Amplification-Polymerase solution added and incubated for 100min at 37°C. The cells were washed in Duolink wash buffer B for 2 x 10mins and then mounted with Duolink in situ mounting medium with DAPI beforevisualization with a Zeiss Confocal 710 microscope (Carl Zeiss). As a negative control, no primary antibodies were applied. A further negative control was the use of iRHOM1 instead of iRHOM2 primary antibody As a positive control, known binding partners (such as Keratin 6 and Keratin 16) primary antibodies were applied. Quantification was performed using ImageJ software analysis programme and analysed by students paired t-test using GraphPad Prism (Graphpad).

2.12 Sh RNA Lentiviral Particle Transduction

shRNA lentiviral particle transduction was used to silence RHBDF2 gene expression in human keratinocyte cell lines.

Lentiviral particles were purchased from Santa Cruz biotechnology (Santa Cruz). The product is a pool of concentrated transduction ready viral particles containing 3 target-specific constructs which encode 19-25 nucleotide (plus hairpin) shRNA designed to knock down gene expression.

Cells were plated at 2 $x10^5$ per well of a 6 well plate, which would resulted in 50-60% confluence after 24 hours. Cells were treated with Polybrene (Santa Cruz), a cation polymer used to increase the efficiency of infection of cells with the retrovirus. Polybrene was added

to the cells and incubated at 37°C for 20 minutes. The Polybrene media was then removed and to this the lentiviral particles (either RHBDF2 or negative scrambled shRNA sequence control) were added. This was optimized using different concentrations of particles. The cells were inclubated overnight at 37°C in complete media. In order to select stably transfected cells, Puromycin selection media was used. Cell lysates were obtained as previously described and analysed using SDS PAGE Electrophoresis and western blotting for iRHOM2 to determine gene silencing.

2.13 Proliferation Assay

Cells were plated at a seeding density of $1x10^4$ per well and harvested at 24 and 72 hours and cell counts were performed using the Nucleocounter/Nucleocasette system (ChemoMetec, Denmark).

2.14 Cell Migration Scratch Assay

Cells were seeded at equal density on a 6 well plate and grown for 24-48 hrs in complete media (as described above) until a confluent monolayer was achieved. Cells were treated with Mitomycin C (400ng/ml) to prevent proliferation. A vertical scratch was performed using a 200□L Gilson pipette tip. Cultures were washed three times in PBS and incubated in media. Photographs were taken at 0, 18 and 24 hours. Wounded areas were measured using Image J software analysis. Results were analysed by students paired t-test using Graphpad Prism (Graphpad, San Diego, USA).

2.15 PMA Treatment and ELISA

Cells were plated at equal density ($3x10^5$ per well) on 6 well plates and grown for 24 hours in complete media. Cells were subsequently treated with 250ng/ml PMA. Media was collected at time points (4h, 24h) for ELISA. Collected medium specimens were analysed for the TNFα using the DuoSet ELISA kit (R&D systems, Abingdon, UK) and compared with untreated controls. In all cases data are presented as mean +/- SEM. Data shown represents the mean of at least three separate experiments for each cell lines. Results were analysed by students paired t-test using GraphPad Prism (Graphpad, San Diego, USA).

2.16 Okadaic Acid Treatment

CTRL and TOC keratinocytes were seeded on coverslips in 12 well plates. After reaching the desired confluence, cells were incubated in media containing 1µM Okadaic Acid (Sigma) for 1H. The media was replaced without Okadaic Acid and cells were fixed for immunostaining as described above at time points following the treatment (0H, 4H, 24H).

2.17 Mouse Tissue

All experiments involving mice followed the UK Animal Welfare Act guidelines and approval of the UK Home Office. *irhom2* $^{-/-}$ mice were generated as previously described (Adrain et al., 2012). All experiments were performed using age and sex matched littermates.

The fore and hind-paw footpad epidermis from 20-week-old gender-matched *irhom2* $^{-/-}$ and *irhom2* $^{+/+}$ mice (n=4 per genotype) were dissected and fixed in OCT on dry ice. 5µm sections were cut and mounted on slides. For histopathological analyses, sections were fixed in 4% PFA and stained with hematoxylin/eosin according to standard protocols. Epidermal thickness was measured using Image J software and analysed by students paired t-test (n=4) using GraphPad Prism (Graphpad, San Diego, CA, USA).

Immunohistochemical staining was performed as previously described and visualised using the Zeiss 710 Confocal Microscope (Carl Zeiss, Germany)

2.18 DNA and RNA methods

2.18.1 Patient samples

All patient samples included in the work presented here were collected in accordance with the Declaration of Helsinki and approval of the East London and City Ethics committee. All informed patients provided written consent.

2.18.2 Extraction of DNA from blood and skin

DNA was extracted from whole blood samples using the QIAamp DNA blood midi/maxi kit (QIAGEN) following the manufacturer's specifications 200 µl proteinase K was mixed with 1-2 ml whole blood. 2.4 ml buffer AL were added and mixed by inversion of the tube, followed by incubation for 2 min. The tubes were incubated at 700C for 10 min, and mixed by inversion 10 times with 2 ml 96-100% ethanol. This mixture was added onto the QIAamp Midi column placed in a 15 ml centrifuge tube and spun at 3000 rpm for 3 min. Firstly the column was washed with 2 ml of buffer AW1 followed by 2 ml buffer AW2 and spun between washes at 5000 rpm for 1 min after the AW1 buffer and 15 min after the AW2 buffer. 300 µl buffer AE were added onto the membrane of the Midi column and incubated at room temperature for 5 min followed by centrifugation at 5000 rpm for 2 min. DNA was resuspended in 200-300 µl distilled water by centrifugation at 5000 rpm for 3 min.

Skin biopsy samples were obtained with written informed consent from patients with ARVC. In each patient, a 5mm punch biopsy was taken from unaffected skin from the left forearm. The fresh tissue was snap frozen on dry ice. 10*10 µm skin cryosections were used for DNA and RNA extractions with the QIAamp DNA and RNeasy mini kits (Qiagen, Hilden, Germany), following the instructions of the manufacturer. RNA was reverse transcribed into cDNA using SuperScript II (Invitrogen, Carlsbad, CA, USA).

2.18.3 Nucleic acid quantification

Nucleic acid concentration was measured using the NanoDrop ND-1000 Spectrophotometer (Thermo Fisher Scientific, Waltham, MA), according to the manufacturer's specifications.

2.18.4 Polymerase Chain Reaction (PCR)

Primer Design and Mutation Screening

All primers were purchased from Sigma-Aldrich and specific primer pairs were designed using Primer3 software (v.0.4.0). The annealing temperature (AT) for each primer pair was optimised using a gradient PCR with temperatures varying between 55-65C PCRs for the screening of all mutations described in this report were performed using either the GoTaq DNA Polimerase (Promega, UK) or the BioTaq PCR Kit(Bioline, UK). 25 µl PCR reaction comprised: 5 µl of 5x (2.5 µl of 10x) reaction buffer, 1.5 µl of 25 mM (0.75 µl of 50 mM) MgCl2, 0.25 µl of 5 U/µl of Taq enzyme; 200 µM of each nucleotide (Bioline, UK); 1 µM of each primer and 20-30 ng of template DNA. Reactions were incubated on a DNA engine Tetrad 2 Peltier Thermocycler (MJ Research) and the cycling conditions consisted of 95°C for 5 min,followed by 35 cycles of 95C for 30 s, optimised primer annealing temperature for 30 s and 72°C for 30 s, with a final extension step at 72°C for 10 min and incubationat 40C for 10 min. In addition to patient DNA, control DNA was used to amplify desired sequences. Resulting PCR products were resolved on a DNA agarose gel electrophoresis or digested with restriction digest enzymes

Reverse Transcription-PCR (RT-PCR)

Extracted RNA was used to make cDNA by RT-PCR. Briefly, 50 ng of RNA were added to 0.64 µl random hexamers (200 µM), 1µl dNTPs (10 mM) made up to 12 µl final volume with dH2O. The reactions were incubated at 65C for 5 min, chilled on ice and 4 µl of 5x first strand buffer, 2 µl of 0.1 M DTT and 1 µl RNase OUT (all Invitrogen, California, USA) were added to the reaction. The mixtures were then incubated at 25°C for 2 min before 1 µl (200 units) of superscript II reverse transcriptase (RT) (Invitrogen) was added. A negative control was simultaneously prepared using RNase free water instead of the enzyme. Samples were incubated at 42°C for 50 min, then by heat inactivation at 70°C for 15 min. 1 µl of cDNA was then added to a standard PCR.

Agarose gels were then used to identify and separate PCR products and restriction digest fragments. To separate fragments shorter than 800 bp, 1.5% (w/v) agarose (Bioline, London, UK) gels were prepared. Agarose was melted in the required volume of Tris-Borate-EDTA buffer and 0.5 µg/ml of ethidium bromide or 10 µl of 10,000x PAGE GelGreen (Biotium) were

then added to the solution. The mixture was poured into a gel tray with a comb to form the sample wells, and allowed left to solidify. The gel was flooded with TBE in an electrophoresis tank. For fragments longer than 800 bp, 1% (w/v) agarose gels were prepared. DNA samples were mixed with 6 x Orange G DNA loading buffer and loaded on the gel alongside a 1 Kb Plus DNA ladder (10% (v/v) (Invitrogen), 16% (v/v) loading buffer). Samples were electrophoresed at a voltage of 80-120V. DNA could be visualised and photographed under UV transillumination (MultiImage Light Cabinet, Alpha Innotech Corporation; pictures printed on Sony P-D890).

Sanger Sequencing

Sequencing was performed using the BigDye Terminator v3.1 Cycle Sequencing Kit (Applied Biosystems, Foster City, CA). The optimal amount of PCR product (0.5-3 µl) was incubated with 6 µl ExoSAP-IT (Affymetrix) at 37°C for 45 min followed by 80°C for 15 min and 40°C for 5 min; this enzymatic reaction removed any unincorporated primers and dNTPs. The Clean sequences were then added to a reaction containing 1 µl of BigDye® Terminator Master mix v3.1, 3 µl of better buffer (Microzone, Ottawa, Canada), 1 µl of 10 µM specific forward or reverse primer and ddH2O, to a final volume of 11.5 µl. Cycling conditions were as follows; 25 cycles at 96°C for 30 s, 58°C for 15 s, 60°C for 1 min, followed by a final incubation at 40°C for 10 min. These reaction products were then precipitated with ethanol and EDTA. This mixture was centrifuged at 4000 rpm at 40C for 20 min and the pellet was washed with 125 µl 70% ethanol and incubated on ice for a further 2 min, then centrifuged for 5 min at 4000 rpm. Precipitated DNA was then air dried at room temperature. Precipitated products were resuspended in 10 µl HiDi formamide (Sigma-Aldrich, UK), incubated at 95°C for 3 min and on ice for 3 min, centrifuged for 2 min to remove air bubbles and loaded on the ABI Prism 3130xl Genetic Analyser (Applied Biosystems, Life Technologies, USA). Traces were visualised using the Chromas LITE v 2.01 software (Free software from Technelysium Pty Ltd).

Capture array

Whole-exome capture performed using SeqCap EZ Human Exome Library v2.0 (Roche NimbleGen, Madison, WI) and sequenced with 100 bp paired-end reads on the HiSeq 2000 platform (Illumina, San Diego, CA). Resulting reads were mapped to the hg18 human reference genome using the Novoalign alignment tool (Novocraft Technologies Sdn Bhd,

Selangor, Malaysia). Sequence variants were called with SAMtools and annotated with ANNOVAR (Wang et al., 2010). variants were filtered for homozygous changes shared by the two affected individuals, of which, 83 homozygous variants reported either as novel, or with an Exome Variant Server (NHLBI GO Exome Sequencing Project (ESP), Seattle, WA) estimated frequency of less than 0.01, were selected as potential candidates.

2.19 Clinical Evaluation of Cardiac Patients for ARVC Project

The project involved 6 families with a history of AC, specifically focusing on a cohort harbouring heterozygous N-terminal loss of function (nonsense/frameshift) mutations of *DSP*. The patients were recruited at the Heart Hospital, University College London Hospitals NHS Trust (UCLH), London, UK. Patients were diagnosed with AC according to the revised Task Force Criteria. Individuals were examined from cardiac and cutaneous perspectives. Systematic evaluation of first and second degree family members was performed in whom mutation-carrier status was verified. In total, personal history of cutaneous features was collected from 58 family members, 38 mutation carriers, including five deceased members, and 20 non-carrier healthy family members. All 33 living mutation carriers were recruited for detailed phenotyping, while 8 of them had 3mm punch biopsies of non-lesional skin of the lower forearm collected for molecular characterisation. Personal history of cutaneous features was collected, and detailed clinical examination of the skin and hair phenotype was carried out by a dermatologist (TM). Cardiac phenotyping was performed according to the protocol described in 30 family members (3 of the 33 carriers resided abroad and were therefore unavailable to participate in cardiac phenotyping). Arrhythmic characterization included arrhythmia recorded during 24 hour ambulatory ECG monitoring and/or exercise testing, cardiac arrest (CA), implantable cardioverter defibrillator (ICD) appropriate discharges. Patients with atypical chest pain, palpitations and/or syncope suggestive of vaso-vagal origin were considered asymptomatic. All patients provided written informed consent.

Chapter 3

iRHOM2 Regulates Cytoskeletal Stress-Associated Keratin 16

3.1 Identifying Novel Interacting Binding Partners of iRHOM2 – Yeast 2 Hybrid Screen

The Yeast 2 Hybrid screen which was performed in a 3-D human skin library (composed of proteins extracted from the Episkin library) to assess for novel protein-protein interactions, yielded 15 potential novel interacting binding partners with the N-terminus (aa1-403) of iRHOM2. Each protein interaction was assigned a confidence score from A to E to rank the plausibility of the interaction. The score is derived from the Hybrigenics database and number of independent prey fragments identified by the screen (Figure 3.1). Scores between A and C are suggestive of a genuine interaction. $112x10^4$ potential preys were screened and 22 positive results were obtained. Of these, 9 positive preys were Type I keratins, each receiving the highest attributable confidence scores (A or B). These three keratins were K10, K14 and K16. All three are highly expressed in mammalian epithelia in a site and situation specific manner.

Bait	**Prey clone library**	**His+/Ade+/Laz+ prey clones**	**True prey clones**	**K10 fragment prey clones**	**K14 fragment prey clones**	**K16 fragment prey clones**
Human RHBDF2 N-Terminus (aa1-403)	112×10^6	28	22	3	4	2

Figure 3.1 Table illustrating the positive prey clones identified by the Yeast 2 Hybrid screen. 9 of the 22 prey clones identified are Type I keratins. The remaining clones scored less than C and are therefore less likely to represent a genuine interaction.

3.2 Identification of Potential Binding Domain

The Yeast 2 Hybrid screen identified a positive interaction between iRHOM2 and multiple fragments of each of the three keratins K10, 14 and 16. In order to identify a potential interacting domain, the overlapping regions of the positive prey fragments were compared.

The overlapping fragments from the two K16 prey fragments were located in their protein maps (www.uniprot.com), and found to correspond to the Coil 1B domain of the keratin filament. This was confirmed using the prey fragments for the two other Keratins identified by the screen (Figure 3.2 and 3.3).

The amino acid sequence of the Coil 1B domain for each of the three keratins was inserted into the Clustal Sequence Alignment tool and sequence homology for this region was determined as 86.67% between the three keratins (Figure 3.4). This fell to 60% homology when type II keratins such as K1 were included suggesting that the conserved Coil 1B domain of the keratins 10, 14 and 16 is the region likely to be interacting with N-Terminus iRHOM2. The high degree of conservation also points to an important role for this region, which will be discussed later in the chapter.

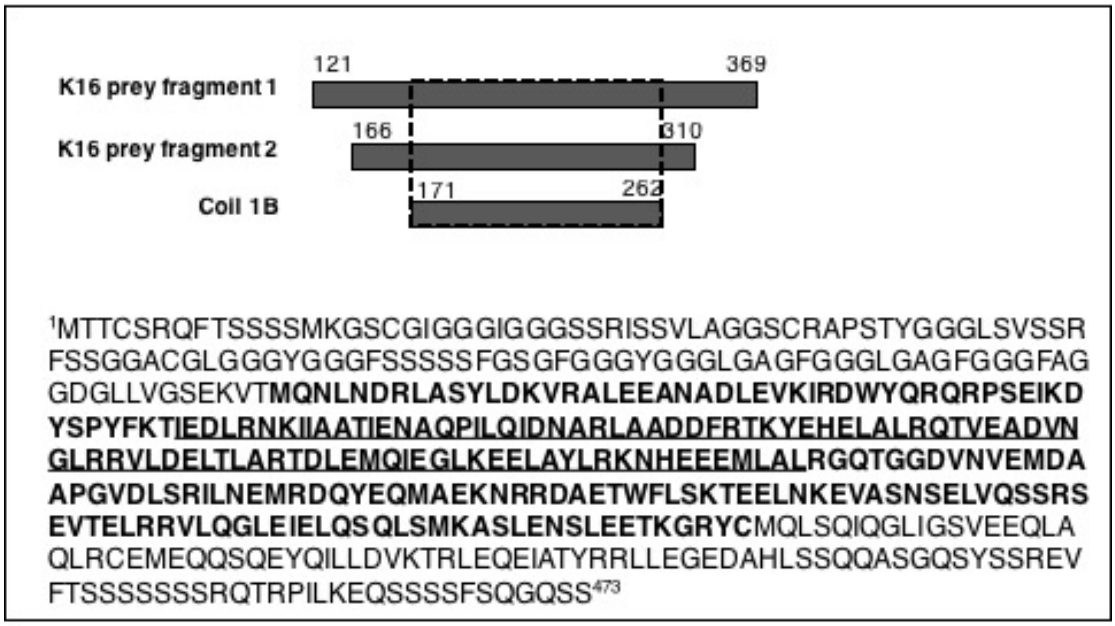

Figure 3.2 K16 prey fragments identified by the Yeast 2 Hybrid screen, both of which span the Coil 1B domain of K16. Below, K16 amino acid sequence. Bold letters refer to identified prey region starting form amino acids 167-310, underlined letters correspond to the Coil 1B domain.

Figure 3.3. Clustal sequence alignment demonstrating sequence homology between the amino acid sequence of K10, K14 and K16 (ordered from highest to lowest line) in a region corresponding to the the Coil 1B Domain (red box).

	K16	**K10**	**K14**
K16	100	81.67	86.87
K10	81.67	100	86.67
K14	86.67	86.67	100

Figure 3.4 Table shows Clustal sequence alignment homology score (%) between the K10, 14 and K16 for the Coil 1B domain.

The interaction between iRHOM2 and Keratin 16 was the focus of further study presented in this chapter. The rationale for this is that Keratin 16 is known to be a wound healing

keratin, and TOC is associated with several features of aberrant wound healing and, patients with TOC show phenotypic features restricted to sites known to express Keratin 16; palms, soles, perifollicular area, oral mucosa and in squamous cell carcinoma of the oesophagus(Brooke et al., 2014, Ellis et al., 2015). Furthermore, Keratin 16 is a known tumour marker in head and neck and oesophageal cancer(Villaret et al., 2000).

3.3 Confirmation of Interaction between iRHOM2 & Keratin 16.

3.3.1 Co-Immunoprecipitation

Co-immunoprecipitation (Co-IP) was used to confirm that iRHOM2 and Keratin 16 form a complex. Initially, the technique was optimized at length with known binding partners, ADAM17 and iRHOM2 (outlined in Materials and Methods). Binding between endogenous ADAM17 and iRHOM2 was confirmed in several cell lines including K17, TYLK1 and TYLK2 (Figure 3.5).

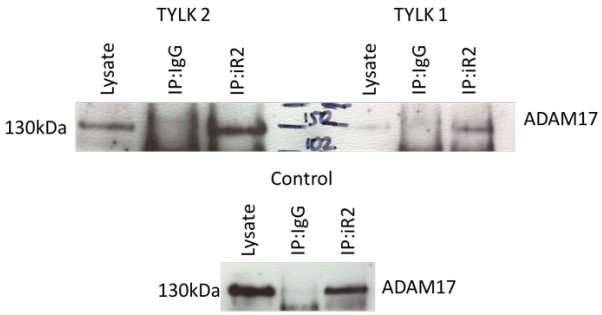

Figure 3.5. Endogenous Co-IP performed in Control and TOC keratinocytes (TYLK1 and TYLK2) using iRHOM2 to pull down ADAM17. Antibodies used: Rabbit anti-RHBDFR (HPA018080 Sigma) and Rabbit anti-ADAM17 (Ab2051, Abcam)

Further Co-IPs were performed using endogenous proteins in HaCaT keratinocytes. This demonstrated that K16 was able to pull-down iRHOM2. Furthermore, iRHOM2 was able to pull down K16. iRHOM1 and iRHOM2 are family members which share the ability to bind ADAM17, therefore it was assessed whether iRHOM1 was able to interact with K16.

However, this pull down experiment was negative, suggesting that the interaction between iRHOM2 and K16 is exclusive (Figure 3.6A).

To further validate the results of the yeast 2 hybrid screen, which used the N-Terminus of iRHOM2 as bait, the N-Terminus of iRHOM2, tagged with GFP, was overexpressed in HaCaT keratinocytes. Co-immunoprecipitation was performed using K16 to pull down GFP, and this confirmed that the N-Terminus region alone is able to bind K16 (Figure 3.6B). Using a construct lacking the N-Terminus of iRHOM2 (ΔNT-iRHOM2) tagged to HA, it was also confirmed that iRHOM2 lacking the N-Terminus domain was unable to bind K16 (Figure 3.6C). These constructs were a kind gift from the Freeman Laboratory.

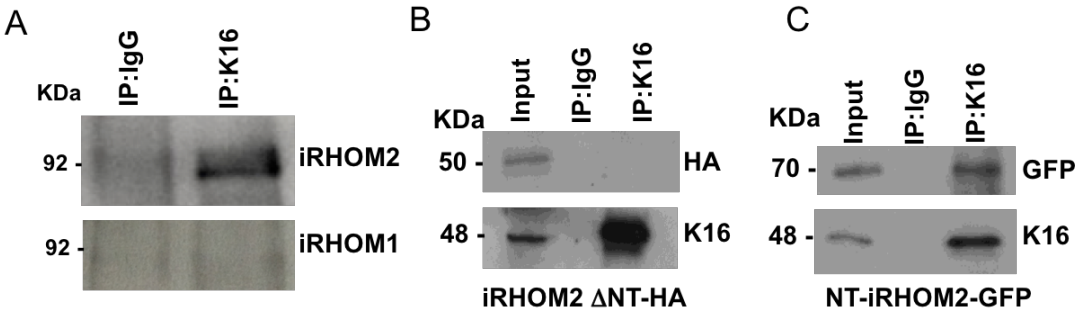

Figure 3.6 (A) Co-immunoprecipitation performed in HaCaT keratinocytes showing pulldown of iRHOM2 by K16. K16 does not pull down iRHOM1 (B) cell extracts from CTRL keratinocytes transfected with a vector expressing HA-tagged iRHOM2 lacking its N-Terminus (iRHOM2-ΔNT-HA) were immunoprecipitated with anti-K16 antibody and analyzed by western blot with anti-HA and anti-K16 antibodies. (C) Cell extracts from Control keratinocytes transfected with a vector expressing NT-iRHOM2-GFP were immunoprecipitated with anti-K16 antibody and analyzed by western blot with anti-GFP and anti-K16 antibodies.

3.3.2 Co-localisation Immunohistochemistry

In cells, iRHOM2 is expressed predominantly in the cytoplasm (particularly endoplasmic reticulum) and at the cell surface memrane. WT-iRHOM2-GFP was overexpressed in HaCaT keratinocytes and co-staining with K16 was performed. Regions of yellow in the merged image suggest that both proteins are present in the same place, at the same time. This can be seen more clearly in the subtraction PDM (Pseudocoloured product of the differences of the mean) images which highlight areas of co-localisation in orange. In addition to diffuse

perinuclear co-localisation, there are also more discrete punctate areas of co-localisation throughout the cytoplasm. Co-localisation was not observed at the cell surface membrane which is likely to be because K16 localisation is predominantly cytoplasmic.

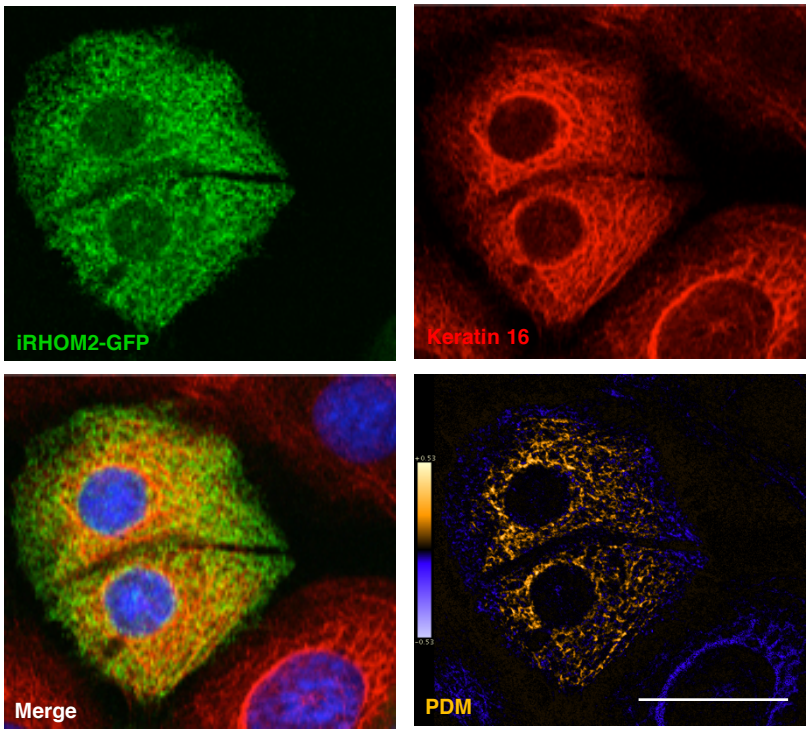

Figure 3.7 Confocal microscopy analysis of GFP-tagged iRHOM2 overexpressed in HaCaT keratinocytes showing co-localisation with endogenous K16 (red). In the merged image, yellow regions are suggestive of co-localisation. Pseudocolored 'product of the differences from the mean' (PDM) image visually quantifies co-localisation, in which each pixel is equal to the PDM value at that location, are shown with a PDM scale. Scale Bar:20 µm.

3.3.3 Proximity Ligation Assay

Proximity ligation assay (PLA) is a technique used to identify protein-protein interactions where each red fluorescent dot suggests a discrete protein-protein interaction. In HaCaT keratinocytes, PLA was used to demonstrate close proximity of endogenous K16 and iRHOM2. In cells, K16 usually exists as a heterodimer with its known Type 1 Keratin binding partner K6 (Moll, 1998), and this interaction was used as a positive control for this experiment. PLA confirmed a positive interaction between iRHOM2 and K16, with red fluorescent signals distributed predominantly within the cytoplasm (Figure 3.8).

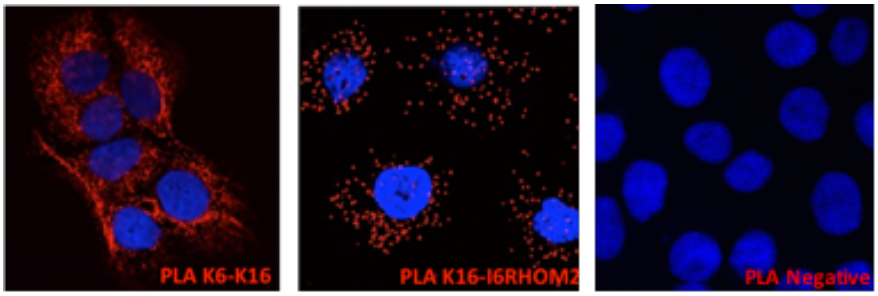

Figure 3.8. PLA in HaCaT keratinocytes shows red fluorescent signals (red dot) in the positive control (K6 and K16) and K16-iRHOM2. Each red dot signifies a single protein-protein interaction. The nucleus is counterstained with DAPI. Negative control performed in the absence of primary antibodies. The left panel is a positive control demonstrating a protein-protein interaction between K6 and K16. The middle panel demonstrates cytoplasmic red fluorescent signals suggesting interaction between iRHOM2 and K16 in HaCaT keratinocytes.

Considered with the binding studies above, these data support a genuine and novel interaction between iRHOM2 and K16.

3.4 iRHOM2-Keratin 16 interaction in TOC

3.4.1 Phenotypic Similarity between TOC and Pachyoncyhia Congenita Type I

TOC bears several phenotypic similarities to Pachyonychia Congenita Type I (PC-1) caused by autosomal dominantly inherited mutations in either K16 or K6A. These include the presence of a focal, non-epidermolytic palmoplantar keratoderma (FNEPPK), perifollicular hyperkeratosis, oral leukokeratoses in addition to the presence of multiple steatocystomas (Figure 3.9). However, the presence of oesophageal SCC is unique to TOC, despite this, the marked clinical similarity between the two inherited diseases supports a shared pathophysiological mechanism. Mutations in K16 associated with PC-1 occur in the 1A and 2B domains and are thought to exert a dominant-negative effect on the wild-type protein (Liao et al., 2007) Over-expression of PC-associated mutant K16 in keratinocytes results

nuclear reorganization of the K16 filament network and some collapse of the endogenous cytoskeletal network (Smith et al., 2000). It is thought that this collapse of the keratin filament network contributes to the clinical phenotype.

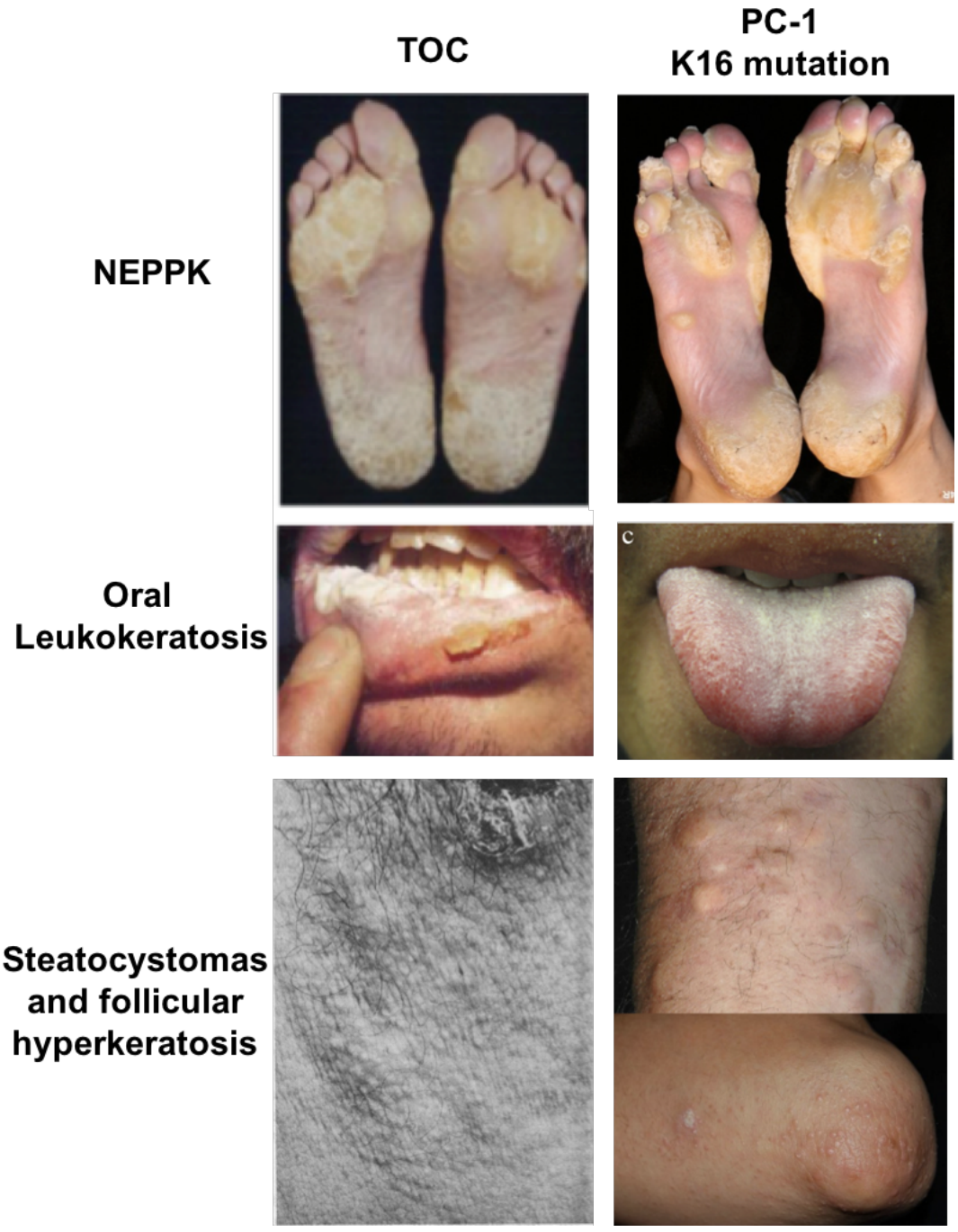

Figure 3.9 Clinical similarities between TOC and PC-1: Yellow, hyperkeratotic thickening of the soles bilaterally at sites of pressure (focal non-epidermolytic PPK), Leukokeratoses of the mouth and tongue (oral mucosal hyperkeratosis), Steatocystomas (sebum-containing dermal cysts) and perfollicular hyperkeratosis (accumulation of scale around the hair follicle)

3.4.2 The Role of K16 in TOC

Tylosis Keratinocytes (TOC) have been derived from patients harboring gain of function mutations in iRHOM2 and were use to gain insight into the functional relevance of the interaction between iRHOM2 and K16. Following informed consent, biopsies were harvested from interfollicular affected skin (papules) from a male and female Tylosis patient. As a normal control, breast skin from a 31 year old healthy female and leg skin from a 45 year old healthy female (K1 and K17 control cell lines) were also collected. Cells were immortalized with HPV16(E6/E7) as described previously (Rheinwald & Green, 1975) and experiments were carried out on cells that had been passaged between 10 and 40 times.

Firstly, western blotting demonstrates that K16 levels are increased in TOC keratinocytes compared with controls (Figure 3.10A). This was confirmed by Immunohistochemistry which showed strikingly increased K16 in lesional TOC skin biopsy compared with control interfollicular skin. In TOC, the epidermis also appears to be slightly thickened compared with normal control skin (Figure 3.10B). TOC keratinocytes have previously been shown to be hyperproliferative and this could explain the presence of a thickened epidermis (Blaydon et al., 2012). K16 is not usually expressed in the normal interfollicular epidermis, however its expression can occur in response to injury and in disease states such as psoriasis and squamous cell carcinomas (Bernot et al., 2002)

Further confirmation of these findings was sought from 3D organotypic human skin equivalents derived from Control (CTRL) and TOC keratinocytes (organotypic culture performed by Benjamin Fell). Like Tylotic skin, the TOC organotypics were thickened and also showed upregulation of K16 throughout the epidermis compared with Control Organotypics (Figure 3.10C). iRHOM2 immunostaining is not shown here but has previously been shown to be comparable between TOC and control skin, with slightly increased cytoplasmic staining in TOC (PhD Thesis, Sarah Etheridge).

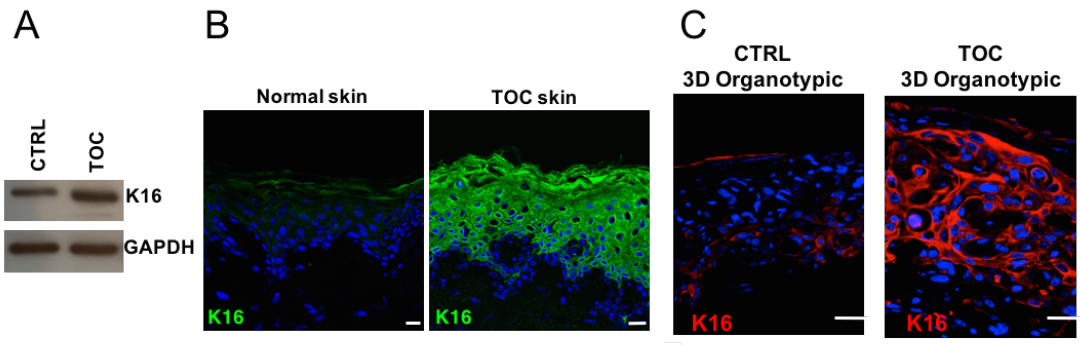

Figure 3.10 (A) Western blotting of cell extracts from Control and TOC keratinocytes immunoblotted for K16 (54KDa) showing upregulation of K16 in TOC. (B) Immunohistochemical staining of K16 (green) in normal and TOC skin. (C) Immunohistochemical staining of K16 (red) in 3 Dimensional Organotypics derived from control or TOC keratinocytes. Scale bars 20µm. Negative controls Appendix Figure B.1.

To determine whether the N-Terminus mutation in iRHOM2 could affect its interaction with K16, Co-IP pull down assays were performed using control and TOC cell lysates, normalized for protein content using a Bradford Assay. This IP confirmed increased interaction between iRHOM2 and Keratin 16 in TOC keratinocytes compared with controls (Fig 3.11A). The extent of binding was quantified by performing densitometry on the IP western blotting bands in control and TOC from three independent experiments and normalized for input. The bar graph demonstrates this quantification, showing that there is a significantly increased iRHOM2-K16 pull-down in TOC compared with control keratinocytes (Figure 3.11B).

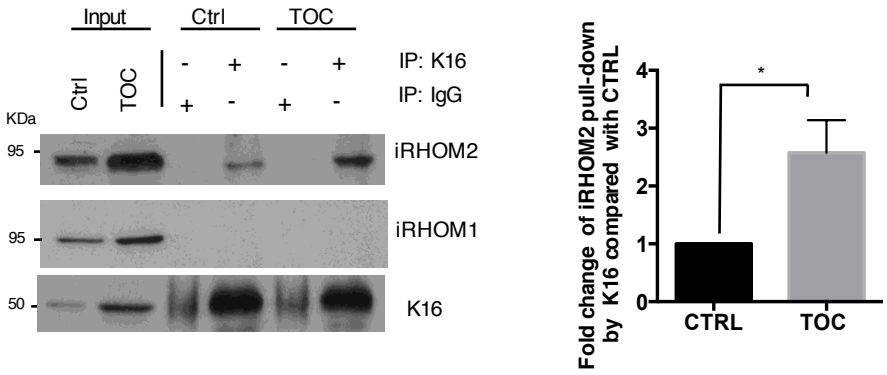

Figure 3.11 (A) CTRL and TOC keratinocyte lysates were immunoprecipitated with anti-K16 antibody and analyzed by western blotting with anti-iRHOM1 and anti-iRHOM2 antibody**.** (B) Graph depicting fold change of iRHOM2 pull-down by K16 in TOC cells compared to CTRL (n=3), error bars denote SD, **P*<0.05

As a negative control, iRHOM1 was shown not to pull down K16 in both control and TOC cells however it could bind to its known partner ADAM17 in the same experiment (3.12A). As a negative control, iRHOM2 was shown not to bind to another intermediate filament (Vinculin) (3.12B).

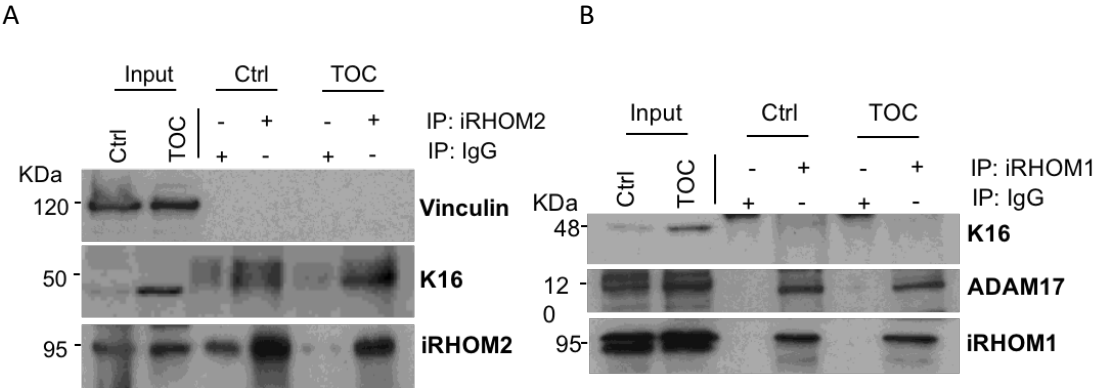

Figure 3.12(A) CTRL and TOC keratinocyte lysates were immunoprecipitated with anti-iRHOM1 antibody and analyzed by western blotting with anti-K16, anti-ADAM17 and anti-iRHOM1 antibody. (B) CTRL and TOC keratinocyte lysates were immunoprecipitated with anti-iRHOM2 antibody and analyzed by western blotting with anti-K16, anti-iRHOM2 and anti-Vinculin antibody.

PLA was used to assess the apparent increased interaction between iRHOM2 and K16 in TOC compared with control keratinocytes. Increased signal intensity was observed in TOC compared with control (Figure 3.13A). Quantification of the signal intensity was performed,

relative to the DAPI to normalize for cell number. In total, 36 images were examined from three independent experiments for each cell type. The data are depicted in the bar graph (Figure 3.13B). Statistical analysis using the unpaired student's t test confirmed a significantly increased interaction between iRHOM2 and K16 in TOC.

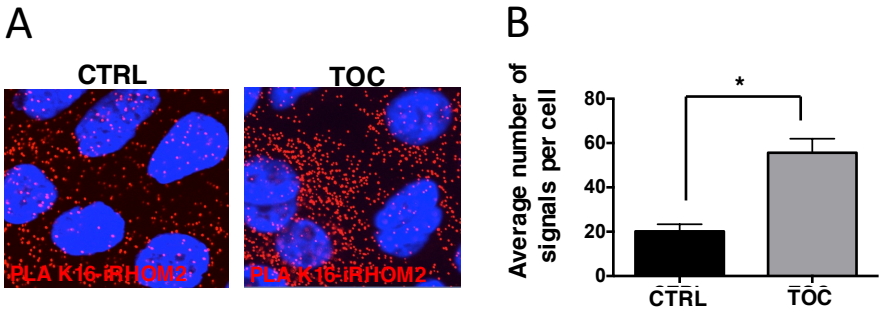

Figure 3.13 (A) Proximity ligation assay (PLA) between iRHOM2 and K16 analyzed by confocal microscopy in CTRL and TOC keratinocytes. (B) Graph represents quantification of red fluorescent PLA signals relative to DAPI. (blue) Mean of 3 experiments, each experiment comprising 12 separate images. Error bars denote SD. *P<0.05.

These findings suggest that the iRHOM2 N-Terminus gain-of-function mutations in TOC are associated with increased interaction with K16.

3.4.3 iRHOM2 regulates the reorganisation of K16 filaments

In humans, TOC manifests itself initially as hyperkeratotic thickening of the plantar and to a less extent palmar epidermis. K16 is one of only three keratins known to be consitutively expressed in the palmoplantar epidermis. Taking this into consideration, and in light of the findings presented so far, it suggests that iRHOM2 may play a role in the epidermal response to physical stress.

In order to recapitulate mechanical footpad stress in vitro, CTRL and TOC keratinocytes were cultured in monolayer on flexible membranes and subjected to 4 hours of oscillating mechanical stress using the Flexcell^{TM} system. The time-point of four hours was selected because K16 has been shown to be rapidly induced in injured epithelia within 4 hours of injury (Paladini et al., 1996) . Both CTRL and TOC cells showed upregulation of K16 and a perinuclear distribution of the filament network (Figure 3.14), which was more pronounced in TOC cells. Although keratins are key scaffolding proteins in epithelia, they are highly

dynamic structures and are able to rearrange themselves in response to specific stimuli to permit alterations in cell size and shape (Windoffer et al.,2011)

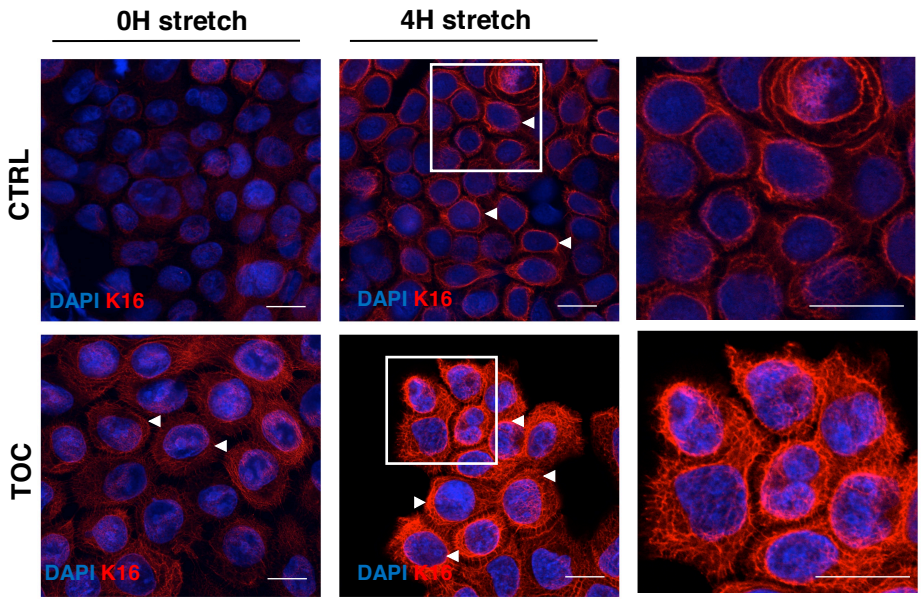

Figure 3.14. CTRL and TOC keratinocytes were subjected to cyclical mechanical stretch at a frequency of 5hz and amplitude 10-13% using Flexcell FX-4000 Tension system for 0h and 4hrs respectively. Stretched cells were immunostained for K16 and and analyzed by confocal microscopy. White arrowheads indicate perinuclear K16 filaments reorganization. Scale Bar: 20µm

In fact, TOC cells demonstrated increased perinuclear localisation of K16 even prior to stress, which is seen more clearly in greyscale images (Figure 3.15A). The percentage of cells with a perinuclear keratin network was quantified using a new methodology previously described by Feng and Coulombe (Feng and Coulombe, 2015). This quantification showed a significantly higher percentage of cells with a perinuclear K16 keratin network in TOC keratinocytes compared with controls (Figure 3.15B)

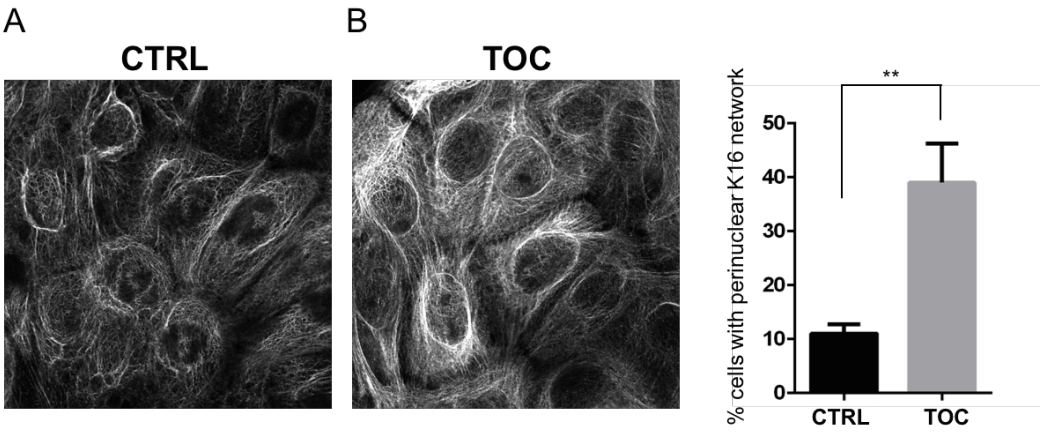

Figure 3.15 (A) 16-bit greyscale images of K16 immuostaining in Control and TOC keratinocytes more clearly reveals the perinuclear arrangement of K16 in TOC cells. (B) Quantification of the perinuclear localization of K16 filaments in CTRL and TOC cells. Data represent the mean of 3 independent experiments, each experiment comprising 30 images per cell line. Error bars denote SD. ***P*<0.01

To more clearly delineate the role of iRHOM2 in perinuclear reorganization of the K16 network, Wild-Type (WT) or TOC iRHOM2-GFP constructs (made by Diana Blaydon) were overexpressed in HaCaT keratinocytes. Immunostaining for K16 was performed and confocal microscopy showed that the K16 filament network was relatively unchanged in cells transfected with WT-iRHOM2-GFP. However, in cells overexpressing TOC mutant-iRHOM2 GFP, K16 showed a perinuclear redistribution. Following mechanical stretching, both WT and Mutant transfected cells showed a striking perinculear relocalisation of the K16 filament network (Figure 3.16).

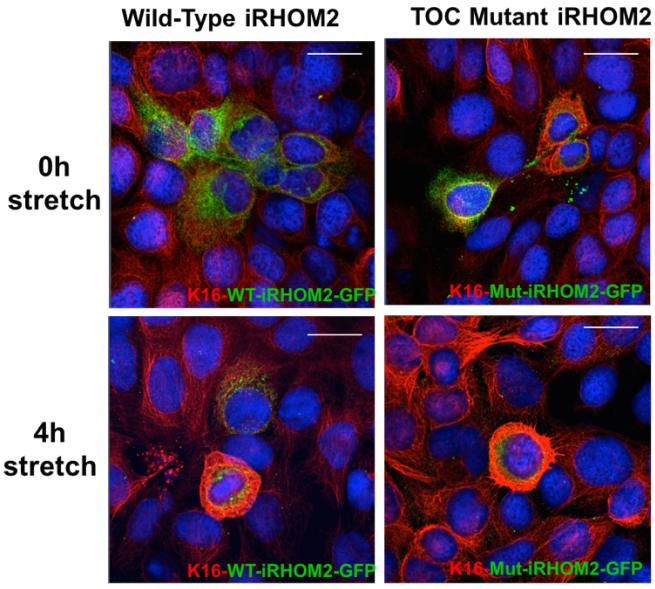

Figure 3.16. HaCaT keratinocytes were transfected with either Wild-type or TOC mutant iRHOM2-GFP and subjected to 4 hours of cyclical mechanical stretching using the Flexcell FX-4000 tension system for 0h and 4 hours respectively. Cells were immunostained for endogenous K16 and analysed by confocal microscopy.

In situ PLA was performed using probes for iRHOM2-GFP and K16 to determine whether the reorganization of K16 in stretched cells was linked to interaction between iRHOM2-GFP and K16. This showed an intense aggregation of peri-nuclear signal intensity, implying that peri-nuclear reorganization of the K16 filament network is associated with iRHOM2-K16 interaction.

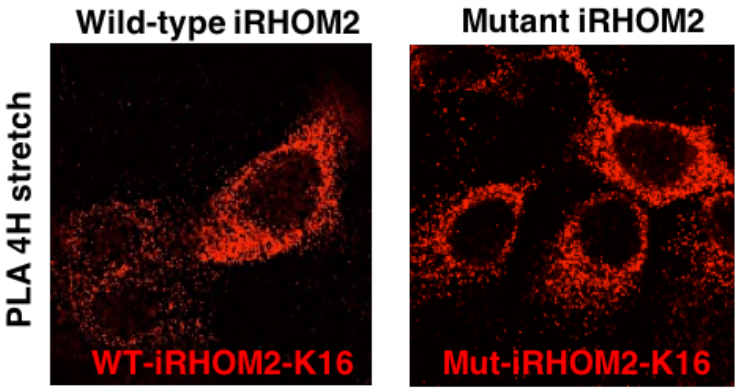

Figure 3.17 PLA of GFP (green) and K6 (red) in cells overexpressing either WT-iRHOM2-GFP or TOC-mutant-iRHOM2-GFP following 4H cyclical stretching. Images analysed by confocal microscopy.

This data suggests that iRHOM2, particularly the TOC-mutant form, plays a role in regulating K16 in response to mechanical stress, specifically, it appears to regulate perinuclear reorganization of the K16 filament network.

3.4.4 K16 and K6 are differentially regulated in TOC

K16 is a type I keratin that forms heterodimers with its type II binding partner K6. To assess the specificity of the effect of TOC on K16, western blotting was also performed for K6. Unexpectedly, levels of K6 were reduced in TOC cell extracts (Figure 3.18A). In addition, immunohistochemistry of TOC skin showed almost absent K6 despite the presence of abundant K16. Confocal analysis of TOC cells showed poorly formed K6 filaments that were reduced to cytoplasmic aggregates compared with the branch like filament network observed in CTRL keratinocytes, whereas K16 had previously been shown to be present in both cell lines (Figure 3.18B).

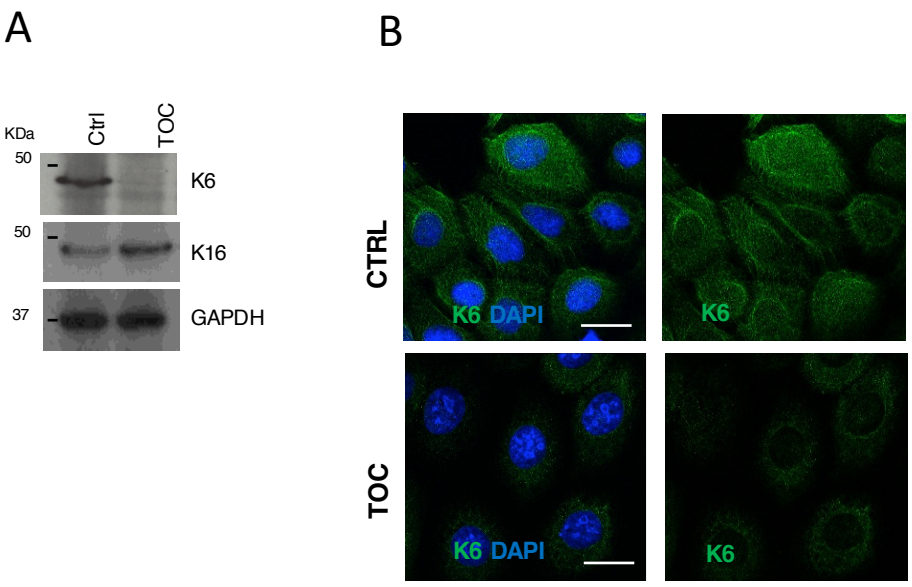

Figure 3.18 (A) Western blot analysis of endogenous expression of K16 and K6 in CTRL and TOC keratinocytes. GAPDH was used as a loading control. (B) Confocal analysis showing reduced K6 expression in TOC keratinocytes. Scale Bar: 20µm Negative control Appendix Figure B.2

PLA was performed in control and TOC keratinocytes to assess the extent of interaction between K6 and K16 in the two cell types. This showed significantly reduced interaction

between K6 and K16 in TOC (Figure 3.19), the same cells which had previously shown increased interaction between iRHOM2 and K16 (Figure 3.12), suggesting a switch in the binding partner of K16 in TOC.

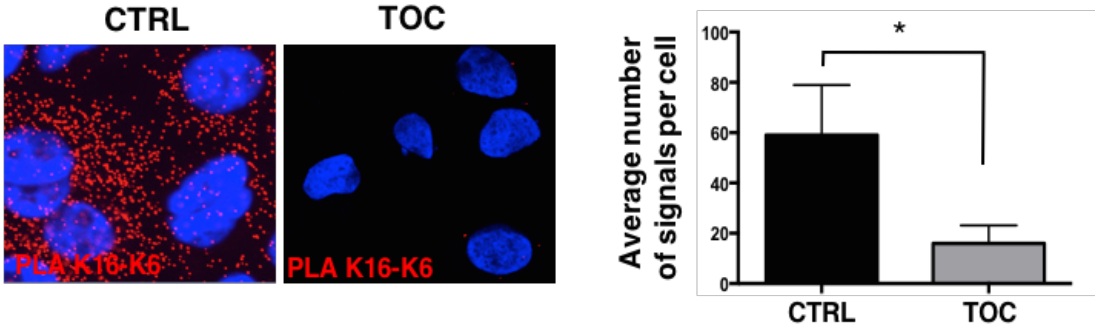

Figure 3.19 PLA between K6 and K16 analyzed by confocal microscopy. The graph shows quantification of red fluorescent PLA signals relative to DAPI. Mean of 3 experiments, each experiment comprising 12 separate images. Error bars denote SD.*P<0.05. Scale Bar: 20µm

Overexpression of both WT and Mutant iRHOM2-GFP in HaCaT Keratinocytes also results in reduced K6. Immunohistochemistry of transfected cells shows reduction of K6 in cells showing GFP signal, and on closer examination, K6 appears distributed as cytoplasmic dots in transfected cells, similar to its appearance in TOC cells (Figure 3.18B) supporting the hypothesis that increased iRHOM2 activity is associated with reduced K6 however the mechanism remains undetermined.

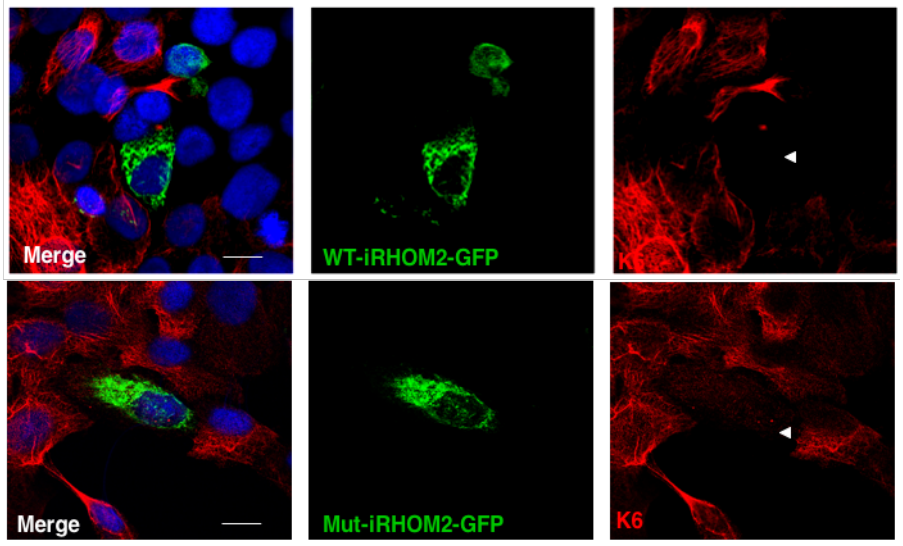

Figure 3.20 CTRL keratinocytes were transfected with either WT-iRHOM2-GFP or TOC Mutant-iRHOM2-GFP and immunostained for endogenous K6 and analyzed by confocal microscopy. K6 expression is reduced in transfected cells (white arrowhead) Scale Bar: 20µm.

In contrast, shRNA knock-down of iRHOM2 in TOC cells resulted in restoration of K6 levels comparable to control keratinocytes (Fig. 3.21A). Re-expression of K6 was also shown to occur in 3-D organotypics derived from sh-iRHOM2 TOC cells (Fig. 3.21B), in contrast to reduced K6 expression in Control 3D cultures, whereas K16 was reduced in both sh-iRHOM2 cell lines (Fig 3d).

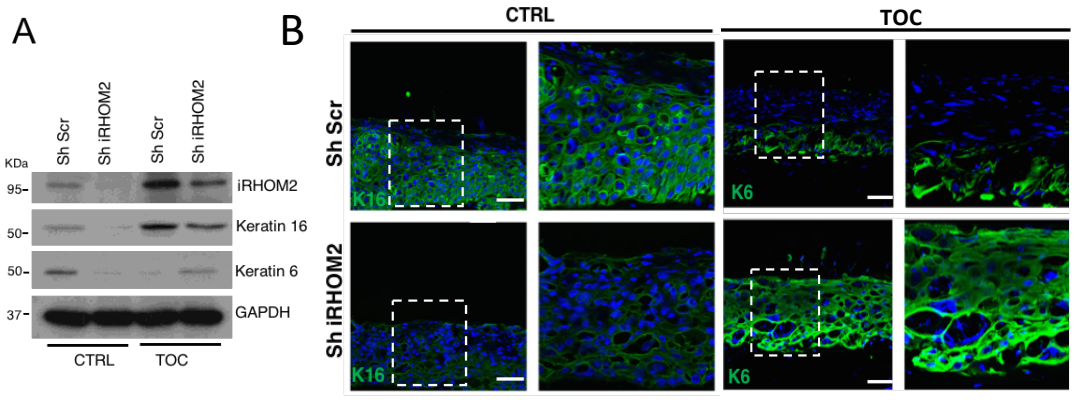

Figure 3.21 (A) Western blot analysis showing that IRHOM2 depletion by ShRNA reduces the expression of K16 in CTRL and TOC keratinocytes while it restores expression of K6 in TOC keratinocytes. GAPDH was used as a loading control (B) Confocal analysis showing the reduction of K16 expression but upregulation of K6 in Sh-iRHOM2 TOC 3D human skin equivalents. Scale bars: 20µm. Negative control Appendix Figure B.3

Intriguingly, qPCR (by Matthew Brooke) showed that K6 mRNA levels were significantly reduced in TOC cells, where K16 mRNA levels were increased, suggesting that the regulation of these two keratins also occurs at transcriptional level (Figure 3.22).

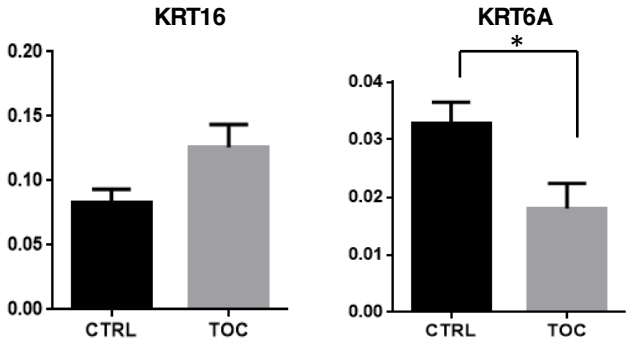

Figure 3.22 Graphs depicting fold change of mRNA expression of K16 and K6 in CTRL and TOC keratinocytes measured by qPCR. (n=3) error bars denote SD, *P<0.05

These data imply that the gain-of-function mutant form of iRHOM2 in TOC, is associated with increased interaction with K16 and reduced levels of K6 at both mRNA and protein level, suggesting a reciprocal regulation of K6 and K16. A potential mechanism for this comes from the results of the Yeast-2 Hybrid screen. The two prey clone K16 fragments found to interact with the iRHOM2 N-Terminus bait, share a 143 amino acid overlapping region which corresponds to Coil 1B of K16 (Figure 3.2). Keratins are composed of head and tail domains well as central helical coiled-coiled domains (Coil 1A, 1B 2A and 2B) each with specific functions (Steinert et al., 1994). The Coil 1B domain plays a role in heterodimerisation between type I and II keratins (Bernot et al., 2005) . Increased binding of iRHOM2 to the coil 1B domain of K16 in TOC could therefore physically impair dimerization with its binding partner K6 and potentially contribute to its downregulation and/or degradation. This data implies that differential modulation of K16 and K6 expression is likely to be iRHOM2-dependent.

3.4.5 iRHOM2 regulates the dynamicity of K16 filaments

Keratin filament cycling plays a key role epithelial migration and proliferation particularly in response to injury. Retraction of rigid keratin filaments from the cell periphery results in cytoplasmic softening, facilitating the changes in cell size and shape required for motility and cell division (Beil et al., 2003) .

In TOC, both migration and proliferation rates are increased compared with control keratinocytes and reportedly similar to those observed in wound-edge keratinocytes

(Blaydon et al., 2012). Therefore, we sought to assess whether the interaction between iRHOM2 and K16 could alter filament cycling.

Okadaic Acid (OA) is a protein phosphatase inhibitor derived originally derived from shellfish and is widely used in Keratin studies to induce hyperphosphorylation of the keratin filaments which then aggregate into cytoplasmic "dots" (Busch et al., 2012). Control and TOC keratinocytes were treated with OA for 1 hour, which disassembled keratin filaments into cytoplasmic aggregates. To determine whether filament cycling was altered in TOC, OA-treated cells were monitored at time-points following treatment to observe how rapidly the K16 cytoskeletal architecture was able to recover (Figure 3.23).

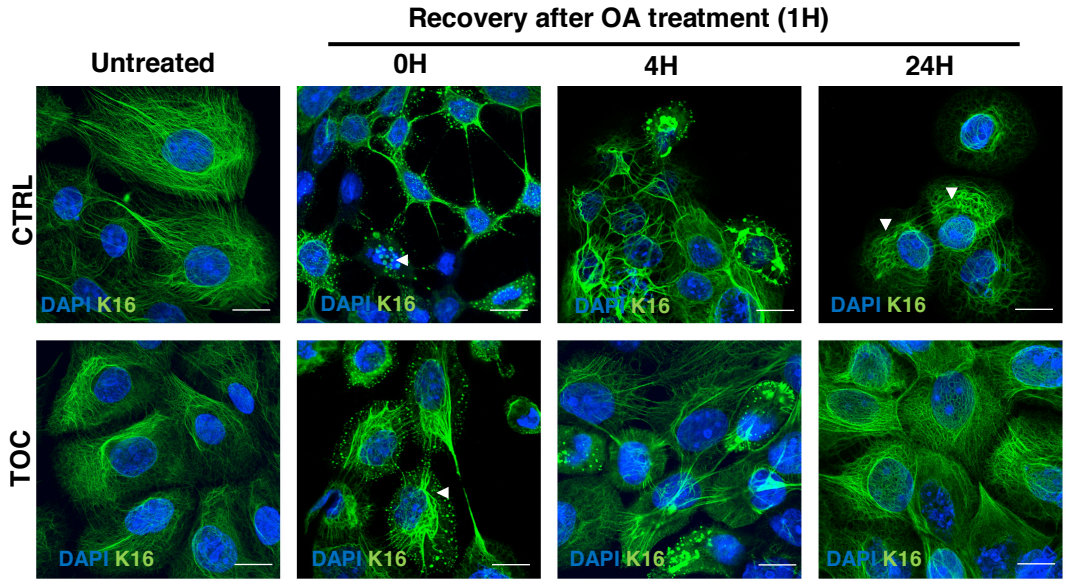

Figure 3.23. Confocal analysis of CTRL and TOC keratinocytes treated with 1µM Okadaic Acid for 1 hour, then fixed at 4H and 24H timepoints following treatment and immunostained for K16. White arrowheads represent aggregated K16 filaments. Scale Bar: 20µm

4 hours following treatment, CTRL cells show limiting recovery, with few filaments reformed. In TOC cells however, there is partial recovery. 24 hours following treatment with OA, TOC cells show almost complete normalisation of K16 filaments however, in CTRL cells, K16 filaments remain partially aggregated in the cytoplasm. These data qualitatively suggest that K16 turnover is more dynamic in TOC keratinocytes because the filaments returned to their normal pattern more rapidly following treatment, and this phenomenon could be related to upregulated iRHOM2 activity.

3.5 The role of iRHOM2 in Migration, Proliferation and Inflammation

As discussed previously, TOC is characterized by features of "constitutive" wound healing, namely, upregulated migration, proliferation and inflammation compared with control keratinocytes. To validate these observations, iRHOM2 was depleted from Control and TOC keratinocytes using shRNA iRHOM2 lentiviral particles. Sh Scramble was used as a control in both cell lines. The efficacy of knock down was checked at mRNA level by qPCR and at protein level by western blotting, both of which showed a robust reduction in the expression of iRHOM2 (Fig 3.24A and B). Western blotting showed reduced K16 in both control and TOC shiRHOM2 cells, with almost complete loss of K16 in control keratinocytes, supporting a link between the expression pattern of the two proteins.

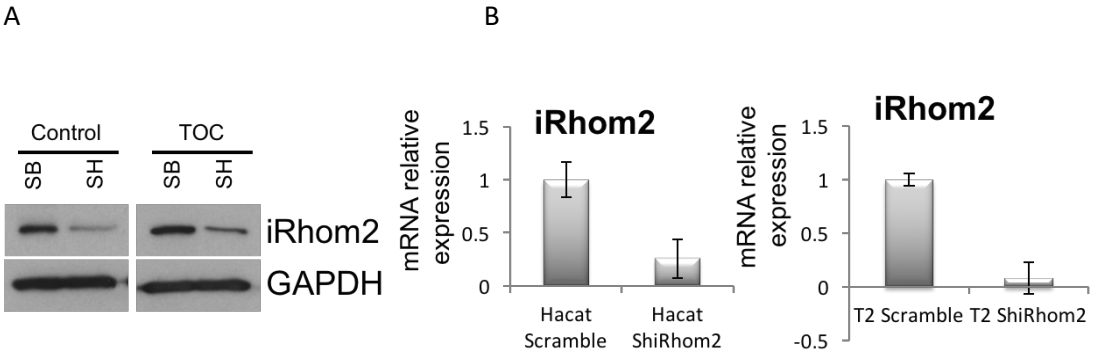

Figure 3.24 (A) Western blotting of iRHOM2 in control and TOC cell lysates, GAPDH used as a loading control.(B) qPCR for iRHOM2 in HaCaT or T2 cells treated with either scramble (SB) or iRHOM2 ShRNA.

K16 is highly expressed at the wound edge and also in several epithelial cancers (Moll et al., 1982). TOC Keratinocytes exhibit increased migration and proliferation rates, similar to that observed in wound edge keratinocytes and epithelial cancers (Blaydon et al., 2012). We therefore hypothesised that the interaction between iRHOM2 and K16 could play a role in these cellular events. A proliferation assay was performed using shiRHOM2 CTRL and TOC

keratinocytes, measuring cell counts at 48 and 72 hours after plating. This showed a reduction in proliferation rates in both cell lines in the absence of iRHOM2 (non significant). In fact, knock-down of iRHOM2 returns the proliferation rates of TOC cells to a level comparable to CTRL keratinocytes, thereby "normalising" their behaviour (Figure 3.25)

.

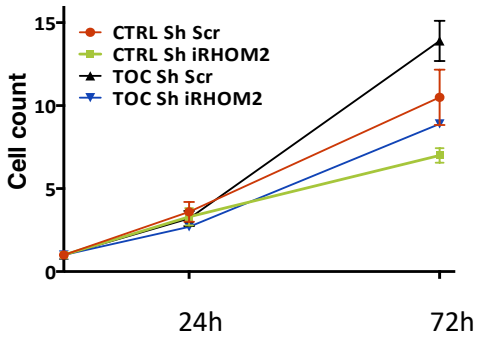

Figure 3.25. Proliferation assay performed in Growth curves of cultured cells for Sh-Scr, Sh-IRHOM2 in CTRL and TOC keratinocytes showing slower growth rates for Sh-iRHOM2 cells in both cell lines. (Mean of 3 experiments ±SD)

shiRHOM2 Control and TOC cells were also used to generate 3-Dimensional organotypics (Benjamin Fell). Immunostaining of these organotypics demonstrated reduced expression of K16 throughout the organotypic "epidermis" (Figure 3.26).

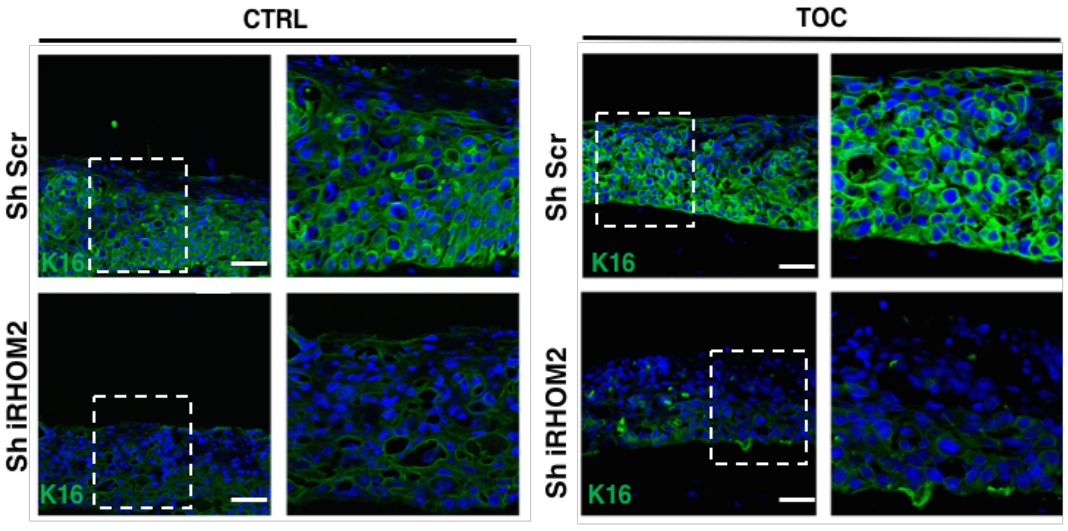

Figure 3.26. Confocal analysis of 3D organotypics derived from shScr or ShiRHOM2 Control and TOC keratinocytes demonstrating reduction of K16 throughout the epidermis when iRHOM2 is depleted. Scale bars: 20µm

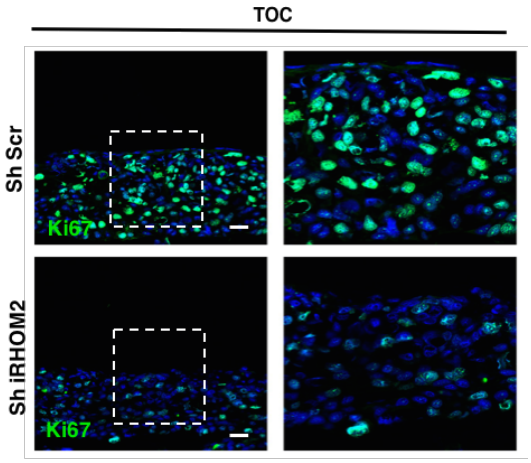

Figure 3.27. Confocal analysis showing the reduction of the proliferation marker Ki67 expression in ShIRHOM2 TOC 3D human skin equivalents. Scale bars: 20µm. Negative control Appendix Figure B.4

The proliferation marker, Ki67 was also reduced throughout the epidermis of shiRHOM2 TOC organotypics (Figure 3.27). Taken together, these observations suggest that depletion of iRHOM2 is associated with reduced K16 and impaired proliferation in control and TOC keratinocytes.

Scratch-wound assays can be used to demonstrate cell migration in monolayer and migration is a key event not only in wound-healing but also tumourigenesis, contributing to metastasis. We performed scratch-wound assays using shiRHOM2 CTRL and TOC cells cultured in a confluent monolayer. These cells were pre-treated with Mitomycin C, a proliferation inhibitor to ensure that closure of the "wound" was not due to cell proliferation. Previously, our group has shown that TOC cells can close a scratch wound rapidly, within 4 hours. However, when iRHOM2 is depleted, migration is significantly abrogated, and as such the scratch remains open even after 24 hours in TOC shiRHOM2 cells (Figure 3.28A). Quantification of the percentage wound closure after 24 hours was performed an confirmed a significant reduction in wound closure in both Control and TOC shiRHOM2 cells, however shiRHOM2TOC cells were still able to migrate slightly faster than shiRHOM2 control cells (21.3% vs 4.9%)(Figure 3.23B). These findings suggest that iRHOM2 contributes to migration in both control and TOC keratinocytes (Figure 3.28B).

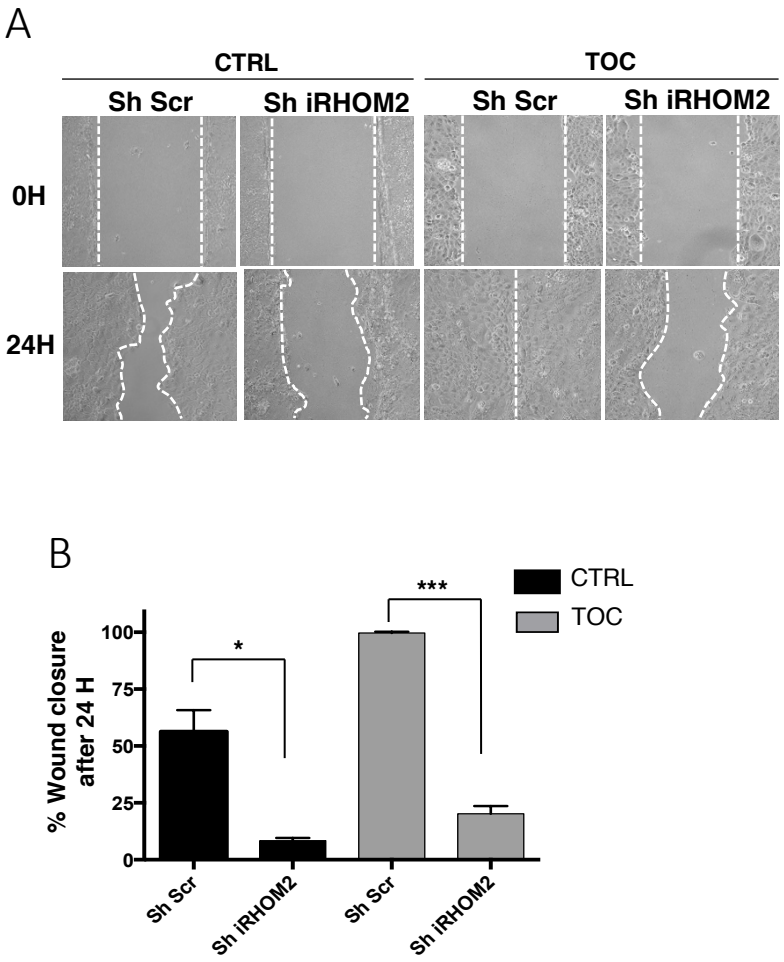

Figure 3.28 (A) Light-microscopy images of CTRL and TOC keratinocyte monolayers 0H and 24H after scratch-wounding. (B)Graph shows quantification of wound closure as a percentage, mean of 3 experiments. Error bars denote SD **P*<0.05, ****P*<0.001

iRHOM2 regulates the trafficking and maturation of ADAM17, a pivotal membrane bound sheddase which cleaves a number of substrates by ectodomain shedding, notably TNFα. Processing of ADAM17 by iRHOM2 results in cleavage of its prodomain, resulting in an active "mature" form (Adrain et al., 2012). Both control and TOC cells depleted of iRHOM2 show decreased levels of mature ADAM17 (Figure 3.29A). Mature ADAM17 is required for TNFα shedding from the cell surface membrane. To test whether depletion of iRHOM2 also results in dampened TNFα release from cells, control and TOC shiRHOM2 keratinocytes were treated with PMA or a vehicle control (DMSO). PMA is known to increase TNFα release from keratinocytes by activating ADAM17. However, in shIRHOM2 cells, TNFα release is significantly reduced at both 4h and 24h timepoints in resonse to PMA (ELISA by Paul Delaney), presumably due to impaired maturation of ADAM17 (Figure 3.29B).

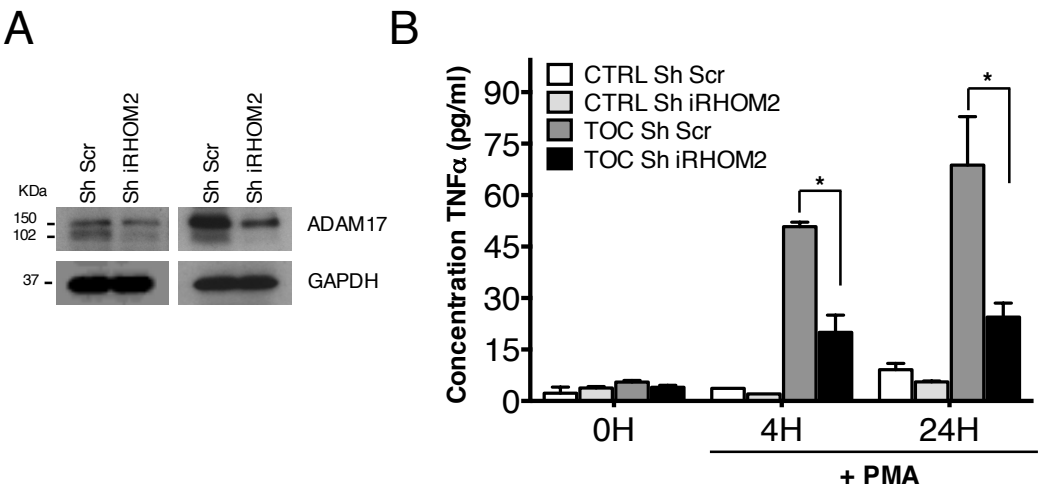

Figure 3.29 (A)Western blot analysis showing the modulation of ADAM17 in normal (K17) and TOC shiRHOM2 keratinocytes. GAPDH is used as a loading control. (B) Reduced shedding of ADAM17 substrate TNFα measured by ELISA in CTRL and TOC keratinocytes depleted of iRHOM2 (shiRHOM2) after stimulation with 250ng/ml PMA for 0, 4 and 24 hours. (n=3) Error bars denote SD *P<0.05.

Although K16 is known to play a pivotal role in both migration and proliferation, substrates of ADAM17, activated by iRHOM2, can also contribute, particularly TNFα. It is therefore possible that reduced ADAM17 maturation and therefore substrate shedding could also cause the changes in cell behavior resulting from iRHOM2 depletion.

3.6 Examination of IRHOM2 KO mice paws reveal a thinner epidermis

To validate the in vitro observations, we collaborated with Prof Matthew Freeman's group at the University of Oxford, who provided us with access to irhom2 knockout (irhom2 KO) mice. These mice have been reported to be physically similar to irhom2 WT mice (McIlwain et al., 2012, Adrain et al., 2012) however, when they were re-examined, a striking difference in the paws of 20 week old adult mice was observed. In all mice examined, the forepaws and hindpaws revealed diminution of the stress-bearing footpads. The footpad skin also appeared pale and translucent when compared with their wild-type littermates who displayed hyperpigmentation and hyperkeratosis typical for their age (Figure 3.30A). The

forepaw and hindpaw footpads of 4 WT and 4 KO littermates were excised. Multiple tissue sections were stained with haematoxylin and eosin and thickness of the epidermis was measured using Image J (Figure 3.30B). Measurements were taken through the thickest part of the footpad epidermis. 10 measurements were taken from each 5 separate sections from each mouse (n=4) and statistically analysed using the unpaired students t test. This data is presented as a bar graph. In keeping with the examination findings, there was a significant reduction in footpad thickness in irhom2 KO mice (Figure 3.30C). However, there was no significant difference in the thickness of their back skin. Interestingly, the back skin does not constitutively express K16 and nor is it subjected to physical stress like the footpads.

Immunohistochemical staining of the paws was performed for K16 and revealed diminished expression throughout the footpad epidermis in irhom2 KO mice compared with wild-types (Figure 3.30D). As a control, the expression of the palmoplantar specific Type 1 Keratin, K9, was also assessed. K9 was not identified by the original Yeast-2-Hybrid screen as a potential interacting binding partner with irhom2. Levels of K9 in the irhom2 KO mice were comparable to WT mice (Figure 3.30E).

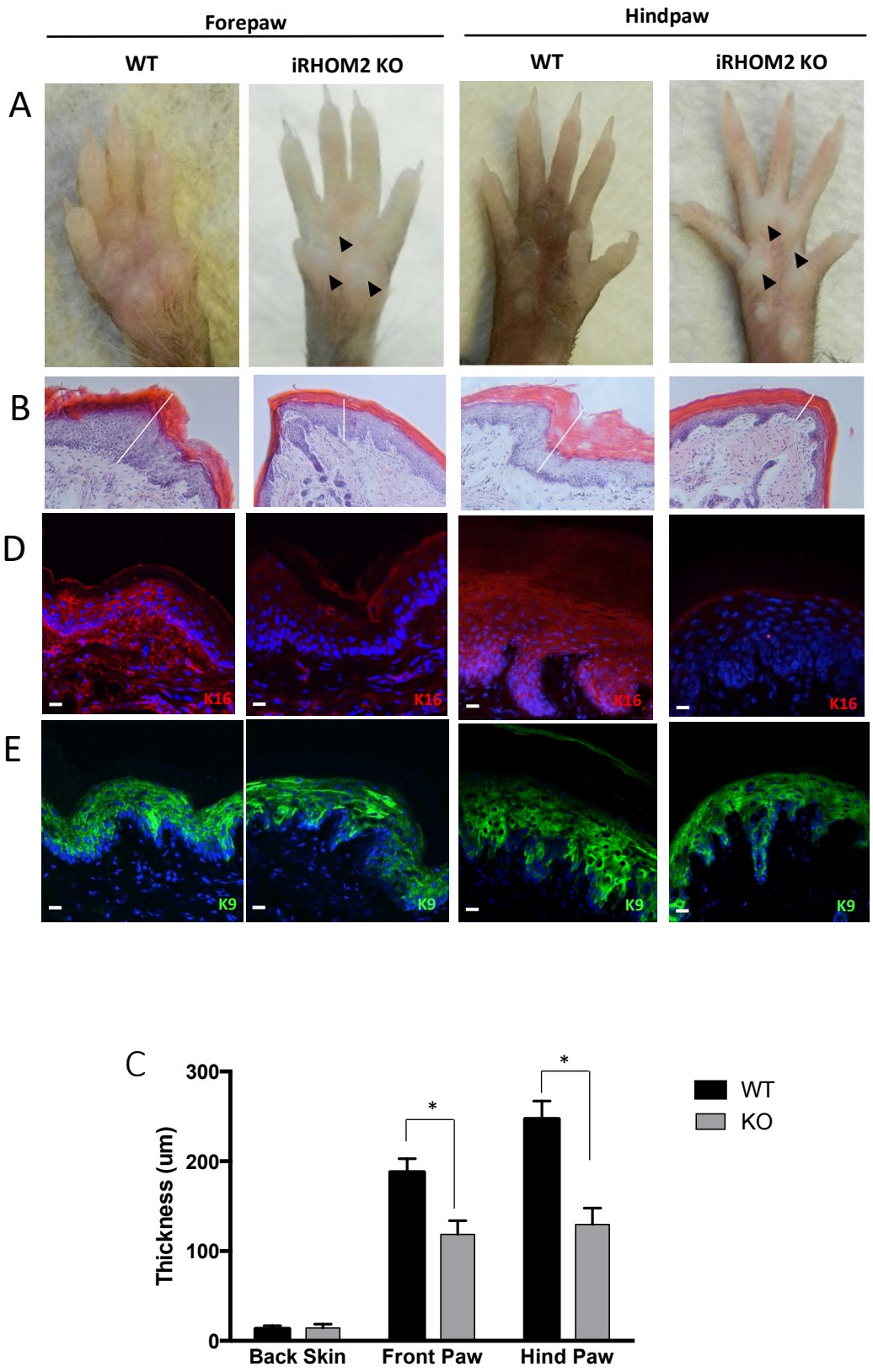

Figure 3.30 (A) The hind paws of 16-week-old irhom2 KO and irhom2 WT littermates (n=4 per genotype) were photographed, revealing pallor and diminution of the major stress-bearing paw footpads calluses (black arrowhead) in adult irhom2 KO mice.(B) Haematoxylin and eosin-stained cross-sections of hind-paw footpads showed a reduction in thickness of

the epidermis (black line) in irhom2 KO mice. Scale bars 50 µm (C) Graph depicts the mean thickness of the epidermis of hind paw and back skin from irhom2 WT and irhom2 KO mice calculated from 10 individual measurements in 5 separate cross sections from each genotype (n=3) error bars denote SD, *P<0.05. (D) Immunohistochemistry demonstrating reduction of K16 expression in paw skin sections. Scale bars: 20 µm.(E) Immunohistochemistry showing similar K9 expression in paw skin sections. Scale bars: 20 µm. Negative control Appendix Figure B.5.

In cells, iRHOM2 depletion by shRNA results in impaired proliferation and reduced Ki67 expression in 3D organotypics derived from these cells. In keeping with this, Ki67 was also reduced in the irhom2 KO mouse footpad epidermis (3.31A). In keeping with the in vitro findings of a reciprocal relationship between K16 and K6 in TOC, the footpad of irhom2 KO mice shows upregulation of K6 throughout the epidermis (3.31B). Reduced proliferation and K16 expression could result in a thinner epidermis in the knockout mice.

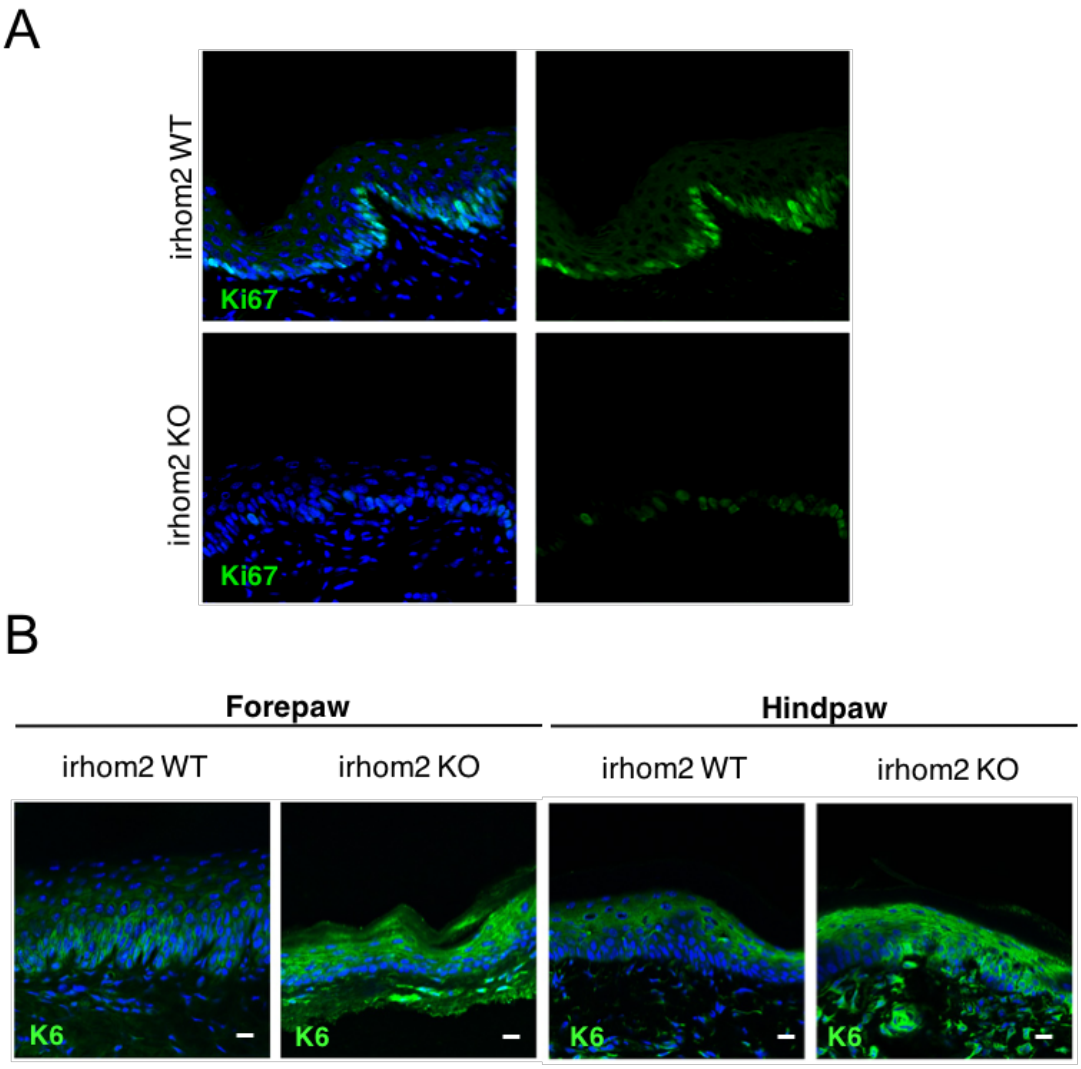

Figure 3.31(A) Confocal analysis confirming the reduction of Ki67 expression in the forepaw epidermis of irhom2 KO mice. Scale bars: 20µm. (B) Immunohistochemistry showing upregulation of K6 expression in the front paw and epidermis of irhom2 KO mice compared with irhom2 WT Scale bars: 20µm.

3.7 Results Summary

1. Identification of a novel interaction between iRHOM2 and K16
2. The interaction between iRHOM2 and K16 is increased in TOC, where K16 is upregulated
3. K16 demonstrates a perinuclear localization in TOC kerationcytes which is increased upon mechanical stress
4. K16 and its partner K6 are differentially regulated in TOC
5. TOC is associated with increased dynamicity of K16 filaments
6. iRHOM2 depletion is associated with reduced proliferation, migration and inflammation
7. iRHOM2 KO mice display a significantly thinned footpad epidermis with reduced expression of K16.

3.8 Discussion

3.8.1 Introduction

To date, very little is known about the substrates which iRHOM2 binds. Initial studies performed in *drosophila* and mice found that iRHOMs target EGF for ERAD (Zettl et al. 2001) and have been shown to regulate the substrate selectivity of protease substrates such as AREG and TGFa (N Nakagawa et al 2005, Maretzky et al 2012; Hosur et al 2014). Regulation of substrate selectivity was shown to be dependent on the N-terminal domain of iRhom2 (Maretzky et al 2012). More recently, two independent groups reported the critical role for iRHOM2 in the maturation and processing of ADAM17 in mice embryonic fibroblasts (MEFs) (Adrain et al., 2012, McIlwain et al., 2012). Both groups showed that in irhom2 KO mice, there was failure of maturation of ADAM17 and as a result stimulation with LPS failed to cause in shedding of TNFα. Beyond EGF and ADAM17 in humans, no further studies have yet shed light on novel binding partners for iRHOM2. The identification of K16 (and potentially other Type 1 keratins) as targets of iRHOM2 therefore represents a novel finding in the field.

3.8.2 Interaction between iRHOM2 and K16

Keratin 16 is a cytoskeletal protein with unique attributes contributing to its expression in specific pathological and physiological situations. It combines the distinct properties of mechanoresilience, flexibility and dynamic turnover, which are necessary in the hyperproliferative "stressed" stratified epithelia where it is expressed including the palmoplantar epidermis (Paladini and Coulombe, 1998, Paladini et al., 1996). Unlike inter-follicular skin, the ridged skin of the palmoplantar epidermis is characterized by the constitutive expression of Keratins 6, 16, 17 and uniquely, Keratin 9 (K9). In addition to its high expression in the palmoplantar epidermis, K16 can be induced in hyperproliferative states such as wounded epithelia(Paladini et al., 1996, McGowan and Coulombe, 1998) and inflammatory skin diseases(Leigh et al., 1995). Upon regeneration, wound edge epithelial cells deviate from their normal expression pattern of K10 and induce K16 within 6 hours of injury(McGowan and Coulombe, 1998, Paladini et al., 1996). K16 is also a biomarker of several cancers particularly squamous cell carcinomas (SCCs), including those originating from cervical, oesophageal and nasopharyngeal epithelia(Karantza, 2011, Moll et al., 1982, Moll, 1998). The tightly restricted expression pattern of K16 supports the notion that this particular keratin bears unique properties, however, how the dynamic regulation of K16 occurs in response to physiological and cellular stress remains poorly understood.

In this report, using human and mouse models, iRHOM2 is shown to be a novel and unexpected regulator of the cytoskeletal response to physical stress through its interaction with K16. Evidence for direct interaction between iRHOM2 and K16 comes firstly from a Yeast-2-Hybrid screen, in which K16 preys were 2 of only 22 positive interactors from a library of over 112 x 10^6 potential preys. Secondly from co-immunoprecipitation experiments performed using endogenous proteins, thirdly from PLA studies (which confirm that the two proteins are within 40nm of one another) and finally from co-localisation immunohistochemistry. The N-terminus of iRHOM2 appears to be functionally important, not only is it the site of all reported TOC-causing mutations in 5 separate large pedigrees, but it is also the domain which interacts with K16. In the absence of the N-terminus, iRHOM2 is no longer able to bind K16. Maretzky et al 2012 also showed similarly that regulation of the substrate selectivity of EGFR in mice is dependent on the N-terminus of iRHOM2.

The positive keratin prey fragments highlighted by the Yeast-2-hybrid screen were used to ascertain a potential site of interaction between iRHOM2 and K16. All 9 prey fragments from K10, K14 and K16 showed sequence overlap directly corresponding to their highly homologous Coil 1B domain. Interestingly, disease-causing mutations in the Coil 1B domain have not been reported to date although several mutations have been ascribed to the other coiled domains including Coil 1A, 2A and 2B, hinting at a functionally important role for this particular region. Within the field of keratin biology, several papers have highlighted the central role for Coil 1B in heterodimerisation between Type I and Type II keratins(Bernot et al., 2005, Wawersik et al., 1997, Wu et al., 2000). In vivo, keratin polymerisation is initiated through the formation of heterodimers involving Type I and II intermediate filament proteins. A small hydrophobic "stripe" located within the Coil 1B domain appears to be key in mediating heterodimerisation (Bernot et al., 2005). Hydrophobic patches on the surface of proteins are thermodynamically unfavourable in aqueous environments and their presence often indicates a region of protein-protein or protein-lipid interaction, making this domain effectively a "docking-site" for interacting proteins (Bernot er al., 2005). Additionally, the Keratin Coil 1B domain displays a 13-residue trigger motif required for stability of their heterodimers. Side directed mutagenesis of critical residues within this trigger motif has been shown to cause near total collapse of the keratin filament network around the nucleus and a reduced ability to form heterodimers (Wu et al., 2000). In TOC we see increased interaction between iRHOM2 and K16 compared with control keratinocytes in co-immunoprecipitation experiments, further quantified by PLA. The increased interaction beween K16 and iRHOM2, likely to be through the coil 1B domain, appears to occur at the expense of binding with its known partner, K6. PLA between K6 and K16 is significantly downregulated in TOC keratinocytes. It is tempting to speculate that greater binding between iRHOM2 and K16 in TOC keratinocytes could physically impair K16 interacting with its partner, K6. This points to an unusual reciprocal regulation between K16 and K6 in TOC. In support of this, shiRHOM2 in TOC keratinocytes results in restoration of K6 expression demonstrated by western blots and 3D organotypic cultures. This occurs despite a reduction in K16, providing further evidence for an "uncoupling" between K6 and K16 in TOC K6 expression appears to be globally reduced in TOC keratinocytes, both at protein level (western blotting and immunohistochemistry) and also at mRNA level (qPCR). It is possible that K6 is less stable as a monomer and may therefore be targeted for degradation. Presumably, a negative feedback loop exists when K6 does not bind to K16, to prevent unstable K6 monomer accumulation in the cytoplasm, however how this occurs this remains

to be explored. Uncoupling of K16 and K6 expression is highly unusual and challenges conventional dogma. Although rarely reported, one circumstance in which K16 is expressed without K6 is in the palmoplantar epidermis. Here, K16 is prominently expressed in the basal layer whereas K6 expression is more restricted, and more similar in distribution to K17 (Swensson et al., 1998). Similarly, transgenic mice lacking K9 develop marked hyperkeratotic thickening and callus formation of their paws in which K16 is highly upregulated in the footpad and interfootpad skin whereas K6 upregulation was restricted to the footpads alone (Fu et al., 2014). Suggesting that surprisingly, differential regulation of K16 and K6 may be more prevalent than previously considered. It may be that in TOC, the interfollicular and potentially oesophageal epithelium adopts a more "palmoplantar" keratin signature, which in turn favours hyperproliferation.

3.8.3 Perinculear Reorganisation of K16 Filaments

Wound edge keratinocytes are poised to undergo proliferation and migration and thus allow tissue regeneration. K16 is rapidly expressed in response to tissue injury and, ultrastructurally, has been shown to adopt a perinuclear arrangement of filaments which proceeds the onset of migratory behaviour (Paladini et al.,1996). Further studies have shown that this delocalization is linked to fragmentation of rigid keratin filaments from the cell periphery, resulting in cytoplasmic "softening", thereby increasing cell plasticity, subsequently facilitating proliferation, migration (Beil et al., 2003, Busch et al., 2012, Rolli et al., 2010). The improved viscoelastic properties resulting from keratin filament reorganisation have also been linked to increased invasion in cancer cells. In particular, Sphingosylphosphorylcholine (SPC), a naturally occurring bioactive lipid present in high density lipoprotein particles found in the blood and malignant ascites of patients with ovarian cancer has been shown to induce perinuclear reorganisation of keratin 8-18 filament networks. Consequently, SPC stimulates migration of cells through pores of limited side and the authors conclude that the metastasis-inducing properties of SPC could result from the high degree of elasticity it causes, enabling cells to squeeze through membranous pores during metastasis (Beil et al., 2003). Intriguingly, iRHOM2 has also been linked to ovarian cancer (Wojnarowicz et al., 2012), however this may be due to loss of heterozygosity at the 17q25 locus. In TOC not only is K16 upregulated, but the filament network itself appears to adopt a different pattern. TOC cells more frequently display a perinculear localisation of K16, even in the absence of mechanical stress. This pattern is further enhanced by subjecting TOC

cells to mechanical stress for four hours. Overexpression of either WT or TOC-mutant iRHOM2 has a similar effect on unstretched control keratinocytes, and results in striking perinculear filament reorganisation following mechanical stress. PLA also confirms binding between iRHOM2-GFP and K16 in the perinculear regions, suggesting that K16 filament reorganisation is mediated by interaction with iRHOM2. How does iRHOM2 cause K16 filament reorganisation? Although this question remains to be answered fully, it is possible to hypothesise that reduced binding between K16 and K6 could be explanatory. As heterodimers, K6 "anchors" K16 to desmosomal cell-cell adhesion structures, stabilising the intermediate filament network which has a branch-like appearance (Kouklis et al., 1994). By contrast, when K6 is down regulated in TOC, K16 is effectively "released" from its tether, and can reorganise itself around the nucleus. Our group have previously shown that desmosomes in TOC skin have an "immature" appearance, lacking the characteristic electron dense midline seen in normal skin (Brooke et al., 2014). In light of the findings presented here, it is possible that this could partly be due to alterations in the dynamics between desmosomes and the keratin intermediate filament network.

3.8.4 iRHOM2 and K16 Filament Dynamicity

Keratin filaments are highly dynamic structures and cycle through stages of assembly and disassembly in a context specific manner. Filament remodelling and turnover are key factors which determine cell growth and turnover (Windoffer et al., 2011, Kolsch et al., 2010). Interference with Keratin filament dynamics in human disease and transgenic mice leads to reduced resilience of epithelia to mechanical and other challenges. One dramatic example is mutation in K5 or K14 underlying Epidermolyis Bullosa which results in severe tissue fragility from birth (Ishida-Yamamoto et al., 1991).

In TOC, we observe enhanced filament turnover demonstrated by rapid recovery from treatment with Okadaic acid. K16 filaments in TOC cells reform within 4 hours after treatment whereas control keratinocytes still show only partial recovery 24 hours following treatment. It is pertinent to note that K16 turnover has been shown to almost double in the absence of K6 (Bernot et al., 2005) and this could explain K16 filament dynamicity in TOC. In conjunction with perinuclear localisation of K16 in TOC, enhanced filament dynamicity would favour the upregulated proliferation and migration observed in TOC keratinocytes compared with controls. By contrast, shiRHOM2 impairs proliferation and migration in both control

and TOC keratinocytes. This could partly be because shiRHOM2 results in reduced K16 in both cell lines. After scratch wounding, abundant keratin filament precursors align at the leading edge of migrating cells, thereby extending the intermediate filament cytoskeleton towards the "wound". Keratin filament particles reorganise and elongate to facilitate changes in cell shape required for motility(Windoffer et al., 2011). It is therefore conceivable that, when K16, the major wound-induced keratin is downregulated, cell migration is impaired.

3.8.5 A Novel Cutaneous Phenotype in irhom2 KO Mice

The irhom2 KO mice displays a clinical phenotype which has not been previously reported in the literature. The presence of "thinned" footpads is somewhat unusual. It would be reasonable to suggest that the "thinned" footpad skin occurs as a result of reduced proliferation and K16 expression throughout the epidermis in the absence of iRhom2. Quite remarkably, K16 KO mice display and altogether opposing phenotype. By 8 weeks of age, K16-KO mice are disabled by painful callous development and palmoplantar hyperkeratosis which demonstrates several hallmarks of inflammatory activation. Inflammatory cytokines, "DAMPs" and "alarmins" are all activated and histologically, there is an influx of inflammatory cells particularly macrophages. The pain resulting from the inflammatory PPK is so severe that mice limp and their mobility is restricted (Lessard et al., 2012). *Irhom2* KO mice show no such features, there is no evidence of inflammation clinically or histologically and quite the opposite of PPK, their footpads are thinner than WT littermates. How can these two phenotypes both linked to reduced K16 expression be reconciled? The answer could lie in ADAM17, the most well-established target of iRHOM2 whose major function is the shedding of inflammatory cytokines. ADAM17 activity is reduced in irhom2 KO mice and thus there is impaired shedding of inflammatory cytokines including TNFα, Amphiregulin and IL6. In this report, shiRHOM2 in both control and TOC human keratinocytes reduces ADAM17 activity and significantly hinders TNFα shedding in response to PMA stimulation. Impaired ADAM17 activity in the irhom2 KO mouse footpad epidermis could exert a protective effect, preventing inflammation and hyperkeratosis in response to physical stress. Potentially, this observation could be significant as therapeutic options in the treatment of PPKs are extremely limited. PPK's can have a profound impact on patients' quality of life, rendering them immobile due to severe pain. Topically formulated specific iRhom2 inhibitors or more specific tissue silencing using intralesional siRNA may be future therapeutic options.

ADAM17 inhibitors have been in development for many years, however concerns about side-effects have been the primary issue, due to widespread tissue expression. Oral or injectable therapies targeting iRhom2 may be a more appealing alternative, as it is more likely to be a skin-specific therapy. Therefore, although the wider role for ADAM17 in inflammatory PPK's remains to be explored, it is likely that further study in this area could prove insightful.

The TOC phenotype in humans diametrically opposes that observed in irhom2 KO mice. It is likely that The combination of high K16 expression in response to mechanical stress and increased cell turnover in the presence of upregulated iRHOM2 activity provide a possible explanation for the presence of palmoplantar keratoderma in TOC. This model could also explain the diminished K16 expression and thinner footpads in irhom2 KO mice. Taken together, the evidence suggests that iRHOM2 and its regulation of K16 play a key role in the dynamic response of the footpad in humans and mice to physical stress.

3.8.6 TOC and PC-1

Looking at the remarkable clinical overlap between the phenotypes of TOC and PC-1 caused by K16 mutation, this functional relationship is in some ways unsurprising. Both conditions are inherited as autosomal dominant traits with high penetrance. They similarly present with marked hyperkeratosis of the plantar, and to a lesser extent, palmar epidermis following weightbearing, I,e. when children begin walking. Typically in TOC this is in early childhood however it can manifest earlier in PC-1. Anecdotally both groups of patients report a marked improvement in their keratoderma following extended periods of rest when walking is restricted e.g. following surgery/childbirth. This implies that the presence of the keratoderma is linked to physical "stress". Both groups can also develop follicular occlusion resulting in steatocystomas (sebum containing dermal cysts) which may be because K16 (amongst other keratins) are expressed within the lumen of sebaceous glands and increased K16 could result in occlusion. Oral leukokeratosis is present in both conditions and is hypothesized to occur as a result of repeated oral trauma due to eating. However, PC-1 has never been linked to oesophageal cancer unlike TOC and this is the key difference between the two conditions.

3.8.7 iRHOM2-K16 Interaction and Disease

In addition to its established role in wound-healing K16 is pathologically expressed in a variety of disease states including squamous cell carcinomas, irrespective of their site of origin and including those arising from the oesophagus, nasopharynx and cervix (Pan X et al, 2013, Karantza et al., 2011). As such it is often referred to as "biomarker" of SCC. In the skin, K16 expression is also used to delineate tumour islands in cutaneous squamous cell carcinomas(Lai et al., 2016). Its expression has also been linked to inflammatory dermatoses, particularly Psoriasis (Leigh et al., 1995). With this in mind, it is possible that there may be a broader significance for the role of iRHOM2 in the pathophysiology of these disorders which remains to be explored.

In TOC, the contribution of iRHOM2-K16 to the development of oesophageal cancer has yet to be studied however, it is the focus of ongoing investigation within the group. The upregulated shedding of proinflammatory and pro-proliferative cytokines by the iRHOM2-ADAM17 pathway is likely to be the major contributor to the development of neoplasia. However, preliminary data points to increased K16 expression in precursor oesophageal lesions in TOC (personal communication: Lisa McGinty, Kelsell Group). This is an area that warrants further study as it could yield insight into the mechanism underlying both TOC and sporadic OSCC.

3.8.8 Conclusions

The data presented here point to a novel and hitherto unidentified role for iRHOM2 in regulating the wound-healing and disease associated keratin, K16. The findings demonstrate direct interaction between iRHOM2 and K16 and show synchronicity between the expression pattern of these two proteins; shRNA mediated knock-down of iRHOM2 in human keratinocytes or *irhom2* $^{-/-}$ in mouse paw skin is associated with depleted K16, and reciprocally, high iRHOM2 activity in TOC is associated with increased K16.

By orchestrating the remodelling and turnover of K16, and uncoupling it from its binding partner K6, iRHOM2 acts as a key regulator of the epithelial response to physical stress. These findings contribute to our understanding of the molecular mechanisms underlying hyperproliferation of the palmoplantar epidermis at sites of high physical stress in both physiological and disease states and how this "stress" keratin, implicated in wound healing, inflammation and cancer, is regulated Thus, pharmacological modulation of iRHOM2 by targeting two stress-response proteins, K16 and ADAM17, could provide a specific therapeutic strategy in the treatment of PPK's, inflammatory epithelial disease and neoplasia.

3.8.9 Further work

The focus of the work presented in this report is the interaction between iRHOM2 and K16, however, the yeast 2 hybrid screen highlighted two additional keratins, K10 and K14 as potential binding partners. K10 and K14 are highly expressed in the interfollicular epidermis and the relevance of this potential interaction would be interesting to study further. Co-immunoprecipitation, colocalisation, and PLA studies could be performed to confirm interactions between iRHOM2 and K10/K14. Immunostaining of TOC and normal skin could also be performed. Furthermore, their binding partners including K1 and K5 should also be assessed. It might be that the effect of iRHOM2 on these keratins differs from K16. K10 is downregulated following injury, where there is a switch from K1/10 to K6/K16. Possibly, iRHOM2 may somehow be regulating this switch. In vivo validation could be performed on irhom2 KO mice. It may also be interesting to examine the expression and activity of iRHOM2 in EBS caused by mutations in K14 or K5 to see if it plays a role in the development of tissue fragility. Immunohistochemical staining and PCR of EBS skin could be performed. The impact of EBS-causing mutations on iRHOM2 binding could also be assessed using Co-immunoprecipitation and Proximity Ligation assay experiments.

More detailed study could be undertaken to further characterise the interaction between iRHOM2 and K16. These could include site-directed mutagenesis and subsequent Co-IP of tagged fragments of irhom2 and K16 to locate the precise binding domain. Live cell imaging of TOC and control keratinocytes could also be performed to more formally quantify the rate of filament turnover. The qPCR findings showing reduced K6 expression in TOC also warrants

further study. Perhaps examining transcription factors known to regulate keratin gene expression including c-Jun and fos could be performed.

As TOC and PC-1 share several phenotypic similarities, iRHOM2 expression at protein and mRNA level in skin samples from PC-1 patients could be performed. It may be that increased iRHOM2 plays a role in the hyperkeratotic skin phenotype observed in these patients. In a similar vein, the broader role of iRHOM2 in other PPK's such as diffuse NEPPK due to Aquaporin 5 mutations, striate PPK's due to desmoplakin mutations and DNEPPK due to K9 mutations could also be studied. It is possible that upregulated iRHOM2 activity is a common feature in the skin of other PPK's. Skin biopsies obtained from patients could be immunostained for iRHOM2 and protein extracted for western blotting. qPCR of mRNA could also be performed. Upregulated iRHOM2, K16 and ADAM17 activity could point to a shared pathophysiolocal mechanism in the formation of PPK.

As K16 has an established role in Psoriasis, this could potentially be an exciting area for further study. The psoriatic epidermis shares similarities with TOC skin, namely hyperproliferation, upregulated inflammation, increased immune cell infiltrate and high K16 expression. Like TOC, psoriasis is also considered similar to exaggerated wound healing. Preliminary data from our group has shown increased expression of iRHOM2, ADAM17 and K16 in Psoriasis RNA sequencing data sets (Matthew Brooke/Professor Nick Reynolds). More detailed study using psoriasis cell lines and patient skin biopsies would be necessary to properly evaluate the contribution of iRHOM2 to the hyperproliferative inflammatory phenotype.

Chapter 4

Loss of function Desmoplakin I and II mutations underlie dominant Arrhythmogenic Cardiomyopathy with a hair and skin phenotype

4.1 Background

4.1.1 Clinical and Genetic Heterogeneity of Arrhythmogenic Cardiomyopathy (AC) due to DSP mutations

Recessively or dominantly inherited mutations in Desmoplakin (DSP) are associated with considerable phenotypic variability. Some mutations result in cardiocutaneous syndromes, others in non-syndromic skin-limited involvement and some forms show cardiac features only. Although this mostly due to the precise location of the mutation, there can also be quite marked variability between individuals from the same family, carrying the same mutation (Sen-Chowdhury et al., 2005, Brooke et al., 2012).

4.1.2 Skin Phenotypes Linked to DSP

Armstrong et al. (Armstrong et al., 1999), reported a large kindred in whom multiple members developed a striate PPK phenotype in the first or early second decade of life revealed a missense mutation in the N-terminal region of DSP resulting in a premature stop codon.

Affected individuals presented with linear thickening along the flexor aspects of the fingers and pressure bearing areas of the soles, exacerbated by use. Hair abnormalities were not detected. This paper did not outline whether cardiac investigations were undertaken, however they do not mention the co-existence of AC and suggest a skin-restricted phenotype. Histologically, the epidermis showed widened intracellular spaces and clumping of the keratin filaments, with loss of connection to the desmosomes. However, it remains a possibility that, as this paper was published before *DSP* was linked to AC and cardiocutaneous disease (Norgett et al., 2000), that specific diagnostic investigations for AC were not undertaken.

Lethal acantholytic epidermolysis bullosa has been reported in a neonate presenting as complete alopecia, neonatal teeth, nail loss, extensive skin erosion and neonatal death. The infant had compound heterozygosity for a recessive nonsense and frameshift *DSP* mutation.

which resulted in near total deletion of the intermediate filament binding sites in the DSP tail domain (Jonkman et al., 2005).

More recently, a recessively inherited missense mutation in *DSP* was linked to "SAM Syndrome" (Severe dermatitis, multiple allergies and metabolic wasting)(McAleer et al., 2015). The resulting amino acid substitution (His586Pro) contributes to the histological features of widened intercellular spaces and defective skin barrier formation, with marked attenuation of cornified envelopes, a virtual absence of corneodesmosomes and abnormalities of the post-secretory maturation and organisation of secreted lamellar body contents. Impaired barrier function would contribute to the formation of severe dermatitis, similar to the pathophysiology of atopic eczema. Interestingly, cardiac involvement was not a reported feature in this patient.

A novel Erythrokeratodermia associated with cardiomyopathy syndrome has also been linked to *DSP* mutations in 3 children (Boyden et al., 2016). The affected individuals were noted to have sparse coarse hair at birth and a persistent pruritic erythrokeratodermia, unreponsive to topical or systemic immunomodulatory agents. The children also demonstrated failure to thrive and marked onychodystrophy. Exome sequencing located three novel, tightly clustered, de novo missense mutations in *DSP* as the underlying cause of this syndrome. The resulting substitution with a proline was suggested to disrupt the conserved a-helical structure of the spectrin-repeat (SR6) at this position. The mutation results in mis-localisation of DSP at the intercellular junction, with formation of focal aggregates. Overexpression of the disease causing mutation in primary human keratinocytes allowed the quanitifcation of Cx43 localisation, which was found to be reduced by 80% at the cell surface membrane (Gutstein et al., 2001).

4.2 RESULTS

4.2.1 Deep Clinical Phenotype of DSP Mutation Carriers and Their Families

Due to the specialist nature of monitoring and treatment, patients with AC are managed at tertiary referral centres with specific expertise. The patients who participated in this study were recruited from a cohort at the The Heart Hospital (originally at UCLH, later, The Heart Hospital at Bart's and the London). At the Heart Hospital, a cardiomyopathy clinic runs weekly, some of the patients who attend this clinic have a confirmed diagnosis of AC. For the purpose of this study, patients with clinically confirmed AC, with autosomal dominantly inherited mutations in the gene encoding *DSP* were selected from this clinic for further evaluation. 6 families (38 patients) were included in the study and underwent cardiac and cutaneous evaluation as well as a skin biopsy (Figure 4.1). Patients were invited to participate in the research project with informed written consent. Clinical photographs were documented. Patients were selected to participate in the study if they had a frameshift or truncating mutation in *DSP* as the impact of the functional effect of missense mutations is considered more complex to determine.

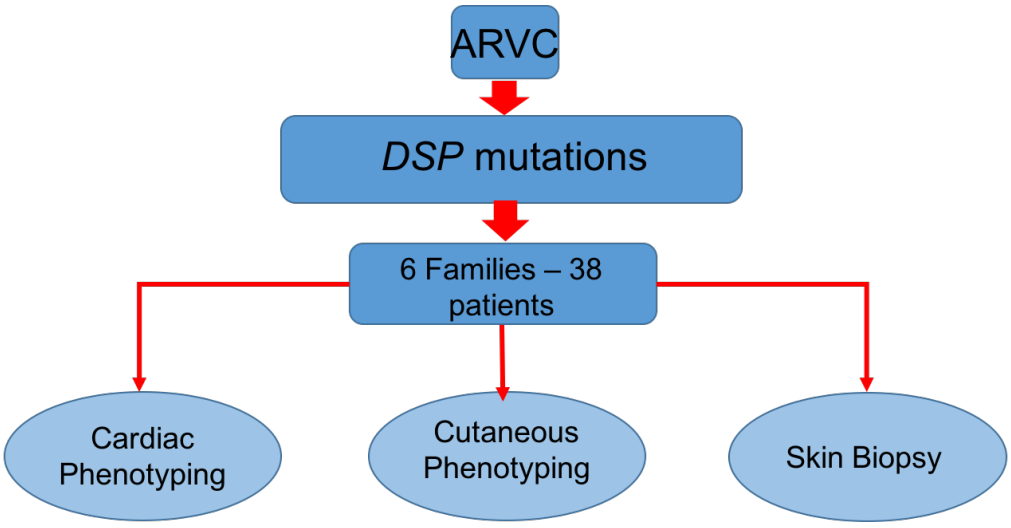

Figure 4.1 Project plan; ARVC/AC Patients with dominantly inherited mutations in *DSP* were selected for deep clinical and genetic phenotyping as well as a skin biopsy from non-lesional skin.

4.2.2. Cutaneous Phenotyping

Family 1 Q273.fs

The 52 year old proband of this particular family presented with Ventricular Fibrillation at rest, in fact, whilst watching television. Following this near-fatal event, clinical evaluation and genetic screening of known ARVC genes identified the presence of a frameshift mutation at p.Q273fs. This mutation is the most proximal of all the patients included in this study. Clinical examination of the patient revealed wavy/kinky hair and linear hyperkeratosis of the forefoot, most prominent between the great toe and second toe. The patient was a physiotherapist and commented that she had suffered from severe dryness of her hands which required regular use of emollients during the winter months due to cracking and fissuring. She also developed marked thickening and hyperkeratosis affecting the heels which developed in adulthood, bilaterally which she scraped and moisturized to keep under control. The patient had an ICD in situ following the VF episode and had received shocks from the device. Her cardiac echo showed a mildly dilated left ventricle, with ejection fraction of 45% and an aneurysmal left apex. After the proband's initial diagnosis, genetic family screening was performed which highlighted 7 further *DSP* mutation carriers including the patients son (3-II) (Figure 4.2) . Clinical examination of the patient's mother (1-II) showed soft curly hair as well as a prominent striate and focal keratoderma (Figure 4.2), with gross thickening and fissuring affecting the heels bilaterally. This individual commented that her feet had caused her "years of trouble" including numerous visits to the GP for topical treatment to relieve the cracking and fissuring. Both mother(1-II) and daughter(2-II) commented that they had "ugly feet". The proband's brother(2-V) was also examined, although he now keeps his hair short, he had wavy hair as a child. Examination of his skin revealed milder linear thickening between the great toe and second toe and to a lesser extent, hyperkeratosis at sites of friction and pressure over the lateral aspects of the forefoot. Clinically, his keratoderma was less marked than in the other two mutations carriers examined. Unfortunately, the sister of the proband (2-III) could not be examined as she now lives in Canada, however through email contact, it was possible to ascertain that she had very curly hair until the menopause, however it was much less curly now. The proband had two children, one of which also carried the mutation (3-II). The affected son also had kinky/wavy hair, whereas the unaffected daughter(3-I) had straight hair. The patients husband(2-I) had straight hair. Patient 2-III's children were both found to be mutation carriers and both have very curly/frizzy hair, however, it is important to note that

the children's father, of Italian descent, also has curly hair. 2-III and both her children (3-III and 3-IV) also have/had moderate eczema requiring the care of a dermatologist during childhood. Patient 2-V has one child who carries the mutation, who also has curly hair, however his unaffected son does not. His partner has straight hair. In summary, in this particular family, 5/8 mutation carriers have curly hair, the remaining 3/8 carriers have wavy/kinky hair. The unaffected offspring (2/2) have straight hair. Overall it appears that there is segregation of the curly/wavy hair phenotype with mutation carrier status in this family.

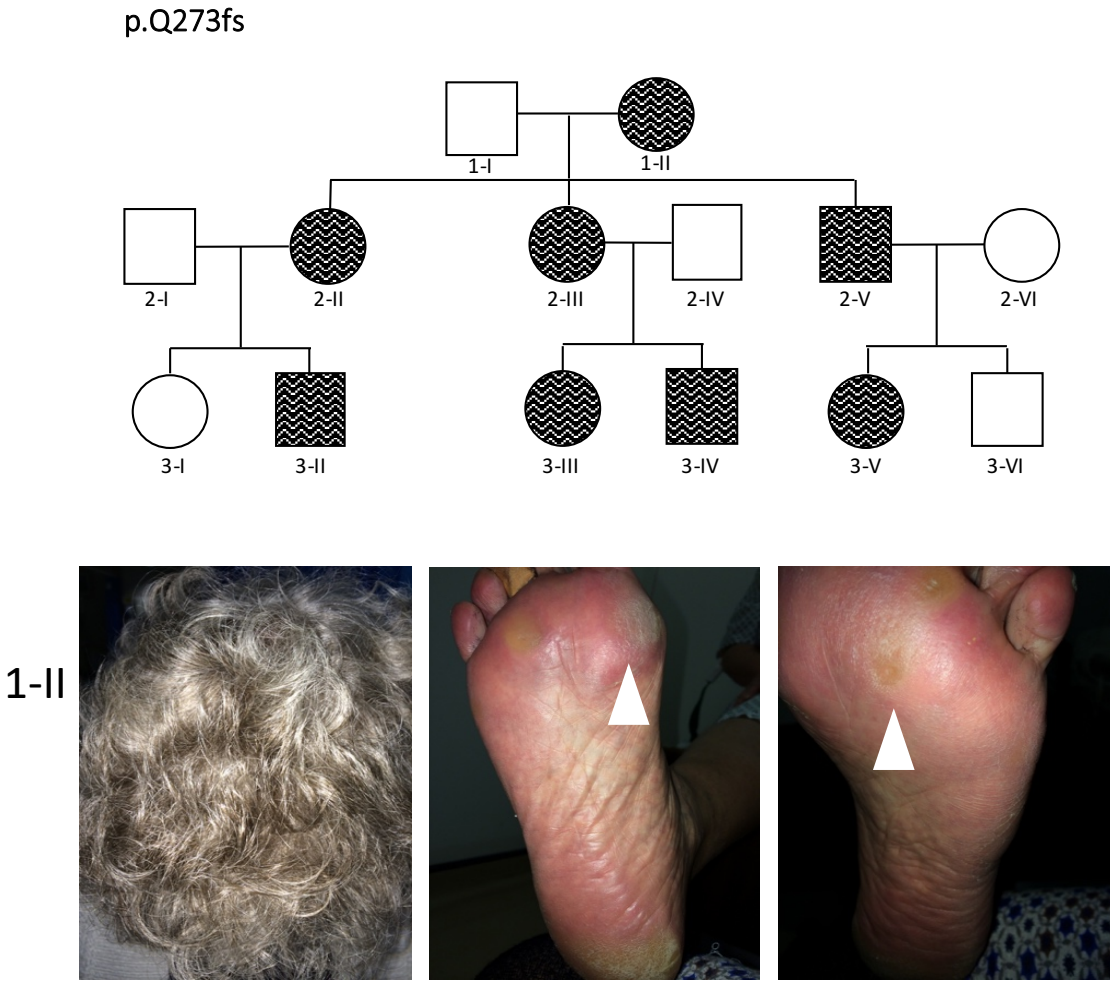

Figure 4.2 Pedigree and clinical photographs of Family 1 (p.Q273.fs). Symbols: circle – female; square – male; Black – mutation carrier, wavy line – curly hair; diagonal line – deceased. Co-segregation of the hair phenotype with the genotype can be observed in all members of this family. Patient 1-II demonstrates the typical curly hair phenotype. White arrowheads mark plantar focal keratoderma with hyperkeratosis and callous formation

Family 2 p.L585fs

The proband in this family (2a-I) died of Sudden Cardiac Death (SCD) aged 22 whilst playing sport. His brother (2a-II) presented on two occasions to A&E at the age of 18 years old with Ventricular Tachycardia whilst playing football that required cardioversion. Following this, and the death of his brother, a diagnosis of AC was made and he was identified to have a causative frameshift mutation in *DSP* at position L585, on screening of a known panel ARVC genes. The family tree from this pedigree is somewhat unclear, and the three families who participated in this project are not known to each other but were located through extensive family screening and as such can be considered distant relatives (Figure 4.3). The full details of the original family trees were no longer available in the current records at the time of writing.

Patient 2a-II was examined during a routine clinic appointment for AC follow up. On examination, the patient had curly and slightly frizzy hair. Examination of the palms was unremarkable, however his feet had caused him trouble for many years. Although previously undiagnosed, examination findings were in keeping with a striate keratoderma affecting the soles of both feet. His heels also showed hyperkeratosis and thickening (Figure 4.3). His keratoderma required him to regularly shave hard skin from his soles. On further questioning he also explained that his brother, the index case, also had very thick hard skin on both feet. Their mother, also a *DSP* mutation carrier, had curly hair but he was unaware of whether her feet were similarly affected. She died of breast cancer in her 50's. 2a-II has a daughter who has undergone genetic screening and was found not to carry the mutation, she was described as having straight hair like her mother. Within this large pedigree was another family who participated in this research through phone consultation. Both mutations carriers, 1b-II (72 years old) and 2a-I (43 years old) had been identified through family screening. Both mother and son had rough curly hair that they commented grew slowly. 2a-I also had suffered from a marked keratoderma for several years that had required specialist care by Dermatology. His mother did not have similar keratoderma of her hands and feet but did have dry skin. His sister (2b-II) had straight silky hair.

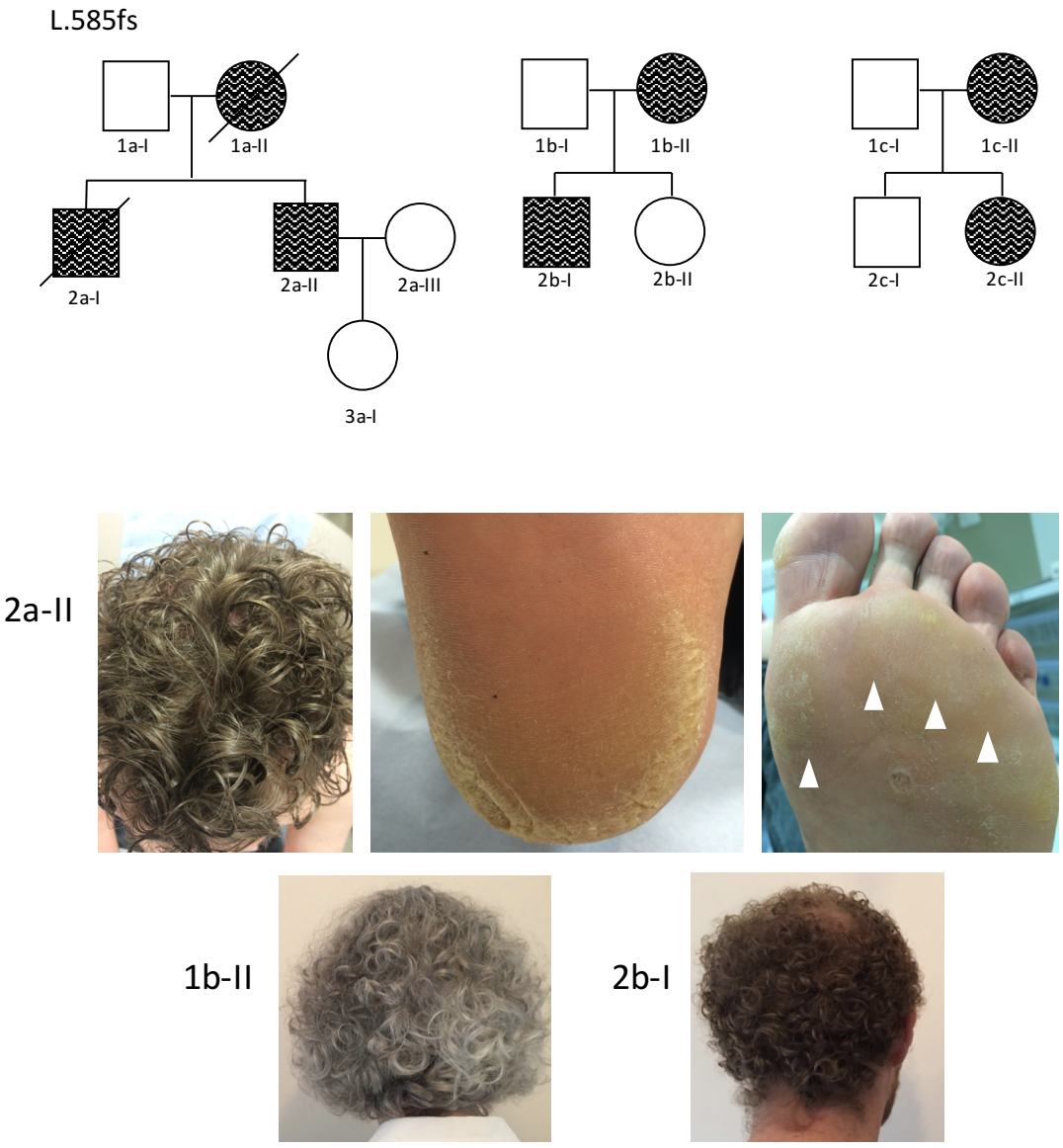

Figure 4.3 Pedigree and clinical photographs of family, black circles/squares with wavy lines indicate curly haired mutation carriers 2 L.585fs. Co-segregation of the hair phenotype with the genotype can be observed in all members of this family. Patient 2a-II demonstrates the curly hair phenotype, heel hyperkeratosis and fissuring and a focal and striate keratoderma (white arrowheads) Patients 1b-II and 2b-I also had tightly curled hair.

Another nuclear family within this pedigree also showed similar segregation of the curly hair phenotype with mutation carrier status. 1c-I, a 62 year old female also had very curly hair and clinical features of a mild striate keratoderma. Her daughter, also a mutation carrier had similar curly hair but lacked palmoplantar involvement. Her brother, who had also been

tested for the mutation had straight hair that differed markedly from the two mutation carriers.

In these 7 *DSP* mutation carriers, we observe the curly hair phenotype shows 100% segregation with disease.

Family 3 p.T922s.fs

This patient is the index case in her family and presented with recurrent palpitations and pre-syncopal episodes. Her hair was tightly curled (Figure 4.4) and she had a striate keratoderma affecting both her feet. Her sister (non-mutation carrier) was unaffected. The parents of this patient lived in New Zealand and had not undergone genetic testing.

Figure 4.4: The proband in this family had tightly curled hair.

Family 4 p.s1015fs

The index case in this large pedigree died of sudden cardiac death in her early 20's whilst playing badminton. Prior to this she had not exhibited any features of AC. Subsequent family screening found 7 further patients who carried the disease-causing mutation p.S1015fs (Figure 4.5). Two sisters 2-II (56yrs) and 2-IV (53yrs) carry the mutation and have tightly curled frizzy hair. None of their other siblings had similar hair. In fact, the sisters had already remarked how those family members who carried the mutation also all had curly hair. Both sisters suffered from painful thickened skin affecting both feet and clinical examination revealed hyperkeratosis and fissuring of the heels bilaterally. 2-IV was a podiatrist and had always been aware that the thickening affecting her feet was unusual, differing from most of the patients she saw. On examination she also had eczematous patches on her upper arm and back which she explained typically developed exacerbated after immersion in water (swimming, baths). She also had to be cautious not to take prolonged showers as this could cause similar lesions, particularly on the upper back. 3-II (31yrs) also had remarkably curly

and frizzy hair whilst his two siblings who did not carry the mutation had straight hair. Clinical examination of a male cousin of the index case (2X, 61 yrs) who also displayed the striking curly phenotype did not show clear evidence of a palmoplantar keratoderma. The patients son (3-VIII) who also carried the mutation had frizzy hair whilst his unaffected siblings did not. In this family we also observe complete segregation of the curly/frizzy hair phenotype with mutation carrier status. Non-carrier offspring do not have curly/frizzy or wavy hair in this family. 2-II and 2-IV also displayed signs of a keratoderma.

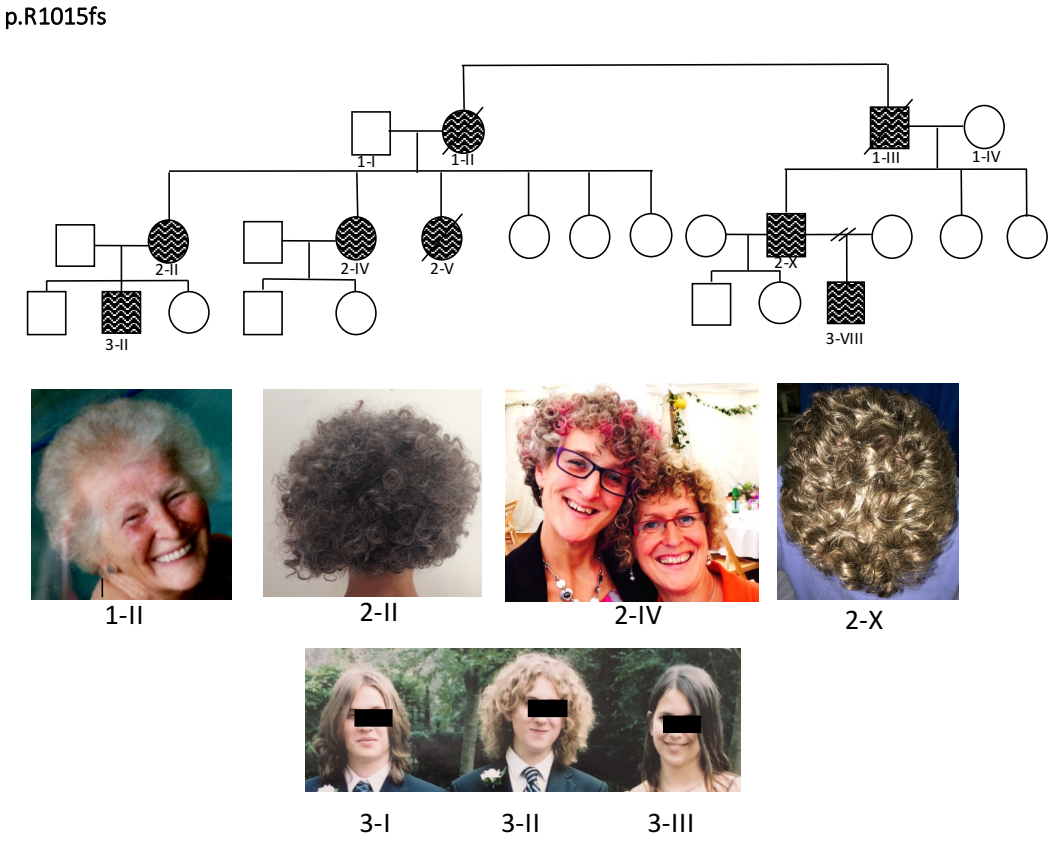

Figure 4.5 Pedigree and clinical phenotype of Family 4 p.1015fs All 8 mutations carriers in this family presented with a curly hair phenotype. Clinical photographs of *DSP* mutation carrying family members exhibit the characteristic tight curls. Patient 3-II has a strikingly different hair phenotype to his two unaffected siblings (3-I and 3-III)

Family 5 p.R1113X

The index case in this family, 2-II died of sudden cardiac death in her early 30's. A stop mutation pR1113X was identified on screening a panel of known ARVC genes. Following her death her family was screened for the causative stop mutation. Her two sons, 3-I and 3-II were found to carry the mutation. Examination of 3-II, a 24 year old male, showed extremely curly, frizzy hair which he confirmed was similar to his mothers hair. He had recently begun working in a warehouse which involved heavy lifting and had since developed subtle linear hyperkeratosis along the palmar aspect of his fingers. He also had focal hyperkeratosis on his toes, which is an unusual site to occur and is suggestive of a pathological keratoderma (Figure 4.6). Although his brother (3-I) was not examined, he was contacted by phone and sent photographs of his hair, which was less curly than his brothers but still showed a similar phenotypic appearance. Images of his feet were not obtained. Their sister (3-III), who did not carry the mutation, had straight hair. The father and both sisters of the index case all shared the same curly/frizzy hair phenotype. Both sisters also showed features of a striate keratoderma and thickened fissure heels (Figure 4.6), as did their father to a lesser extent. Both of the mutation carrier daughters of 2V, shared the curly hair phenotype, and one of them also had gross thickening between the great and second toe (3-VI) whereas their non-carrier cousins 3-IV and 3-V did not. In this family, 8 of the affected mutation carriers had curly/frizzy hairs whereas all non-carrier offspring do not. Furthermore, five of the carriers showed overt features of a palmoplantar keratoderma. It is pertinent to note that the palmar keratoderma in patient 3-II was brought on by increased activity – since he had started lifting heavy boxes, supporting the hypothesis that "stress" is an important aetiological factor in the presence of skin involvement.

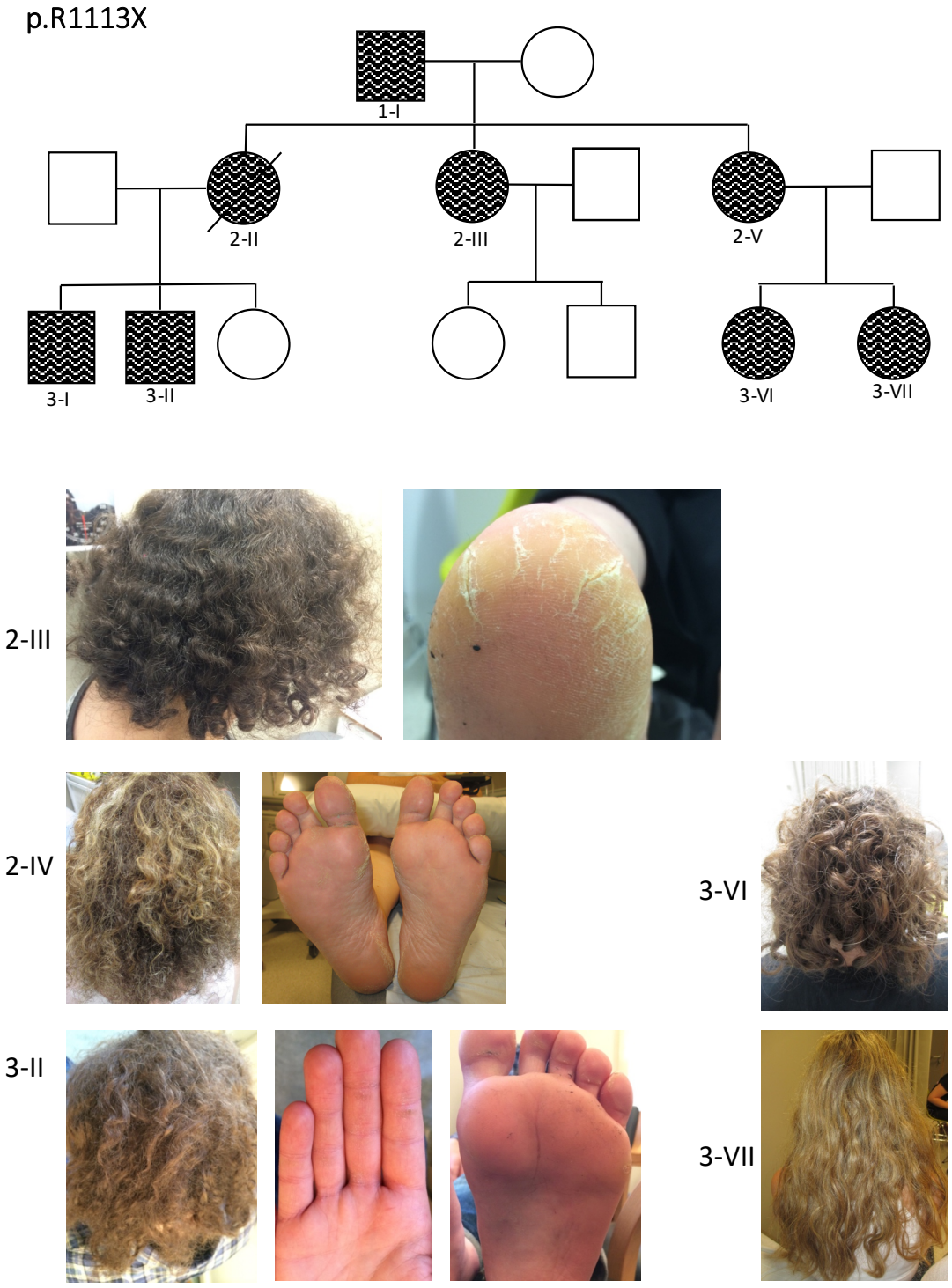

Figure 4.6. Pedigree and clinical photographs of Family 5 p.R1113X. All mutation carriers exhibit the curly hair phenotype. They also demonstrate hyperkeratosis and fissuring of the heels.

Family 6 p.E1493X

The index case in this family (1-V) died in his 40's from sudden cardiac death, which prompted further family screening. The actual pedigree is in fact much larger than that shown here, however these family members were not examined as part of this study as they do not attend the clinic at the Heart Hospital. The 64 year old brother of the index case (1-II) was examined for cutaneous signs. This individual had soft curly hair and a focal plantar keratoderma on clinical examination. He worked as a joiner and his hands were dry and fissured (Figure 4.7). His two affected children, 2-II and 2-IV however did not have curly or even wavy hair, in fact, both had straight hair, as did both of their unaffected siblings. Their cousin, 2-VI was also examined. She had straight hair and no evidence of a keratoderma Further questioning revealed that in this family, 6 of the 7 mutation carriers had straight hair and also did not have skin involvement. The correlation of hair and cutaneous phenotype with mutation-carrier status in this family appears to differ markedly from the other 5 families examined in this study.

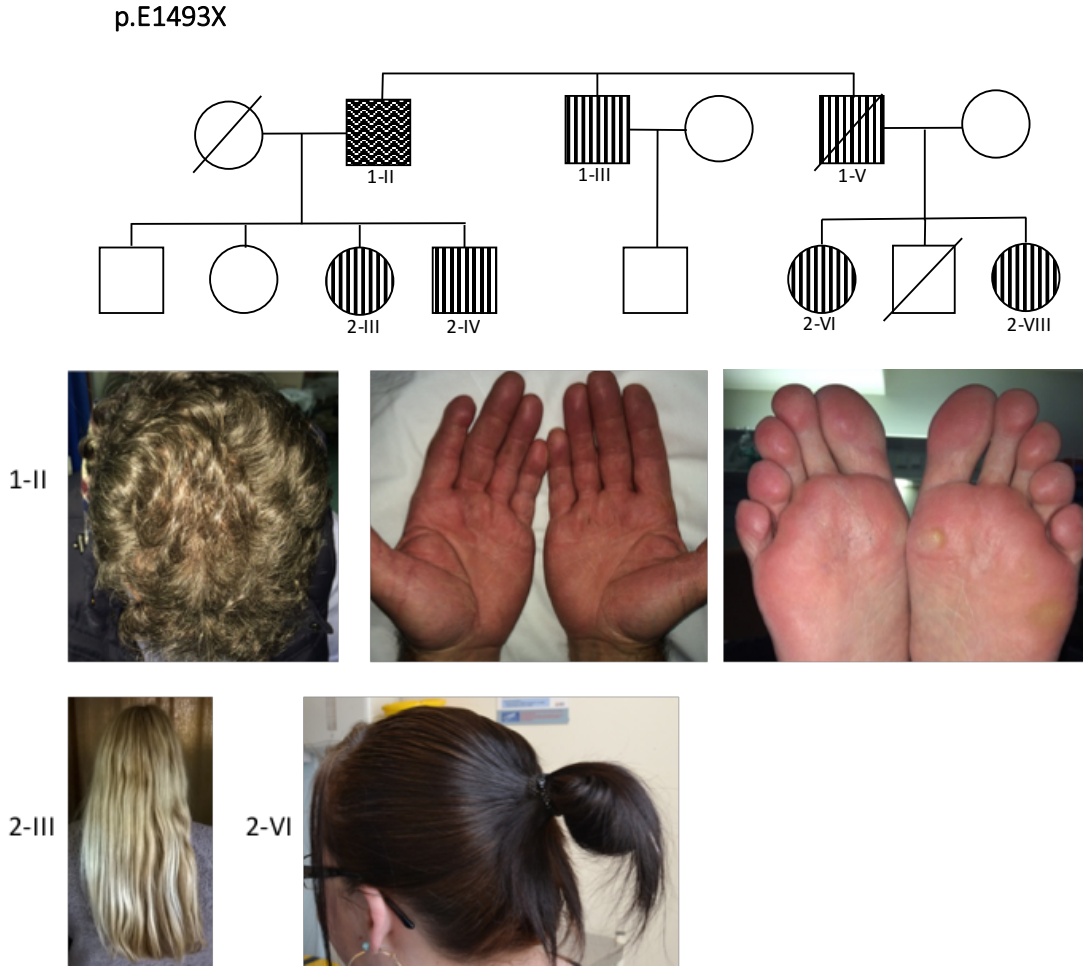

Figure 4.7 Pedigree and clinical photographs of family 6 p.E1493X. Square with wavy lines indicates curly haired carrier, Square or circle with straight lines indicates straight haired carrier. Unlike the other pedigrees examined in this study, only 1 of the 7 mutation carriers exhibited a curly hair, hyperkeratotic skin phenotype. Other mutation carriers such as 2-III and 2-VI had straight hair.

4.2.3 Summary of Hair Findings

In summary, 6 families in which members carried *DSP* gene mutations were phenotyped with respect to their skin and hair. Of the 39 mutation carriers in the families examined, 29 (74.4%) had curly hair, a further 4 (10.2%) had wavy hair and 6 (15.4%) had straight hair.

Intriguingly, none of the non-carrier offspring showed the curly hair phenotype in these families. All the families who participated in this study were Caucasian. In the European population, the incidence of curly has been estimated at 15%, which is significantly lower than in the *DSP* mutant cohort studied here (P=0.0012)(Figure 4.8).

DSP mutation	Carriers	Curly	Wavy	Straight	Non-Carriers Curly
p.Q273fs	8	5/8	3/8	0	0/2
p.H586fs	7	7/7	0	0	0/3
P.922fs	1	1/1	0	0	0/1
p.1015fs	8	7/8	1/8	0	0/11
p.R1113X	8	8/8	0	0	0/3
p.E1493X	7	1/7	0	6/7	0/3
Total	39	29 (74%)	4 (10%)	6 (15%)	0 (0%)

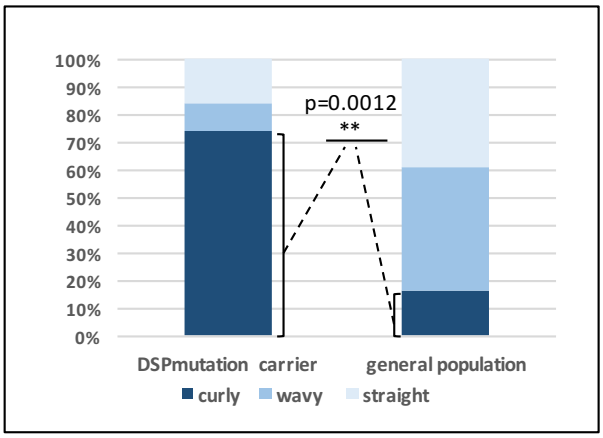

Figure 4.8 Table summarizing hair phenotype in the 6 pedigrees examined in this study. Bar chart showing that 74% of *DSP* mutation carriers exhibited a curly hair phenotype, significantly higher than observed in the general population.

Family 6 does not fit the phenotype inheritance pattern clearly observed in the other 5 families, with 6/7 members having straight hair and also lacking a skin phenotype. Initially this was felt to be rather unusual, however further examination of the location of the disease-causing mutation provided potential insight into the underlying mechanism. The mutation site in this family, a stop mutation at p.1493, occurs in the *DSP* I isoform specific region of the protein (Figure 4.9). As previously discussed in the introduction, *DSP* undergoes alternative splicing to yield two isoforms, DSP I being the full-length form and DSP-II lacking approximately two thirds of the residues within the rod domain. The p.1493 mutation would therefore only affect DSPI, and should not affect DSPII. DSPII is thought to be the major functional isoform in the skin and hair (Cabral et al., 2012), it could be "protective" in these individuals and preclude the presence of a skin/hair phenotype.

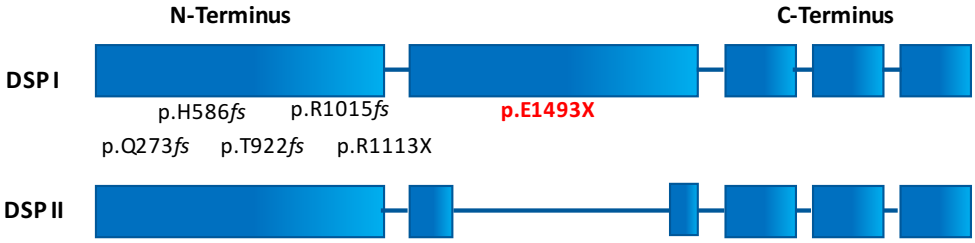

Figure 4.9 Schematic representation of DSP I and II isoforms. The mutations of the pedigrees in this study are predominantly located in the N-Terminus of both DSP I and II. However, the causative mutation in Family 6 (red) lies within the DSP I specific region.

Despite this, it is evident from the patients examined in this study that there is a high degree of segregation between the curly hair phenotype with *DSP* mutation carrier status in the families examined. Looking at the 24 mutation-carrying offspring of curly haired patients with AC due to *DSP* mutation, 22 of these (92%) also carried the mutation. Suggesting that, the presence of curly hair in a family member in which the proband has curly hair is highly suggestive of mutation carriage in that family member. This novel phenotypic finding may be useful in highlighting family members for genetic screening.

The curly hair in this patient cohort has an unusual texture and also tends to be frizzy, with a coarse "wire wool" texture in several of the individuals examined. Some patients commented that the texture was rough and required careful styling as it became knotted easily. Several members of independent families also commented that their hair grew slowly, or was difficult to grow longer. However, they did not describe hair breakage, fragility or excessive thinning of the hair. Interestingly, the curly hair phenotype could vary between individuals within the same family, carrying the same mutation suggesting additional factor. For example, in family 5, R1113X, although 3-I and 3-II both have curly hair, the appearance of their hair differs, the curl is looser in 3-II, whereas in 3-II its appearance is more typical of the "woolly" hair described associated with Naxos or Carvajal disease. Other patients described their hair becoming less curly with time (e.g. 2-III and 2-IV). We were unable to obtain scalp biopsies for further evaluation and no hair microscopy was performed. Overall, the hair phenotype in the curly-haired *DSP*-mutation carriers appeared to be less striking than that observed in Naxos or Carvajal disease but still present. Nevertheless, these finding suggest a marked clustering of the curly hair phenotype with mutation carrier status with the exception of Family 6. The variability in the hair phenotype in members of the same family could be attributed to genetic or epigenetic modifiers for example by DNA methylation or histone modification.

4.2.4 Summary of Skin Findings

Unlike the hair phenotype, the skin finding, although present in several patients, were altogether subtler. Some patients had evidence of a striate PPK with linear hyperkeratosis affecting the feet and/or palms. Patients showed variable hyperkeratosis, particularly between the great toe and second toe or painful hyperkeratotic fissuring of the heels. Several patients also described marked dryness of the skin, particularly the hands, and some had even developed clinical features similar to eczema. Another important factor to consider was that the skin phenotype in many families appeared to become more prominent in later life. For example, in Family 5. Although in this family, the skin features were less clearly defined than the hair phenotype, the youngest family members, aged 15 and 19 showed very little thickening of the plantar skin however their mother, aunts and grandfather all had more overt features of plantar keratoderma. Although the skin findings were more variable, there was a correlation between their presence and skin "stress". For example, several individuals

mentioned that their keratoderma deteriorated following walking/exercise and their hands became very dry when washed frequently or in the winter months. Others also mentioned that exposure to water, such as swimming, bathing or long showers, exacerbated the formation of eczematous patches on the interfollicular skin. Although the skin features were somewhat less striking than the hair phenotype, they were nonetheless present. Simply asking the question of whether the patient had ever had problems with their hands and feet often led to an animated discussion with several replying "how did you know" or "you don't want to see my feet they have always been so ugly" etc. This response was not generally observed in unaffected carriers or the partners of mutation carriers. Several patients described time-consuming foot-care regiments, for example shaving or scraping hard skin, foot soaks and regular application of emollients. Although patients were aware that little could be done therapeutically for their keratoderma, there was some sense of relief to them that it was in fact due to their underlying *DSP* mutation.

4.2.5 Mechanism of Disease – Haploinsufficiency

How these autosomal dominantly inherited mutations in *DSP* actually cause disease has remains somewhat controversial. To address this question, it was important to determine whether the mutant allele was being expressed at the mRNA and protein level. The following experiments were carried out by Dr Anna Posafalvi (Kelsell Group). Skin biopsies were taken from non-lesional skin on the patients forearm with written informed consent. cDNA and mRNA were extracted from patient and control skin. Specific primers were designed targeting either wild-type *DSP* or the particular mutant sequence. Sanger Sequencing revealed that in all six samples analyzed, the mutant allele was present only the genomic DNA but not in the mRNA, where only the wild-type allele transcript was detected (Figure 4.10). Physiological mechanisms exist to prevent the transcription/translation of mutant mRNA, and it is likely that if the mutant mRNA is transcribed, it undergoes nonsense-mediated decay to prevent it being translated and producing an aberrant protein product.

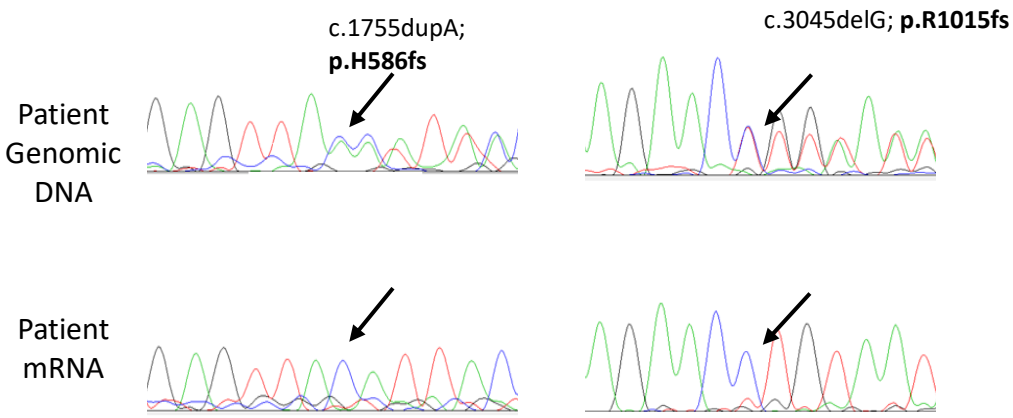

Figure 4.10 Sanger Sequencing traces showing that the causative mutation is present in genomic DNA (upper panel) but absent from mRNA from each patient using specifically designed primers, where only the wild-type allele was detected. This suggests that the mutant allele is not being transcribed/translated and that the downstream effects are due to haploinsufficiency.

4.2.6 Immunohistochemical Staining of Patient Skin Biopsies

Towards understanding how the disease-causing mutations could contribute to the skin phenotypes observed linked to AC, immunohistochemical staining was performed of the patient skin biopsy samples. (Dr Anna Posafalvi performed the immunohistochemical staining and the confocal imaging was performed by myself)

DSP and PG

In normal control skin, DSP staining (using an antibody directed at the N Terminus of both isoforms I and II -Materials and Methods) and PG (PG) show a predominantly membranous staining pattern throughout the epidermis, including the basal layers. However, in mutant Q273fs skin, DSP is mislocalised (Appendix Figure C.1), forming intercellular aggregates in the basal layers extending to the mid-epidermis. Also, cytoplasmic localisation of DSP seen here, which is less evident in control skin, also suggesting mislocalisation. PG expression appears to be fainter in patient skin than control, with the formation of intercellular aggregates in the basal layers. There is also both cytoplasmic and membranous localization in the suprabasal epidermis. The size and shape of the cells does not appear to be altered and there

is no evidence of clefting or widened intercellular spaces. Immunostaining for Connexin 43 (Cx43) was also performed, as this Gap Junction protein is also essential for electromechanical conduction in cardiac myocytes. Improperly located Cx43 in has been shown to occur in cardiac biopsies from patients with AC. In control skin, Cx43 is located at the intercellular membrane in the basal and spinous layers. In Q273fs however, it is almost entirely absent from the basal layers and instead, is irregularly accumulated in the upper epidermis. All three junctional proteins fail to localize correctly in the basal and suprabasal layers of the skin from patients with this particular mutation.

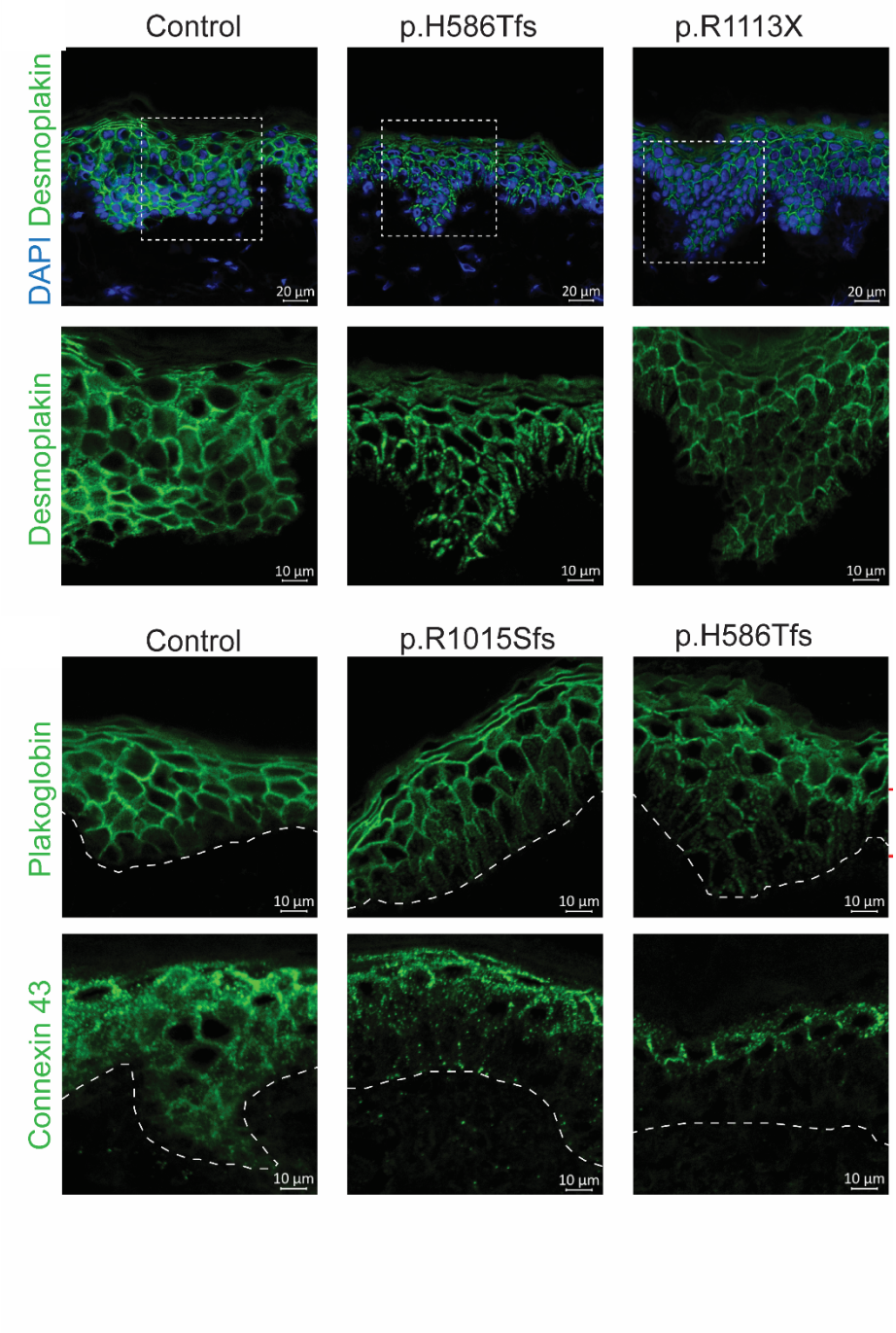

Figure 4.11. Immunohistochemical staining of patient and control skin. DSP immunostaining shows a granular membranous distribution in the basal and mid-epidermis. PG immunostaining appears faint and speckled in the basal layers of patient skin. Cx43 immunostaining is virtually absent in the basal layers of patient skin. Scale bars marked on individual images. Negative control Appendix Figure C.4.

Patient H586fs shows impressive mislocalisation of DSP in the epidermis. Rather than a continuous membrane localization, It forms irregularly distributed dense intercellular aggregates which occur more extensively than in Q273fs, extending to the superficial epidermis (Figure 4.11). PG staining is also markedly different from control skin. In the patient skin, its expression appears diminished however, where it is present, it forms aggregates and accumulates abnormally in the cytoplasm. By contrast, the signal intensity in the upper epidermis appears more intense than control skin, possibly suggesting that there may be increased expression of PG in the upper layers to compensate for reduced DSP. Cx43 immunostaining reflects the distribution of both PG and DSP, its expression is reduced in the basal and suprabasal layers and restricted to the upper stratum spinosum.

In both Q273fs and H584fs, the overall levels of DSP appear to be qualitatively somewhat reduced, although more striking in H585fs. By contrast, T922fs shows robust downregulation of DSP throughout the epidermis compared with control skin. Very faint intercellular staining is observed in the mid-epidermal layers, predominantly as aggregates (Figure 4.11). It is possible that this particular mutation results in addition to haploinsufficiency, a dominant-negative effect of the mutant allele on the wild-type. With regards to PG in T922fs, the immunostaining is much less prominent than in control skin, and appears slightly irregularly distributed compared with control skin (Appendix Figure C.2). Cx43 staining is also unusual. It appears upregulated in the upper spinous layers and stratum granulosum but almost completely absent from the basal and suprabasal layers (Appendix Figure C.3).

R1015fs shows a similar staining pattern for DSP as Q273fs and H585fs, with intercellular aggregates of DSP seen in the basal and suprabasal layers (Appendix Figure C.1). Although this is less apparent in the superficial epidermis, there is also a slight reduction of the overall intensity of the green signal in this staining. PG staining was distributed in a similar fashion

to DSP in this patient's skin, also showing reduced intercellular deposition in the basal layers, and the formation of faint intercellular aggregates. Cx43 immunostaining differed markedly from control skin. The intensity of staining appeared reduced and formed ill-defined "dots" or diffuse cytoplasmic staining in the lower epidermis (Appendix Figure C.3).

The immunohistochemical staining pattern of the three proteins, DSP, PG and Cx 43 are also abnormal in skin from R1113X (Figure 4.11 and Appendix Figures C.1-C.3). DSP is abnormally distributed in the basal and suprabasal epidermis, where it is present in the cytoplasm and forms discrete foci at the intercellular membrane. The PG signal shows reduced intensity in the basal layers and Cx43 is almost entirely absent in the basal and suprabasal layers, save for a few speckles. This differs significantly from its expression pattern in normal skin. Where it is located throughout the epidermis.

E1493X

In the skin biopsies taken from family members carrying this mutation, the localization of DSP in the skin actually appeared unchanged compared with control skin. It is correctly localized intercellularly without cytoplasmic distribution and minimal formation of intercellular aggregates in the basal layers. PG staining was also preserved compared with control skin. Cx43 immunostaining appeared comparable with control skin (Figure 4.12).

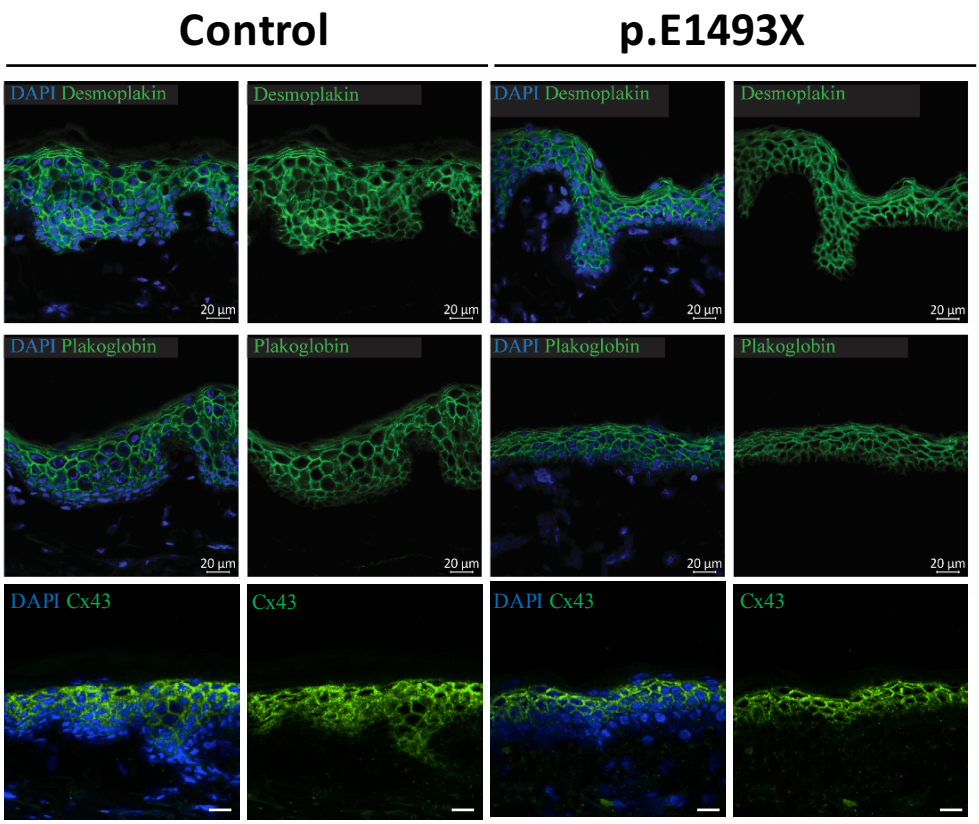

Figure 4.12 Immunohistochemical staining of control and patient (p.E1493X) skin. The distribution of DSP, PG, and Cx43 is comparable between patient and control skin. Scale bar 20µm. Negative control Appendix Figure C.4

It has been previously shown by selectively depleting HaCaT keratinocytes of either DSP-I or DSP-II by siRNA, that DSP-II is the key isoform mediating intercellular adhesion in response to mechanical stress (Flexcell stretch assay)(Cabral et al., 2012). A Dispase assay was performed to assess the role of each isoform in desmosomal adhesion. This showed that siDSP-I did not result in a significant increase in the number of fragments produced upon agitation, whereas siDSP-II did. This suggests that DSP-II is able to compensate for DSP-I function with respect to intercellular adhesion in keratinocytes. Therefore, it is relatively unsurprising that the DSP-I specific mutation, Q1493fs does not result in a cutaneous phenotype, as cutaneous mechanoresilience is predominantly maintained DSP-II (Cabral et al. 2012). Furthermore, PG and Cx43 localization is also preserved in this patient, further emphasizing that heterozygous loss of DSP-I can be compensated in the skin.

4.2.7 Summary of Immunohistochemical Findings

Reviewing the results of the immunohistochemical findings, some consistent trends are observed. In skin from Q273fs, H585fs, T922fs, R1015fs and R1113X, DSP immunostaining was reduced in the basal and suprabasal layers and, where present, it appeared to form intercellular aggregates and speckles. PG immunostaining was also reduced in the basal and suprabasal layers in these samples and importantly, Cx43 immunostaining revealed a similar expression pattern. Suggesting that, these mutations in DSP result in mislocalisation of the three proteins and in some cases reduced expression in the basal layers. It is particularly interesting that these changes are observed in skin biopsies taken from clinically normal appearing skin in all five families. In cardiac tissue from patients with AC, it has been shown that PG immunostaining at the intercalate disc is consistently reduced (Asamaki et al., 2009). This includes archival autopsy cardiac tissue from the index patient carrying the mutation R1113X, whose sister and son donated skin biopsies used for the immunostaining shown here. Furthermore, mislocalised Cx43 is also observed in AC. Taken together, these observations suggest that clinically unaffected skin from patients with AC can show mislocalisation of desmosomal and gap junction proteins that are also found in the heart. It is possible to therefore extrapolate that perhaps, the skin in these patients reflects their heart. Interestingly, the changes observed in the skin are predominantly confined to the basal and suprabasal epidermis whereas the upper epidermis appears relatively unaffected with regards to distribution of DSP, PG and Cx43. The desmosomal components present in the basal layer of the skin are highly similar to those present in the cardiac intercalate disc, however their composition differs in the upper stratum spinosum and stratum granulosum. Importantly, in addition to DSP and PG, the desmosomal proteins DSC2, DSG2 and PKP2 are all preferentially expressed in the basal and suprabasal epidermis and also the intercalate disc but not in stratified epithelia. Therefore, the basal and suprabasal epidermis could histologically provide a “mirror” for the cardiac intercalate disc. Clinically this could be very useful as obtaining a cardiac biopsy is difficult and carries risks during the procedure including aneurysm formation and haemorrhage. Obtaining a skin biopsy is markedly easier, particularly from clinically unaffected skin.

4.2.8 Correlation of Cardiac and Cutaneous Phenotypes

There can be marked clinical heterogeneity in the cardiac phenotype in patients with AC, even amongst individuals within the same family, carrying the same disease-causing mutations. To examine the cardiac phenotype of mutation carriers included in this data set, retrospective analysis of clinical data from patients was performed. The patients demographics and clinical features, according to the most recent AC Task Force Criteria were ascertained from their electronic records by Dr Silvia Castelletti. The data examined include age, sex, family history, symptoms, echo findings, the presence of T-wave inversion, signal averaged ecg (SAECG), presence of arrhythmia on 24 hour tape, the presence of an ICD, whether the ICD had emitted shocks, and whether the patient fulfilled criteria for a diagnosis of AC based on the task force guidance. The clinical characteristics of patients who fulfilled or borderline fulfilled the criteria for AC are shown summarized in Table 1.

	Variant	Patient	*DSP* mutation carrier	Age/ sex	Major Criteria	Minor Criteria	Curly/ wavy hair	Skin
	pQ273fs							
1		2-II	y	53 F	*c, e*	*a, d*	yes	yes
2		1-II	y	71 F	*f*	*a, d*	yes	yes
3		3-V	y	17 F	*f*		yes	No
4		3-II	y	17 M	*f*		yes	yes
5		2-V	y	46 M	*f*	*d*	yes	no
6		2-III	y	54F	*N/A*	*N/A*	yes	no
7		3-III	y	18F	*N/A*	*N/A*	Yes	No
8		3-IV	y	17M	*N/A*	*N/A*	yes	No
9		3-I	n	26 M			no	no
10		3-VI	n	16 M			no	N/A
	pH586fs							
8		2a-I	y	55 M	*		yes	N/A
9		2a-II	y	50 M	*a, e, f*	*d*	yes	yes
10		1c-II	y	61 F	*a, c, f*	*d, e*	yes	yes
11		2c-II	y	36 F	*e, f*	*d*	yes	yes
12		2b-I	y	42 M	*e, f*	*a*	yes	yes
13		1a-II	y	71 F	*f*		yes	N/A
14		1b-II	y	76 F	*e, f*	*d*	yes	yes

15		3a-I	n	20 F			no	no
16		2c-I	n	42 M			no	no
17		2b-II	n	39 F			no	N/A
	pT922fs							
18		1-I	y	30 F	*b, e*	*c, d*	yes	yes
19		1-II	n	28 F			no	no
	pR1015fs							
20		2-V	y	26 F	*		yes	N/A
21		2-II	y	53 F	*a, b, e, f*	*d*	yes	yes
22		2-IV	y	56 F	*a, e, f*	*d*	yes	yes
23		2-X	y	61 M	*c, e, f*	*a, d*	yes	no
24		3-II	y	31 M	*f*	*a*	yes	yes
25		3-VIII	y	18 M	*f*		yes	no
26		3-I	n	30 F			no	No
27		3-III	n	27 F			no	no
28		3-IV	n	16 F			no	No
29		3-V	n	17 M			no	no
30		3-VI	n	33 M			no	N/A
31		3-VII	n	32 F			no	N/A
32		3-XII	n	64 F			no	N/A
33		3-XIII	n	52 F			no	N/A
	pR1113x							
		2-II	y	30 F	**1*		Yes	N/A
34		1-I	y	84 M	*f*	*d, e*	yes	yes
35		2-III	y	54 F	*c, f*	*a, d*	yes	yes
36		2-V	y	50 F	*c, f*	*a, d*	yes	yes
37		3-I	y	26 M	*f*		yes	yes
38		3-II	y	24 M	*f*		yes	yes
39		3-VI	y	20 F	*f*		yes	Yes
40		3-VII	y	15 F	*f*		yes	no
41		3-V	n	23 M			no	No
42		3-IV	n	25 F			no	no
43		3-III	n	22 F			no	no
	pE1493x							
		1-V	y	38 M	** 1*			
44		1-II	y	64 M	*f*	*a, c, d*	yes	yes
45		1-III	y	59 M	*a, f*	*d*	yes	no
46		2-IV	y	34 M	*f*	*d*	no	no
47		2-VI	y	32 F	*f*	*a, d*	no	yes
48		2-VIII	y	31 F	*f*		no	no
49		2-III	y	36 F	*f*	*d*	no	no

Table 4.1. Cardiac and cutaneous phenotype in *DSP* mutation carriers and non-carrier family members

Categories of fulfilled diagnostic criteria are reported.

*index case: died suddenly ǂ post-mortem diagnosis

a, global or regional dysfunction and structural alterations; *b*, tissue characterization of wall; *c*, repolarization abnormalities; *d*, depolarization abnormalities; *e*, arrhythmias; *f*, family history.

Among all patients, 12/30 (40%) fulfilled the 2010 Task Force Criteria for AC diagnosis. The fulfilment of the diagnostic criteria is presented in Table 4.1. Ten patients (33%) had history of arrhythmic symptoms, inverted T waves on electrocardiogram (ECG) were present in 9 (30%) patients whilst signal-averaged ECG (SA-ECG) was positive in 12 (40%) mutation carriers. Ejection fraction was impaired in 9 (30%) patients at echocardiogram. During 24 hour ambulatory ECG monitoring, >500 ventricular ectopics were noted in 13 (43%) mutation carriers, in particular, in 7 of these a non-sustained ventricular tachycardia (NSVT) was recorded. Cardiac Magnetic Resonance (CMR) showed fibrofatty infiltration in 10 patients (33%) and 11 (37%) patients had an ICD implanted, two of these for secondary prevention. A representative cardiac MRI is shown below (Figure 4.13). 72% of patients were found to have a skin phenotype. As desmoplakin is a critical component of the intercalate disc, mutations in *DSP* impair conduction as well as cell-cell adhesion, resulting in fibrofatty infiltration and arrhythmia.

p.R1015fs

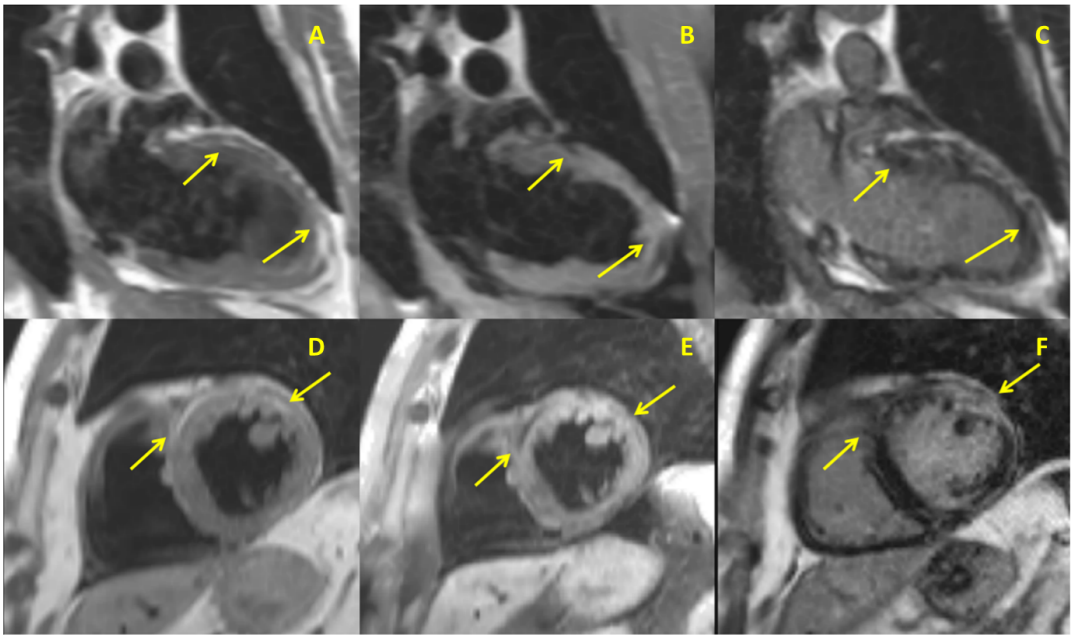

Figure 4.13. A representative cardiac MRI image from patient II:10 in Family 4. It shows 2 chambers and short-axis LV turbo spin echo images with and without fat saturation and late gadolinium enhancement image on the same slice of a AC patient positive for a mutation in *DSP*. Arrows indicate some areas of fat infiltration (A, B, D, E) and fibrosis (C, F).

The exact mechanisms underlying the development of a striate keratoderma remain largely unknown however, it is thought that it arises because the footpad epidermis is not able to adequately withstand mechanical stress and therefore develops compensatory thickening as a "stress response". This may be akin to fibrosis seen in the hearts of patients with AC, essentially also an impaired response to physical stress. As the histological findings observed in patients skin (mislocalised and/or downregulated desmosomal proteins DSP, JUP and Cx43) are similar to the typical features observed in myocardial biopsies from patients with AC, it suggests therefore that the desmosome dysfunction in the skin could reflect a similar occurrence the heart. Extrapolating this hypothesis further, we questioned whether the presence of skin involvement could therefore confer a poorer outcome for patients with AC or be linked to disease severity. Although there is relatively little data available for risk stratification in patients with AC, there is a broad agreement that ICD implantation is recommended in patients with documented sustained ventricular arrhythmias due to the high incidence of arrhythmia recurrence (Brugada et al., 2012) but also those presenting with high risk symptoms such as syncope and NSVT. ICD therapy occurs in approximately 10% of

AC patients per year, with an estimated survival benefit of around 25-30% at 3 years (Carrado et al., 2003). Therefore the placement of an ICD is suggestive of a more severe disease phenotype. In this cohort, 12 of the 18 patients (67%) had an ICD in place at the time of writing. All of these patients had clinical evidence of a striate keratoderma. Anecdotally, within the same family (p.S1015.fs) two sisters with marked skin involvement of their plantar epidermis (2-II and 2-IV) required ICD placement, whereas their cousin (2-X), who did not have involvement of the plantar epidermis, does not require an ICD. These findings could suggest that the presence of cutaneous involvement may be associated with a more severe cardiac phenotype. Functionally, this would be logical as both skin and cardiac involvement indicates defective desmosomal dysfunction and an impaired cutaneous and myocardial response to physical strain would therefore be seen in both tissues. Interestingly, all four patients carrying the DSP-1 specific mutation p.E1493X appear to have a milder cardiac phenotype than the other families, all family members have normal echocardiograms and do not have TWI in V1-V3. Nor do any of the members of this family have an ICD. It has previously been shown that DSP-I is the predominant isoform in the heart, with DSP-II expression found only in small amounts in the left atrium and ventricle (Ucuzmu et al., 2006). However, the seemingly milder cardiac phenotype in this family would suggest otherwise, and raises the possibility that in fact, DSP-II could be compensating for DSP-I haploinsufficiency in the heart, perhaps in response to stress. Interestingly, the skin from these patients also shows relatively normal expression of PG and Cx43 despite reduced levels of DSP-I throughout the epidermis.

4.3 Summary of Findings and Discussion

1. Novel cutaneous phenotype in Dominantly Inherited AC
2. Haploinsufficiency is the molecular mechanism in the skin
3. Differential expression of DSP I and II isoforms in the skin.
4. Correlation between cardiac and cutaneous phenotype

The data presented above support a novel cutaneous phenotype in dominantly inherited AC caused by mutations in *DSP*, namely the presence of curly hair and PPK, including striate keratoderma, focal keratoderma, hyperkeratosis and fissuring of the heels. The presence of curly hair is found in 76% of all mutation carriers, with a further 10% having wavy hair, significantly higher than in the control Caucasian population (p=0.0012). The curly hair phenotype is highly penetrant, such that 92% of offspring of curly-haired mutation carriers who also carry the mutation, will also have curly hair. This phenotypic feature may prove to be useful in genetic screening of susceptible family members. Furthermore, it could also aid the timely diagnosis of AC, which as previously eluded to, can be complex due to the vast heterogeneity of the clinical presentation. A proportion of the mutation carriers also had evidence of a striate keratoderma and/or hyperkeratosis and fissuring of the heels. This could manifest initially as linear thickening between the great toe and the second toe in several of the patients examined. The striate keratoderma in the mutation carriers is a much milder phenotype than that observed due to homozygous mutations in *DSP* (Armstrong et al., 1999, Norgett et al., 2000) and appears to become more prominent with age, suggesting exposure to mechanical force may be a contributory factor. Some patients also described developing very dry hands, particularly in winter, which could manifest as fissures and hyperkeratosis along the fingers. Recently, a homozygous missense mutation in the N-terminus region of *DSP* has been linked to "SAM" syndrome (McAleer et al., 2015). Ultrastructural analysis of patient skin revealed marked attenuation of cornified envelopes and a virtual absence of corneodesmosomes, pointing to a defective skin barrier in the pathophysiology of the disease. It is possible that a similar defect could exists in our cohort and contribute to a compromised skin barrier, which would explain the presence of dry, cracked fissuring skin, worsened by exposure to cold weather and water.

By extracting mRNA and protein from patient skin biopsies, experiments performed by Dr Posafalvi confirmed that haploinsufficiency is the likely underlying molecular mechanism in the skin of these patients. The mutant allele does not appear to be expressed at mRNA, and

therefore at protein level, there may be a reduced level of DSP in the skin which could explain mislocalisation of DSP, PG and Cx43 in the basal and suprabasal layers of the patients' skin. Using a murine model with a conditional genetic deletion of one allele of *DSP* in the adult heart (DSP+/-), Gomes et al., (Gomes et al., 2012) demonstrated that haploinsufficiency of DSP could mimic the cardiac phenotype observed in AC. Furthermore, they also showed reduced DSP and PG at the intercalate disc and mislocalisation of Cx43. These observations are similar to what was observed by immunohistochemical staining performed in the skin of patients with AC in this study. However, it is pertinent to note that Armstrong et al., (Armstrong et al., 1999) identified a truncating mutation affecting the n-terminal region of *DSP* as the underlying cause of a striate keratoderma in a large pedigree who intriguingly did not have underlying ARVC, nor have they since developed it (personal communication), suggesting the role of DSP in the development of cardiac and cutaneous features of ARVC is complex and likely to be multifactorial.

In the family carrying the mutation p.1493X however, the clinical and histological findings were significantly different to those observed in all 5 other families. In this family, there was a notable absence of the curly hair phenotype, with 6/7 family members having straight hair. Furthermore, the same 6 family members also did not have features of a keratoderma or dry skin/xerosis. As previously discussed, the location of the mutation is likely to explain the difference. The mutation occurs in the DSP-I specific region of the gene, which would effectively be "spliced out" in DSP-II. The presence of "normal" DSP-II in the presence of DSP-I haploinsufficiency appears to rescue the clinical phenotype, such that hair development also occurs normally. PG, DSP (using DSP-I and II antibody) and Cx43 immunostaining all appeared comparable between patient and control skin. This observation is consistent with previous studies which has confirmed that DSP-II is the isoform required for mechanoresilience in keratinocytes (Cabral et al., 2012).

To gain further understanding into the correlation of cutaneous and cardiac findings in this cohort, detailed cardiac phenotypic analysis was performed for patients who fulfilled/borderline fulfilled the criteria for AC in this cohort. 78% of patients with AC criteria also had skin involvement. Of particular interest was that 100% of patients who required an ICD to manage their disease also had skin involvement. It is likely that the critical role of the desmosome in maintaining skin integrity and cardiac function reflects the shared phenotype in this cohort. The presence of skin involvement is suggestive of defective desmosome

function and could perhaps represent a surrogate marker for defective desmosome function in the heart. In fact, within the same family, the presence of skin involvement delineated two sisters who required an ICD from their cousin who did not, which is particularly unusual as all three members carry the same mutation. This points to additional factors (genetic or epigenetic modification) which could exacerbate both the cardiac and cutaneous phenotypes. Moreover, the family carrying the DSP-I specific mutation p1493X, appeared to have a milder cardiac phenotype than the other families, none of these family members required an ICD and all had normal echocardiograms. From this it could be inferred that despite haploinsufficiency of DSP-I, DSP-II is able to compensate not only in the skin, but also in the heart. A role for DSP-II in the heart has not yet been clearly elucidated and further work would be necessary to establish its function more clearly.

In clinical practice, the presence of curly hair and keratoderma is likely to be a useful additional clinical identifier of AC patients. When incorporated into family screening for AC, it could be particularly useful in persuading individuals to partake in genetic screening programmes and identify high risk family members who warrant further diagnostic tests, lifestyle changes and participating in regular follow-up. This study did not include pedigrees with missense mutations in *DSP*, nor did it examine carriers of other desmosomal AC gene mutations. All pedigrees included in this study happened to be of Caucasian origin, however it would be important to consider the significance of the cutaneous phenotype in other populations including those in which curly hair is known to be more highly prevalent. Although our study includes the largest number of *DSP* mutation carriers reported, and the first systematic approach of a well-defined mutation subtype cohort, larger-scale genotype-phenotype correlation studies are necessary to confirm these dermatological findings.

Chapter 5

Mutations in FAM83G Cause Autosomal Recessive Palmoplantar Keratoderma with Leukonychia and Abundant Curly Hair

5.1 Introduction

5.1.1 FAM83 Family of Proteins

The FAM83A-H (FAMily with sequence similarity 83) comprise a novel group of signalling proteins about which relatively little is known. They were Initially described as “hypothetical proteins”, however mass spectrometry has since confirmed the expression of all 8 proteins (Cipriano et al., 2013). FAM83A-H are highly conserved in jawed vertebrates, and are characterised by the presence of conserved N-Terminal “domain of unknown function”; DUF 1669 (Figure 5.1). Within this region is a putative phospholipase D motif however it lacks the functionally important histidine residues required for enzymatic activity and its molecular role remains unknown.

Sequence alignment of members of the FAM83 family show that there is between 32% and 48% sequence homology within the DUF 1669 region however, outside of this domain (Cipriano et al., 2013), the proteins are divergent, sharing very little protein sequence similarity. Since their identification, the function of FAM proteins are slowly being uncovered, with a predominant focus on their potential role as oncogenes (Bartel et al., 2016) however the role of the DUF1669 domain remains to be determined.

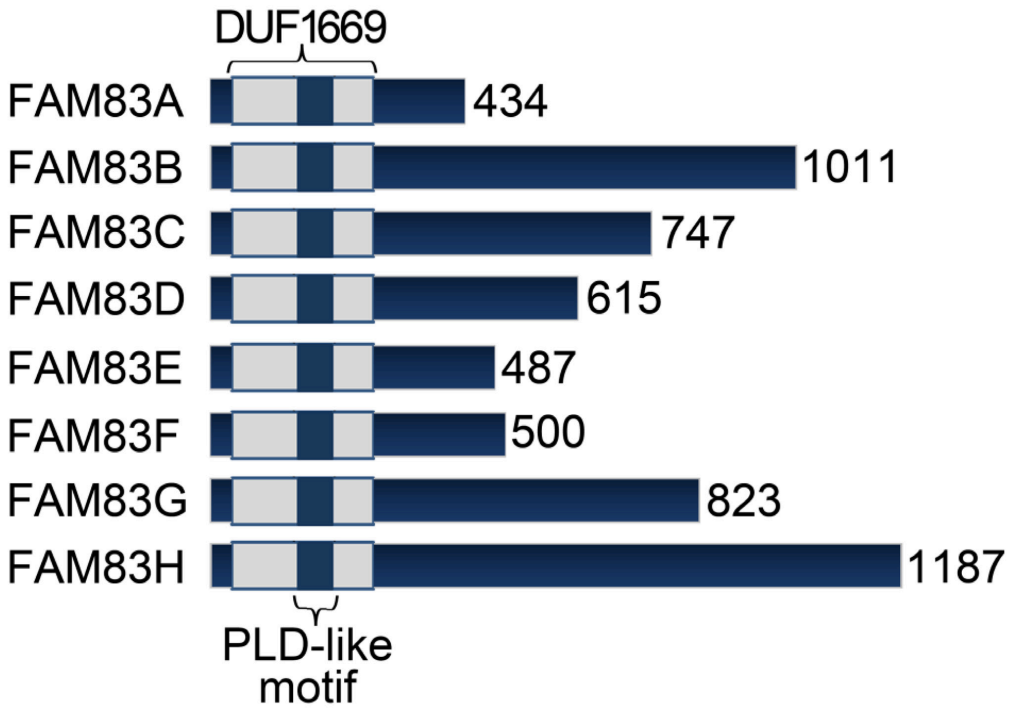

Figure 5.1 The eight FAM83 proteins (A-H) share a common N-terminal domain and Domain of Unknown Function (DUF1669) however differ considerably in their C-terminus region. The DUF1669 contains a putative phospholipase D motif (PLD). (Adapted from Bartel et al., 2016).

Overexpressed or dysregulated FAM83 proteins have been identified as regulators of cell growth, proliferation and metastasis and can be markers of resistance to targeted therapies in breast cancer (Cipriano et al., 2014). FAM83A, for example confers resistance to an EGFR tyrosine kinase inhibitor (TKI) in tumorigenic mammary epithelial cells (Lee S-Y et al., 2012). Subsequently, FAM83B was found in an independent mutagenesis screen at the Jackson Lab, to drive mammary epithelial cell transformation, in a fashion similar to active RAS (Cipriano et al., 2012). These data suggest that FAM83 A and B play a role in EGFR and RAS signalling pathways and could contribute to malignant transformation in breast tissue. Further evidence for the role of FAM83 proteins in cancer comes from gene expression studies, which have shown that FAM83A, B, D and E are highly expressed in ovarian cancers, whereas A, C and D are increased in bladder cancer (Cipriano et al., 2014).

Beyond malignancy, autosomal dominantly inherited mutations in FAM83H have been shown to underlie Amelogenesis Imperfecta (AI) (Kim et al., 2008, Lee et al., 2008). This rare disorder is characterised by impaired mineralisation of the tooth enamel, and as a result, the dental enamel of affected individuals is “cheesy soft” in consistency. FAM83H was the first non-extra cellular matrix protein found to cause Amelogenesis Imperfecta. All reported

mutations introduce premature stop codons in exon 5 which results in deletion of part of the C terminal domain ranging from 503-880 amino acids in length. FAM83H has been shown to regulate the cytoplasmic localisation of Casein Kinase Ie by direct interaction. The C-terminal truncated protein occurring in AI is thought to have gain-of-function activity leading to mislocalised nuclear Casein Kinase Ie that is toxic to ameloblasts (Wang et al., 2016). Interestingly, AI-causing mutations in FAM83H have not been linked to malignancy although FAM83H is overexpressed in colon cancer where it disorganises the keratin cytoskeleton through its interaction with Casein Kinase 1e (Kuga et al., 2016). As described in Chapter 1, keratin filament assembly/disassembly plays a key role in cell proliferation, invasion and migration and could explain the role of FAM83H in colon cancer invasion and metastasis. In AI, disruption of the cytoskeleton by disease causing mutations in FAM83H also impairs the formation of desmosomes. Both keratins and desmosomes are required for the proper formation of dental enamel in ameloblastoma cells.

Other members of the FAM83 family, FAM83C, E and F remain to be characterised and are yet to be linked to function or disease.

5.1.2 FAM83G

FAM83G is an 823 amino acid long protein encoded by the *FAM83G* gene located on chromosome 17p11.2. It is highly conserved in eutherians (placental mammals) however in more distantly related vertebrate species, the predicted FAM83G orthologs show reduced homology. RNA and protein expression studies reveal that FAM83G expression is highest in the skin, followed by the colon and oesophagus (www.proteinatlas.org). FAM83G expression is specifically enriched (> five-fold) in the skin compared with 26 other tissue types (Edqvist et al., 2015).

To date, it has been the subject of only four publications, three linking it to disease in animals (Radden et al., 2013, Drogemuller et al., 2014, Sayyab et al., 2016) and one functional study (Vogt et al., 2013). Using a proteomic approach, Vogt et al. 2013, identified FAM83G as a novel Smad1-interacting protein, where it promotes smad4-independent signalling and transcription of non-BMP target genes *NEDD9* and *ASNS*.

5.1.3 Recessively Inherited Mutations in FAM83G in Animal Models

In 2013, the Jackson laboratory reported the identification of a spontaneously occurring phenotype in mouse with a woolly coat evident at 3-4 weeks of age and named it the "*wly"* mouse (Radden et al., 2013) (Figure 5.2). No other phenotypic abnormalities were seen and affected mice had a normal life expectancy.

Figure 5.2 The *wly* mouse exhibits a striking, woolly coat. Histopathology of murine skin demonstrated "giant hair follicles in anagen" (adapted from Radden et al.,2013)

A recessively inherited frameshift mutation resulting in a 995bp deletion in *FAM83G* was determined as the underlying cause of the *wly* mouse by exome sequencing. The authors suggested that this deletion is likely to result in a severely truncated non-functional protein product, at least partially removing the conserved DUF1669**.** Although no functional work was carried out in this paper, a skin biopsy from an affected mouse revealed "giant" hair follicles with all hairs in the anagen phase of the hair cycle (Radden et al., 2013).

Purebred dogs are particularly well suited to genetic analysis due to their limited population structure. In 2014, Drogemuller et al. (Drogemuller et al., 2014) used a genome wide association (GWAS) approach combined with whole genome sequencing (WGS) to identify missense mutations in FAM83G as the underlying cause of the recessively inherited disorder "Hereditary Footpad Hyperkeratosis" in Kromfohrlander and Irish Terrier dog breeds. The variant c.155G>C was predicted to change an evolutionarily conserved arginine into a proline (p.R52P) and occurs within the DUF1669. Further genotyping confirmed that this variant was present in more than 500 HFH dogs. Like the "wly" mouse, the phenotype in affected dogs is a bushy coat presenting from a few weeks of age. In addition, the dogs also have

hyperkeratotic, fissured footpads and hard, rapidly growing nails that require frequent trimming (Figure 5.3).

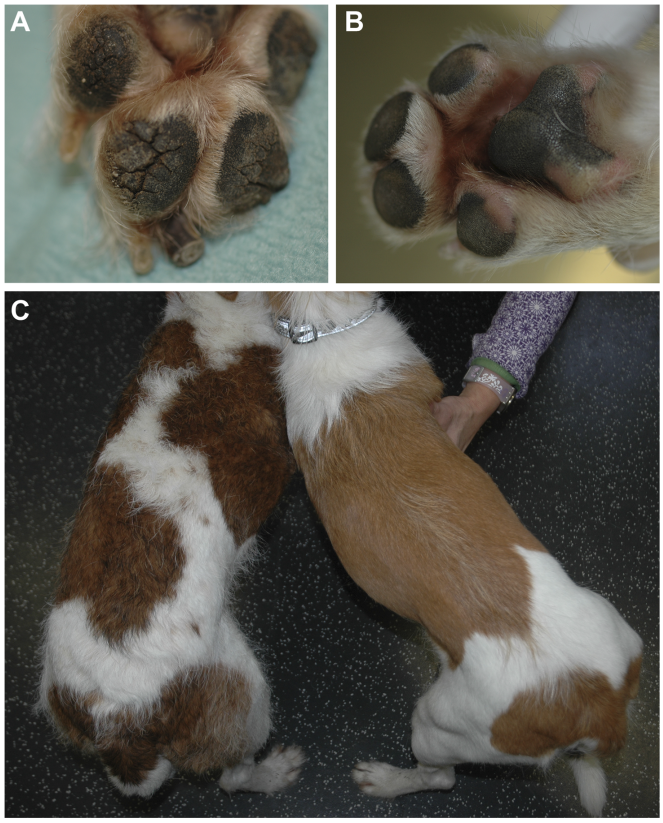

Figure 5.3 Hereditary Footpad hyperkeratosis in Irish Terrier dogs. **(A)** Marked hyperkeratosis and fissuring of the footpads as well has rapidly growing nails are observed in mutation carriers compared with normal controls **(B)**. **(C)** Affected dogs are identifiable by the presence of a woolly, wavy coat (left) compared with normal control (right). Figure adapted from Drogemuller et al., 2014.

Although there is no reduction in life expectancy, pain and discomfort resulting from footpad thickening and superadded infection can contribute to lameness. Biopsies taken from the paw of an affected dog revealed marked hyperkeratosis and acanthosis of the epidermis (Drogemuller et al., 2014). As a consequence of this discovery, dog breeders can now use commercially available genetic screens for variants in FAM83G to screen for HFH.

As the reported deletion in mice results in a severely truncated and probably non-functional protein, it is likely that the mutation in dogs, with a similar clinical phenotype is also loss of function.

Tightly regulated homeostatic mechanisms determine the turnover of skin and hair and nail matrix cells to maintain stable epidermal thickness and rate of hair and nail growth The animal phenotypes reported, comprising bushy hair, rapid nail growth and footpad thickening suggest that loss of functional FAM83G results in an imbalance of epidermal homeostasis.

5.1.4 Maintaining Epidermal Homeostasis – The Stem Cell

Over the course of a human lifetime, the outer layers of the epidermis are replaced over a thousand times. Intricate regulatory mechanisms govern the balance between proliferation and differentiation of cells in the basal layer that give rise to distinct epidermal lineages. Self-renewing stem cells residing in the basal layer of the epidermis play a critical role in replenishing the epidermis during homeostasis and in response to injury (Solanas and Benitah 2013). The key defining characteristics of stem cells are as follows:

1. It Is not itself terminally differentiated
2. It can divide without limit
3. Its daughters have the choice to either remain a stem cell or commit to terminal differentiation.

To maintain a steady state within the epidermis, precisely 50% of the daughters of stem cells in each generation must remain as stem cells. Stem cells are also required for skin appendages such as the hair and nails. The nail matrix contains a small population of self-renewing stem cells which sustain continuous growth of the nail. These cells can even orchestrate reconstruction of a partially amputated digit (Tekeo et al. 2013). Stem cells in the hair follicle have been intensively studied and will be discussed later in this chapter.

5.1.5 Canonical Wnt Signaling Pathway

Wnt signalling is a highly conserved pathway which is required for the maintenance of adult epithelial stem cells of various lineages. They are well known to regulate stem cell pluripotency and regulate multiple processes during development, such as cell polarity and embryonic induction and the specification of cell fate. Stem cell proliferation and malignant transformation are often considered " two sides of the same coin" and as such, misregulation

of Wnt signalling is widely implicated in human cancer (Solanas et al., 2014). Several components of the pathway are known oncogenes or tumour suppressors and this is the focus of much investigation for therapeutic discovery. Although both canonical and non-canonical Wnt signalling pathways exist, this chapter will focus on canoncical Wnt signalling which plays a key role in the skin and its appendages.

Canonical Wnt signalling is mediated by its intracellular signal transducer protein, β-catenin. It is initiated by the binding of Wnt ligands to the extracellular binding domain of their corresponding 7 pass transmembrane G-coupled receptors (Frizzled, Fz) and the activation of Disheveled (Dvl). These receptors then form a complex with co-receptors LRP5/6 which results in their activation. In the absence of Wnt signalling, β-catenin is sequestered and degraded at the cell surface membrane by a "destruction complex" comprising AXIN, APC, GSK3, Casein Kinase 1a and PP2A, which phosphorylate the amino terminal of β-catenin and leads to its recognition by E3 ubiquitin Ligase B-TrCP which targets it for proteosomal degradation (Stamos and Weis, 2013). This continual degradation prevents β-catenin translocating to the nucleus.

When Wnt is activated, the destruction complex is inhibited because Axin is recruited to the complex. β-catenin phosphorylation and degradation is reduced and it becomes stabilized, accumulating in the cytoplasm and subsequently translocating to the nucleus (Figure 5.4). Although nuclear β-catenin does not bind DNA itself, it does interact with the TCF/LEF family of transcription factors leading to transcription of pro-proliferative Wnt target genes such as *c-myc* and *c-jun.* The details of how β-catenin shuttles between the cytoplasm and nucleus remain largely unknown however, microtubules and active transport are thought to be involved (Sugioka et al., 2011).

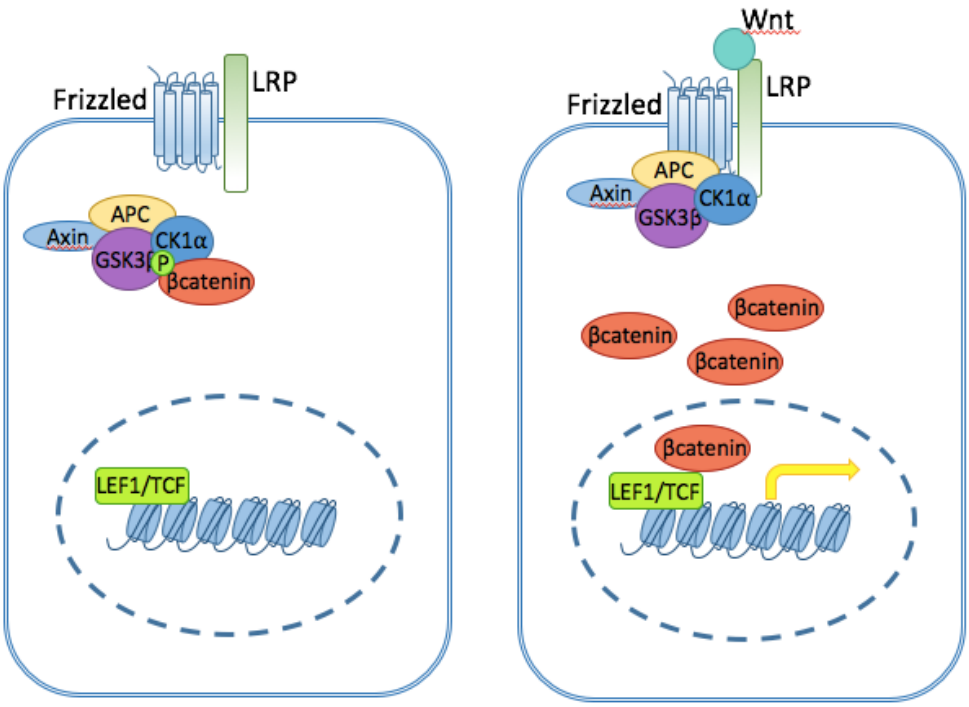

Figure 5.4 Canonical Wnt signalling. **(A)** In the absence of Wnt signalling, phosphorylated B Catenin is sequestered in its destruction complex in the cytoplasm. **(B)**When Wnt ligands bind to Frizzled/LRP complexes at the cell membrane, the destruction complex is recruited, releasing β-catenin, now in its dephosphorylated "activated" state. It can then translocate to the nucleus and activate transcription factors such as TCF/LEF1 leading to the transcription of Wnt target genes (yellow arrow)

Constitutive activation of Wnt signalling has been linked to carcinogenesis. For example, autosomal dominantly inherited mutations in *APC* are linked with the familial cancer syndrome "Familial Adenomatosis Polyposis". Mutant APC prevents inhibition of β-catenin and results in a high risk of developing colorectal carcinoma in affected individuals. Furthermore, global exome-sequencing has confirmed that the majority of colorectal cancers carry inactivating APC mutations (Wood et al., 2007). Patients with hereditary Axin 3 mutations also carry a predisposition to colon cancer and have tooth agenesis (Lammi et al.,2004).

5.1.6 R Spondins and LGRs

The strength of Wnt signalling can be further fine-tuned in vertebrae by the R-spondin family of ligands and leucine rich repeat (LGR) G-coupled family of receptors (Clevers et al., 2014). R Spondins are ligands for LGR5, 5 and 6, a subgroup of the Rhodopsin family of GPCR's (de Lau et al 2012) and act as secreted ligands of Wnt signalling. The important role that R-Spondins play in embryogenesis has been shown by loss of function mutations in humans and mice. Inactivation of the R-Spondin 2 gene results in a "foot-less" mouse (Nam et al., 2007). R Spondin 1 mutations underlie gonadal development in XX individuals. R Spondin 3 regulates placenta development and causes embryonic death. Our group have previously found that loss of function mutations in R-Spondin 4 cause congential anonychia (absent or severely hypoplastic nails on fingers and toes) in humans (Blaydon et al. 2006).

LGR4-6 bind R-spondins in response to canonical Wnt signalling, which results in phosphorylation of LRP 5/6 and stabilised β-catenin (de Lau et al 2011).

LGR5 is a highly specific marker of actively proliferating stem cells in the intestine and hair stem cell bulge. They have been shown to mark long-lived yet slowly cycling cells in the hair stem cell bulge, which result in increased hair growth when transplanted into nude mice (Jaks et al., 2008).

5.1.7 Wnt/ β-catenin Signaling in the Hair Follicle Stem Cell Niche

The hair follicle has proved to be an ideal tissue in which to study stem cell behaviour due to its accessibility, and the well characterised anatomical nature of individual components of the hair stem cell niche. Wnt signalling is critical for hair follicle development and regeneration. When Wnt signalling is inhibited by ectopically expressed Dickkopf1 (DKK1), a secreted Wnt antagonist, in the skin of transgenic mice, there is complete failure of formation of the placode, the initial embryonic structure required for hair follicle development and this results in a hairless mouse (Andl et al. 2002). By contrast, sustained Wnt activity and nuclear translocation of β-catenin has been shown to induce *de novo* hair follicles within the epidermis of transgenic mice (Lo Celso et al, 2004) by redirecting keratinocytes in the interfollicular epidermis and sebaceous glands to differentiate along the hair follicle lineage.

5.1.8 Anatomy and Function of the Hair Follicle

Hair follicles are self-renewing structures containing distinct reservoirs of multipotent stem cells that are able to entirely regenerate the epithelium. At the base of the hair follicle is a pocket of dermal cells known as the dermal papilla, from which signals arise instructing epithelial stem cells in the hair bulge to divide and migrate to the base of the hair follicle and, in response to further cues from the dermal papilla, differentiate to form the hair shaft (Alonso and Fuchs, 2006). Hair does not grow continuously, but instead passes through sequential cycles of growth (Anagen), rest (Telogen) and shedding (Catagen). During each anagen phase, hair cycles are able to generate an entire hair shaft from root to tip. Cyclical growth and shedding of hair occurs throughout postnatal life and is influenced by hormonal changes, for example androgens in both men and women contribute to shortened anagen phase and miniaturisation of scalp hair follicles which cause androgenetic alopecia (AGA), a common form of hair loss. By contrast, during pregnancy, high levels of oestrogen lengthen anagen and reduces hair shedding (Langan et al., 2010).

Hair follicle cycling is governed by two opposing regulatory pathways – inhibitory Bone Morphogenic Protein (BMP) and activating Wnt signalling. During phases where BMP signalling predominates, hair enters the telogen (resting phase). Once Wnt signals surpass the threshold for activation, and β-catenin is translocated to the nucleus, the follicle is primed undergo telogen-anagen transition. Hair is then regenerated by stem cells located in the bulge, which migrate to the matrix at the tip of the hair bulb, and differentiate to form the multiple layers of the outgrowing hair shaft and inner root sheath. The rapidly dividing cells within the matrix elongate into the dermis by rapidly expanding during anagen (Alonso and Fuchs 2006). Distinct markers define bulge stem cells, these include LGR5, CD34 and Keratin 15. The inductive properties of hair bulge stem cells has been shown in an elegant series of experiments by Jahoda et al. (Jahoda et al., 1984) who demonstrated by transplantation, that adult bulge stem cells can induce the growth of hair when transplanted into follicles which would otherwise not grow hair. The regeneration of hair follicles requires activated β-catenin in dermal papilla cells (Enshell-Seijffers et al 2010). More recently, Zhou et al (Zhou et al. 2016) overexpressed a stabilised form of β-catenin in the dermal papilla which led to an accelerated rate of hair growth in mice by increased matrix cell proliferation and differentiation in hair follicles.

5.2 RESULTS

5.2.1 Clinical Phenotype

Two adult siblings from a Pakistani family with a history of parental relatedness presented with progressively deteriorating palmoplantar keratoderma. They reported marked thickening of the skin of the soles and to a lesser extent the palms since childhood. They also had thick, bushy and curly scalp hair, noticeable since the age of 2-3 years old, which they both commented grew very quickly, requiring frequent haircuts. The female siblings' hair could grow easily below her waist and was extremely thick. Examination revealed severe diffuse, verrucous hyperkeratosis with deep fissuring affecting the soles (Figure 5.5) and to a lesser extent, the palms. The hyperkeratosis was more marked at pressure bearing sites. Some hyperkeratosis was also noted in the interdigital spaces. There was no evidence of transgradiens. The toenails were dystrophic with onycholysis and leukonychia was also present, most evident in the finger nails. There was also some proximal nail fold erythema and periungual swelling. Onychomycosis was excluded by negative fungal culture. No abnormalities of teeth or sweating were identified. Both siblings had abundant curly, dense scalp hair. The affected females' hair had a matted appearance and was difficult to brush. There was no evidence of hair breakage and no scalp abnormalities were observed. Neither sibling described excessive hair growth elsewhere on the body and clinical examination did not reveal hirsutism. Both parents were examined and did not share any phenotypic similarity to their offspring. Neither sibling reported any further symptoms and a full skin examination did not reveal any additional phenotypic features. Both parents were examined and found to be unaffected and both had straight hair. Clinical photographs were taken with written patient consent.

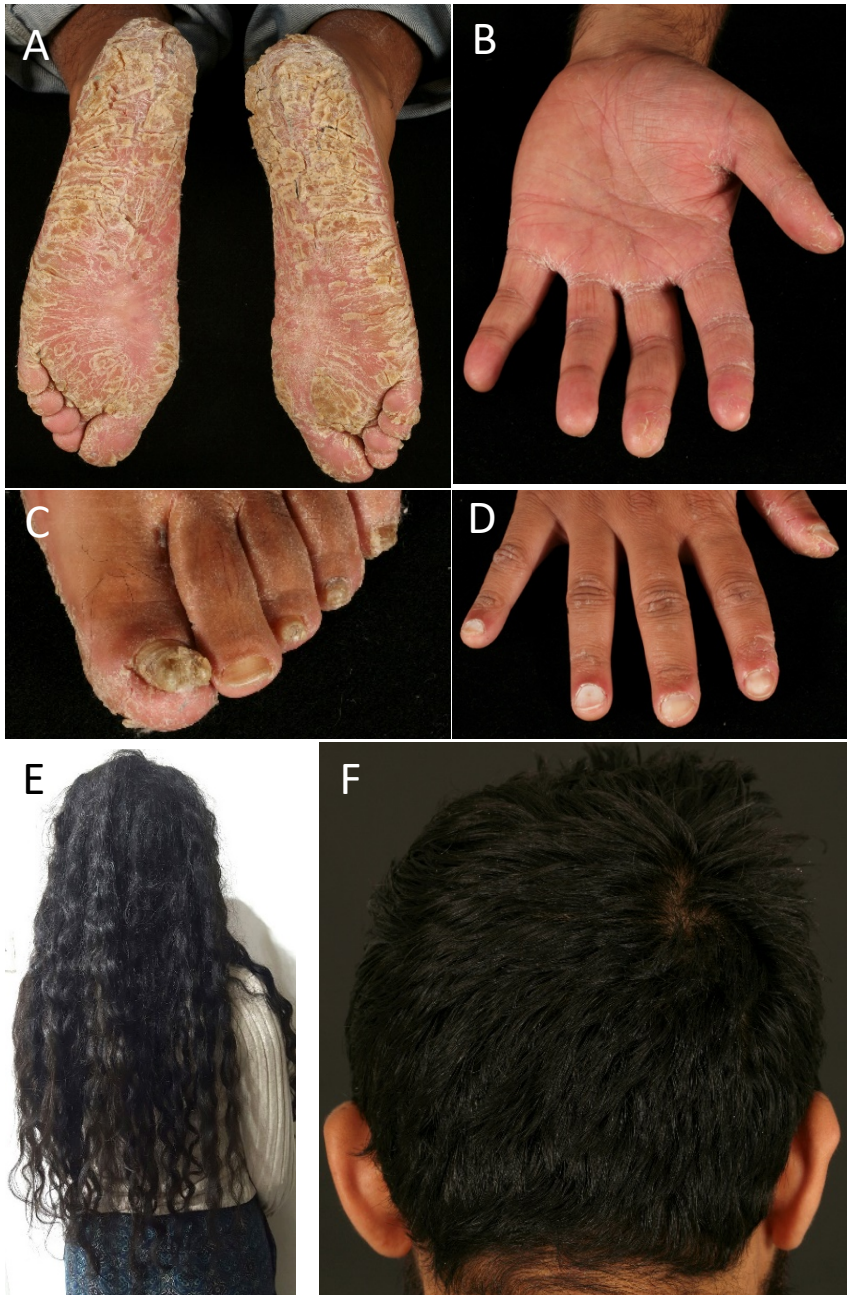

Figure 5.5 (A) Two siblings presented with diffuse, gross palmoplantar keratoderma, displaying marked hyperkeratosis and fissuring particularly affecting the soles and to a lesser extent the interdigital space **(B)**. The toenails were dystrophic **(C)** and leukonychia was observed in the hands **(D)**. The scalp hair was curly, thick, dense and had a matted appearance. The affected female could grow her hair beyond the waist **(E and F)**.

5.2.2 Exome Sequencing

Peripheral blood samples were collected for exome sequencing from all four family members after written informed consent in adherence with the Declaration of Helsinki Principles and approval of the East London and City Health Authority. Exomes were captured and enriched using SeqCap EZ Human Exome Library v3.0 (Roche NimbleGen, Madison, WI) and were sequenced on a Hiseq 2000 platform (Illumina, San Diego, CA) according to the manufacturer's instructions. Sequence variants were filtered against public databases (dbSNP137, 1000 Genomes Project, HapMap8). Given the history of parental relatedness of the family, the variants were filtered for homozygous changes shared by the two affected individuals, of which, 83 homozygous variants (i.e. variants identified in both chromosomes) were reported either as novel, or with an Exome Variant Server (NHLBI GO Exome Sequencing Project (ESP), Seattle, WA) estimated frequency of less than 0.01, were selected as potential candidates. These candidates included a homozygous C to A transversion, c.C101A, in exon 2 of *FAM83G* (NM_001039999) a gene reported to be mutated in Hereditary Footpad Hyperkeratosis (HFH) in Kromfohrländer and Irish terrier dog breeds, which presents with fissuring hyperkeratosis of the paws and a bushy coat (Drogemuller et al., 2014, Sayyab et al., 2016). Furthermore, the bushy hair phenotype of the "woolly" mice (*wly* mouse) has been linked to a 995bp deletion in *fam83g* (Radden et al., 2013). Therefore, the variant in *FAM83G* presented as an obvious candidate for further analysis. The homozygous c.C101A variant in *FAM83G* was confirmed by Sanger sequencing in both siblings and both parents were heterozygous carriers (Primer sequences: FAM83G-F: 5'CCGGGCTCATCAGGTCTTT 3' and FAM83G-2R: 5' GAGCGGTCCGACTTCTGG 3'; Figure 5.6A and D.1). The c.101C>A mutation results in loss of a Cac8I restriction endonuclease consensus site and segregation of the mutation with the condition was confirmed by RFLP (restriction fragment length polymorphism) analysis (Figure 5.6B) which was performed by Dr Diana Blaydon (Kelsell Group). The mutation c.C101A is predicted to change an evolutionary conserved alanine to glutamate (p.A34E) in the protein FAM83G. This missense mutation was absent from dbSNP, ExAC, 1000 genomes, gnomAD and EVS. It is predicted to be deleterious to the protein structure (Polyphen2 score 1.00, SIFT score 0.00) as the resulting amino acid change is from a non-charged, non-polar residue to a charged polar residue. This particular residue is conserved across 29 vertebrate species examined, 5 of which are shown here (Figure 5.6C) as well as between members of the FAM83 family of

proteins. The FAM83A-H family are characterized by the presence of a conserved N-terminal domain of unknown function; DUFI 669. Like the missense variant, p.A34E, reported in this study, the missense variant, p.R52P, underlying HFH in dogs is also located in the DUF 1669 domain (Figure 5.6D). FAM83G expression is specifically enriched (> five-fold) in the skin compared with 26 other tissue types (Edqvist et al., 2015). FAM83G has been implicated as a regulator of BMP signaling (Vogt et al., 2014)

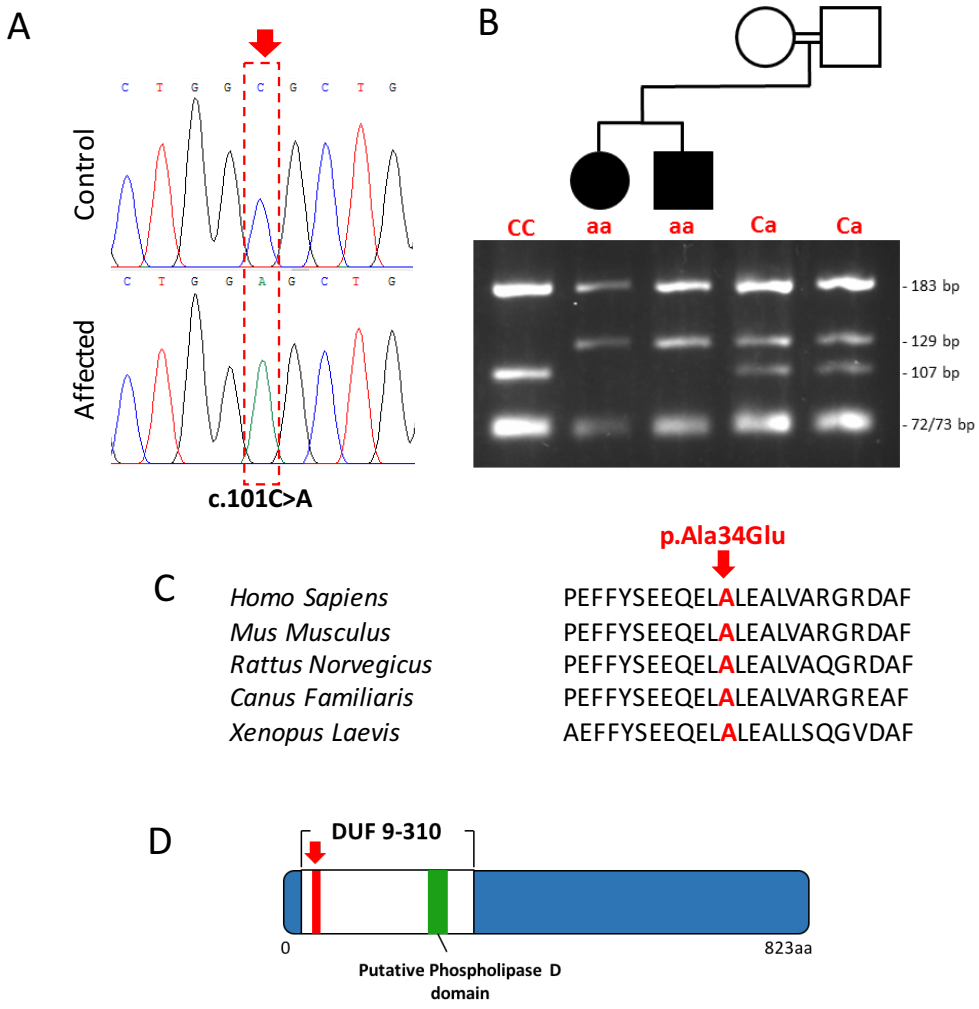

Figure 5.6 (A) Homozygous C to A mutation, c.101C>A, in *FAM83G* identified by exome sequencing was confirmed by Sanger sequencing **(B)** Segregation of the mutation within the family was confirmed by RFLP analysis (genotypes in red). **(C)** The mutation c.101A is predicted to result in the missense variant, p.A34E, in the FAM83G protein affecting an

alanine residue (indicated in red) that is evolutionary conserved across vertebrates. **(D)** The mutation occurs within the DUF1669 (red arrowhead)

5.2.3 Histology and Immunohistochemistry

With informed consent, a 5mm punch biopsy was taken from the right thigh of the affected male sibling. The skin at this site appeared clinically normal. Unfortunately, both siblings declined a biopsy being taken from the scalp, palms or soles. H&E staining of the patients skin showed some evidence of an acanthosis, and thickening compared with site-matched normal skin. There was no evidence of hyperkeratosis (Figure 5.7).

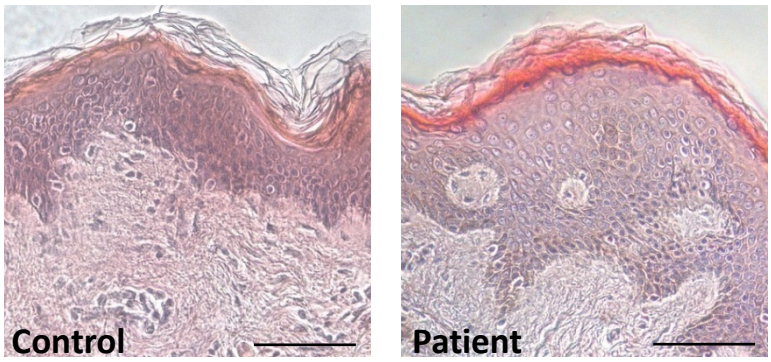

Figure 5.7 H&E staining of patient skin reveals acanthosis compared with site matched control skin (Scale bar 50 µm) .

Immunohistochemistry for FAM83G (Abcam ab121750, Cambridge, UK) revealed that its expression was diminished throughout the epidermis of the patients' skin. In control skin, FAM83G was observed throughout the epidermis, more prominently in the basal layers in keeping with previous reports (Drogemuller et al., 2014 (Figure 5.8).

As the H&E and the clinical phenotype were suggestive of a hyperproliferative aetiology, immunohistochemistry was performed for known proliferation markers; Ki67 (Abcam ab15580) and K14 (CRUK LL001). Both appeared upregulated in the patient skin compared with control. Interestingly, K14 immunostaining which is usually confined to the basal layer in the normal epidermis, extended to the suprabasal layers (Figure 5.8). These observations support the hypothesis of increased keratinocyte proliferation in the patient skin.

As epidermal homeostasis is a balance between proliferation and differentiation, immunohistochemistry for epidermal differentiation markers K10 (Ab9026, Abcam, UK),

Loricrin (Ab85679) and Filaggrin (Ab81468) were also performed (Figure 5.9). Their distribution and expression appeared to be similar between control and patient skin. Suggesting that, at least in clinically normal-appearing skin, the missense mutation in FAM83G results in increased proliferation without altering differentiation.

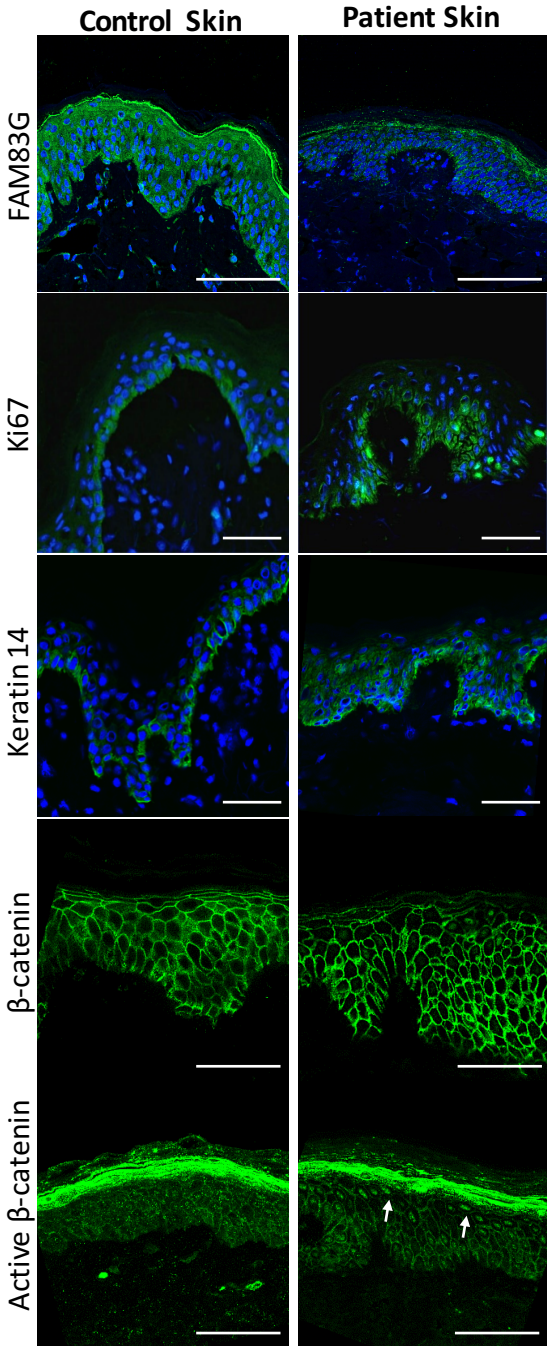

Figure 5.8 Patient epidermis displays reduced FAM83G expression. Upregulation of Ki67 is observed in the basal layers. Keratin 14 expression appears increased and extends to suprabasal layers. Total β-catenin expression appears similar between patient and control skin, although some nuclear staining is seen in the upper layers. Active nuclear β-catenin

expression is markedly increased in patient skin compared to control and extends to the upper layers (white arrow) (Scale bars 50µm). Negative control Appendix Figure D.2.

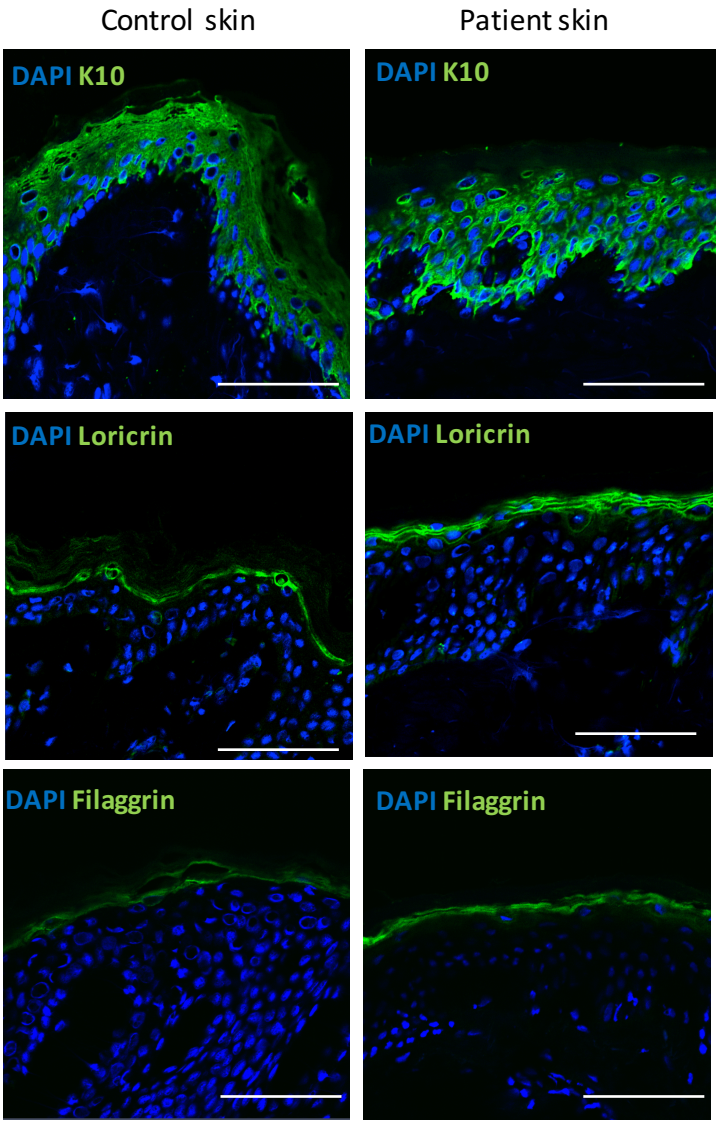

Figure 5.9 Immunohistochemical staining of differentiation markers K10, Loricrin and Filaggrin showed similar localisation and expression between patient and control skin. (Scale bars 50µm). Negative control Appendix Figure D.2

5..2.4 Confocal Hair Analysis

As the hair phenotype in both affected siblings and the animal models appears to have a striking hair component, we performed confocal hair analysis in collaboration with the Maatta Lab (University of Dundee). Hair samples from both parents and the affected son were sent for analysis. Confocal imaging of hairs revealed membrane bound deposits on the outer cuticle of the hair shaft in 30% of the patients' hairs (Figure 5.10 A arrowhead), which were absent in the parents' hair shaft. This was confirmed by transmission electron microscopy (X4000) (5.10 B) and was felt to be consistent with poorly differentiated cuticle cells. It is possible that this could occur in the presence of increased proliferation within the hair follicle. No other abnormalities of the hair shaft were identified.

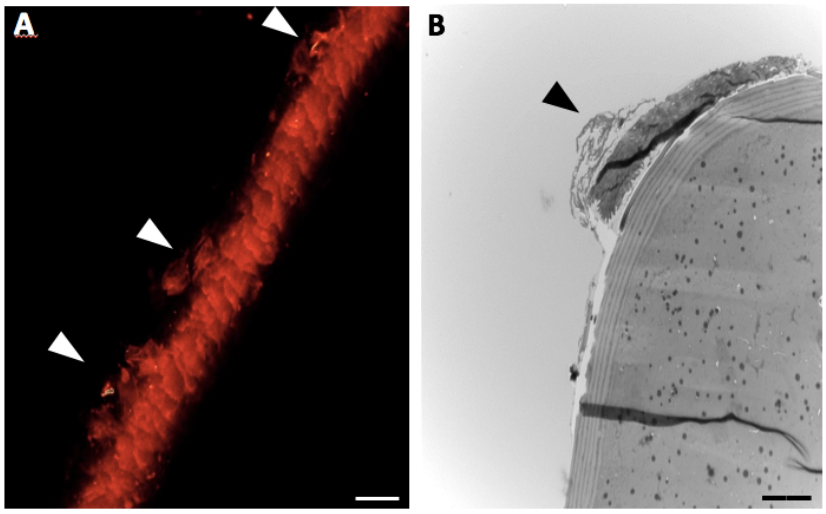

Figure 5.10 (A) Confocal imaging of the hair shaft from the affected sibling shows membrane bound deposits on the outer cuticle of the hair shaft (white arrowhead) (Scale bar 25µm). **(B)** TEM of a cross section of the affected siblings' hair shaft show regions of poorly differentiated cuticle cells (black arrowhead)(Scale bar 4µm).

5.2.5 FAM83G expression profiling

Publicly available large scale datasets can provide a useful tool in identifying the potential role for novel genes. The Lifemap discovery website (www.discovery.lifemapsc.com) holds a repository of numerous microarray datasets derived from the literature. A search for FAM83G in this repository highlighted that it was found in three individual microarray analyses of hair bulge stem cells. In one study by Greco et al. (Greco et al., 2009), FAM83G was one of 102 genes found to be differentially upregulated in hair bulge stem cells compared with dermal papilla cells in adult mice, with a 6.12 fold change observed. Although not conclusive, taken together with the strikingly similar clinical phenotypes in humans, dogs and mice, this could suggest a hitherto unidentified role for FAM83G in hair follicle stem cells.

5.2.6 FAM83G and β-catenin

The most striking and unifying feature of the three reported phenotypes in animals and humans is the presence of bushy, thick hair that is also longer than the hair of their wild type littermates. Histological evaluation of the hair follicle of the *wly* mice has previously shown "giant" follicles all in anagen (Radden et al., 2013). The duration of anagen is the main determinant of hair length. This led us to hypothesise whether the mutation in FAM83G could result in increased Wnt activity, which could subsequently maintain hair in the anagen phase. β-catenin is a critical signalling molecule at the centre of canonical Wnt signalling and plays a pivotal role in hair and nail growth and skin homeostasis. We performed immunohistochemical staining with a total β-catenin antibody (BD Transduction Labs 610153, Oxford, UK) (Figure 5.8) in the patients skin and observed that β-catenin expression appeared similar between patient and control skin cells but subtle nuclear localisation was evident in the upper layers in patient skin. Nuclear B Catenin suggests its activation and propogation of downstream Wnt signaling. To confirm that β-catenin was indeed activated, immunohistochemical staining was performed with an active β-catenin antibody (Merck Millipore 05-655 Clone 8E7, Watford, UK) and this demonstrated rather strikingly, nuclear accumulation throughout the epidermis in patients' skin compared with control skin where its expression was minimal (Figure 5.8). Initial staining was performed by myself and repeated by Lisa McGinty (PhD student, Kelsell group) for the purposes of publication.

5.2.7 FAM83G Expression in Murine Hair Follicles

To further explore the role of FAM83G in hair follicles, immunohistochemical staining was performed in hair follicles from the back skin of control mice in different phases of the hair cycle. FAM83G was found to be expressed during the anagen growth phase (P28) (Figure 5.11 A) and exhibited high levels of staining intensity at the IRS as well as in the dermal papilla. The expression of FAM83G appeared to be maintained in catagen/early telogen (P42), within the IRS (Figure 5.11 B). As outlined previously, FAM83G has previously been identified as a differentially expressed gene in adult mouse hair bulge stem cells compared with dermal papilla cells during telogen (P56) (Greco et al., 2009).

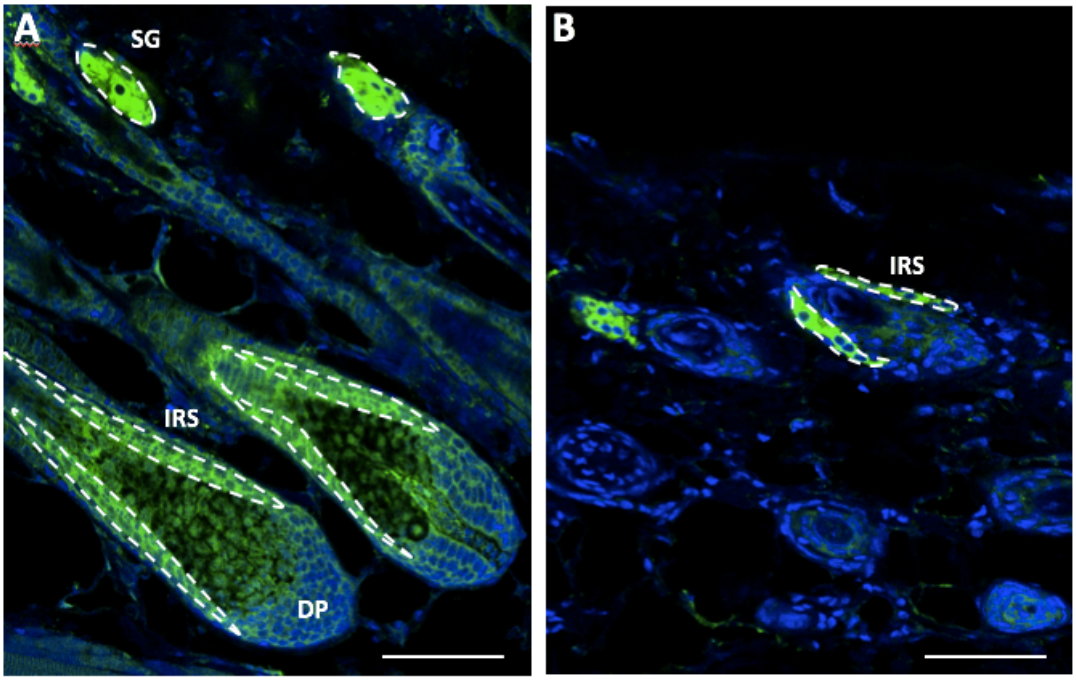

Figure 5.11 (A) FAM83G expression in the murine hair follicle during anagen (P28) is observed in the Inner Root Sheath (IRS), Dermal Papilla (DP) and sweat glands (SG). **(B)** FAM83G expression is observed in the IRS during catagen/early telogen (P42). Scale bar 50µm. Negative control Appendix Figure D.2

5.2.8 FAM83G Knock-Down in HaCaT Keratinocytes

HaCaT cell lysates in which FAM83G had been knocked-down by sh-RNA were received as kind gift from the Sapkota Lab (Dundee, UK) for this project. These lysates were immunoblotted and probed for β-catenin and Active β-catenin (Anti-ABC Clone 8E7, Merck, Millipore, dephosphorylalted Ser37 or Thr41)). Western blotting of these lysates showed no differences in total β-catenin. However Active β-catenin appeared to be upregulated at protein level in FAM83G-KO cells (n=3). Other downstream markers of Wnt signalling such as Axin, c-myc, TCF, R Spondin 1 and 4 were also assessed but differences were not observed (Figure 5.12) . It is important to note that this data is preliminary and at the time of writing, the role of FAM83G in Wnt signalling is unknown. This preliminary data suggests that there may be a relationship between FAM83G and active β-catenin however further investigation of downstream markers such as LEF1, Cyclin D1, c-myc and c-jun are necessary to characterise this relationship further.

One hypothesis that could explain our findings is that FAM83G could be part of the β-catenin destruction complex. Unpublished work by Hans Clevers lab have identified FAM83G as a novel binding partner for AXIN2. A further potential area of study could be whether FAM83G interacts with keratins. FAM83H has been shown to regulate keratin filament spatial organisation by interaction with CK1a. It is possible that FAM83G, which also shares the same DUF region as FAM83H could also interact with the keratins but at present this remains speculative. Wnt signalling in humans is complex and affected by multiple converging signalling pathways, therefore although some novel findings are observed here, a great deal of further work is necessary to unravel the complexities of FAM83G in the skin. A more recent study has identified the DUF domain as a requirement for interaction with CK1a for the FAM83 family of proteins, highlighting their novel role of FAM83 proteins in Wnt signalling (Fulcher et al., 2018).

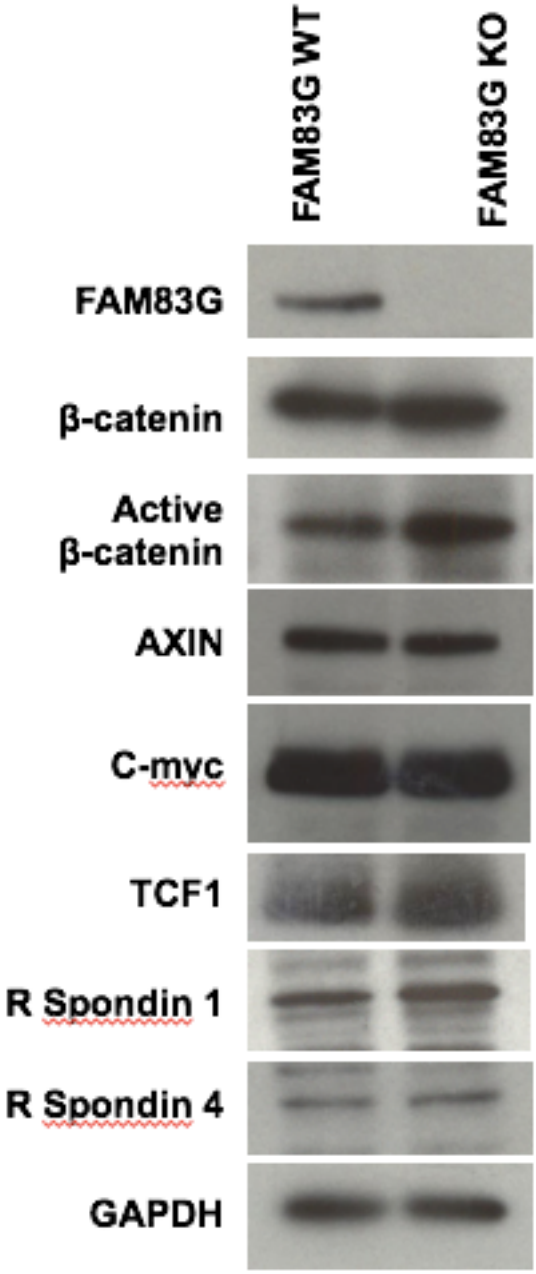

Figure 5.12 Immunoblotting of lysates extracted from FAM83G KO cells was performed and showed upregulation of active β-catenin but no clear differences in Axin, C-myc, TCF1, R spondins 1 and 4. GAPDH was used as a loading control.

5.3 Discussion

5.3.1 A novel role for FAM83G in human skin, hair and nail homeostasis

The predominant focus of this work is the novel identification of a disease-causing mutation in FAM83G in humans. The missense mutation identified is predicted to be damaging, suggesting a loss-of-function effect. This work presented here formed the basis of a paper published by Maruthappu et al., 2018. The findings highlight a hitherto unidentified role for FAM83G in the homeostasis of the palmoplantar epidermis and hair follicle. Across all three species identified in this and previous publications, mutations in FAM83G affect the highly conserved DUF1669, and result in a similar clinical phenotype. We have highlighted a a role for this novel protein in skin, hair and nail homeostasis. A challenge faced during the publication of this work is that at the time of writing, very little was known about the function of FAM83G in human skin therefore it was possible only to speculate on its role.

5.3.2 Mutations in FAM83G are associated with increased proliferation markers in the epidermis

In patient skin, we have shown evidence for hyperproliferation, with increased K14 and ki67 in the basal layers. This is particularly interesting because the site of the biopsy used for these studies was the patients' thigh, and appeared phenotypically normal with no overt evidence of thickening of the epidermis. Differentiation markers, K10, Loricrin and Filaggrin all showed comparable immunostaining to control skin, suggesting that in patient skin, there is increased basal proliferation without overt changes in differentiation. It is possible that these patients have increased turnover of clinically normal appearing skin.

One interesting finding was the increased nuclear localization of β-catenin in patient skin compared with control skin. This was observed using an antibody for "active" B Catenin (Merck, Millipore AE07). Total β-catenin however was comparable between the two samples. Nuclear β-catenin was observed throughout the epidermis in patient skin. Nuclear β-catenin is rarely seen in the normal adult human epidermis but does occur in non-melanoma skin cancers such as Basal cell carcinomas, Squamous cell carcinomas and

Pilomatrixomas (Doglioni et al., 2003). It has also been observed in the suprabasal layers of hyperproliferative psoriatic skin and in the wound healing state (H Clevers., 2006). Full skin examination of our patients have not revealed such tumours but they remain under regular surveillance. It is possible that upregulated β-catenin activity in the palmoplantar epidermis of affected patients skin and nails contributes to the development of the marked hyperproliferative palmoplantar keratoderma. Furthermore, recent research has linked a close family member FAM83H to upregulated Wnt/ β-catenin signaling and a similar mechanism is highly likely to contribute to the skin hair and nail phenotype observed (Yang et al., 2018).

The findings above led us to consider whether FAM83G could in fact play a role in canonical Wnt signaling. Previous publications have shown that overexpression of active β-catenin in the murine epidermis increases the thickness (with increased density of hair follicles) and length of hair growth (Zhou et al., 2016), which bears similarity to the hair phenotype observed in our affected patients.

5.3.3 Mutations in FAM83G result in a striking hair phenotype

Our patients exhibited a striking exuberant curly/wavy hair phenotype, which is also observed in both animal models. Anecdotally, our patients also reported rapid hair growth, with the affected male cutting his hair every month. The affected female could easily grow her hair beyond the waist. Neither parent exhibited a similar phenotype. Unfortunately, our patients declined a scalp biopsy, which could have shed further light on the role of FAM83G in the human hair follicle. However, confocal microscopy of the hair shaft of affected patients uncovered the presence of deposits on the cuticle in 30% of the patients' hair samples, absent from both parents and control hair. Electron microscopy suggested that these were poorly differentiated cuticle cells. This could result from hyperproliferation within the hair follicle.

Murine hair follicles undergo predictable cycling and therefore allow examination of the hair follicle at different phases of the hair growth cycle. Murine hair follicles in Anagen (P28) and Telogen (P42) were a kind gift from Dr Kristin Braun. Immunohistochemistry of FAM83G showed it localized to the inner root sheath and dermal papilla during anagen and in the inner root sheath during telogen.

The inner root sheath is composed of the inner root sheath cuticle, Henley's and Huxley's layers. BMP, Wnt/ β-catenin and Notch signaling are responsible for the normal differentiation of matrix cells into the hair shaft and IRS envelope. Mutations in genes such as Gata3, which is expressed in the IRS, can lead to alterations in the hair shaft (Kaufman et al., 2003). FAM83G also localized to the Dermal Papilla during anagen. Dermal papilla cells have been shown to instruct surrounding matrix cells to proliferate and move upwards subsequently differentiating into the various layers of the hair shaft and the inner root sheath (Millar et al., 2002). Although several pathways have been implicated in the reciprocal signaling between the DP and matrix cells, Wnt signaling has emerged as dominant (Millar et al., 2002). Furthermore, inhibition of β-catenin signaling in the DP has been shown to induce catagen and prevent anagen induction (Enshell-Seijffers et al., 2010). By contrast, Zhou et al., (2016) demonstrated that overexpression of a stabilized form of β-catenin (resistant to degradation as it lacks key ubiquitination sites) promoted hair follicle neogenesis and accelerated hair growth. Of note, the hair follicles were significantly denser and hair shafts were longer than in controls. They were also found to remain in anagen longer than in controls. It is interesting to consider these findings in light of the fact that histopathology from the *wly* mouse demonstrates "giant hair follicles in anagen" (Radden et al., 2013).

What is particularly unusual is why increased body hair growth was not observed in either affected patient. It may be that FAM83G exerts specific actions within the scalp hair follicle or that the threshold for activation of hair growth differs between body hair and scalp hair.

5.3.4 Recent insights into FAM83G

Since the publication of this work (Maruthappu et al., 2018a), very recently published work by the Sapkota group (Dundee) have shed further light on the role of FAM83G through experiments performed in vitro and in *Xenopus* (Fulcher et al., 2018, Bozatzi et al., 2018)

Although it was initially felt that the role of FAM83G was to interact with SMAD1 and subsequent regulation of BMP signaling, this group now feels that this is actually a more minor function, and the predominant role of FAM83G, and the FAM group of proteins is in interacting with casein kinase isoforms. They have identified that the DUF1669 domain is critical for this interaction to occur in FAM83A-H (Fulcher et al., 2018). They also discovered

that mutations in the DUF1669 impaired the ability of FAM proteins to interact with CK1 isoforms and interfered with its proper subcellular localization. Furthermore, the group have shown that FAM83G does indeed regulate Wnt signaling at the level of the destruction complex. They show that overexpression of FAM83G mRNA results in complete axis duplication in Xenopus embryos, a feature of heightened Wnt signaling (Bozatsi et al., 2018).

Although exciting, their findings appear to somewhat contradict what we have observed in our patients. Patient skin carrying homozygous recessive mutations in FAM83G within the DUF1669, which are assumed to be loss-of-function because of the predicted effects on protein structure, show increased nuclear β-catenin, a feature of upregulated Wnt signaling. Furthermore, the clinical phenotype supports hyperproliferation in human skin, hair and nails. Although this appears to be in contrast with work from the Sapkota lab, it could potentially be reconciled if the mutant FAM83G in our patients, fails to sequester CK1a because it occurs within the DUF1669 domain, potentially resulting in relative overexpression of CK1 isoforms and subsequent propogation of Wnt signaling and associated nuclear translocation of β-catenin. Moreover, our studies were performed in humans, whereas these two publications primarily used human cell lines (U2OS bone cells) and *Xenopus* for their studies. Intriguingly, immunoblotting of FAM83G KO U2OS lysates gifted from the Sapkota lab appeared to show increased active β-catenin (Figure 5.12) but not other downstream markers of Wnt activity. However, after discussion with Dr Sapkota, it was revealed that they have also observed increased β-catenin GS3KB phosphorylation sites (Ser37 and Thr 41) in this cell line, (which is in fact the target of the ABC antibody used in our experiments) at basal unstimulated conditions (Bozatzi et al., 2018 - Figure 9A.) However, following stimulation of Wnt and using a Wnt3A reporter assay, mRNA expression and cell fractionation, they were able to demonstrate reduced nuclear localisation of active β-cateninin FAM83G KO cells (Bozatsi et al., 2018). An alternative hypothesis is that the mutation observed in our patients are not loss-of-function as originally hypothesized but gain-of-function. One way to investigate this would be to clone the mutation in human keratinocytes and perform co-immunoprecipitation to determine its impact on CK1 binding. It would then also be possible to assess the downstream impact on Wnt signaling.

5.3.5 Clinical Relevance

The data presented in this chapter provide for the first time, an introduction to the possible role of FAM83G in human skin, hair and nail growth. This is particularly interesting because despite an obvious hair skin and nail phenotype, these patients are otherwise healthy. If FAM83G does indeed play a role in the regulation of human scalp hair growth, resulting in increased density and length of hair growth, it may well be an attractive target for therapeutic development. Dampened Wnt/β-catenin signaling is a feature of several common forms of hair loss, including alopecia areata and androgenetic alopecia (Lim et al., 2016). Further studies of FAM83G, in particular regarding its role in hair biology and the hair cycle, may support targeting FAM83G and associated pathways in scalp hair disorders

Chapter 6

Final Discussion & Future Work

6.1 Background

At birth, the epidermal skin of our palms and soles has a similar thickness to the skin elsewhere such as the forearm. As we expose these areas to physical stresses such as gripping and walking, the skin adapts by thickening to protect it against substantial external forces. Abnormally thickened skin affecting the palms and soles occurs in the PPK's. As described earlier, the PPK's have an intriguingly diverse range of genetic and acquired causes (Blaydon and Kelsell, 2014, Maruthappu et al., 2014). A subset of PPKs are also associated with diverse syndromes linked to other cutaneous features (Betz et al., 2012) and also non-cutaneous conditions such as hearing loss, cardiomyopathy and oesophageal cancer (Blaydon et al., 2012, Kelsell et al., 2001). The varied mechanisms underlying the development of keratodermas therefore lends itself more broadly to the exploration of the genetic basis of human disease. The focus of this thesis is the study of mutations underlying three distinct keratodermas, and how these mutations contribute to the development of the clinical phenotype observed, using three approaches:

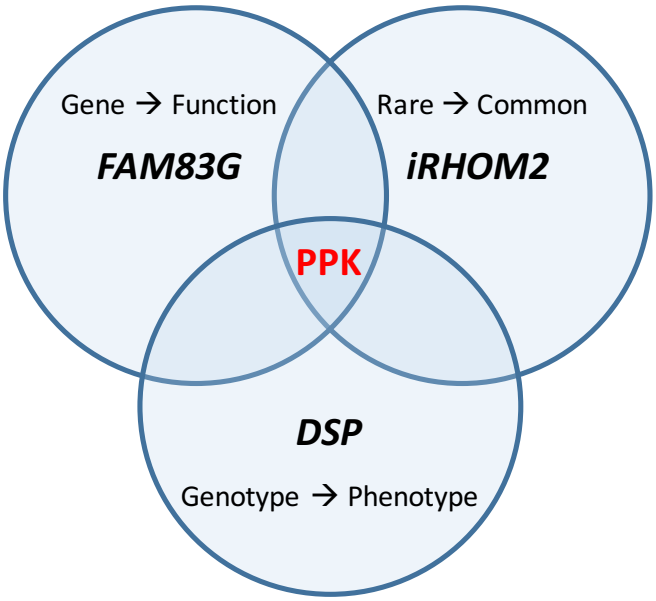

6.2 iRHOM2 and K16

Keratin 16 (K16) is a major cytoskeletal stress keratin, providing resilience at pressure-bearing sites such as the human palms and soles and mammalian footpad. It is also well established as a bio-marker, upregulated in hyperproliferative disorders including psoriasis and several cancers. Using *in vivo* and *in vitro* material from human and mouse, the work presented in this thesis identifies the inactive rhomboid protease iRHOM2 as a direct regulator of K16 (Maruthappu et al., 2017).

Historically, it has been considered that the keratins were simply structural components within the cell, providing mechanoresiliance in a site and situation specific manner. However, more recent evidence points to a more dynamic role for these proteins within the cell. For example, K17 has been found to regulate expression of Aire (Autoimmune regulator) and does so by translocating to the nucleus (Hobbs et al., 2015). Downstream effects include the transcription of pro-inflammatory genes. K16 has also been shown to regulate NRF2 and it is thought that oxidative stress resulting from hyperphosphorylated NRF2 in K16-/- mice contributes to the development of painful callouses and a Pachyonychia Congenita-like

phenotype (Kerns et al., 2016). More recently, iRHOM2 has been shown to play a key role in the cellular response to oxidative stress through the master regulator p63 (Arciadicono P et al., 2018), providing a mechanistic understanding for the role of K16 in oxidative stress.

K16 is highly upregulated at the wound edge, in specific carcinomas and in psoriasis. Previously, this has been attributed to the fact that K16 is highly dynamic and therefore expressed in hyperproliferative states. However, it would be interesting to determine whether in fact, the interaction between iRHOM2 and K16 influences its expression in these situations. iRHOM2 has been clearly implicated in the maturation of ADAM17 (TACE) and subsequent cleavage of TNFα (Adrain et al., 2012, McIlwain et al., 2012, Brook et al., 2014). As ADAM17 has also been implicated in wound healing, carcinomas and psoriasis (Gooz et al., 2010), it would be of interest to explore whether K16 plays an additional regulatory role in this interaction.

The discoveries made during the course of this thesis with regards to iRHOM2 and its role in keratinocyte biology may also have wider implications, namely the role of iRHOM2-K16 in keratinocyte hyperproliferation in psoriasis. Following on from this, studies are underway in the Kelsell group to investigate the role of iRHOM2 in psoriasis using iRHOM2 mice models in which a psoriatic phenotype has been induced. The aim of such studies is to determine whether irhom2KO can attenuate the development of psoriasis using the Imiquimod mouse model. In addition, iRHOM2 expression in lesional, non lesional and normal skin will be compared by immunohistochemistry and PCR studies.

6.3 *FAM83G* and its role in human skin and hair growth

The data presented in Chapter 5 are based on the identification of the first reported human disease-causing mutation in *FAM83G* associated with striking hyperproliferative skin, hair and nail phenotypes. The findings are comparable the to two animal models (Drogemuller et al., 2014, Radden et al., 2013). The involvement of skin, hair and nail phenotypes suggested a role for FAM83G in Wnt signalling. More recent studies have now shown that FAM83G forms part of the β-catenin destruction complex and may therefore regulate Wnt signalling (Bozatzi et al., 2018). Although aberrant Wnt signalling has strongly been implicated in oncogenesis, it is pertinent to note that the affected humans appear healthy, and all reported animal models have normal life expectancies. Therefore, the precise role of

FAM83G in Wnt signalling remains a promising area for further investigation, and one which Dr Sapkota's lab (MRC Protein Phosphorylation Unit, Dundee UK) continues to research.

One of the most striking and unique features of the cutaneous phenotype in the affected patients was the presence of abundant curly hair. Anecdotally, both affected patients reported rapidly growing hair and the affected female could grow her hair well beyond her waist. β-catenin/Wnt signalling is critical to the development of hair follicles and therefore precisely how FAM83G regulates this pathway is intriguing. The work presented in this thesis suggests that loss of FAM83G function appears to promote hair growth via upregulated β-catenin activity. Active β-catenin is located in the nucleus in patient skin, whereas it is expressed at low levels in control skin (Maruthappu et al., 2018a). β-catenin/Wnt signalling pathways have been studied in great detail so it is relatively surprising that FAM83G has not previously been identified as a component of this pathway. However, this study demonstrates how monogenic diseases can provide unique insights into the function of previously unknown genes.

The potential clinical relevance of *FAM83G* is compelling. Hair loss remains a significant concern to patients and can cause genuine distress. As such, the value of the global hair loss treatment market is over $2.8 billion and few effective treatments are available. The most common cause of hair loss is androgenetic alopecia, and over 85% of males over the age of 50 are affected, in addition to many women. Therefore, the discovery of a gene whose function is potentially linked to increased hair growth could benefit a large population. Androgenetic alopecia has been linked to dysregulated β-catenin/Wnt signalling via the androgen receptor (AR) (Kretzchumar et al. 2015). The AR has been shown to negatively impact on β-catenin signalling in mouse hair follicle bulb cells through reciprocal regulation. Further work would be required to characterise the role of FAM83G in different phases of the human hair cycle and in pathological states such as androgenetic alopecia.

6.4 Novel Cutaneous Phenotypes linked to Arrhythmogenic Cardiomyopathy

AC is a highly heterogeneous disorder with an incidence ranging from 1:5000 to 1:1000 depending on the population studied (Sen-Chowdhury et al., 2010). Due to the variability in presentation, the foremost clinical challenge in AC is making an accurate and timely

diagnosis. This is complicated by the fact that clinical features may be subtle or absent, and mutations in desmosomal genes contribute only up to 50% of cases. Further investigations into additional candidate genes have implicated non-desmosomal proteins such as *TGF-B3*, and *TMEM43* (Beffagna et al., 2005, Merner et al., 2008). In those patients who carry a desmosomal mutation, studies have shown that only 30-50% fulfill the AC Task Force Criteria (Towbin et al., 2008). One theory is that modifier genes may play a role in the variability of presentation particularly phenotypic differences within the same family. Genetic diagnosis may also be in part hampered by the incomplete sensitivity of mutation screening techniques which may miss mutations such as deletions and insertions or regulatory non-coding variants. It is likely that the advent of whole genome sequencing in a timely and cost-effective manner, will uncover hitherto unidentified causative genes in AC.

The work presented in this thesis identifies a cutaneous phenotype in autosomal dominantly inherited AC caused by mutations in *DSP*. Haploinsufficiency is likely to be the mechanism underlying the development of curly hair and PPK in the cohort of patients examined (Maruthappu et al., 2018b). The presence of a readily recognisable phenotype could facilitate diagnosis in AC, and is currently being considered for inclusion in the revised AC Task Force Criteria. However, mutations in *DSP* underlie only 10-15% of AC cases.

Mutations in *PKP2* are most common, contributing to 40% of causative desmosomal mutations (Sen-Chowdhury et al., 2010). AC caused by *PKP2* mutations appears to be non-syndromic and cutaneous features have not been reported to date. PKP2 is the only isoform expressed in the heart, whereas in the skin, both PKP1 and PKP3 are also expressed, and may compensate for PKP2 deficiency. Mutations in *DSG2* are responsible for 10-15% of desmosomal AC mutations. Again, hair and skin features have not been reported in those carrying *DSG2* mutations (Syrris et al., 2006, Awad et al., 2006). Functional redundancy of DSG2 in the skin, rescued by the presence of DSG1 and DSG3, may explain the lack of skin/hair features in these patients.

Despite this, it would be of interest to broaden the scope of the work presented here and undertake formal dermatological examination of patients with *PK2P*, *JUP*, *DSG2* and *DSC* mutations to determine whether subtle hair and skin features are evident. To date, these studies have not been performed involving a dermatologist. During the course of this study, one patient with a PKP2 mutation was reviewed, anecdotally he reported severe blistering

of both his feet after walking long distances. It may be that cutaneous features could become apparent under increased stress in such patients. It may also be fruitful to examine patients with AC in whom the genetic diagnosis remains unknown, to explore the presence of hair and skin features. It is plausible that even if the genetic causes is unknown, the similarities between the components of the intercalate disc and epidermis could result in a cutaneous phenotype

Skin biopsies taken from unaffected sites of patients with AC could demonstrate mislocalisation of desmosomal proteins. If validated against cardiac biopsies from the same patients and normal controls, this could potentially be of diagnostic benefit. Cardiac biopsies are difficult to obtain and carry procedural risks including precipitating arrhythmias and cardiac haemorrhage. By contrast, skin biopsies are much more straightforward to obtain, and could hypothetically be used for screening and diagnostic purposes. Asimaki et al. (Asimaki et al., 2017) have demonstrated changes in the distribution of cell junction proteins in buccal mucosa cells from patients with ARVC, similar to those observed in their cardiomyocytes. They propose that these cells could prove useful in studying disease mechanisms and potential therapies. However, the very nature of buccal mucosal cells is that they are prone to shedding. Therefore, studying adhesion complexes in these cells is likely to be fraught with complexities and less likely to be a true representation of cardiomyocytes. By contrast, cell-cell adhesion in the skin is critical to its function and robust, similar to that required in cardiomyocytes. The skin, and in particular the basal layer of the epidermis is therefore more likely to authentically represent the cardiac intercalate disc. If the findings of this thesis were validated, it could be a potentially useful aide in the early diagnosis of AC, which at present, remains the foremost clinical challenge.

6.5 Conclusions

The development of PPK's as a result of a diverse array of genetic mutations is a curious phenomenon. The palmoplantar skin is unique in its ability to withstand phenomenal physical stress. This remarkable adaptation may also be its vulnerability. Mutations in epidermal genes may be relatively compensated in the skin, but reveal themselves at stressed sites such as the palmoplantar epidermis. Consequently, of the known keratodermas, mutation carriers do not present with PPK at birth, but instead typically develop thickening of the palms and soles once they start walking or during times of

increased physical exertion. Mechanical stress in the skin can also act as a surrogate for "stress" elsewhere. For example, in TOC, we now know that epithelial "stress" caused by exposure to toxins e.g. alcohol and cigarette smoking, accelerates the development of oesophageal cancer. In AC, the presence of PPK is linked to impaired adhesion in cardiomyocytes and results in fibrofatty replacement in the myocardium. AC is exacerbated by "stress" and as such, patients are advised to limit strenuous activities.

The PPK's studied as part of this Thesis have provided a unique mechanistic insight into three diverse diseases. This adds to the significant body of work linking PPK's to numerous systemic disorders and highlights this peculiar phenomenon as an abundant resource for investigating genotype-phenotype correlation.

Bibliography

Adrain, C., Zettl, M., Christova, Y., Taylor, N., & Freeman, M. (2012). Tumor necrosis factor signaling requires irhom2 to promote trafficking and activation of TACE. *Science, 335*, 225–228.

Alcalai R., Metzger S., Rosenheck S., Meiner V., & Chajek-Shaul, T. (2003). A recessive mutation in desmoplakin causes arrhythmogenic right ventricular dysplasia, skin disorder, and woolly hair. *J Am Coll Cardiol, 42*, 319–327.

Alonso, L., & Fuchs, E. (2006). The hair cycle. *Cell Sci, 119*, 391–393.

Amagai, M., Matsuyoshi, N., Wang, Z. H., Andl, C., & Stanley, J. R. (2000). Toxin in bullous impetigo and staphylococcal scalded-skin syndrome targets desmoglein 1. *Nat Med, 6*(11), 1275–1277.

Amagai, M., Yamaguchi, T., Hanakawa, Y., Nishifuji, K., Sugai, M., & Stanley, J. R. (2002). Staphylococcal exfoliative toxin B specifically cleaves desmoglein 1. *J Invest Dermatol, 118*(5), 845–850.

Amagai, M. I., Klaus-Kovtun, V., & Stanley, J. R. (1991). Autoantibodies against a novel epithelial cadherin in pemphigus vulgaris, a disease of cell adhesion. *Cell, 67*(5), 869–877.

Andl, T., Reddy, S. T., Gaddapar, T., & Millar, S. E. (2002). Wnt signals are required for the initaiton of hair follicle development. *Dev Cell, 2*, 643–653.

Angst, B. D., Marcozzi, C., & Magee, A. I. (2001).The cadherin superfamily. *J Cell Sci, 114,* 629–641.

Armstrong, D. K., McKenna, K. E., Purkis, P. E., et al. (1999). Haploinsufficiency of desmoplakin causes a striate subtype of palmoplantar keratoderma. *Hum Mol Genet, 8,* 143–148.

Asimaki A., Syrris P., Wichter, T., Matthias, P., Saffitz, J. E., & Mckenna, W. J. (2007). A novel dominant mutation in plakoglobin causes arrhythmogenic right ventricular cardiomyopathy. *Am J Hum Genet, 81*, 964–973.

Asimaki, A., Protonotarios, A., James, C. A., Chelko, S. P., Tichnell, C., Murray, B., Saffitz, J. E. (2016). Characterizing the molecular pathology of arrhythmogenic cardiomyopathy in patient buccal mucosa cells. *Circulation: Arrhythmia and Electrophysiology, 9*(2), e003688.

Awad, M. M., Dalal, D., Cho, E., Amat-Alarcon, N., James, C., Tichnell, C., Judge, D. P. (2006). DSG2 mutations contribute to arrhythmogenic right ventricular dysplasia/cardiomyopathy. *Am J Hum Genet, 79*(1), 136–142.

Baroni, A., Buommino, E., De Gregorio, V., Ruocco, E., Ruocco, V., & Wolf, R. (2012). Structure and function of the epidermis related to barrier properties. *Clinics in Dermatology, 30,* 257–62.

Bauce, B., Basso, C., Rampazzo, A., et al. (2005). Clinical profile of four families with arrhythmogenic right ventricular cardiomyopathy caused by dominant desmoplakin mutations. *Eur. Heart J, 26,* 1666–16675.

Beffagna, G., Occhi, G., Nava, A., Vitiello, L., Ditadi, A., Basso, C., Rampazzo, A. (2005). Regulatory mutations in transforming growth factor-beta3 gene cause Arrhythmogenic right ventricular cardiomyopathy type 1. *Cardiovasc Res, 65,* 366–373.

Bergbold, N., & Lemberg, M. K. (2013). Emerging role of rhomboid family proteins in mammalian biology and disease. *Biochim Biophys Acta, 1828*, 2840–2848.

Bernot, K. M., Lee, C. H., & Coulombe, P. A. (2005). A small surface hydrophobic stripe in the coiled-coil domain of type I keratins mediates tetramer stability. *J Cell Biol, 168*, 965–974.

Bhonsale A., Groeneweg J. A., James, C. A., et al. (2015). Impact of genotype on clinical course in arrhythmogenic right ventricular dysplasia/cardiomyopathy-associated mutation carriers. *Eur Heart J, 36,* 847–855.

Blaydon, D. C., Ishii, Y., O'Toole, E. A, Unsworth, H. C., Teh, M.T., Ruschendorf, F., Kelsell, D. P. (2006). The gene encoding R-spondin 4 (RSPO4), a secreted protein implicated in Wnt signaling, is mutated in inherited anonychia. *Nat Genet, 38,* 1245–1247.

Blaydon, D. C., Biancheri, P., Di, W. L., Plagnol, V., Cabral, R. M., Brooke, Kelsell, D. P. (2011). Inflammatory skin and bowel disease linked to ADAM17 deletion. *N Engl J Med,* 365, 1502–1508.

Blaydon, D. C., Etheridge, S. L., Risk, J. M., Hennies, H. C., Gay, L. J., Carroll, Kelsell, D. P. (2012). RHBDF2 mutations are associated with tylosis, a familial esophageal cancer syndrome. *Am J Hum Genet, 90,* 340–346.

Blaydon, D. C., Lind, L. K., Plagnol, V., Linton, K. J., Smith, F. J., Wilson, Kelsell, D. P. (2013). Mutations in AQP5, encoding a water-channel protein, cause autosomal-dominant diffuse nonepidermolytic palmoplantar keratoderma. *Am J Hum Genet, 93,* 330–335.

Bolling, M. C., & Jonkman, M. F. (2009). Skin and heart: Une liaison dangereuse. *Exp Dermatol, 118,* 658–668.

Bonazzi, M., & Cossart, P. (2011). Impenetrable barriers or entry portals? The role of cell-cell adhesion during infection. *J Cell Biol, 195*, 349–

Bozatzi, P., Dingwell, K. S. 2., Wu, K. Z. 1., Cooper, F., Cummins, T. D. 1., Hutchinson, L. D., & Sapkota, G. P. (2018). PAWS1 controls Wnt signalling through association with casein kinase 1a. *EMBO Rep. 19*(4), e44807.

Brennan, D., & Mahoney, M. G. (2009). Increased expression of Dsg2 in malignant skin carcinomas: A tissue-microarray based study. *Cell Adh Migr*, *3*, 148–154.

Brooke, M. A., Nitoiu, D., & Kelsell, D. P. (2012). Cell-cell connectivity: Desmosomes and disease. *J Pathol, 226*, 158–171.

Brooke, M. A., Etheridge, S. L., Kaplan, N., Simpson, C., O'Toole, E., Ishida-Yamamoto, A., & Kelsell, D. P. (2014). Irhom2-dependent regulation of ADAM17 in cutaneous disease and epidermal barrier function. *Hum Mol Genet, 23*(15), 4064–4076.

Brooke, M. A., Nitoiu, D., & Kelsell, D. P. (2012). Cell-cell connectivity: Desmosomes and disease. *J Pathol, 226,* 158–171.

Broussard, J. A., Getsios S., & Green, K. J. (2015). Desmosome regulation and signaling in disease. *Cell Tissue Res, 360*, 501–512.

Cabral, R. M., Tattersall, D., Patel, V., et al. (2012).The DSPII splice variant is crucial for desmosome-mediated adhesion in HaCaT keratinocytes. *J Cell Sci, 125,* 2853–2861.

Castelletti S., Vischer A. S., Syrris, P., et al. (2017). Desmoplakin missense and non-missense mutations in arrhythmogenic right ventricular cardiomyopathy: Genotype-phenotype correlation. *Int J Cardiol, 249*, 268–273.

Cerrone, M., Noorman, M., Lin, X., Chkourko, H., Liang. F.X., van der Nagel, R., Delmar M. (2012). Sodiumcurrent deficit and arrhythmogenesis in a murine model of plakophilin-2 haploinsufficiency. *Cardiovasc Res, 95,* 460–468.

Chen, H., Bonifas, J. M., Matsumura, K., Ikeda, S., Leyden, W. A., & Epstein, E. H. J. R. (1995). Keratin 14 gene mutations in patients with epidermolysis bullosa simplex. *J Invest Dermatol*, *105,* 629–632.

Christova, Y., Adrain, C., Bambrough, P., Ibrahim, A., & Freeman, M. (2013). Mammalian irhoms have distinct physiological functions including an essential role in TACE regulation. *EMBO Rep, 14*, 884–890.

Cipriano R., Graham, J., Miskimen, K. L. S., Bryson, B. L., Bruntz, R. C., Scott, S. A, Jackson, M. W. (2012). FAM83B mediates EGFR- and RAS-driven oncogenic transformation. *J Clin Invest, 122,* 3197–3210.

Cipriano, R., Miskimen, K. L. S., Bryson, B. L., Foy, C. R., Bartel, C. A., & Jackson M. W. (2014). Conserved oncogenic behavior of the FAM83 family regulates MAPK signaling in human cancer. *Mol Cancer Res, 12,* 1156–1165.

Cipriano, R., Miskimen, K. L. S., Bryson, B. L., Foy, C. R., Bartel, C. A., & Jackson M. W. (2013). FAM83B-mediated activation of PI3K/AKT and MAPK signaling cooperates to promote epithelial cell transformation and resistance to targeted therapies. *Oncotarget, 4*, 729–738.

Clark, R. A. (2010). Skin-resident T cells: The ups and downs of on site immunity. *J Invest Dermatol, 130,* 362–370.

Clevers, H., Loh, K. M., & Nusse, R. (2014). Stem cell signaling. An integral program for tissue renewal and regeneration: Wnt signaling and stem cell control. *Science, 346,* 6205

Clevers, H. (2006).Wnt/beta-catenin signaling in development and disease. *Cell, 127*, 469–480.

Coats, C. J., Quarta, G., Flett, A. S., et al. (2009). Arrhythmogenic left ventricular cardiomyopathy. *Circulation, 120,* 2613–2614.

Corrado, D., Basso, C., & Judge, D. P. (2017). Arrhythmogenic cardiomyopathy. *Circ Res, 121*, 784–802.

D'Alessandro, M., Russell, D., Morley, S. M., Davies, A. M., & Lane, E. B. (2002). Keratin mutations of epidermolysis bullosa simplex alter the kinetics of stress response to osmotic shock. *J Cell Sci, 115,* 4341–4351.

De Lau, W, Barker, N., Low, T. Y, Koo, B. K., Li, V. S., Teunissen H., & Clevers, H. (2011). Lgr5 homologues associate with Wnt receptors and mediate R-spondin signalling. *Nature, 476*(7360), 293–297.

Delmar, M., & McKenna, W. J. (2010). The cardiac desmosome and arrhythmogenic cardiomyopathies: From gene to disease. *Circ Res*, *107*(6), 700–714.

Desai, B. V., Harmon, R. M., & Green, K. J. (2009). Desmosomes at a glance. *J Cell Sci*, *122*(24), 4401–4407.

Ding, X., Diaz, L. A., Fairley, J. A., et al. (1999). The anti-desmoglein 1 autoantibodies in pemphigus vulgaris sera are pathogenic. *J Invest Dermatol, 112,* 739–743.

Doglioni, C., Piccinin, S., Demontis, S., et al. (2003). Alterations of beta-catenin pathway in non-melanoma skin tumors: Loss of alpha-ABC nuclear reactivity correlates with the presence of beta-catenin gene mutation. *Am J Pathol, 163*(6), 2277–2287.

Drogemuller, M., Jagannathan, V., Becker, D., Drogemuller, C., Schelling, C., Plassais, J., et al. (2014). A mutation in the FAM83G gene in dogs with hereditary footpad hyperkeratosis (HFH). *PLoS Genetics, 10*(5), e1004370.

Edqvist, P., Fagerberg, L., Hallstrom, B., Danielsson, A., Edlund, K., et al. (2015). Expression of human skin-specific genes defined by transcriptomics and atnibody-based profiling. *J Histo & Cyto, 63*(2), 129–141.

Ellis, A., Risk, J. M., Maruthappu, T., & Kelsell, D. P. (2015).Tylosis with oesophageal cancer: Diagnosis, management and molecular mechanisms. *Orphanet J Rare Dis, 29*(10), 126.

Enshell-Seijffers, D., Lindon, C, Wu, E. L., Taketo, M., & Morgan, B. A. (2010). B catenin activity in the dermal papilla of the hair follicle regulates pigment type switching. *PNAS, 107*(50), 21564–21569.

Etheridge, S. L., Brooke, M. A., Kelsell, D. P., & Blaydon, D. C. (2013). Rhomboid proteins: A role in keratinocyte proliferation and cancer. *Cell Tissue Res, 351*, 301–307.

Feng, X., & Coulombe, P. A. (2015). A role for disulfide bonding in keratin intermediate filament organization and dynamics in skin keratinocytes. *J Cell Biol, 209*, 59–72.

Frank, J., Cserhalmi-Friedman, P. B., Ahmad, W., Panteleyev, A. A., Aita, V. M., & Christiano, A. M. (2001). Characterization of the desmosomal cadherin gene family: Genomic organization of two desmoglein genes on human chromosome 18q12. *Exp Dermatol, 10*(2), 90–94.

Freeman, M. (2004). Proteolysis within the membrane: Rhomboids revealed. *Nat Rev Mol Cell Biol, 5,* 188–197.

Freeman, M. (2009). Rhomboids: 7 years of a new protease family. *Semin Cell Dev Biol, 20,* 231–239.

Freeman, M. (2016). Rhomboids, signalling and cell biology. *Biochem Soc Trans, 44*, 945–950.

Fu, D. J., Thomson, C., Lunny, D. P., Dopping-Hepenstal, P. J., Mcgrath, J. A., Smith, F., Pedrioli, D. M. (2014). Keratin 9 is required for the structural integrity and terminal differentiation of the palmoplantar epidermis. *J Invest Dermatol, 134,* 754–763.

Fuchs, E., & Green, H. (1980). Changes in keratin gene expression during terminal differentiation of the keratinocyte. *Cell, 19*, 1033–1042.

Fulcher, L. J., Bozatzi, P., Tachie-Menson, T., Wu, K. Z. L., Cummins, T. D., Bufton J. C., Dunbar K. (2018). The DUF1669 domain of FAM83 family proteins anchor casein kinase 1 isoforms. *Sci Signal,* (11) 531–535.

Goldberg, G. S., Valiunas, V., & Brink, P. R. (2004). Selective permeability of gap junction channels. *Biochim Biophys Acta, 1662*, 96–101.

Gomes, J., Finlay, M., Ahmed, A. K., et al. (2012). Electrophysiological abnormalities precede overt structural changes in arrhythmogenic right ventricular cardiomyopathy due to mutations in desmoplakin-A combined murine and human study. *Eur Heart J, 33,* 1942–1953.

Goodenough, D. A., Goliger, J. A., & Paul, D. L. (1996). Connexins, connexons, and intercellular communication. *Annu Rev Biochem, 65*, 475–502.

Gooz, M. (2010). Adam-17: The enzyme that does it all. *Crit Rev Biochem Mol Biol,* 45, 146–169.

Greco, V., Chen, T., Rendl, M., Schober, M., Pasolli, H. A., Stokes, N., et al. (2009). A two-step mechanism for stem cell activation during hair regeneration. *Cell Stem Cell, 4*(2), 155–169.

Green, K. J., & Gaudry, C. A. (2000). Are desmosomes more than tethers for intermediate filaments? *Nat Rev Mol Cell Biol, 1*, 208–216.

Green, K. J., Getsios, S., Troyanovsky, S., & Godsel, L. M. (2010). Intercellular junction assembly, dynamics, and homeostasis. *Cold Spring Harb Perspect Biol, 2,* a000125.

Gutstein, D. E., Morley, G. E., Tamaddon, H., et al. (2001). Conduction slowing and sudden arrhythmic death in mice with cardiac-restricted inactivation of connexin43. *Circ Res, 88*(3), 333–339.

Kanter, H. L., Laing, J. G., Beyer, E. C., Green, K. G., & Saffitz, J. E. (1993). Multiple connexins colocalize in canine ventricular myocyte gap junctions. *Circ. Res, 73*, 344–350.

Haines, R. L., & Lane, E. B. (2012). Keratins and disease at a glance. *J Cell Sci, 125*, 3923–3928.

Heathcote, K., Syrris, P., Carter, N. D., & Patton, M. A. (Year). A connexin 26 mutation causes a syndrome of sensorineural hearing loss and palmoplantar hyperkeratosis. *Periodical Title, x*(x), xx–xx.

Hobbs, R. P., DePianto, D. J., Jacob, J. T., Han, M. C., Chung, B. M., Batazzi A. S., Coulombe, P. A. (2015). Keratin-dependent regulation of Aire and gene expression in skin. *Nat Genet, 47*(8), 933–938.

Hosur, V., Burzenski, L. M., Stearns, T. M., Farley, M. L., Sundberg, J. P., Wiles, M. V., & Shultz, L. D. (2017). Early induction of NRF2 antioxidant pathway

by RHBDF2 mediates rapid cutaneous wound healing. *Exp Mol Pathol, 102*(2), 337–346.

Hosur, V., Burzenski, L. M., Stearns, T. M., Farley, M. L., Sundberg, J. P., Wiles, M. V., & Shultz, L. D. (2017). Early induction of NRF2 antioxidant pathway by RHBDF2 mediates rapid cutaneous wound healing. *Exp Mol Pathol, 102*(2), 337–346.

Howel-Evans, W., Mc, C. R., Clarke, C. A., & Sheppard, P. M. (1958). Carcinoma of the oesophagus with keratosis palmaris et plantaris (tylosis): A study of two families. *Q J Med, 27,* 413–429.

Ishida-Yamamoto, A., Mcgrath, J. A., Chapman, S. J., Leigh, I. M., Lane, E. B., & Eady, R. A. (1991). Epidermolysis bullosa simplex (Dowling-Meara type) is a genetic disease characterized by an abnormal keratin-filament network involving keratins K5 and K14. *J Invest Dermatol, 97,* 959–968.

Itin, P. H., & Fistarol, S. K. (2005). Palmoplantar keratodermas. *Clin Dermatol, 23*, 15–22.

Jahoda, C. A. B., Horne, K. A., & Oliver, R. F. (1984). Induction of hair growth by implantation of cultured dermal papilla cells. *Nature, 311,* 560–562.

Jaks, V., Barker, N., Kasper, M., Van, E. J. H., Snippert, H. J., Clevers, H., & Toftgard R. (2008). Lgr5 marks cycling yet long-lived hair follicle stem cells. *Nat Genet, 40*(11), 1291–1299.

Jonkman, M. F., Pasmooij, A. M., Pasmans, S. G., van den Berg, M. P., Ter Horst, H. J., Timmer A., & Pas H. H. (2005). Loss of desmoplakin tail causes lethal acantholytic epidermolysis bullosa. *Am J Hum Genet, 77*(4), 653–660.

Kanter, H. L., Saffitz, J. E., & Beyer, E. C. (1992). Cardiac myocytes express multiple gap junction proteins. *Circ Res, 70*(2), 438–444.

Kapplinger, J. D., Landstrom, A. P., Salisbury, B. A., et al. (2011). Distinguishing arrhythmogenic right ventricular cardiomyopathy/dysplasia-associated mutations from background genetic noise. *J Am Coll Cardiol*, 57, 2317–2327.

Karantza, V. (2011). Keratins in health and cancer: more than mere epithelial cell markers. *Oncogene, 30,* 127–138.

Kaufman, C. K., Zhou, P., Pasolli, H. A., et al. (2003). GATA-3: An unexpected regulator of cell lineage determination in skin. *Genes Dev, 17*(17), 2108–2122.

Kelsell, D. P., Di, W.-L., & Houseman, M. J. (2001). Connexin mutations in skin disease and hearing loss. *American Journal of Human Genetics, 68*(3), 559–568.

Kelsell, D. P., Dunlop, J., Stevens, H. P., Lench, N. J., Liang, J. N., Parry, G., .Leigh, I. M. (1997). Connexin 26 mutations in hereditary non-syndromic sensorineural deafness. *Nature, 387*, 80–83.

Kerns, M. L., Hakim, J. M., Lu, R. G., Guo, Y., Berroth, A., Kaspar R. L., & Coulombe, P. A. (2016). Oxidative stress and dysfunctional NRF2 underlie pachyonychia congenita phenotypes. *J Clin Invest, 126*(6), 2356–2366.

Kim, J.-W., Lee, S.-K., Lee, Z. H., Park J.-C., Lee, K-E, Simmer, J. P. (2008). FAM83H mutations in families with autosomal-dominant hypocalcified amelogenesis imperfecta. *American Journal of Human Genetics*, *82*, 489–494.

Kim, H. J., Choi, W. J., & Lee, C. H. (2015). Phosphorylation and reorganization of keratin networks: Implications for carcinogenesis and epithelial mesenchymal transition. *Biomol Ther (Seoul), 23*, 301–312.

Kljuic, A., Gilead, L., Martinez-Mir, A., Frank, J., Christiano, A. M., & Zlotogorski, A. (2003b). A nonsense mutation in the desmoglein 1 gene underlies striate keratoderma. *Exp Dermatol, 12*, 523–527.

Kolsch, A., Windoffer, R., Wurflinger, T., Aach, T., & Leube, R. E. (2010). The keratin-filament cycle of assembly and disassembly. *J Cell Sci, 123*, 2266–2272.

Kouklis, P. D., Hutton, E., & Fuchs, E. (1994). Making a connection: Direct binding between keratin intermediate filaments and desmosomal proteins. *J Cell Biol, 127,* 1049–1060.

Kretzschmar, K., Cottle, D. L., Schweiger, P. J., & Watt, F. M. (2015). The androgen receptor antagonizes Wnt/β-catenin signaling in epidermal stem cells. *J Invest Dermatol, 135*(11), 2753–2763.

Kuga, T., Kume, H., Kawasaki, N., Sato, M., Adachi, J., Shiromizu T., Tomonaga T. (2013). A novel mechanism of keratin cytoskeleton organization through casein kinase I and FAM83H in colorectal cancer. *Journal of Cell Science, 126*, 4721–4731.

Lai, C., August, S., Albibas, A., Behar, R., Cho, S. Y., Polak, M. E., Healy, E. (2016). OX40+ regulatory T cells in cutaneous squamous cell carcinoma suppress effector T-cell responses and associate with metastatic potential. *Clin Cancer Res, 22,* 4236–4248.

Lammi, L., Arte, S., Somer, M., Jarvinen, H., Lahermo P, Thesleff I., Nieminen P. (2004). Mutations in AXIN2 cause familial tooth agenesis and predispose to colorectal cancer. *Am J Hum Genet, 74*(5), 1043–1050.

Langan, E. A., & Paus, R. (2010). Female pattern hair loss: beyond an androgenic aetiology. *Br J Dermatol, 163* (5) 1140-1141

Lee, S.-K., Hu, J. C. C., Bartlett, J. D., Lee, K.-E., Lin, B. P. J.. Simmer. J. P., & Kim J.-W. (2008). Mutational spectrum of FAM83H: The C-Terminal portion is required for tooth enamel calcification. *Human Mutation, 29,* E95–E99.

Lee. S.-Y., Meier, R., Furuta, S., Lenburg, M. E., Kenny, P. A., Xu, R., & Bissell, M. J. (2012). FAM83A confers EGFR-TKI resistance in breast cancer cells and in mice. *The Journal of Clinical Investigation, 122,* 3211–3220.

Lee, S. S., Jung, N. J., Im, M., Lee, Y., Seo, Y. J., & Lee, J. H. (2011). Acral-type malignant acanthosis nigricans associated with gastric adenocarcinoma. *Ann Dermatol, 23*, S208–S210.

Leigh, I. M., Navsaria, H., Purkis, P. E., Mckay, I. A., Bowden, P. E., & Riddle, P. N. (1995). Keratins (K16 and K17) as markers of keratinocyte hyperproliferation in psoriasis in vivo and in vitro. *Br J Dermatol, 133*, 501–511.

Lessard, J. C., & Coulombe, P. A. (2012). Keratin 16-null mice develop palmoplantar keratoderma, a hallmark feature of pachyonychia congenita and related disorders. *J Invest Dermatol, 132*, 1384–1391.

Leube, R. E., Moch, M., Kolsch, A., & Windoffer, R. (2011). “Panta rhei”: Perpetual cycling of the keratin cytoskeleton. *Bioarchitecture, 1,* 39–44.

Liao, H., Sayers, J. M., Wilson, N. J., Irvine, A. D., Mellerio, J. E., Baselga, E., Smith, F. J. (2007). A spectrum of mutations in keratins k6a, K16 and K17 causing pachyonychia congenita. *J Dermatol Sci, 48,* 199–205.

Lim, X., Tan, S. H., Yu, K. L., Lim, S. B., & Nusse, R. (2016). Axin2 marks quiescent hair follicle bulge stem cells that are maintained by autocrine Wnt/β-catenin signaling *Proc Natl Acad Sci, 113*(11) E1498-505

Lin, Z., Chen, Q., Lee, M., Cao, X., Zhang, J., Ma, D et al. (2012). Exome sequencing reveals mutations in TRPV3 as a cause of Olmsted syndrome. *Am. J. Hum. Genet, 90*, 558–564.

Lo Celso, C., Prowse, D. M., & Watt, F. M. (2004). Transient activation of beta-catenin signalling in adult mouse epidermis is sufficient to induce new hair follicles but continuous activation is required to maintain hair follicle tumours, *Development, 131*, 1787–1799.

Loussouarn, G., Garcel, A. L., Lozano, I., et al. (2007). Worldwide diversity of hair curliness: A new method of assessment. *Int J Dermatol, 46*(1), 2–6.

Marcus, F. I., McKenna, W. J., Sherrill, D., et al. (2010). Diagnosis of arrhythmogenic right ventricular cardiomyopathy/dysplasia: Proposed modification of the Task Force criteria. *European Heart Journal, 31*, 806–814.

Maruthappu, T., Chikh, A., Fell, B., Delaney, P. J., Brooke, M. A., Levet, C., Kelsell, D. P. (2017). Rhomboid family member 2 regulates cytoskeletal stress-associated Keratin 16. *Nat Commun, 27*(8), 14174.

Maruthappu, T., McGinty, L. A., Blaydon, D. C., Fell, B., Mattaa, A, Duit R, Kelsell, D. P. (2018a). Recessive mutation in FAM83G associated with PPK and exuberant scalp hair. *J Invest Dermatol, 138*(4), 984–987.

Maruthappu, T., Posafalvi, A., Castelletti, S., Delaney, P. J., Syrris, P., O'Toole, Kelsell D. P. (2018b). Loss of function desmoplakin I and II mutations underlie dominant arrhythmogenic cardiomyopathy with a hair and skin phenotype. *Br J Dermatol, 10.1111/bjd.17388. [Epub ahead of print]*

Maruthappu, T., Scott, C. A., & Kelsell, D. P. (2014). Discovery in genetic skin disease: The impact of high throughput genetic technologies. *Genes (Basel), 5*(3), 615–634.

Maruthappu, T., & Kelsell, D. P. (2018). "Chapter 23.3: Inherited skin disease," in A. Editor & B. Editor (Eds.), *Oxford Textbook of Medicine* (6th ed.) (pp. xx–xx). Location: Oxford University Press.

McAleer, M. A., Pohler, E., Smith, F. J., et al. (2018). Severe dermatitis, multiple allergies, and metabolic wasting syndrome caused by a novel mutation in the N-terminal plakin domain of desmoplakin. *J Allergy Clin Immunol, 136*(5), 1268–1276.

McGowan, K., & Coulombe, P. A. (1998). The wound repair-associated keratins 6, 16, and 17. Insights into the role of intermediate filaments in specifying keratinocyte cytoarchitecture. *Subcell Biochem, 31,* 173–204.

McGrath, J. A., Mcmillan, J. R., Shemanko, C. S., Runswick, S. K., Leigh, I. M., Lane, E. B., Eady, R. A. (1997). Mutations in the plakophilin 1 gene result in ectodermal dysplasia/ skin fragility syndrome. *Nat Genet, 17,* 240–244.

Mcilwain, D. R., Lang, P. A., Maretzky, T., Hamada, K., Ohishi, K., Maney, Mak, T. W. (2012). Irhom2 regulation of TACE controls TNF-mediated protection against Listeria and responses to LPS. *Science, 335,* 229–232.

McKoy, G., Protonotarios, N., Crosby, A., et al. (2000). Identification of a deletion in plakoglobin in arrhythmogenic right ventricular cardiomyopathy with palmoplantar keratoderma and woolly hair (Naxos disease). *Lancet, 355,* 2119–2124.

Mclean, W. H., Morley, S. M., Higgins, C., Bowden, P. E., White, M., Leigh, I. M., & Lane, E. B. (1999). Novel and recurrent mutations in keratin 10 causing bullous congenital ichthyosiform erythroderma. *Exp Dermatol, 8,* 120–123.

Medland, S. E., Nyholt, D. R., Painter, J. N., et al. (2009). Common variants in the trichohyalin gene are associated with straight hair in Europeans. *Am J Hum Genet, 85,* 750–755.

Medland, S. E., Nyholt, D. R., Painter, J. N., et al. (2009). Common variants in the trichohyalin gene are associated with straight hair in Europeans. *Am J Hum Genet, 85,* 750–755.

Mckenna, W., Gallagher, B., Morris-Larkin, L., & Bassett, A. S. (Year). Cardiomyopathy type 5 is a fully penetrant, lethal arrhythmic disorder caused by a missense mutation in the TMEM43 gene. *Am J Hum Genet, 82,* 809–821.

Merner, N. D., Hodgkinson, K. A., Haywood, A. F., Connors, S., French, V. M., Drenckhahn, J. D., Young, T. L. (2008). Arrhythmogenic right ventricular Cardiomyopathy type 5 is a fully penetrant, lethal arrhythmic disorder caused by a missense mutation in the TMEM43 gene. *Am J Hum Genet, 82*, 809–821.

Millar, S. E. (2002). Moleclar mechanisms regulating hair follicle development. *J Invest Dermatol, x*(x), 216–225.

Moll, R., Franke, W. W., Schiller, D. L., Geiger, B., & Krepler, R. (1982). The catalog of human cytokeratins: Patterns of expression in normal epithelia, tumors and cultured cells. *Cell, 31,* 11–24.

Nam, J. S., Park, E., Turcotte, T. J., Palencia, S, Zhan X, Lee J., Yoon, J. K. (2007). Mouse R-spondin2 is required for apical ectodermal ridge maintenance in the hindlimb. *Dev Biol, 311*(1) 124-35

Navarcikova, S., Hatala, R., Zlatos, L., & Hulin, I. (2005). Arrhythmogenic right ventricular cardiomyopathy/dysplasia. *Bratisl Lek Listy, 106*, 257–261.

Nitoiu, D., Etheridge, S. L., & Kelsell, D. P. (2014). Insights into desmosome biology from inherited human skin disease and cardiocutaneous syndromes. *Cell Commun Adhes, 21,* 129–140.

Norgett, E. E., Hatsell, S. J., Carvajal-Huerta, L., et al. (2000). Recessive mutation in desmoplakin disrupts desmoplakin-intermediate filament interactions and causes dilated cardiomyopathy, woolly hair and keratoderma. *Hum Mol Genet, 9*, 2761–2766.

Norgett, E. E., Lucke, T. W., Bowers, B., et al. (2006). Early death from cardiomyopathy in a family with autosomal dominant striate palmoplantar keratoderma and woolly hair associated with a novel insertion mutation in desmoplakin. *J Invest Dermatol, 126*, 1651–1654.

Norman, M., Simpson, M., Mogensen, J., et al. (2005). Novel mutation in desmoplakin causes arrhythmogenic left ventricular cardiomyopathy. *Circulation, 112*, 636–642.

Nousari, H. C., & Anhalt, G. J. (1999). Pemphigus and bullous pemphigoid. *Lancet, 354*, 667–672.

Oda, H., & Takeichi, M. (2011). Evolution: Structural and functional diversity of cadherin at the adherens junction. *J Cell Biol, 193*, 1137–1146.

Paladini, R. D., & Coulombe, P. A. (1998). Directed expression of keratin 16 to the progenitor basal cells of transgenic mouse skin delays skin maturation. *J Cell Biol, 142,* 1035–1051.

Paladini, R. D., Takahashi, K., Bravo, N. S., & Coulombe, P. A. (1996). Onset of re-epithelialization after skin injury correlates with a reorganization of keratin filaments in wound edge keratinocytes: defining a potential role for keratin 16. *J Cell Biol, 132,* 381–397.

Patel, D. M., Dubash, A. D., Kreitzer, G., & Green, K. J. (2014). Disease mutations in desmoplakin inhibit Cx43 membrane targeting mediated by desmoplakin–EB1 interactions. *J Cell Biol, 206*(6), 779–797.

Patel, D. M., & Green, K. J. (2014). Desmosomes in the heart: A review of clinical and mechanistic analyses. *Cell Commun Adhes, 21*(3), 109–128.

Paul, M., Wichter, T., Gerss, J., Arps V, Schulze-Bahr E, Robenek H, . . . Weissen-Plenz, G. (2013). Connexin expression patterns in arrhythmogenic right ventricular cardiomyopathy. *Am J Cardiol, 111*(10), 1488–1495.

Pigors, M., Schwieger-Briel, A., Cosgarea, R., et al. (2015). Desmoplakin mutations with palmoplantar keratoderma, woolly hair and cardiomyopathy. *Acta Derm Venereol, 95*, 337–340.

Pilichou, K., Nava, A., Basso, C., Beffagna, G., Bauce, B., Lorenzon A., Rampazzo, A. (2006). Mutations in desmoglein-2 gene are associated with arrhythmogenic right ventricular cardiomyopathy. *Circulation, 113*, 1171–1179.

Protonotarios, N., Tsatsopoulou, A., Patsourakos, P., Alexopoulos, D., Gezerlis, P., Simitsis, S., & Scampardonis, G. (1986). Cardiac abnormalities in familial palmoplantar keratosis. *Br Heart J, 56*(4), 321–326.

Protonotarios, N., & Tsatsopoulou, A. (2004). Naxos disease and Carvajal syndrome: Cardiocutaneous disorders that highlight the pathogenesis and broaden the spectrum of arrhythmogenic right ventricular cardiomyopathy. *Cardiovasc Pathol, 13*(4), 185–194.

Radden, L. A., Child, K. M., Adkins, E. B., Spacek, D. V., Feliciano, A. M., & King, T. R. (2013). The wooly mutation (wly) on mouse chromosome 11 is associated with a genetic defect in Fam83g. *BMC Research Notes, 6,* 189.

Rampazzo, A., Nava, A., Malacrida, S., et al. (2002). Mutation in human desmoplakin domain binding to plakoglobin causes a dominant form of arrhythmogenic right ventricular cardiomyopathy. *Am J Hum Genet, 71,* 1200–1206.

Rasmussen, T. B., Hansen, J., Nissen, P. H., et al. (2013). Protein expression studies of desmoplakin mutations in cardiomyopathy patients reveal different molecular disease mechanisms. *Clin Genet, 84,* 20–30.

Rasmussen, T. B., Nissen, P. H., Palmfeldt, J., et al. (2014). Truncating plakophilin-2 mutations in arrhythmogenic cardiomyopathy are associated with protein haploinsufficiency in both myocardium and epidermis. *Circ Cardiovasc Genet*, *7*, 230–240.

Reis, A., Hennies, H. C., Langbein, L., Digweed, M., Mischke, D., Drechsler, & Sperling, X. (1994). Keratin 9 gene mutations in epidermolytic palmoplantar keratoderma (EPPK). *Nat Genet, 6,* 174–179.

Rickman, L., Simrak, D., Stevens, H. P., Hunt, D. M., King I. A., Bryant, S. P., Buxton R. S. (1999). N-terminal deletion in a desmosomal cadherin causes the autosomal dominant skin disease striate palmoplantar keratoderma. *Hum Mol Genet, 8,* 971–976.

Rose-John, S. (2013). ADAM17, shedding, TACE as therapeutic targets. *Pharmacol Res, 71,* 19–22.

Sayyab, S., Viluma, A., Bergvall, K., Brunberg, E., Jagannathan V., Leeb, T., et al. (2016). Whole-genome sequencing of a canine family trio reveals a FAM83G variant associated with hereditary footpad hyperkeratosis. *G3 (Bethesda, Md), 6*(3), 521–527.

Sen-Chowdhry, S., Syrris, P., & McKenna, W. J. (2005). Desmoplakin disease in arrhythmogenic right ventricular cardiomyopathy: Early genotype-phenotype studies. *Eur Heart J, 26,* 1582–1584.

Sen-Chowdhry, S., Syrris, P., & McKenna, W. J. (2007). Role of genetic analysis in the management of patients with arrhythmogenic right ventricular dysplasia/cardiomyopathy. *J Am Coll Cardiol, 50*, 1813–1821.

Shimizu, H., Masunaga, T., Ishiko, A., Kikuchi, A., Hashimoto, T., & Nishikawa, T. (1995). Pemphigus vulgaris and pemphigus foliaceus sera show an inversely graded binding pattern to extracellular regions of desmosomes in different layers of human epidermis. *J Invest Dermatol, 105*, 153–159.

Simcha, I., Shtutman, M., Salomon, D., Zhurinsky, J., Sadot, E., Geiger, B., & Ben-Ze'ev, A. (1998). Differential nuclear translocation and transactivation potential of beta-catenin and plakoglobin. *J Cell Biol, 141*(6), 1433–1448.

Simpson, C. L, Patel, D. M., & Green, J. K. (2011). Deconstructing the skin: Cytoarchitectural determinants of epidermal morphogenesis nature reviews. *Molecular Cell Biology, 12*, 565–580.

Smith, F. J., Fisher, M. P., Healy, E., Rees, J. L., Bonifas, J. M., Epstein, . . . Mclean, W. H. (2000). Novel keratin 16 mutations and protein expression studies in

pachyonychia congenita type 1 and focal palmoplantar keratoderma. *Exp Dermatol, 9,* 170–177.

Smith, F. J., Liao, H., Cassidy, A. J., Stewart, A., Hamill, K. J., Wood, P., Mclean, W. H. (2005). The genetic basis of pachyonychia congenita. *J Investig Dermatol Symp Proc, 10,* 21–30.

Solanas, G., & Benitah, S. A. (2013). Regenerating the skin: a task for the heterogeneous stem cell pool and surrounding niche. *Nat Rev Mol Cell Biol, 14,* 737–748.

Stamos, J. L., & Weis, W. I. (2013). The B Catenin destruction complex. *Cold Spring Harb Perspect Biol, 5*(1) a007898

Steinert, P. M., North, A. C., & Parry, D. A. (1994). Structural features of keratin intermediate filaments. *J Invest Dermatol, 103,* 19s–24s.

Stephens, K., Zlotogorski, A., Smith, L., Ehrlich, P., Wijsman, E., Livingston, R. J., & Sybert, V. P. (1995). Epidermolysis bullosa simplex: A keratin 5 mutation is a fully dominant allele in epidermal cytoskeleton function. *Am J Hum Genet, 56,* 577–585.

Stevens, H. P., & Rustin, M. H. (1994). Keratin gene mutations in human skin disease. *Postgrad Med J, 70,* 775–779.

Sugioka, K., Mizumoto, K., & Sawa, H. (2011). Wnt regulates spindle asymmetry to generate asymmetric nuclear β-catenin in C. elegans. *Cell, 146*(6), 942–954.

Swensson, O., & Eady, R. A. (1996). Morphology of the keratin filament network in palm and sole skin: Evidence for site-dependent features based on stereological analysis. *Arch Dermatol Res, 288*, 55–62.

Syrris, P., Ward, D., Evans, A., Asimaki, A., Gandjbakhch, E., Sen-Chowdhry, S., & Mckenna, W. J. (2006). Arrhythmogenic right ventricular

dysplasia/cardiomyopathy associated with mutations in the desmosomal gene desmocollin-2. *Am J Hum Genet, 79,* 978–984.

Takeo, M., Chou, W. C, Sun, Q., Lee, W., Rabbani, P., Loomis C, Ito, M. (2013). Wnt activation in nail epithelium couples nail growth to digit regeneration. *Nature, 11*(499), 228–232.

Terrinoni, A., Smith, F. J., Didona, B., Canzona, F., Paradisi, M., Huber, M., .Mclean, W. H. (2001). Novel and recurrent mutations in the genes encoding keratins K6a, K16 and K17 in 13 cases of pachyonychia congenita. *J Invest Dermatol, 117*, 1391–1396.

Thiers, B. H., Sahn, R. E., & Callen, J. P. (2009). Cutaneous manifestations of internal malignancy. *CA Cancer J Clin, 59*, 73–98.

Towbin, J. A. (2008). Arrhythmogenic right ventricular cardiomyopathy: A paradigm of overlapping disorders. *Ann Noninvasive Electrocardiol, 13*, 325–326.

Urban, S., Lee, J. R., & Freeman, M. (2001). Drosophila rhomboid-1 defines a family of putative intramembrane serine proteases. *Cell, 107,* 173–182.

Uzumcu, A., Norgett, E. E., Dindar, A., Uyguner, O., Nisli, K., Kayserili, H., .Wollnik, B. (2006). Loss of desmoplakin isoform I causes early onset cardiomyopathy and heart failure in a Naxos-like syndrome. *J Med Genet, 43,* xx–xx.

Villaret, D. B., Wang, T., Dillon, D., Xu, J., Sivam, D., Cheever, M. A., & Reed, S. G. (2000). Identification of genes overexpressed in head and neck squamous cell carcinoma using a combination of complementary DNA subtraction and microarray analysis. *Laryngoscope, 110,* 374–381.

Vogt, J., Dingwell, K. S., Herhaus, L., Gourlay, R., Macartney, T., Campbell, D., et al. (2014). Protein associated with SMAD1 (PAWS1/FAM83G) is a substrate for type I bone morphogenetic protein receptors and modulates bone morphogenetic protein signalling. *Open Biology, 4,* 130210.

Wang, K., Li, M., & Hakonarson. H. (2010). ANNOVAR: Functional annotation of genetic variants from high-throughput sequencing data. *Nucleic Acids Research, 38*(16), e164.

Wang. S.-K., Hu, Y., Yang, J., Smith, C. E., Richardson, A. S., Yamakoshi, Y., Simmer, J. P. (2016). Fam83h null mice support a neomorphic mechanism for human ADHCAI. *Molecular Genetics & Genomic Medicine, 4*, 46–67.

Wawersik, M., Paladini, R. D., Noensie, E., & Coulombe, P. A. (1997). A proline residue in the alpha-helical rod domain of type I keratin 16 destabilizes keratin heterotetramers. *J Biol Chem, 272*, 32557–32565.

Wei, C. J., Xu, X., & Lo, C. W. (2004). Connexins and cell signaling in development and disease. *Annu Rev Cell Dev Biol, 20*, 811–838.

Wilgoss, A., Leigh, I. M., Barnes, M. R., Dopping-Hepenstal, P., Eady, R. A. J., Walter, J.,Kelsell, D. P. (1999). Identification of a novel mutation R42P in the gap junction protein beta-3 associated with autosomal dominant erythrokeratoderma variabilis. *J. Invest. Derm, 113,* 1119–1122.

Wilson, N. J., Leachman, S. A., Hansen, C. D., Mcmullan, A. C., Milstone, L. M., Schwartz, .. Smith, F. J. (2011). A large mutational study in pachyonychia congenita. *J Invest Dermatol, 131,* 1018–1024.

Windoffer, R., Beil, M., Magin, T. M., & Leube, R. E. (2011). Cytoskeleton in motion: The dynamics of keratin intermediate filaments in epithelia. *J Cell Biol, 194,* 669–678.

Wojnarowicz, P. M., Provencher, D. M., Mes-Masson, A. M., & Tonin, P. N. (2012). Chromosome 17q25 Genes, Rhbdf2 and Cygb, in ovarian cancer. *Int J Oncol, 40,* 1865–1880.

Wu, K. C., Bryan, J. T., Morasso, M. I., Jang, S. I., Lee, J. H., Yang, J. M., Steinert, P. M. (2000). Coiled-coil trigger motifs in the 1B and 2B rod domain segments are required for the stability of keratin intermediate filaments. *Mol Biol Cell*, *11,* 3539–3558.

Xu, H., Ramsey, I. S., Kotecha, S. A., Moran, M. M., Chong, J. A., Lawson, D., .Clapham, D. E. (2002). TRPV3 is a calcium-permeable temperature-sensitive cation channel. *Nature, 418,* 181–186,

Shirakata, Y., Amagai, M., Hanakawa Y., Nishikawa, T., & Hashimoto, K. (1998). Lack of mucosal involvement in pemphigus foliaceus may be due to low expression of desmoglein 1. *J Invest Dermatol, 110*, 76–78.

Yamada, S., Wirtz, D., & Coulombe, P. A. (2002). Pairwise assembly determines the intrinsic potential for self-organization and mechanical properties of keratin filaments. *Mol Biol Cell, 13,* 382–391.

Yang, J. M., Chipev, C. C., Digiovanna, J. J., Bale, S. J., Marekov L. N., Steinert, P. M., & Compton, J. G. (1994). Mutations in the H1 and 1A domains in the keratin 1 gene in epidermolytic hyperkeratosis. *J Invest Dermatol, 102,* 17–23.

Yin, T., & Green, K. J. (2004). Regulation of desmosome assembly and adhesion. *Semin Cell Dev Biol, 15,* 665–677.

Zettl, M., Adrain, C., Strisovsky, K., Lastun, V., & Freeman, M. (2011). Rhomboid family pseudoproteases use the ER quality control machinery to regulate intercellular signaling. *Cell, 145,* 79–91.

Zhou, L., Yang, K., Xu, M., Andl, T., Millar, S. E., Boyce, S., & Zhang, Y. (2016). Activating β-catenin signaling in CD133-positive dermal papilla cells increases hair inductivity. *The FEBS Journal, 283*(15), 2823–2835.

Appendices

Appendix A - Buffers

Buffer Reagents:

RM+
40µg/ml Hydrocortisone
500µg/ml Insulin
1µg/ml EGF
10-8 (0.84 µg/ml) Cholera toxin
500µg/ml Transferrin
1.3µg/ml Lyothyronine (L4)

Normal media (add to DMEM)
10% (v/v) FBS
2 mM L-glutamine
100 U/ml Penicillin
100 µg/ml Streptomycin
1% RM+

TBE Buffer 9M Tris base
9M Boric acid
0.2M EDTA, pH 8.0

DNA Loading Buffer 50% (v/v)
Glycerol 0.2% (w/v) Orange G

Western Blotting Polyacrylamide Running Gel (10%) in 5 ml
1.7 ml of Acrylamide mix [Protogel 30% (w/v)
acrylamide : 0.8% (w/v) Bis-acrylamide
stock solution (37.5:1)]

1.9 ml of ddH2O
1.3 ml of 1.5 M Tris, pH 8.8
0.05 ml of 10% SDS
0.05 ml of APS
0.002 ml of TEMED

Western Blotting Polyacrylamide Stacking Gel (5%) in 1 ml
0.17 ml of Acrylamide mix [Protogel 30% (w/v)
acrylamide : 0.8% (w/v) Bis-acrylamide
stock solution (37.5:1)]
0.68 ml of ddH2O
0.13 ml of 1.0 M Tris, pH 6.8
0.01 ml of 10% SDS
0.01 ml of APS
0.001 ml of TEMED

SDS Protein Loading Buffer
0.100 M Tris-HCl, pH 6.8
4% SDS
20% Glycerol
0.001% Bromophenol Blue
1.44 M Beta-mercaptoethanol (10%)

Western Blotting 10x Running Buffer
0.25M Tris base
1.92M Glycine
1% SDS

Western Blotting
10 x Transfer Buffer
0.48M Tris base
0.30M Glycine
0.37% (w/v) SDS
Add 20% (v/v) Methanol to 1 x Transfer Buffer

10 x TBS
0.5M Tris-HCl, pH 7.5
1.5M NaCl

1 x T-TBS
(Tween 20-TBS)
0.05M Tris-HCl, pH 7.5
0.15M NaCl
0.1% (v/v) Tween-20

Appendix B- Results Chapter 3 - Negative Controls

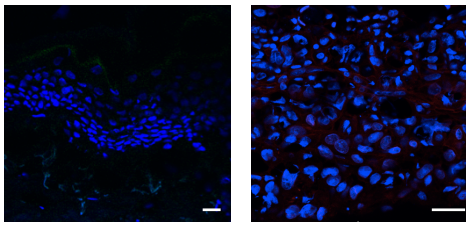

Figure B.1 Negative control for K16 in normal skin (left) and CTRL organotypic (right) staining Scale bar 20 µm

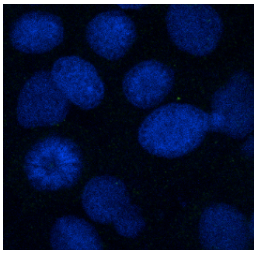

Figure B.2 Negative control for K6 staining in CTRL keratinocytes.

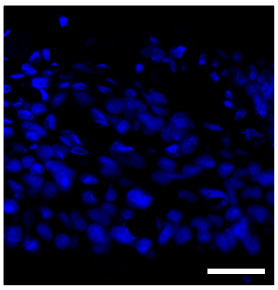

Figure B.3 Negative control for K6 staining in CTRL organotypics. Scale bar 20 µm

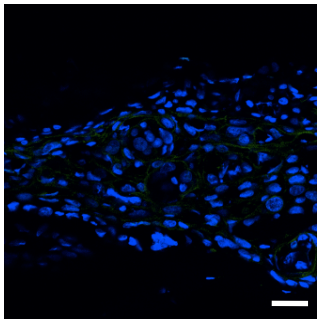

Figure B.4 Negative control for Ki67 staining in CTRL organotypics. Scale bar 20 µm

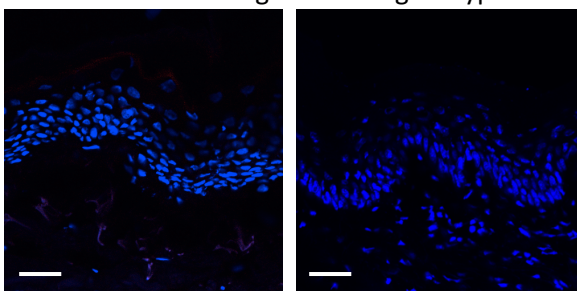

Figure B.5 Negative control for mouse paw staining K16 (left) and K9 (right) Scale bar 20 µm

Appendix C - Results Chapter 4 Additional immunostaining and negative controls.

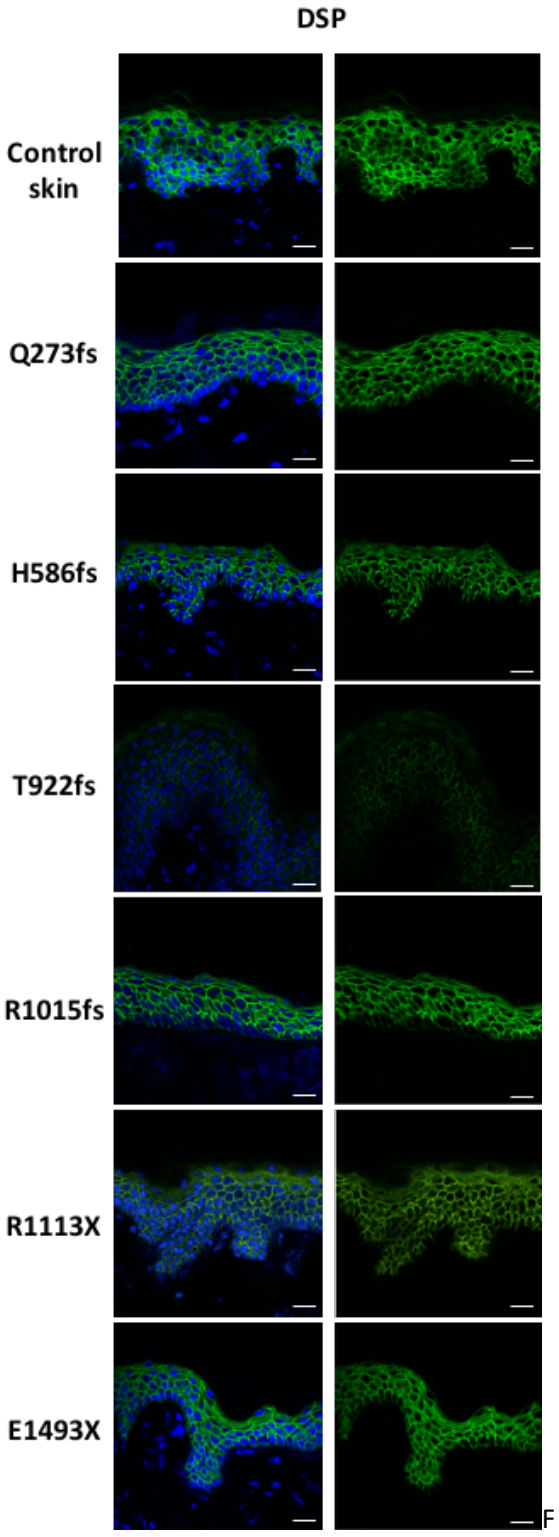

Figure C.1
Immunohistochemical staining of DSP in control and patient skin. Scale bar 20 µm

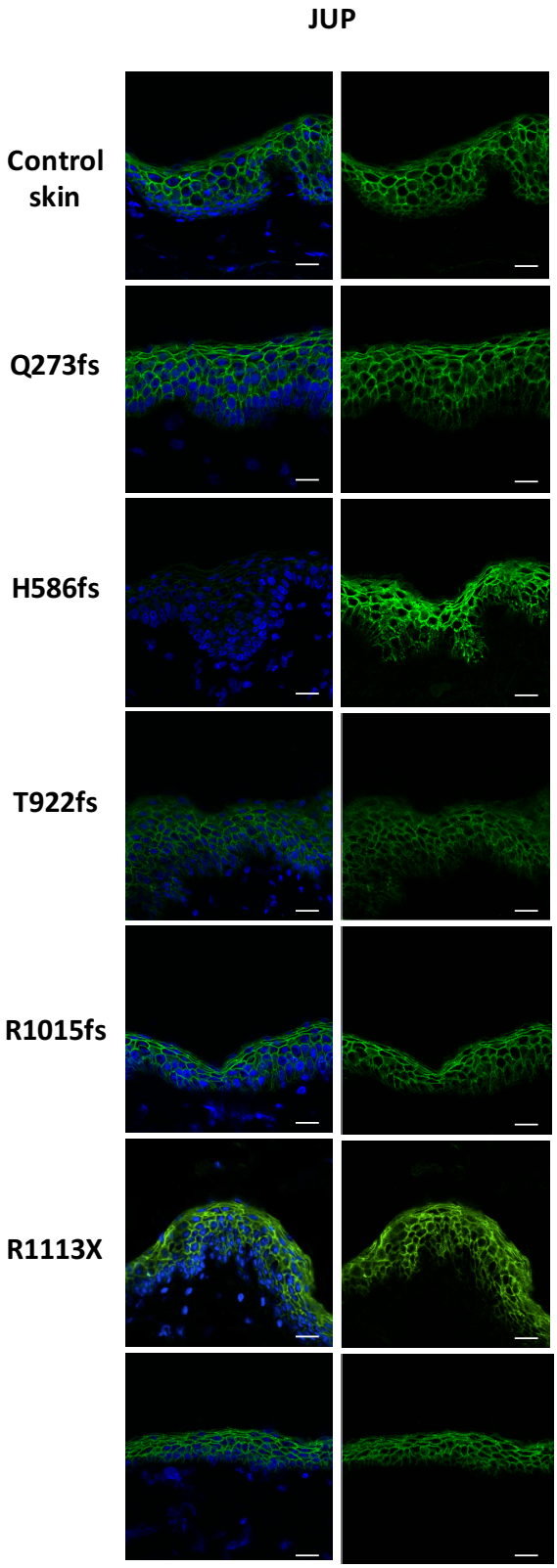

Figure C.2
Immunohistochemical staining of JUP in control and patient skin. Scale bar 20 µm

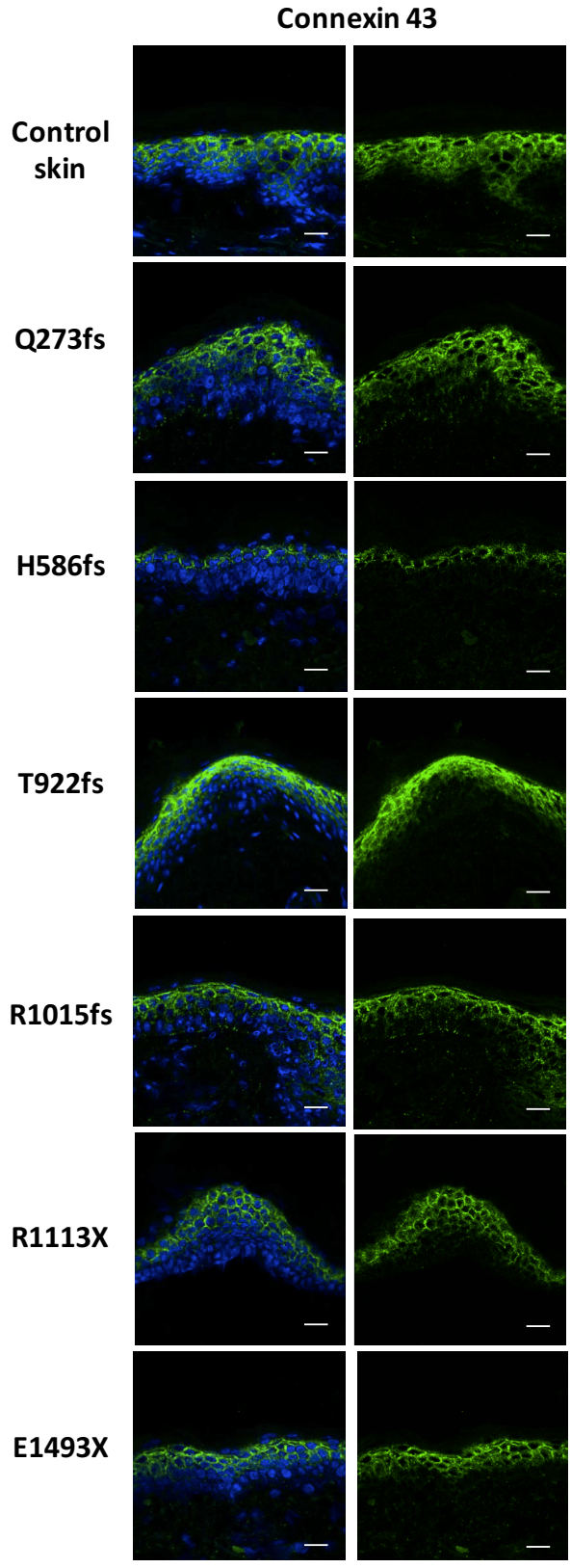

Figure C.3
Immunohistochemical staining of Connexin 43 in control and patient skin. Scale bar 20 µm

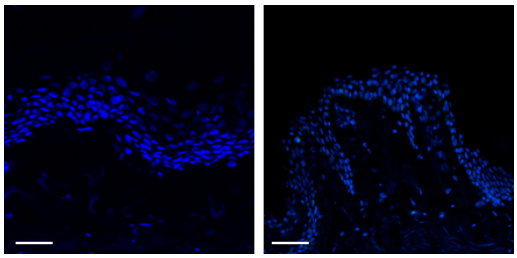

Figure C.4 Negative controls performed with secondary antibody only, anti-rabbit (left) and anti-mouse (right). Scale bar 20 µm

Appendix D - Results Chapter 5 – Primer sequences and negative controls

Primer Sequences – FAM83G

FAM83G-F: 5'CCGGGCTCATCAGGTCTTT 3'
FAM83G-R: 5' GAGCGGTCCGACTTCTGG 3';

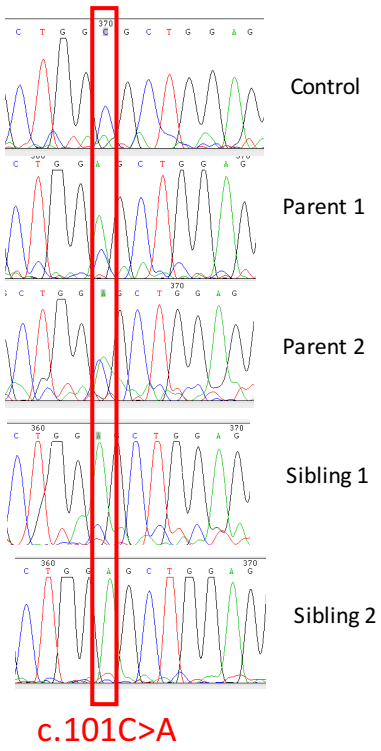

Figure D.1 Sequencing trace showing homozygous missense mutation c.101C>A, resulting in A34E in both siblings. Both parents were heterozygous carriers of the mutation

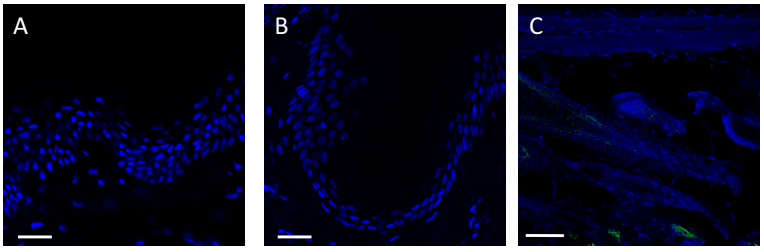

Figure D.2 Negative controls using anti-rabbit (A) and anti-mouse (B) secondary antibodies in normal human skin. Negative control for FAM83G mouse hair follicle immunostaining. Scale Bar Scale bar 20 µm.